Structural and Luminescent Properties of Rare Earth Activated Calcium Aluminozincate Phosphor for Solid State Lighting Applications

Thesis

Submitted to the Delhi Technological University

for the Award of the Degree of

DOCTOR OF PHILOSOPHY

in

APPLIED PHYSICS

Submitted by

SUMANDEEP KAUR

(2K14/Ph.D/AP/04)

DEPARTMENT OF APPLIED PHYSICS
DELHI TECHNOLOGICAL UNIVERSITY
DELHI-110 042, INDIA

JULY 2019

This thesis is dedicated to my family

DECLARATION

This is to certify that the thesis entitled ***"Structural and Luminescent Properties of Rare Earth Activated Calcium Aluminozincate Phosphor for Solid State Lighting Applications"*** submitted to the Delhi Technological University, Delhi for the award of degree of Doctor of Philosophy is based on the original research work carried out by me under the joint supervision of Prof. A.S. Rao and Dr. M. Jayasimhadri, Department of Applied Physics, Delhi Technological University, Delhi. It is further certified that the work embodied in this thesis has neither been partially nor fully submitted to any other university or institution for the award of any degree or diploma.

Sumandeep Kaur
Research Scholar
(Reg. No. 2K14/Ph.D/AP/04)

DELHI TECHNOLOGICAL UNIVERSITY
Formerly Delhi College of Engineering
(Under Delhi Act 6 of 2009, Govt. of NCT of Delhi)
Shahbad Daulatpur, Bawana Road, Delhi-110042

CERTIFICATE

This is to certify that the thesis entitled ***"Structural and Luminescent Properties of Rare Earth Activated Calcium Aluminozincate Phosphor for Solid State Lighting Applications"*** submitted to the Delhi Technological University, Delhi for the award of degree of Doctor of Philosophy is based on the original research work carried out by me under the joint supervision of Prof. A.S. Rao and Dr. M. Jayasimhadri, Department of Applied Physics, Delhi Technological University, Delhi. It is further certified that the work embodied in this thesis has neither been partially nor fully submitted to any other university or institution for the award of any degree or diploma.

Sumandeep Kaur
Research Scholar
(Reg. No. 2K14/Ph.D/AP/04)

This is to certify that the above statement made by the candidate is correct to the best of our knowledge.

Prof. A.S. Rao
Supervisor

Dr. M. Jayasimhadri
Supervisor

Prof. Rinku Sharma
Head, Department of Applied Physics
Delhi Technological University, Delhi

Acknowledgement

Thanks giving is a delightful job when sincerely expressed in words. Though these humble words, articulations and gratitude cannot really convey the deep feelings of my heart. While going through different stages during the last five years working in Delhi Technological University and specifically within the Luminescent Material Research Laboratory (LMRL) and Materials and Atmospheric Science Research Laboratory (MASRL), I take this opportunity to express my sincere thanks to those who helped me in this modest attempt of writing this thesis. Prior to all, I would like to thank ***Almighty****, who showered constant blessings upon me and made me able to carry out the present study successfully.*

I feel great honour in expressing my profound sense of gratitude, indebtedness and reverence to my supervisors ***Prof. A.S. Rao*** *and* ***Dr. M. Jayasimhadri****, Department of Applied Physics, Delhi Technological University, Delhi. It has been an honour to work under excellent, enthusiastic and distinguished supervisors. Their unremitting encouragement, constant help, meticulous supervision and constructive criticism throughout the course of my study for carving another milestone in my academic journey. Their immense knowledge of the subject, analytic gaze, farsightedness and perseverance were a constant source of inspiration during the course of this thesis work. I feel privileged to have worked under such a great supervision.*

I further stand ovated to ***Prof. Rinku Sharma****, Head, Department of Applied Physics, DTU, for her valuable help and suggestions.*

My heartfelt recognitions for ***Prof. S.C. Sharma****, DRC Chairman, former Head Department of Applied Physics, DTU, my SRC & DRC committee members for their enduring support and appropriate propositions.*

I would grab this opportunity to thank ***Dr D. Haranath****, Associate Professor, National Institute of Technology (NIT), Warangal and* ***Dr. Bathula Sivaiah****, Scientist, CSIR-National Physical Laboratory (NPL), Delhi, for providing necessary facilities, giving valuable suggestions and discussion. All this proved as a leading light throughout pursuit of my studies and research endeavours.*

I owe my sincere gratitude to ***Prof. G. Vijaya Prakash****, Indian Institute of Technology (IIT) Delhi, for his timely advice and support.*

It is my pleasure to express my sincere thanks to all the ***faculty*** *members of Department of Applied Physics for their continuous encouragement and help during my research work. I*

am also grateful to ***Mr. Sandeep Mishra*** *and other* ***technical and non-technical staff*** *for their timely support and cooperation whenever required.*

My deepest regards to ***Mr. Anil Kumar****, Deputy Registrar, Delhi Technological University,* ***Prof. J.L. Rao****, Sri Venkateswara University, Tirupati and* ***Dr. Swapna Koneru, K.L. University,*** *and* ***Dr. Mahamuda Shaik, K.L. University, Vijayawada*** *for their valuable suggestions during my Ph.D.*

Now it's time to sincerely thank my dear former and present lab mates whose support helped in accomplished my work. It is my pleasure to thank ***Dr. Amit K. Vishwakarma, Dr. Kaushal Jha, Dr. Nisha Deopa, Dr. Ritu Sharma, Dr. Arti Yadav*** *and other lab mates* ***Ms. Harprret kaur, Mr. Mukesh K. Sahu, Mr. Aman Prasad, Mrs. Yasha Tayal, Mrs. Kartika Maheshwari, Mr. Mohit Tyagi, Mr. Shankar Subhramanian, Mr. Rajat Bajaj, Mrs. Ravita Pilania, Ms. Pooja Rohilla, Ms. Shristi Malik*** *and* ***Ms. Deepali*** *for their support. I would also like to thank all the other scholars of Department of Applied Physics, Delhi Technological University, Delhi for their help and advice.*

I wish to acknowledge the enjoyable company and suitable help rendered by my dear friends, ***Dr. Savvi Mishra, Dr. G. Swati, Ms. P. Rekha Rani,*** *and* ***Mr. Rupesh A.Talwar*** *for their help and support during this tenure. It is my pleasure to thank* ***Mr. Vishnu Vikesh Jaiswal*** *for his continuous help, support, and care. My special thanks to* ***Dr. Jyotsna Panwar*** *with whom I have spent memorable time, who made my life easier and happier in Delhi Technological University.*

This endeavour would not have been a success without the persistent support and encouragement of my dearest friends ***Mr. Manish, Mr. Manoj, Mrs. Anjuma, Mrs. Vandana, Mr. Dheeraj, Mr. Rakesh Sharma, Mrs. Amandeep Kaur, Mrs. Riajeet Kaur, Mrs. Gagandeep Kaur*** *and* ***Mrs. Inderpreet Kaur****. I am glad to thank* ***Mr. Karandeep Singh*** *for his extended support and earnest concern that help me to tide over the occasional moments of stress at various stages of this tenure. My deep regards to his family for their support and encouragement.*

The love, pamper, support, encouragement, understanding and blessings of my parents gave me the strength to take up this work and complete it to the best of my ability. With heartful gratitude and love, I express my gratefulness to my grandmother ***Mrs. Ajeet Kaur****, father* ***Mr. Jatinder Singh****, mother* ***Mrs. Balvinder Kaur****, sister* ***Ms. Amandeep Kaur****, brother* ***Mr. Sandeep Singh****, my extended maternal and paternal family who have always been my pillars of strength and they enabled me to maintain a positive attitude throughout my studies.*

I always thank all my beloved friends across the globe for sharing my happy and sorrow moments.

*I extend my gratitude to **Delhi Technological University** and staff in Administration, Accounts, Store & Purchase, Library and Computer centre for their help and services.*

*I am grateful to the **University Grants Commission (UGC), Govt. of India, New Delhi,** for extending and providing financial assistance in the form of **Junior Research Fellowship** and **Senior Research Fellowship** during the period of my research.*

Thank you all!!!

Sumandeep Kaur

LIST OF PUBLICATIONS

Thesis Work

1. Synthesis optimization, photoluminescence and thermoluminescence studies of Eu^{3+} doped calcium aluminozincate phosphor.
   Sumandeep Kaur, *A.S. Rao, M. Jayasimhadri, B. Sivaiah, D. Haranath*
   Journal of Alloys and Compounds, 802 (2019) 129-138, ***IF-4.175***
2. Color tunability and energy transfer studies of Dy^{3+}/ Eu^{3+} co-doped calcium aluminozincate phosphor for lighting applications.
   Sumandeep Kaur, *A.S. Rao, M. Jayasimhadri*
   Materials Research Bulletin, 116 (2019) 79-88, ***IF-3.355***
3. Enhanced red down-conversion luminescence and high color purity from flux assisted Eu^{3+} doped calcium aluminozincate phosphor.
   Sumandeep Kaur, *A.S. Rao, M. Jayasimhadri*
   Journal of Luminescence, 202 (2018) 461-468, ***IF-2.961***
4. Spectroscopic and photoluminescence characteristics of Sm^{3+} doped calcium aluminozincate phosphor for applications in w-LED.
   Sumandeep Kaur, *M. Jayasimhadri, A.S. Rao*
   Ceramics International, 43 (2017) 7401-7407, ***IF-3.450***
5. A novel red emitting Eu^{3+} doped calcium aluminozincate phosphor for applications in w-LEDs.
   Sumandeep Kaur, *A.S. Rao, M. Jayasimhadri*
   Jouurnal of Alloys and Compounds, 697 (2017) 367-373, ***IF-4.175***

Other than thesis Work

1. Spectroscopic studies of Dy^{3+} doped borate glasses for cool white light generation.
   Sumandeep Kaur, *Amit kumar Vishwakarma, Nisha Deopa, Aman Prasad, M. Jayasimhadri, A.S. Rao*
   Mater Res. Bull., 104 (2018) 77-82.
2. Intense green emission from Tb^{3+} ions doped zinc lead alumino borate glasses for laser and w-LEDs applications.
   Sumandeep Kaur, *Nisha Deopa, Aman Prasad, Rajat Bajaj, A.S. Rao*
   Opt. Mater. 84 (2018) 318-323.

3. Spectral studies of Eu^{3+} doped lithium lead alumino borate glasses for visible photonic applications.
   *Nisha Deopa, **Sumandeep Kaur**, Aman Prasad, Bipin Joshi, A.S. Rao*
   Opt Laser Technol., 108 (2018) 434-440.
4. Spectroscopic investigations on Dy^{3+} ions doped zinc lead alumino borate glasses for photonic device applications.
   *Nisha Deopa, Shubham Saini, **Sumandeep Kaur**, Aman Prasad, A.S. Rao*
   J. Rare Earth 37 (2019) 52-59.
5. UV radiation emitting Gd^{3+} activated Sr_2SiO_4 host system prepared by sol–gel procedure: structural, electron paramagnetic resonance, and luminescence studies.
   *V. Singh, N. Singh, M. S. Pathak, **Sumandeep Kaur**, M Jayasimhadri, S Watanabe*
   J. Mater. Sci.: Mater. Electron. 29 (2018) 20759–20767.
6. UV emitting Pb^{2+} doped $SrZrO_3$ phosphors prepared by sol-gel procedure.
   *V. Singh, N. Singh, **Sumandeep Kaur**, M. Jayasimhadri, M. S. Pathak, S. Watanabe, T.K. Gundu*
   Ceram. Inter., 44 (2018) 17074-17078.
7. An Electron Paramagnetic Resonance and Photoluminescence Investigation of UVB Radiation Emitting Gadolinium-Activated $CaY_2Al_4SiO_{12}$ Garnet Compound.
   *V. Singh, **Sumandeep Kaur**, A.S. Rao, N. Singh, M. S. Pathak, J. L. Rao*
   J. Electron. Mater., 48 (2019) 4092-4098.
8. Spectroscopic properties of deep Red Emitting Tm^{3+} doped ZnPbWTe Glasses for Optoelectronic and Laser Applications.
   *Ritu Sharma, Aman Prasad, **Sumandeep Kaur**, Nisha Deopa, Rekha Rani, M. Venkateswarlu, A. S. Rao*
   J. Non-Cryst. Solids, 516 (2019) 82-88.

Abstract

Recently, the increasing requirement for energetically efficient, high resolution displays and lighting devices necessitate the development of such devices with enhanced brightness and good color purity. Solid state lighting (SSL) technology involves white Light Emitting Diodes (wLEDs) which are globally used for wide-spread applications in consumer electronics and general illumination. It offers many scientific and technological patronages such as environmental friendliness, lower operating temperature and effective energy utilization by saving 80% of energy consumption over conventional lighting devices. In the light of the aforementioned advantages, wLEDs are considered to be the next generation lighting technology. Generally, there are three different approaches which can be used for generating white light based on solid state lighting LEDs: (1) by mixing red, green, blue (RGB) LEDs, (2) by using an ultraviolet (UV) LED to stimulate RGB phosphors, and (3) by using a blue-emitting GaN LED chip that excites a yellow-emitting phosphor (YAG: Ce) embedded in an organic material; the combination of blue and yellow light makes a white-emitting LED (pc-wLEDs). However, pc-wLEDs made by means of blue-LED + YAG: Ce yellow phosphors suffer some weaknesses, such as poor color rendering index (CRI) and low stability of color temperature. Since the white light is generated by the combination of blue light emitted by an LED chip and yellow light emitted by YAG: Ce phosphors, deterioration of the chip or YAG: Ce phosphors would cause some significant color changes. The instability of color temperature also exists for RGB LEDs as the degradation of different color LEDs or variations of driving current which also complicate its fabrication. In tricolor (RGB) phosphors, the excitation is achieved by n-UV/UV LEDs. Moreover, in tricolor pc-wLED the efficiency of red phosphors is low in comparison with green and blue phosphors and the rate of degradation of tricolor phosphors is different. Therefore, it is necessary to develop single phase phosphor

with tunable emission containing white emission or new red phosphor such that luminous efficiency, CRI and correlated color temperature (CCT) can be improved.

Phosphors have been considered as key and technologically important components of the functionality and success of many lighting and display systems over the past several years. Versatile physical properties of the phosphors facilitate their usage in many areas, both scientific research and practical applications. Inorganic compound incorporated with the rare earth (RE) elements is the most prevalent protocol to synthesize brilliant luminescence phosphor in visible region. Among different inorganic oxides, zincates have been long studied because of its high chemical stability, high brightness, high melting point, and long persistence time without radioactive radiations. Moreover, zincate-based compounds in suitable composition could be potential candidates for white light emitting phosphors. When excited with LED emission in UV or n-UV region, these novel materials have the capability to convert the ultraviolet emission of a UV-LED into visible emission. Therefore, the work done for the thesis is based on novel ternary calcium aluminozincate ($Ca_3Al_4ZnO_{10}$,) as a host material for SSL application. By incorporating suitable RE ions, the present host can be tuned for different emissions in visible region of the electromagnetic spectrum for SSL applications. The present thesis embraces seven chapters to accomplish the research objectives. The brief summary of each chapter is as follows:

Chapter1 emphasize on the brief history and technological advancements of white light generation, their advantages, related issues. Spectroscopy of RE ions and theoretical models adopted for the analysis of observed spectral data, ionic interaction and energy transfer between RE ions. The Judd-Ofelt (J-O) theory that elucidates radiative transition probability (A_R), branching ratio (β) and radiative lifetime (τ_R). The emission spectral data enables to evaluate the CIE coordinates, color purity and correlated color temperature (CCT).

Chapter 2 describes the methods to prepare calcium aluminozincate ($Ca_3Al_4ZnO_{10}$: CAZ) phosphors activated with different RE ions (Eu^{3+}, Sm^{3+}, and Dy^{3+}) with varying concentrations. It also explains the experimental tools/equipment's used to analyse structural, morphological and optical properties of the CAZ phosphors. The thermal, structural and vibrational properties determined from thermal gravimetric analysis (TGA), X-ray Diffractometer, Fourier transform infrared (FT-IR) spectroscopy, Diffuse reflectance absorbance (DRA) have also been discussed. The morphology of the as-prepared phosphors investigated from scanning electron microscopy and the photoluminescence properties of the CAZ phosphors doped with different RE ions were also discussed in this chapter.

Chapter 3 explains single phase CAZ phosphor doped with Sm^{3+} ions with varying concentrations prepared at 1300˚C by conventional solid-state reaction (SSR) method. The crystal structure and phase analysis of the as-prepared phosphor has been carried out by XRD studies. Morphology and functional groups present in the phosphor have been investigated thoroughly by using SEM and FT-IR spectral measurements respectively. Under 401nm excitation, the as-prepared phosphor exhibits intense visible orange emission at 601nm. The Sm^{3+} ions concentration is optimized to 1.0 mol% to achieve intense visible orange emission. The PL analysis reveals that the dipole-dipole interaction is primarily responsible for the concentration quenching observed beyond 1.0 mol% of Sm^{3+} ions. The PL decay study reveals bi-exponential behaviour of decay curves with an average lifetime of the order of microseconds. The CIE coordinates (x= 0.574 and y= 0.424) measured for the optimized phosphor are very close to the intense orange emission coordinates specified by Nichia Corporation developed Amber LED NSPAR 70BS (0.57, 0.42). The Spectroscopic, PL and PL decay studies suggest the potential use of Sm^{3+} doped CAZ phosphors for display and white light emitting devices.

Chapter 4 describes about the Eu^{3+} ions doped CAZ phosphors without flux and blended with various fluxes (NaF, NaCl and $Na_2B_4O_7$) synthesized by using conventional SSR method and characterized by employing XRD, SEM, DRA and Spectrofluorophotometer to study the structural, morphological and PL properties. The Judd-Ofelt (J-O) analysis has been carried out to get insights of optical properties. All the XRD peaks are matching well with the standard ICDD card confirms that all the prepared phosphors consist of single phase with orthorhombic structure. The band gap has been calculated from DRA spectra. The PL spectra recorded under near-UV/blue excitations demonstrate a very distinct and intense red emission from all the phosphors. The intensity of emission in these phosphors increases up to 2.0 mol% of Eu^{3+} ions concentration and beyond concentration quenching is observed. The PL studies exhibit significant enhancement in the red emission for Eu^{3+} doped CAZ phosphor with the incorporation of $Na_2B_4O_7$. The emission intensity has been found to increase approximately 1.5 times using NaCl and 2.5 times for $Na_2B_4O_7$ in Eu^{3+} doped CAZ phosphor as compared to the phosphor without any flux. The energy transfer mechanism has also been studied in detail. The CIE chromaticity coordinates measured from the PL spectra of the prepared samples lies in the red region of the visible spectrum. From the measured PL and CIE chromaticity co-ordinates, it was found that Eu^{3+} doped CAZ phosphors with optimized concentration of Eu^{3+} ions as 2.0 mol% and optimized flux ($Na_2B_4O_7$) could be used as red phosphor in the development of white LEDs.

Chapter 5 described about the Eu^{3+} doped CAZ phosphors synthesized via solid-state reaction (SSR), combustion (CS) and Pechini sol-gel (SG) methods for better luminescent properties and optimization of the synthesis method. The XRD, SEM, PL and PL decay curve measurements have been recorded for the detailed investigation of the luminescence properties of the as-synthesized phosphor. The XRD peaks indicate the complete matching of the diffraction peaks of the as-synthesized sample with the standard data for $Ca_3Al_4ZnO_{10}$. The

morphology of the sample synthesized via SG method shows homogeneous distribution of agglomerated particles with smaller particle size than those obtained from CS and SSR methods. The detail investigation shows significant red emission enhancement in Eu^{3+} doped CAZ phosphors synthesized via SG method. The obtained results suggest that the Eu^{3+} doped CAZ phosphor synthesized via SG method could be a great choice as red emitter for SSL applications.

Chapter 6 describes the preparation and characterization of a series of Dy^{3+} doped and Dy^{3+}/Eu^{3+} co-doped CAZ phosphors using Pechini sol-gel method. The crystal structure was analysed by recording XRD patterns and further it was confirmed from Rietveld refinement using Fullprof suite software. The morphology of the as-prepared phosphors was studied by recording SEM images. The PL properties were analysed from excitation and emission spectra. The colorimetric properties were studied by evaluating CIE coordinates and CCT. The decay curves were recorded, and energy transfer mechanism was analysed using I-H model, Dexter theory and Reisfeld's approximation. The obtained results indicate that the white light from warm to neutral to cool emission can be achieved and color tunability can also be achieved in Dy^{3+}/Eu^{3+} co-activated CAZ phosphor by varying the excitation or activator concentration in the host lattice.

Chapter 7 summarizes the results obtained from the content presented in chapters 3 to 6. The futuristic scope of the thesis work has also been elaborated with respect to the expected applications of these phosphors in versatile fields.

CONTENTS

LIST OF TABLES

LIST OF FIGURES

Chapter-1

General Introduction

Lighting technology is progressing in wide field of applications including flat panel displays and solid-state lighting owing to their high luminescence efficiency, less energy loss and cost effectiveness. The luminescent materials comprise of phosphors received attention for research in lighting technology. This chapter give prominence to the basics of luminescence, its mechanism, rare earth (RE) elements, and methods of generating white light. This chapter also embraces brief description of some theories given by Dexter and Judd- Ofelt. Further this chapter is comprising of importance of the host $Ca_3Al_4ZnO_{10}$ and objectives of the presented work.

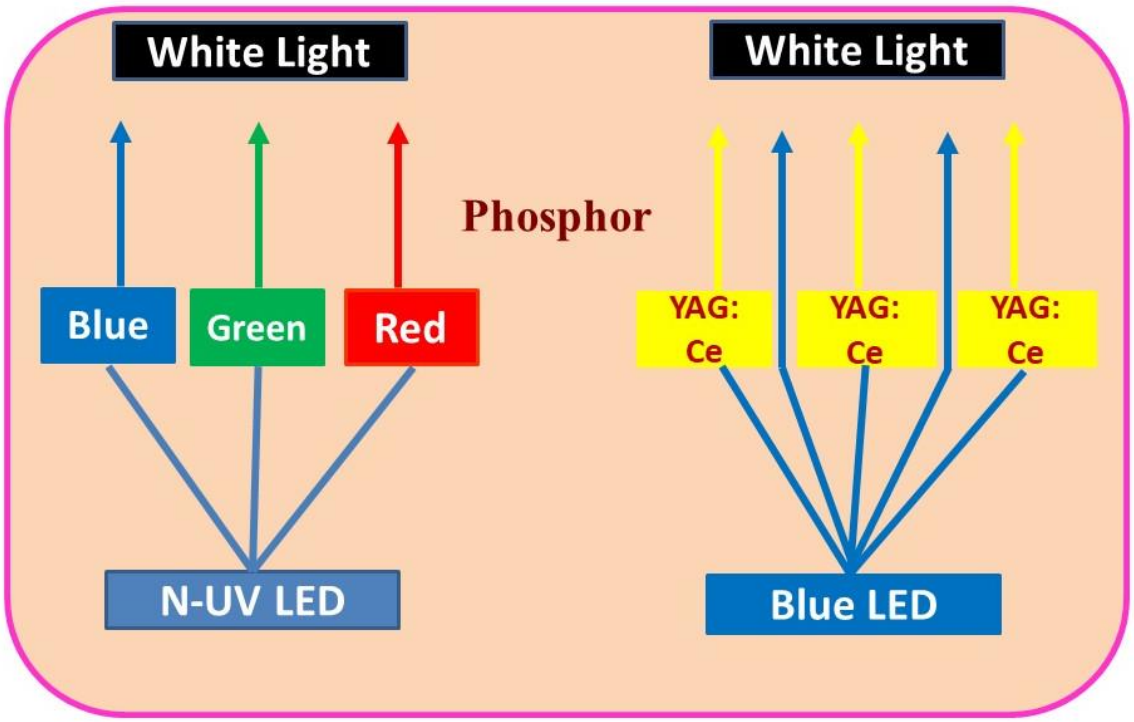

1.1. Luminescence:

Light is a form of energy that give sensation of vision. Naturally, light is abundantly available from the Sun that can be captured and transformed into electricity. But all the new technologies simply cannot rely on natural source of light (sunlight), which necessitates the need of generating light artificially. There are broadly two phenomena that emanates light artificially namely, incandescence and luminescence. Luminescence is a process of emitting electromagnetic radiation (preferably in the visible region) which takes place after being exposed to X-ray, ultraviolet (UV), infrared (IR) radiations without heating the material. Incandescence is a phenomenon in which the material is heated to such a high temperature that the atoms vibrate and emit light. Therefore, incandescence is known as hot process and luminescence is termed as a cold process in comparison with incandescence [1,2]. The emission in case of incandescence bulbs is due to heating of the filament, which in turn causes a enormous energy loss in the form of heat [3]. Moreover, the life span of these incandescent bulbs is approximately 1000 h which is short in comparison with compact fluorescent lamps (6,000-15,000 h) and very short when compared with that of light emitting diodes (50,000 h) [4].

Figure 1.1. Examples of Incandescence (a) Fire, (b) Hot iron and (c) Bulb.

Figure 1.2. Examples of Luminescence (a) CFL and (b) LED screen.

Since the luminescence phenomenon is a cold process, the materials undergo luminescence offer better efficiency. The emission process involved in luminescence stimulates either internally or externally. Fig. 1.1 & 1.2 show examples of incandescence and luminescence, respectively. The various luminescence processes can be defined on the basis of source used to excite the matter as enumerated below:

I. ***Photoluminescence (PL):*** In this process, the electrons get excited by absorbing photons and relaxing to the ground state emanates the energy loss to visible emission. PL is further classified into fluorescence and phosphorescence.

i. *Fluorescence:* In this process, electrons from ground state get excited to upper vibrational level of excited energy state by absorbing photons of sufficient energy and come back to the lowest energy state. By removing excitation source, the emission process ceased.

ii. *Phosphorescence:* In this process, electrons after absorbing excitation energy reach excited state having different spin, after absorption of photons and returned to the ground state. After the removal of the excitation source, the emission process continues for a long time in comparison with emission from singlet state. This process is also known as afterglow [5,6].

II. ***Cathodoluminescence:*** In this process, the energetic electrons or cathode rays bombard and excite the electrons which emits light while returning to the ground state. Cathodoluminescence is observed in cathode ray tubes (CRT), display monitors and TV sets.

III. ***Electroluminescence (EL):*** In this process, photons generation take place when excess electron hole pairs gets created by passing electric field or current through the substance [7,8].

IV. ***Radioluminescence (RL):*** When ionising radiations such as X-rays, γ-rays, β-rays or cosmic rays interact with some polymer/organic molecules, visible light emits, thereby showing luminescence.

V. ***Sonoluminescence (SL):*** In this process light is produced by sound waves (in general, ultrasonic waves).

VI. ***Chemiluminescence (CL):*** It is the emission of light that occur during chemical reaction between reactants, where the intermediate product goes to excited state and emits light while coming back to the ground state. The oxidation and reduction type of chemical reaction leads to such kind of luminescence and other biological systems in which decay of organic material takes place with visible emission [9].

VII. ***Bioluminescence (BL):*** It is a special type of CL in which reaction occurs in living organisms through biological process.

VIII. ***Mechanoluminescence (ML):*** The emission of light occurs when some external mechanical energy applied on solid substances to cut, grind, rub, or compress the material or deformed solids through some impulse reaction.

   i. *Triboluminescence:* When bonds between some atoms or ions are broken due to scratching, rubbing or crushing, the material emits light.

ii. *Fractoluminescence:* When fractures in a crystal break the bond and generate luminescence, it is termed as fractoluminescencce.

iii. *Piezoluminescence:* By applying pressure on certain materials luminescence can be produced and is known as piezoluminescence.

IX. Thermoluminescence (TL): TL is basically thermally stimulated luminescence in which the luminescent material initially gets irradiated by UV rays, γ-rays, β-rays or X-rays. The absorbed radiations in the material create defects, that after thermal stimulation radiate energy in visible region [10,11].

1.2. Important definitions:

I. Absorption: The energy of incident photon is taken up by the electrons of an atom. A light beam gets attenuated after passing through a material due to absorption of light by the material.

II. Excitation: The absorbed energy of incident radiation add to the energy of electron that leads to excitation from lowest state to certain upper excited state. Therefore, excitation can also be called as elevation in energy level.

III. Emission: It is a spontaneous process of electron transition from higher to lower energy level that results in emission of photon having energy equals the difference in the energies of the two states involved in the process. This process is also called as luminescence [6].

IV. Activators: When small amount of impurities doped in the main composition of the host, it will create defects or traps in the host lattice and are responsible for luminescence. Such impurities are referred as activators/dopants [12].

V. Sensitizers: When some another impurity is being added to the main composition, then such impurities absorbs the incident energy and transfer it to activators by sensitizing it

and are referred as sensitizers. Sensitizers are used along with the activator in the main host composition if the optical absorption of the activator is weak [12].

VI. ***Energy levels:*** Lattice defects, impurities and other perturbations creates discrete energy levels in the forbidden region of the host material. These energy levels are liable for luminescence [13].

VII. ***Trap centres:*** The centres get created in the host lattice when irradiated with β, γ-radiations or some defects created with the addition of impurities give rise to trap centres. These traps are responsible for phosphorescence and thermoluminescence.

VIII. ***Fluxes:*** These are inorganic salts with very low melting point as compared with the precursors taken up for the synthesis of desired material and helps in the early fusion of the chemical precursors to synthesize the material. In general, fluxes include alkali or alkali earth metal halides, borates and sulphides [14].

IX. ***Host:*** Inorganic or organic compounds in which imperfection or defects get created with the addition of some impurities as activators are treated as host. In general, these materials are colourless, or light coloured with high melting point, high solubility of impurities such as rare earths (REs) or transition metals. Inorganic oxides such as silicates, borates, molybdates, aluminates, zincates, etc [15].

X. ***Killers/Quenching centres:*** When the excitation energy migrates among large number of centers and then these centers exude their energy by relaxing to the ground state by multiphonon emission or by IR emission. These are the centres from where the probability of radiative transition is low. These quenching centres serves as an energy sink for the energy migration chain that leads to the quenching of luminescence [6].

XI. ***Energy Transfer (ET):*** When excitation energy is being absorbed by the host or sensitizer, the energy is being transferred to the activator radiatively or non-radiatively. The ET helps in achieving color tunability in phosphors [16].

XII. ***Relaxation:*** The process of energy loss to the lattice in either radiative or non-radiative manner is known as relaxation process. The efficiency of the emission depends on the relaxation process and heat loss should be minimized to get maximum luminescence efficiency [17,18].

1.3. Phosphor and luminescence process:

The materials that exhibit the phenomenon of luminescence is known as "luminescent materials" or "phosphors". The mantle of phosphors is to convert incident radiation energy into visible or IR region. The word "phosphor" means the "light bearer". In general, the phosphors are the solid crystalline inorganic materials doped with small quantity of impurities composed (i.e., host lattice and activator, respectively). These activators (lanthanide ions or transition metal ions) serve as luminescence centre which implies that the luminescence occurs at the sites of activators. The absorption of radiation is basically done either by these activators or the host lattices [19]. The host lattices have potential to absorb the excitation energy of a particular frequency from different sources. This is known as host excitation. After the excitation of the host lattice, it releases its energy via the following routes:

i. The host lattice itself can release energy and give visible emission. This process is known as characteristic/pure/host sensitized luminescence as shown in Fig. 1.3 (a). Such kind of phosphors are known as host luminophores, for example vanadate and tungstate.
ii. The host lattice can give off the absorbed energy non-radiatively and produce heat as represented in Fig. 1.3 (b).
iii. The host lattice can migrate the energy to the activator ion. In this case, host lattice/sensitizer sensitizes the activator by transferring energy to the activator. The activator after being excited to upper level releases its energy and get back to the ground state by emanating visible emission. If the activator radiates non-radiatively then the

activator is said to be killer, since it quenches the luminescence. This type of luminescence is known as non-characteristic or impure luminescence. Impure luminescence is further classified into two categories: (a) host + activator type, in which host absorbs the incident energy and excite the activator as represented in Fig. 1.3 (c). (b) Host + sensitizer + activator type, in which sensitizer after absorbing incident energy transfer it to the activator and hence emission from activator is observed as represented in Fig. 1.3 (d) [20].

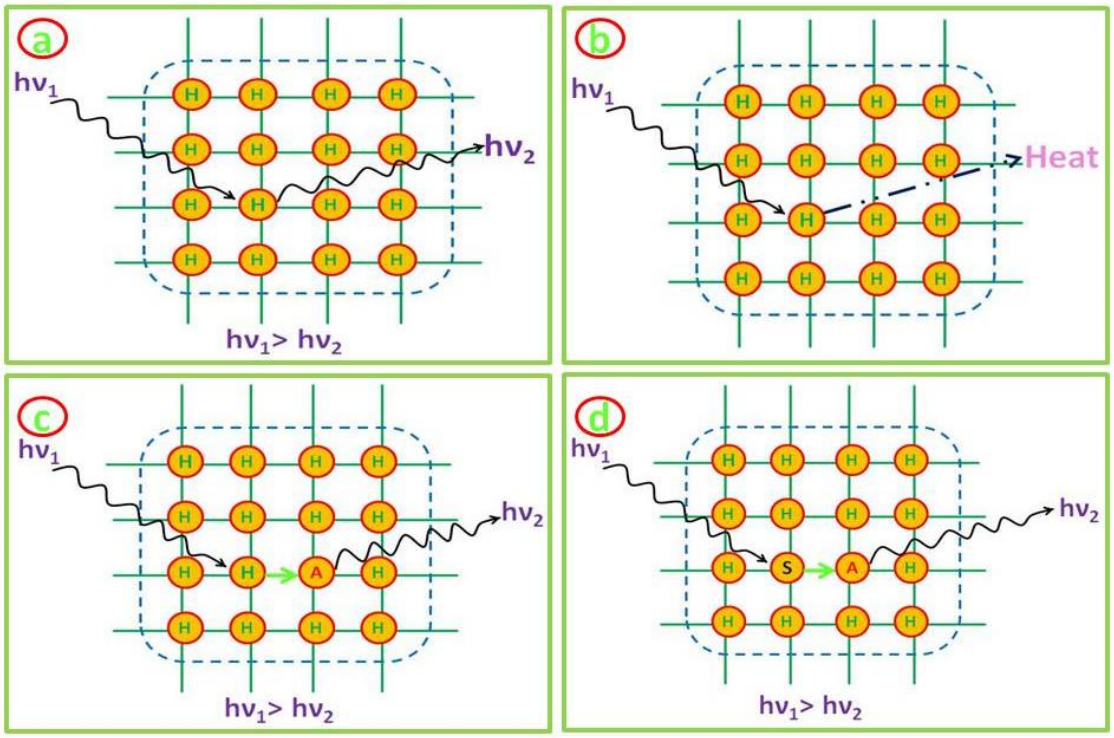

Figure 1.3. Absorption of incident energy, energy transfer, and emission (a) Host sensitized luminescence, (b) Non-radiative relaxation, (c) Host + Activator type luminescence and (d) Host + Sensitizer + Activator type luminescence.

If the excitation energy gets directly absorbed by the activator ion followed by the radiative or non-radiative emission. This is known as direct excitation process [2,19,21]. When a high energy photon is being absorbed and low energy photon emits, the process is known as stokes (wavelength shows red shift/shift toward lower energy) emission or down-conversion. On the other hand, if low energy photons (two or more) are being absorbed and high energy photon

gets emitted, then the process is known as anti-stokes (wavelength shifts to lower value/blue shift/shift toward higher energy) emission or up-conversion process. These processes are represented in Fig. 1.4 (a & b), respectively [2,22].

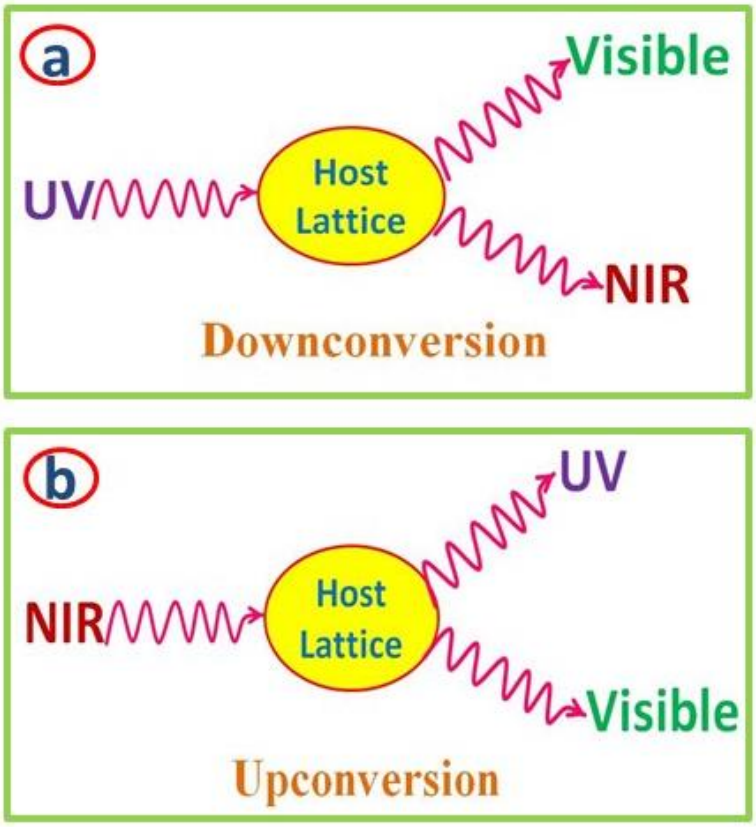

Figure 1.4. (a) Down-conversion and (b) Up-conversion process.

1.4. Rare Earth (RE)/Lanthanides:

RE are the elements of the lanthanide series starting from Lanthanum (La) up to Lutetium (Lu) along with Scandium (Sc) and Yttrium (Y). The RE elements are relatively obtained in abundance [23]. The RE are disseminated and not available as dense minerals in economically exploitable ore deposits, that's why the name Rare Earths. Scandium and Yttrium are also included in the list of RE due to their occurrence in the same ore and show similar properties as lanthanides. Although these elements evince similar chemical behaviour, yet their physical characteristics are unique such as color, luminescence behaviour, and nuclear magnetic properties. The electronic configuration of REs is $[Xe]4f^n$ (n=0-14). These configurations can

give various electronic levels specified by three quantum number L, S, and J values as a result of spin-orbit coupling. These levels are well defined, and their energy is fixed since 4f electrons remain unaffected by the external electronic field due to $5s^2$ and $5p^6$ electrons serve as protective shielding to 4f electrons and also these levels are independent of environment [24–26]. Some of the RE ions shows $4f^{n-1}5d$ state in which electron transfer takes place from 4f to 5d orbital and charge transfer state in which electron in the neighbouring anion transferred to 4f orbital. The $4f^{n-1}5d$ and charge transfer state gets affected by the local environment around these RE ions [27,28]. Therefore, RE ions show +3 oxidation state in general and some RE ions also show +2 oxidation state. Moreover, these RE ions exhibit large stokes shift which is a prerequisite for designing a phosphor. In RE doped solids, photoluminescence is observed due to the presence of partially filled 4f subshell and are either due to intra-configurational $4f^n$ transitions or inter-configurational $4f^n$-$4f^{n-1}5d^1$ transitions or charge transfer transitions [29,30]. The RE ions incorporated into the host, beget energy levels within the optical band gap of host. Some of the unique properties of RE ions that discriminate between REs and other optically active ions are as follows:

- RE ions exhibit luminescence in various spectral regions such as visible and NIR regions of the electromagnetic spectrum.
- RE ions exhibit narrow spectral lines and have relatively long emission lifetimes.
- They exhibit large stoke shift upon ligand excitation (gap between excitation and emission wavelength is large).
- Their $4f^n$ transitions exhibit small homogeneous linewidths.
- They possess several energy levels suitable for optical pumping
- To systematically analyse energy levels, transition intensities, excited state dynamics, theoretical models are available.

The abovementioned beguiling properties of these divalent and trivalent RE ions facilitate their utility in myriad of applications in display and solid-state lighting [24,31–34].

1.5. Radiative and non-radiative transitions:

In luminescence, the host or sensitizer sensitizes the activator and transfers the energy to the activator. These activators take the energy, reaches the excited state and make radiative or non-radiative transition from the higher excited states to lower states.

I. ***Radiative transition:*** When an electron absorbs the excitation energy, it attains the highest vibrational level of the excited state, from where it relaxes to the lowest vibrational level releasing excess energy to the lattice. Then the radiative emission is observed from this vibrational level. Fig. 1.5 represents configurational coordinate diagram for radiative and non-radiative transitions. The phenomenon of luminescence is observable when the emission from a luminescent centre is radiative in nature.

II. ***Non-radiative transition:*** In general, luminescence is accompanied by some non-radiative transitions. Non-radiative transition can take place through any of the below mentioned channels:

(i) If the rotational level of excited state crosses the level of ground state, the nature of relaxation from excited to ground state will be non-radiative. The excess energy is lost to the host as heat.

(ii) If the frequency is same, then the parabolas will be parallel. If the excitation is much higher than the stokes shift, then from higher vibrational level, the excess energy is lost for radiation of phonons. This process is known as multiphonon relaxation [26].

(iii) In some cases, resonant energy transfer take place between two indistinguishable adjoining centers and electron may attain an intermediate level by giving off the excess energy to another nearby electron which after

absorbing the energy rises to the same intermediate or some other level having the same energy difference. This process is known as cross-relaxation [5,17].

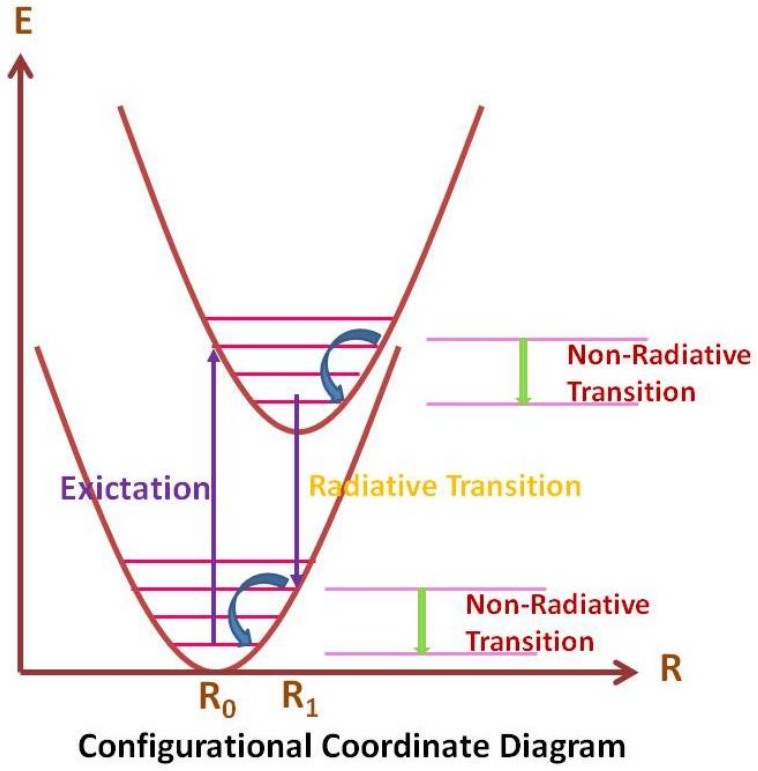

Figure 1.5. Configurational coordinate representation for radiative and non-radiative transitions.

1.6. Types of interaction: Broadly the interaction between different level is classified on the basis of transition between f-f levels and $4f^{n-1}5d^1$-$4f^n5d^0$.

I. ***Intra-configurational f-f interaction.*** The RE ions doped materials shows various narrow lines attributed to the electronic transitions between $^{2S+1}L_J$ to free ion level or J-manifolds in 4f subshell. They are spin forbidden. In f-f transitions, excitation and emission energies remain independent of the host into which the activator is substituted as they are effectively shielded from 5s and 5p electrons. That's why these spectra exhibit narrow line width. The interaction of the RE ions in the host with the light give rise to different types of transitions as mentioned below:

i. Magnetic dipole (MD) transition: When the magnetic field facet of the incident light interacts with the RE ion through a magnetic dipole, a weakly intense

transition is observed and termed as magnetic dipole (MD) transition. When the charges get displaced rotationally and direction of rotation remains same under inversion through a point, MD transition occurs. The MD transition has even transformation under inversion and it exhibits even parity which means it allows transition between states having same parity. Therefore, a MD transition is endorsed by the Laporte selection rule ($|\Delta l|=\pm1$, $|\Delta s|=0$, $|\Delta L|\leq0$, $|\Delta J|=0, \pm1$; $J=0\leftrightarrow0$ transition is forbidden) [35,36].

ii. *Forced electric dipole (ED) transition*: An ED transition takes place when the RE ion interacts with the electric field facet of the incident electromagnetic radiation through an electric dipole. The electric dipole results in linear movement of charges. The ED transition has odd transformation properties under inversion and has odd parity. This transition is forbidden in RE doped materials, since the start and end states of $4f^n$ transition have the same parity (absence of states with different parity). Hence, these ED transitions are restricted by the Laporte selection rule ($|\Delta l|=\pm1$, $|\Delta s|=0$, $|\Delta L|\leq6$, $|\Delta J|\leq6$). However, the non-centro symmetrical interactions of electronic states allow the mixing of states of opposite parity that induces the ED transition and therefore known as induced ED transition. Some of the induced ED transitions are sensitive to the surrounding environment of RE ions and therefore also known as hypersensitive transition that follow the selection rules ($|\Delta S|=0$, $|\Delta L \leq6$, $|\Delta J|\leq6$). These hypersensitive transitions are also termed as pseudo quadrupole transitions as they obey same selection rules as followed by quadrupole transitions [37]. These hypersensitive transitions originate from an asymmetrical distribution of dipoles induced by the electromagnetic radiation in the surrounding of the RE ions. The intensity of these

transitions gets enticed by the local field symmetry and inhomogeneity in the dielectric medium around RE ion.

iii. *Induced electric quadrupole transition:* The electric quadrupole transition becomes apparent with displacement of quadrupole charges. An electric quadrupole is composed of four-point charges or two dipoles arranged in such a way that their net dipole moments is zero. An electric quadrupole has even parity. Electric quadrupole transitions are frail in correlation with MD and induced ED transitions [38].

II. ***Inter-configurational ($4f^n5d^0$-$4f^{n-1}5d^1$) interaction:*** The transfer of 4f electrons in to 5d subshell is parity allowed. Since d orbitals get greatly swayed by the ligand field effect, the intensity of such transitions are highly susceptible to the surrounding of RE ions and their energy is high [33]. The transitions between $4f^{n-1}5d^1$ and $4f^n5d^0$ levels give rise to a broad range of excitation and emission wavelengths compared with the very narrow peaks from transitions between 4f-4f levels. The broad range of f-d transitions can be described on the basis of two phenomena: the Franck-Condon principle and breaking of the degeneracy of the 4f ground state. According to the Franck-Condon principle, there are different vibrational states in two rotational states, that results in transitions with many different energies. The wide range of transition energies results in inhomogeneous broadening in solids. Furthermore, the 4f degeneracy breaks due to spin-orbit coupling into multiple levels. Moreover, activator ion in a host crystal may undergo centroid shift and/or crystal field splitting. The centroid shift is defined as shift in 5d energy levels to lower side due to decrease in the interelectronic repulsion. The crystal field splitting, as the name suggests, is the splitting of 5d energy levels due to the environment provided by the host to the activator ion in which it is doped. The factor on which the magnitude of crystal field effect depends include bond length between activator ion and the ligand,

the overlapping of molecular orbital or nature of bond (ionic or covalent), the surrounding environment, and the site symmetry of the activator ion. The crystal field splitting reciprocate to the change in bond length, or polyhedral volume in opposite manner [39].

1.7. Solid state lighting (SSL):

Artificial light provides substantial contribution in expanding the prolific day into non-sunlit hours of the evening and night and in daytime productivity enlarge as it reaches the places where sunlight is not prevailing. Globally, artificial lighting production includes immense amounts of energy. Earlier, the conventional lighting devices such as incandescent lamps and CFLs were used for artificial lighting which rely either on heat or discharge of gases. These lighting devices involve high temperature that leads to large energy losses. Moreover, these devices release toxic substances and more CO_2 is released into the environment [40]. Over the last few decades, the immense global awareness of energy saving has aroused the revolutionary growth and development of lighting technology and transit from the incandescent and fluorescent lamps towards SSL based on LEDs [41]. White LEDs (wLEDs) have brought significant thrust in the development of lighting technology for general illumination, automotive lighting applications, and sensors. SSL based on wLEDs replacing conventional light sources such as incandescent and fluorescent lamps owing to their supercilious characteristics such as higher luminous efficiency, low energy consumption, eco-friendly as it does not release any toxic compound in the environment, greater reliability, optically tunable and more durable as compared to conventional lighting devices [42,43]. The wLEDS using InGaN or GaN chips are broadly classified into two categories: (i) multichip (mc) wLEDs, and (ii) phosphor converted (pc) wLEDs. The mc-wLEDs comprises of individual red, green, and blue (RGB) LEDs and their emission covers the visible spectrum and thus the white light is generated [41,43,44]. These mc-wLEDs offer good luminous

efficiency and color rendering index (CRI) but driving circuit used to produce white light is complex that leads to high cost of LEDs and complex fabrication [45]. Also, different driving currents leads degradation of different color LEDs and results in instability of color temperature. Moreover, the pc-wLEDs are rather more efficient than mc-wLEDs, since it comprises of yellow phosphor (YAG: Ce^{3+}) or red, green, blue (RGB) phosphors embedded in epoxy dome, coated over the surface of blue GaN (450 nm) or ultraviolet (UV) InGaN LED chip, respectively. These pc-wLEDs uses blue or n-UV LED chips to excite the phosphor and thus generate white light. In blue LED and yellow phosphor based wLEDs, the change in emission color occurs due to the deterioration of blue LED chip or yellow phosphor [46,47]. Since the blue + yellow combination is depriving of red component and due to halo effect, the CRI is low and the correlated color temperature (CCT) is high in these pc-wLEDs [48,49]. In case of UV/near-UV (n-UV) LED + RGB phosphor-based pc-wLEDs, high luminous efficiency in comparison with blue chip along with high CRI and high chromatic stability can be achieved. However, this approach of generating white light have some pitfalls, such as complex blending of tri color phosphors and different degradation of each phosphor. In RGB phosphors, the blue light emitted is being reabsorbed by green and red light which further reduce the efficiency of these pc-wLEDs [50]. The pc-wLEDs are extensively used in lighting devices on the grounds of their simple structure, high durability, excellent luminous efficiency, cost effectiveness and their spectral design flexibility. Table 1.1 presents the pros and cons of different methods to generate white light.

Table 1.1. Pros and cons in different methods for white light generation.

	RGB LEDs	**Binary Complimentary**	**UV-LED + RGB Phosphor**
Advantages	• Light source with variable color point. • High efficiency.	• Low cost. • Easy fabrication.	• High efficiency. • High CRI • High chromatic stability.

Disadvantages	• Need variable driving current to operate red, green and blue LEDs. • Instability of color temperature.	• Low efficiency. • Low CRI. • Low chromatic stability. • Lack of efficient red component.	• Complex blending of different phosphors.

1.8. Color rendering index:

It is a unitless index, abbreviated as CRI or R_a, measured as the difference in perceiving the color of object under source illumination and a reference source such as natural light source/sunlight. CRI can be indexed as integral value from 0 to 100. The low CRI ratings suggested that less accurate color will be reproduced. The CRI value of 100 would signify that the perceived color of all the samples illuminated by a light sources and incandescent light source have high CRI since all colors in their spectrum are rendered equally [2,39,51].

1.9. CIE color chromaticity coordinates & color purity:

To characterize or express the color, the Commission Internationale de l'Eclairage (CIE) is used to describe the color of any object in terms of three primary color. The CIE chromaticity coordinates determined from emission spectra using color matching function $\bar{x}(\lambda)$, $\bar{y}(\lambda)$ and $\bar{z}(\lambda)$ defined in CIE 1931 and spectral power density $P(\lambda)$ of the light source. The chromaticity coordinates can be obtained using tri-stimulus values X, Y and Z, as [2,52]:

$$x = \frac{X}{X+Y+Z} \quad (1)$$

$$y = \frac{Y}{X+Y+Z} \quad (2)$$

where, degree of stimulation (tri-stimulus values: X, Y, and Z) required to match the color of $P(\lambda)$ is given by the following equations:

$$X = \int \bar{x}(\lambda)P(\lambda)d\lambda \quad (3)$$

$$Y = \int \bar{y}(\lambda)\mathrm{P}(\lambda)\mathrm{d}\lambda \quad (4)$$

$$Z = \int \bar{z}(\lambda)\mathrm{P}(\lambda)\mathrm{d}\lambda \quad (5)$$

The value of CIE coordinates along the perimeter of the CIE diagram signifies the monochromaticity. Therefore to ascertain monochromaticity of the material under consideration using as obtained CIE coordinates, the color purity can be evaluated by using the expression as follows [43]:

$$color\ purity = \frac{\sqrt{(x-x_{ee})^2+(y-y_{ee})^2}}{\sqrt{(x_d-x_{ee})^2+(y_d-y_{ee})^2}} \quad (6)$$

where (x, y) are the coordinates of the sample under consideration, (x_{ee}, y_{ee}) are the coordinates of white point, and (x_d, y_d) are the coordinates of dominant wavelength point. The color purity of the monochromatic emitters should be 100%.

1.10. Correlated color temperature (CCT):

It is defined as the absolute temperature of a blackbody whose chromaticity resembles the same color as that of the light source [51]. As the temperature increases, hot objects will subsequently glow in red, orange, and yellowish white and bluish white. CCT is a method that manifest the color characteristics of light, such as low CCT indicate warm light with more of yellow and red perception while high CCT appears to be a more blue light indicates cold white light, by measuring it in degrees Kelvin (K) [39]. Typical CCT of the white region diagram is in the range between 2000 and 10000 K. The CCT can be calculated by using the equation given by McCamy [53]:

$$CCT = -437\left[\frac{x-x_e}{y-y_e}\right]^3 + 3601\left[\frac{x-x_e}{y-y_e}\right]^2 - 6861\left[\frac{x-x_e}{y-y_e}\right] + 5514.31 \quad (7)$$

Here, (x, y) are the CIE coordinates obtained for the sample under consideration and (x_e=0.3320, y_e=0.1858) are the coordinates for epicentre.

1.11. Excited state dynamics of RE ions:

The PL decay is a non-linear optical process described by non-linear polarization of the incident light beam. Nonlinear emission responses of luminescent materials manifest excited-states dynamics such as radiative and non-radiative relaxation, inter system crossing of a molecule from singlet to triplet state, conformational properties such as trans-cis isomerisms and energy transfer mechanism of samples under investigation. The intensity in PL decay spectroscopy is monitored at different time delays after excitation, allowing for high temporal resolution. Temporal resolution should be fast in comparison with the excited-state lifetime of the RE ions on the appropriate time scale. The fluorescence decay time evaluated from decay profiles provides valuable information about the excited state decay dynamics of RE ions, charge and energy transfer, molecular interaction with the surroundings, and optical gain of the samples for advancement in optoelectronics, photosynthetic systems, nanoelectronics and biological applications [9]. Fluorescence lifetime depend on the rate of radiative and non-radiative relaxations. The lifetime value decreases with increase in non-radiative relaxation rates due to increased surface defects or quenching centres. The lifetime depends on:

(i) Non-solid surrounding medium

(ii) Size of the particles

(iii) Lattice constant that varies the odd crystal field component.

1.12. Energy transfer mechanism:

Energy transfer between two neighbouring ions take place only if resonance occurs in their ground and excited states energy difference and if suitable interaction exists between the two. The two neighbouring ions can interact viz exchange interaction or multipolar interaction [54]. To identify the type of multipolar interaction, Dexter theory and Reisfeld's

approximation can be employed on emission spectra or Inokuti-Hirayama (I-H) model on PL decay curves.

I. ***Dexter theory and Reisfeld's approximation:*** In the process of identifying the type of multipolar interaction, the luminescence quantum efficiency can be related to the concentration of RE ions according to Dexter's as follows [55]:

$$\frac{\eta_0}{\eta} \propto C^{n}/_{3} \qquad (8)$$

where η_0 and η represents luminescence quantum efficiencies of donor ions in the absence and presence of acceptor ions, respectively, the value of C depicts the total concentration (in mole% of donor and activator ions), and the value of n represents the type of interaction. The n = 3, 6, 8 and 10 corresponds to exchange interaction, dipole-dipole (d-d), dipole-quadrupole (d-q) and quadrupole-quadrupole (q-q) interaction, respectively. The ratio of quantum efficiencies of donor in absence and in presence of acceptor can be approximated with their respective emission intensities. Therefore, the above relation can be re-written as [21,56]:

$$\frac{I_{s0}}{I_s} \propto C^{n}/_{3} \qquad (9)$$

where I_{s0} and I_s are the integrating emission intensities of hypersensitive transition of RE ions in the absence & presence of co-dopant ions, respectively. A plot between I_{s0}/I_s versus $C^{n/3}$ for n = 6, 8 and 10. By analysing the linear fitting factor R^2 for the plot obtained as mentioned above, the energy transfer mechanism can be studied. The high value of R^2 obtained for the corresponding 'n' value suggests the type of interaction between the sensitizer and activator.

II. ***Inokuti-Hirayama (I-H) model:*** According to I-H theory, the luminescent intensity can be expressed as [57,58]:

$$I_t = I_0 * \exp(-\frac{t}{t_0} - Q * (\frac{t}{t_0})^{3/s}) \quad (10)$$

here, I_t denotes the luminescent intensity at time t after excitation, t_0 is the lifetime of the donor in the absence of acceptor, s represents index of multipole interaction (6, 8 and 10 for d-d, d-q and q-q interaction between sensitizer and activator ions, respectively, and Q is fitting parameter [21].

1.13. Judd-Ofelt (J-O) parameters using emission spectra:

The J-O theory can be pertained to the emission spectra of RE ions in any host lattice that emerge from the transitions within $4f^n$ configuration to ascertain its optical properties and to have a deeper insight into the quantitative analysis of Eu^{3+} emissive properties in matrix [59]. The evaluated parameters (Ω_λ) allows the researcher to elucidate the local structure and bonding of RE ions with the ligands. Henceforth, the J-O analysis of the emission expound radiative transition rates of different levels of the RE ions and luminescence branching ratios (β_R) can also be determined [60,61].

MD transitions of RE ions are practically independent of its surroundings. The radiative transition rate for such transitions are evaluated using the equation [62]:

$$A_{0-1} = \frac{64\pi^4 \nu_1^3}{3h(2J+1)} S_{MD} n^3 \quad (11)$$

where, ν is the average transition energy (in cm^{-1}) of $^5D_0 \rightarrow {}^7F_1$ transition, h is the Planck's constant, n is the medium refractive index, S_{MD} is the MD line strength which is not affect by the structure of host lattice and therefore is a constant (7.83×10^{-42} esu^2cm^2) [63,64]. The other characteristic transitions of Eu^{3+} ions for J = 2, 4, and 6 are induced electric dipole transitions. The radiative transition rate for forced ED transition can be written as [65]:

$$A_{0-J\,(J=2,4,6)} = \frac{64\pi^4 \nu_j^3 e^2}{3h(2J+1)} \frac{n(n^2+2)^2}{9} \sum_{J=2,4,6} \Omega_J \langle 5D_0 | U^J | 7F_J \rangle^2 \quad (12)$$

where, ν_J is the average transition energy (in cm^{-1}) of $^5D_0 \rightarrow {}^7F_J$ (J = 2, 4, 6) transition, e is the elementary charge of electron, Ω_J is the intensity parameter, $\langle {}^5D_0 | U^J | {}^7F_J \rangle^2$ is the squared reduced matrix with values 0.0032, 0.0023, 0.0002 for J = 2, 4, and 6 respectively, cannot be influenced by the chemical environment of RE ions. The $^5D_0 \rightarrow {}^7F_J$ transitions are forbidden by the selection rule as aforesaid and therefore, the squared reduced matrix values are zero for these transitions. The term $n(n^2+2)^2/9$ is the correction term result from local field corrections, which convert the external electromagnetic field into an effective field at the location of the active centre in the dielectric medium [66]. The radiative transition rates, $A_{0\text{-}J}$ are obtained by using the relation:

$$A_{0-J} = A_{0-1} \frac{S_{0-J}}{S_{0-1}} \frac{\nu_J}{\nu_1} \quad (13)$$

where $A_{0\text{-}1}$ is taken as 50 s^{-1} [66], $S_{0\text{-}1}$, $S_{0\text{-}J}$ are the areas under the curve related to $^5D_0 \rightarrow {}^7F_1$ and $^5D_0 \rightarrow {}^7F_J$ transitions, respectively obtained from the emission spectra and ν_1 and ν_J have been discussed above. The branching ratio (β_R) is determined by the expression given as:

$$\beta_R = \frac{A_{0-J}}{\sum_J A_{0-J}} \quad (14)$$

The branching ratio symbolizes the lasing potentiality of the transition if the value of β_R is more than 50% in comparison with the other transitions originating from an excited level [67,68]. Further, the J-O parameters (Ω_J) can be evaluated from the ratio between ED and MD transition rates using the following equation [69]:

$$\frac{A_{0-J\,(J=2,4,6)}}{A_{0-1}} = \frac{e^2 \nu_J{}^3 (n^2+2)^2}{9 S_{MD} \nu_1{}^3 n^2} \Omega_J \|U^J\|^2 \quad (15)$$

where the transition rate for each energy level is directly proportional to the integrated emission intensity.

1.14. Importance of host:

An awe-inspiring lighting technology with many advantages can compete with the traditional lighting technology and can approach the theoretical limits of luminescence efficiency. Notwithstanding many phosphor materials have been reported in support of fourth generation lighting technology, there are challenges to develop novel luminescent materials that meet the requirement of wLEDs based SSL technology. Major challenges that can be elucidate from the requirements in phosphor converted (pc)-wLEDs as: (1) High absorption rate in the emission region of LED used to pump the phosphor and emission spectrum should exhibit desirable visible emission for white light generation; (2) high luminescence efficacy with improved quantum efficiency at working temperature; (3) High thermal quenching temperature; (4) Excellent chemical, thermal and irradiation stability as desired for diversified applications. An exhaustive analysis of the nature and limitations of phosphors enforce to discover a novel potential phosphor by emphasizing the selection of non-hazardous host lattice, modifying chemical constituents, doping activators into host lattice, possibility of sufficient energy transfer from host/sensitizer to activator and limit to level-headed production costs for the bulk production and breakthrough application of phosphors [70].

The zincates have been long studied because of its high chemical stability, high brightness, high melting point, lower chemical toxicity and long persistence time without radioactive radiations. Zincates doped with RE ions have tremendous application in lighting devices. [58-62]. They have also been studied due to their interesting properties like high thermal stability, high mechanical strength, low surface acidity, hydrophobicity which make them suitable carrier for their applications in display devices, sensors, ceramic materials and catalytic activity [62-64]. When excited with LED emission in UV or n-UV region, these novel materials are proficient to convert the emission of a UV-LED to generate white light

[62, 67-68]. A host material with wide band gap and low vibrational energy can significantly transfer energy from host to activator, which is requisite in designing efficient phosphor.

Therefore, based on literature, we have chosen novel ternary calcium aluminozincate ($Ca_3Al_4ZnO_{10}$, named as CAZ in forthcoming chapters) as a host material for SSL applications.

1.15. Objective of thesis:

- To synthesize RE doped calcium aluminozincate ($Ca_3Al_4ZnO_{10}$) CAZ phosphors by using different chemical synthesis techniques to achieve single phase structure.
- To study structural, morphological, optical and luminescence properties of CAZ phosphors for their application in SSL and display devices.
- To improve the emission intensity:
    - By exciting at different wavelengths
    - By varying dopant ion concentration
    - By co-doping with suitable activator/sensitizer ions
    - By appropriate incorporation of fluxes.
- Preparation of phosphors for multicolour emissions and optimization of process for each color emitting phosphor and all relevant characterization needed.

Finally, to develop environment friendly pc-wLED by appropriate mixing and coating of phosphors onto the commercially available LED.

Chapter-2

Experimental and Characterization Techniques

The development of high-quality material requires adequate knowledge of various synthesis methodologies along with the relevant characterization techniques. The purpose of this chapter is to explain the synthesis methods adopted in the present work. The structural, morphological, photoluminescent properties of the synthesised powder phosphor samples have undergone various characterizations by employing tools such as X-ray diffraction (XRD), scanning electron microscopy (SEM), field emission scanning electron microscopy (FE-SEM), UV-Vis spectrophotometer and spectrofluorophotometer etc. The working principles and experimental tools used in the current work are also explained in this chapter.

2.1. Experimental:

The pre-eminent step during the experimental research is the synthesis and characterization of the material. This chapter is focused on the synthesis method and the characterization techniques required to characterize the material to understand their utility in wLED applications. The dry and wet chemical synthesis methods along with experimental setup have been discussed in detail in this chapter. The characterization techniques such as thermogravimetric analysis (TGA), X-ray diffractometer, diffuse reflectance absorbance (DRA), Fourier transform infrared (FT-IR) spectroscopy, scanning electron microscope (SEM), field emission (FE)-SEM are utilized to analyse structure, morphology and optical characteristics of the synthesized materials. The spectrofluorophotometer is used to examine the luminescence behaviour of the synthesized materials. TLD reader Nucleonix used to study different traps centres.

The quality of phosphors is said to be excellent if reproducible luminescent properties of the phosphor can be achieved. To prepare phosphors, many factors need to be considered meticulously such as choice of host, activator, purity of chemicals used, sintering temperature, duration of sintering, stirring of chemical solutions, fluxes and many more [71]. There are various physical and chemical techniques to prepare phosphors as reported in the literature, where physical synthesis methods include ball milling and chemical synthesis techniques include traditional solid-state reaction (SSR), sol-gel, combustion, molten salt, co-precipitation, spray pyrolysis and hydrothermal [72]. The synthesis technique is an indispensable constraint to govern the structure, morphology, distribution of particles and particle size. Moreover, the luminescence properties, and quantum efficiency can be altered by changing the method of synthesizing the phosphor. Among all the synthesis techniques, solid-state reaction technique is prevailing for the bulk production as the cost of production is low and easy fabrication [73]. However, this synthesis technique suffers some serious implications

such as creating defects that leave an unpropitious impact on the luminescent properties of the synthesized phosphor. When the reacting species diffuse exponentially, the reaction does not complete 100% that leads to some residue which results in some defects. To vaporize the residue, grinding of raw materials is followed by sintering. Moreover, fluxes can be added to a host material for ameliorating structure and morphology of the host matrix by providing a surface for faster diffusion of reacting species [74]. The improved structure and morphology induces enhancement in the luminescence characteristics of the as-prepared phosphors [75,76]. The wet chemical synthesis method used to produce smaller size, homogeneous particles with uniform distribution of particles [77]. Among different wet chemical synthesis methods, combustion, and Pechini sol-gel method were employed in synthesizing the phosphor to optimize the phase and luminescence behaviour of the phosphor.

2.2. Chemicals used:

For the synthesis of luminescent materials, a host lattice, activators, sensitizers, fuels and some fluxes are required. The various chemicals availed for the purpose of synthesizing phosphors explored in this thesis are listed below:

Table 2.1. List of chemicals used to synthesize CAZ phosphor to accomplish present thesis work.

S.No.	Name of the Chemicals	Chemical Formula	Purity (%)	Supplier
1	Calcium Oxide	CaO	99.90	Fisher Scientific
2	Zinc Oxide	ZnO	99.50	Fisher Scientific
3	Aluminium Oxide	Al_2O_3	99.90	Fisher Scientific
4	Europium Oxide	Eu_2O_3	99.99	CDH
5	Samarium Oxide	Sm_2O_3	99.99	CDH
6	Calcium Nitrate Tetrahydrate	$Ca(NO_3)_2.4H_2O$	99.90	CDH

7	Zinc Nitrate Hexahydrate	$Zn(NO_3)_2.6H_2O$	99.90	Fisher Scientific
8	Aluminium Nitrate Nonahydrate	$Al(NO_3)_3.9H_2O$	99.90	Fisher Scientific
9	Dysprosium Oxide	Dy_2O_3	99.99	CDH
10	Citric Acid (CA)	$C_6H_8O_7$	99.50	Fisher Scientific
11	Urea	CH_4N_2O	99.50	Fisher Scientific
12	Polyethylene Glycol (PEG)	$H-(O-CH_2-CH_2)_n-OH$		Fisher Scientific
13	Nitric Acid	HNO_3	69.71	Fisher Scientific
14	Sodium Fluoride	NaF	99.00	Fisher Scientific
15	Sodium Chloride	NaCl	99.90	Fisher Scientific
16	Sodium Tetraborate	$Na_2B_4O_7$	99.90	Fisher Scientific

Other chemicals such as acids and solvents used were of reagent grade/analytical grade.

2.3. Synthesis Methods:

2.3.1. Solid-state reaction method (SSR): The SSR method, known as dry media reaction is used to synthesize phosphors for industrial purpose where high volume production and low cost are prerequisites within short period of time [78]. In this method high purity chemical are weighed in stoichiometric ratio and dispersed in acetone. The chemicals are then grinded for an hour to ensure homogeneous grinding of the precursors. These solid chemical in powder form does not react at room temperature even kept for hours and therefore, it become essential to heat the chemical reactant at high temperatures. Therefore, the grinded samples after pouring in alumina crucible were kept for high temperature (>1000°C) sintering in a programmable muffle furnace. After allowing natural cooling of samples to room temperature, the obtained phosphor is grinded to ensure uniform sintering of the samples.

In the work submitted in this thesis, CAZ)phosphor were prepared by using conventional SSR method by taking highly pure chemicals CaO, Al_2O_3, ZnO as chemical precursors and

RE_2O_3 (RE = Sm and Eu) used as an activator. The prior chemicals taken in suitable amounts were collected in an agate pestle mortar and grinded for an hour by adding acetone for uniform mixing of the constituent chemicals. The grinded samples were collected in an alumina crucible and placed inside a programmable muffle furnace at 1300°C for five hours to obtain a pure phase of $Ca_3Al_4ZnO_{10}$. The sintered samples were naturally cooled down to the room temperature and again grinded for various characterizations. Fig. 2.1 (a) represents flow chart of SSR method used to synthesize CAZ phosphor.

2.3.2. Combustion method (CS): The combustion synthesis comprises of heating metal nitrate solution as oxidizer and fuel or complexing agent such as urea, glycine, CA, carbohydrazide. In the combustion synthesis, the reaction is very fast, self-sustaining and highly exothermic, which after reaction gives product [78]. This method is prevailing owing to its simple experimental setup, fast reaction rate, it does not require big experimental setup or energy and uses low cost chemicals to obtain the final product that make it cost effective and increase the level of reproducibility. The important parameter for complete combustion is to maintain oxidizer to fuel ratio as 1, which can be obtained from the valences of oxidizers and fuel. In combustion reaction, metal nitrates serve as oxidizing reactant and fuel as reducing reactant. The high energy released in exothermic reaction increase the temperature of the reacting species and ignite to fire. Combustion reaction is self-propagating reaction that take place with evolution of gases to obtain the desired product.

In this thesis work, to optimize the synthesis method for CAZ phosphor, combustion method was also explored. For this, the analytically pure calcium nitrate tetrahydrate, aluminium nitrate nonahydrate, zinc nitrate hexahydrate, RE oxide dissolved in nitric acid, were taken in stoichiometric amount without any further purification. All the nitrate precursors taken in stoichiometric ratio were individually dissolved in de-ionized (DI) water and then mixed together (solution A). RE_2O_3 dissolved in HNO_3 (solution B) is poured into the solution

A, the resultant solution is referred as solution C. The solution so obtained (solution C) is kept on a magnetic hot plate for uniform mixing under constant heating at 80°C for an hour. Urea dissolved in DI water has been taken as fuel for the combustion to occur, and then added into the solution C under constant stirring and heating at 120°C for 2 h. By constant heating and stirring, dehydration occurs with release of gases. After dehydration, the temperature of the hot plate is raised to 500°C, where spontaneous combustion occurs with liberation of large amount of heat. As the combustion process finished, white solid flakes obtained cooled to room temperature and then the grinded samples are sintered at 1100°C for 2 h.

2.3.3. Pechini sol-gel method (SG): In Pechini sol-gel method, metal salt solution reacts under mild heat treatment in an acidic or alkali medium. From a sol, a gel is formed with an interconnected network having pores and polymeric chain.

In later chapters of this thesis, CAZ phosphors were prepared using Pechini sol-gel method. In Pechini solgel method, all the nitrate metal precursors were dissolved in DI water and RE oxide dissolve in nitric acid is added into the solution of metal nitrates and stirred on magnetic hot plate for its uniform mixing. CA is used as chelating agent in this method. The metal:CA ratio is taken as 1:2 and polyethylene glycol has been taken which helps in making a polymeric network of metal citrate complex [79]. In solution C as mentioned in the above section, CA solution (CA dissolved in DI water) is added and kept oiver a magnetic hot plate under constant heating at 120°C for 10 h. The control of pH in this method is very crucial for maintaining the homogeneity of the gel and particle size of the resultant powder sample. In the present case, the pH of the solution is maintained at ~2. As the gel formation takes place, it is fired at 500°C and the obtained brown foamy solid is grinded and sintered at 1000°C. The as-synthesized white powder phosphor is taken for characterizations.

The details of combustion and sol-gel synthesis methods employed in this article is represented in Fig. 2.1 (b).

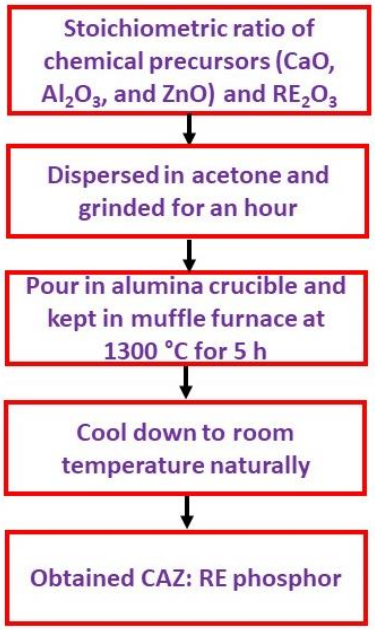

Figure 2.1(a). Flowchart of CAZ phosphor synthesized by SSR method.

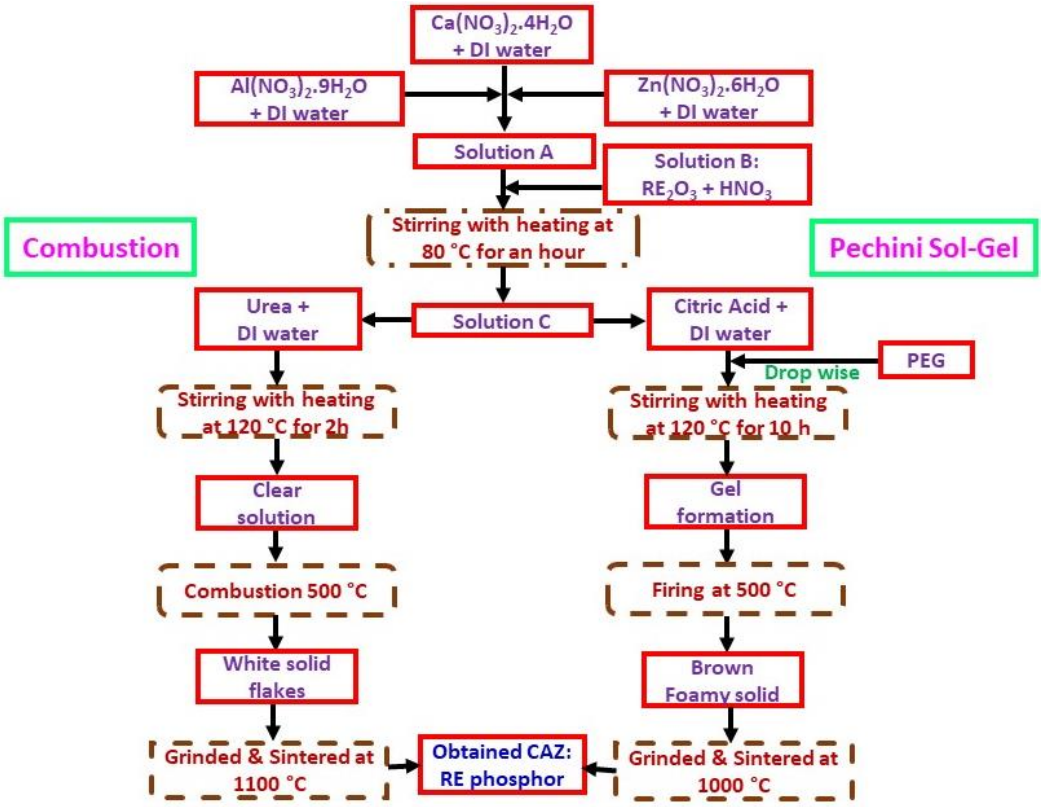

Figure 2.1(b). Flow chart of Combustion and Pechini sol-gel synthesized CAZ phosphor.

2.4. Structural characterization techniques:

The characterization of the synthesized phosphors is important to know the various parameters for the optimization and utilization of the as synthesized phosphors as luminescent materials in lighting devices. The as synthesized phosphors have been characterized using the standard instruments, which is utilized for the determination of the structure, morphology and luminescence behaviour of the phosphors. The experimental tools used for characterization of the as synthesized phosphors are discussed in detail in the subsequent topics of this chapter.

2.4.1. Thermal analysis: The thermal analysis is a technique to determine physical properties of the material under investigation or reaction products as a function of temperature, stress and environmental factors. Thermal analysis provides insight of certain properties such as topography, phase transition, crystallization, adsorption, desorption, melting, enthalpy thermal capacity, mass changes, and thermal stability. Generally, the substance is heated in a controlled manner for the analysis of the substance.

There are various thermal analysis techniques such as:

- Thermogravimetry analysis (TGA).
- Differential Scanning Calorimetry (DSC).
- Differential Thermal Analysis (DTA).
- Differential Photo Calorimetry (DPC).
- Thermo Mechanical Analysis (TMA).
- Dialometry (DIL)
- Evolved Gas Analysis (EGA).

However, in the present thesis work, we have used only TGA to know the crystallization of the phosphor.

2.4.1.1 Thermogravimetric analysis: In TGA, the mass or weight of a sample is measured with gradual increase in temperature or time in a controlled atmosphere. A graph is plotted for mass or mass percentage with respect to time or temperature and the plot is said to be thermogram

or thermal decomposition curve. This plot provides the information about decomposition, oxidation, vaporization, sublimation and desorption. The first order derivative of mass versus time or temperature is termed as differential thermal decomposition curve [80]. The mass change in TGA curve indicates adsorption or desorption of gases from the substance under observation. An increase in the mass indicates adsorption and decrease in the mass indicates desorption, whereas negligible mass change specifies stability of the substance. In the present thesis, TGA analysis was carried out by using Perkin Elmer Pyris diamond (TGA/DTA/DSC) system as shown in Fig. 2.2.

Figure 2.2. Perkin Elmer TGA system.

2.4.2. X-ray diffraction (XRD): It is the standard and potential probe for the phase and crystal structure determination of the synthesized materials. The X-rays are electromagnetic waves in the electromagnetic spectrum having wavelength in the range of few angstroms which are used to probe the materials for structural discern. X-rays used in XRD have typical range of 0.5-2.5 Å.

The crystalline materials show periodic arrangement of atoms in three-dimensional array, known as lattice. The smallest building block of crystal structure is known as unit cell. The translational vectors a, b and c specify the position of atoms in a lattice also known as the length of edges, where α, β and γ are the angles between these vectors. The crystalline solid can be classified within the seven crystal systems, which are further sub divided into 14 Bravais lattices.

2.4.2.1. Basic theory of XRD:

When the wavelength of X-rays matches well with the inter-planar spacing, then the periodic lattice serves as a diffraction grating and produces diffraction called X-ray diffraction or XRD. The matching of wavelength of X-rays with inter-planar spacing make it possible to study the structural arrangement of atoms in a crystal [81].

Bragg's Law: In general, crystal lattice acquires three dimensional arrangements of atoms in such a fashion that they form parallel plane having interplanar spacing d. When the electromagnetic radiation incident on crystal lattice at particular angles, it gets reflected from the surface and from the plane inside crystal. The reflected beams interact and undergo constructive interference. Fig. 2.3 (a) represents the set of atoms arranged parallel with interplanar spacing 'd'. Consider a monochromatic beam of wavelength λ irradiate lattice at an angle θ. The constructive interference is observed if the path difference between two reflected rays is integral of λ.

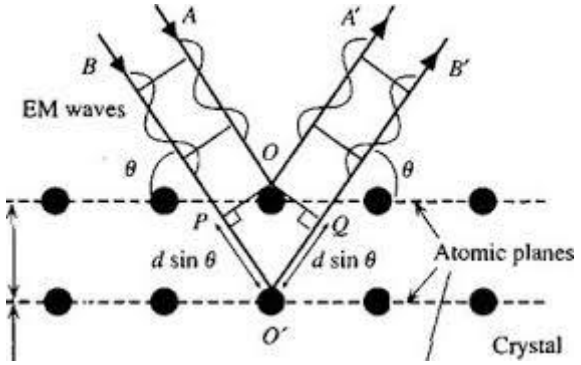

Figure 2.3 (a). Bragg's Diffraction from crystal planes.

The difference between ray A′ and B′ is PO′+O′Q.

PO′+O′Q = dsinθ + dsinθ

For constructive interference, path difference = nλ; n is integer.

∴, 2d sinθ = nλ

This relation is known as Bragg's diffraction law or Bragg's law. The intensities of scattered waves is collected versus angle to obtain the diffraction pattern. The diffraction peaks indicate the presence of different phases and its lattice structure [81].

2.4.2.2. Powder diffraction method:

X-ray Diffractometer is made up of X-ray tube, sample holder and X-ray detector. The X-ray tube produce X-rays of known wavelength, crystal is positioned at any arbitrary angle with respect to incident wave by rotating the crystal about an axis through the geometrical centre of the spectrometer as shown in Fig. 2.3 (b). The purpose of detector is to determine the intensity of the diffracted X-rays; it can also be set at any desired angular position through rotation about the geometrical centre of spectrometer. The crystal is placed at positions to satisfy the condition of diffraction so that its reflecting planes make some particular angle θ with the incident beam and the position of D is made at the corresponding angle 2θ [81].

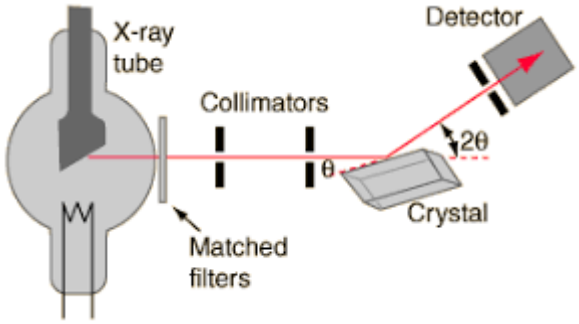

Figure 2.3 (b). Schematic representation of X-ray diffractometer.

In the finely powdered sample, crystals occupy every possible orientation about the incident beam and the diffracted beams appear as the cone of radiation emitted from the sample. A powder diffraction pattern has three main features that may be measured quantitatively. In decreasing order of relative importance, these are (a) d-spacings, (b) intensities and (c) line profiles. Powder diffraction method utilized in determining the average crystallite size of powder sample. The obtained diffraction lines in a powder diffraction pattern possess finite width at half maximum and the lines become broader for smaller sized particle.

2.4.2.3. Structure analysis and crystallite size:

Every crystalline material is endowed with its own characteristics diffraction pattern which help to identify the phase of the material. Standard patterns published by the Joint Committee on Powder Diffraction Standards (JCPDS) or International Crystallographic diffraction data (ICDD) are considered for reference to study the pure phase formation of the sample under investigation. The peaks other than the reference data are considered as the impurities and can be identified as a separate crystalline phase.

Applications of X-ray diffraction:

- Qualitative phase analysis.
- Determination of crystallite size and strain.
- Orientation of crystalline materials.
- Determination of atomic position and atomic number.
- Determination of the lattice parameters, like, a, b, c, α, β, γ and thus the crystal structure.

The crystallite size from XRD patterns can be calculated using Debye-Scherrer formula given by [82]:

$$D = k\lambda/\beta cos\theta \quad (1)$$

in which k is the shape factor (= 0.94), λ is the wavelength of X-ray used, β is the full width at half maximum (FWHM), θ is the Bragg's diffraction angle, D is the crystallite size [83]. There is another method known as Williamson-Hall (W-H) method to determine the crystallite size [84,85]:

$$\beta cos\theta = \frac{k\lambda}{D} + 4\varepsilon sin\theta \quad (2)$$

where, ε is the lattice strain and other symbols have their usual meanings. W-H graph has been plotted between βcosθ/λ versus sinθ/λ, intercept and slope give crystallite size (D) and the value of lattice strain (ε), respectively.

2.4.2.4. Rietveld analysis:

It is a technique described by Hugo Rietveld to characterize crystalline materials using diffraction data obtained from powder diffraction method. The X-ray diffraction pattern is characterized by reflections obtained as intensity for certain angles. The (h k l) miller indices of these reflections are useful in figuring out many facets of the structure of material.

Figure 2.3 (c). X-ray Diffractometer (Bruker D8).

The Rietveld method uses a least square fitting analysis to refine a theoretical line profile under "n" number of iterations to match the measured profile. This method uses predetermined parameters to minimalize the error between an experimentally observed data and a hypothetically determined crystal structure and instrumental parameters (calculated pattern). Refinement parameters like background, peak shape, lattice parameters can be refined using a Rietveld refinement software such as Full Prof Suite, PANanalytical X'Pert HighScore Plus etc. The Rietveld refinement is useful for quantitative phase analyses, microstructural

analyses, texture and residual stress. For the determination of crystal structure, it requires reflection positions, cell size, space group symmetry, intensities and atomic positions. Thus, the parameters are refined to the precise values using least square fit approach.

In this thesis work, the XRD data were observed in the 2θ range from 20° to 70° at room temperature using Bruker D8 Advance Diffractometer. The diffractometer equipped with a Ni filtered Cu-Kα source (λ=1.5406 Å) and was operated at 40 kV and 30 mA. The XRD diffractometer used in the present thesis work is shown in Fig. 2.3 (c). Rietveld refinement of the samples was carried out using Full Prof Suite.

2.4.3. Scanning electron microscope (SEM): It is an awfully resourceful mode to provide thorough details of structure over a wide range of magnification. It is used to inspect topography of specimen or surface sensitive compositional information at a very high magnification. It produces the image of a material by scanning over the surface with a focussed beam of electrons. When a highly focussed electron beam is incident on the specimen, secondary electrons (SE) get ejected from the surface. To produce SEM micrograph by collecting ejected SE, the electron probe is swept two dimensionally over the surface of the specimen.

The SEM instrument involves an optical system to generate a focused electron beam, a platform to place the sample, a detector to detect secondary electrons, an image display system, and an operation system to perform various operations. Generally, in SEM tungsten filament is used to produce an electron beam, or in some cases, a crystal of lanthanum hexafluoride (LaF_6) is mounted on the tungsten filament to produce electron beam. The schematic diagram is shown in Fig. 2.4 (a).

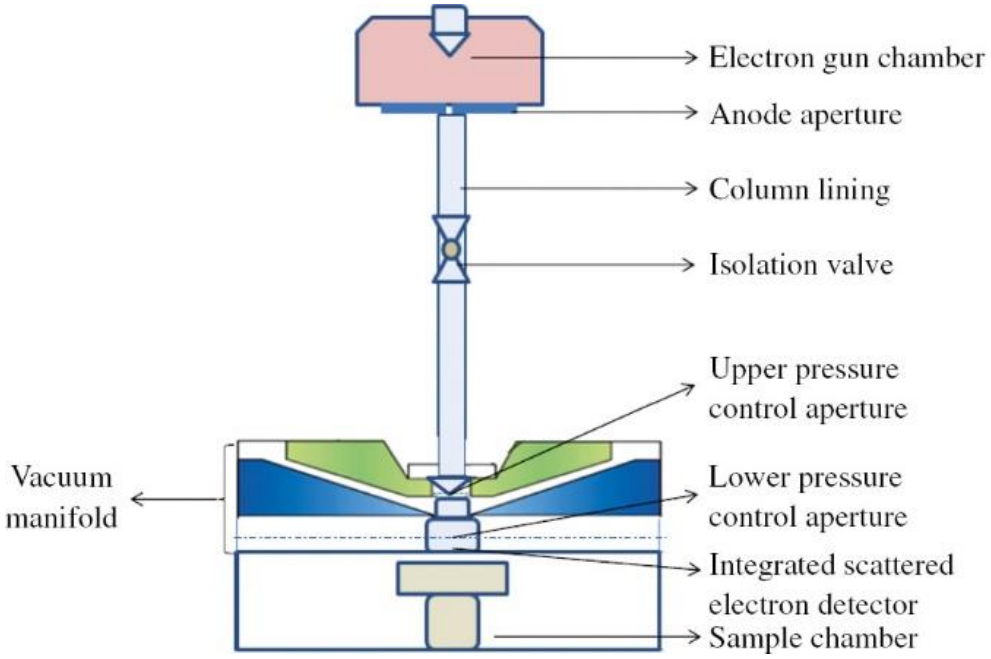

Figure 2.4 (a). The electron optic column design.

The highly focused electron beam scans the surface of the sample with the help of scanning coils to produce the image. The accelerated electron beam after interacting with the specimen produces electromagnetic signal. The SE and/or backscattered electrons (BSE), are collected by the detector and amplified signal unveil on display screen. The resulting SEM image appears on display screen. The magnification (M) of displayed SEM image can be altered by varying the scan width of electron probe. The magnification can be calculated using the expression M= D/d, where D is the width of monitor screen on which the image is displayed, and d is the scan width of electron probe. Since the size of monitor is fixed, if scan width decreases magnification increases and vice versa. The following characteristic information can be obtained from SEM:

(a) Topography: The surface appearance of specimen, its texture; and material properties.

(b) Morphology: The shape, size and arrangement of the particles on the surface of the sample; relation between material and its structure.

(c) Composition: The chemical constituents of the sample in elemental form and their relative ratios.

(d) Crystallographic information: The atomic arrangement and their degree of order.

The surface of non-conductive materials is rendered conductive usually by coating an extremely thin layer of gold/gold-palladium/carbon, the last one being specifically suited for EDX. The sample is mounted on a metallic platform after making its surface conductive and kept for scanning across the surface. The SEM used to conduct morphological observations is S-3700 N microscope in Fig. 2.4 (b).

Figure 2.4 (b). S-3700 N scanning electron microscope.

2.4.4. Field emission (FE)-SEM: The FE-SEM is an electron microscope that scans across the sample surface when high energy electron beam interacts with the sample surface in raster scan pattern. In FE-SEM instead of heating, cold source (field emitter gun) is used to liberate electrons. An exceptionally pointed tungsten needle with a tip diameter of the order of an

angstrom serves as a cathode in front of a primary and secondary anode. The voltage between cathode and anode is in the order of magnitude of 0.5 to 30 KV. Under high vacuum conditions, these primary electrons get focussed and generate a narrow beam that reaches the sample surface. The SE after emission from each spot of the sample surface reaches the detector and produces an electronic signal. The amplified electronic signal is converted into a scan-image and displayed on screen. The FE-SEM is used to get ultra-high resolution image at low accelerating voltages and small working distances. The FE-SEM used in this thesis to record the micrograph is ZEISS Gemini FE-SEM as shown in Fig. 2.4 (c).

Figure 2.4 (c). ZEISS FE-SEM instrument (GEMINI SEM-500).

2.4.4.1. Energy dispersive spectroscopy (EDS): Sometimes SEM/FE-SEM is provided with energy dispersive spectroscopy (EDS) analysis system to gather elemental information of the sample under investigation. EDS is a dynamic technique to gather information about materials, impurities, and the relative proportion of chemical composition of micro features in the sample under investigation without any destruction of the sample. The characteristics X-rays are being

emitted by the sample placed under electron beam to loss the excess energy. The energy of X-rays produced signifies their corresponding atoms and appear as specific peaks in the spectrum. The intensity represents the concentration of element present in the specimen. The X-ray mapping and line profiles can be developed to illustrate the compositional information about the specimen.

2.5. Optical characterization techniques:

2.5.1. Diffuse reflectance absorbance (DRA): It is an explicit technique that provide microscopic details of surface and facilitate the analysis of solids. DRA is used to analyse material with internal inhomogeneity. In general, when light is incident on the sample, some amount of light gets absorbed, some gets reflected back, and some get scatter in all possible directions within the sample. For inhomogeneously distributed particles, the resultant of reflection, refraction, diffraction, and absorption in all possible directions is called diffuse (or volume) reflection, whereas in homogeneous media regular (or directional) reflection is observed from a plane phase boundary. Ideally, the angular distribution of the reflected radiation should be independent of the angle of incidence to observe diffuse reflectance. A reflectance spectrum is basically collection of electromagnetic radiation reflected from the surface in correlation with frequency or wavenumber. Reflectance is the ratio of power of reflected radiation to the power of incident radiation [86].

2.5.1.2. Working of diffuse reflectance: As discussed above, in diffuse reflectance, the highly focussed incident beam gets reflected, scattered and some of the incident beam get transmitted through the sample as shown in Fig. 2.5 (a). The beam which is scattered within a sample and returns to the surface is considered as diffuse reflection and this signal is collected by the detector. For better results, the sample is diluted to ensure the deep penetration of incident beam which in turn increase the chance of diffuse reflection and reduce specular reflection.

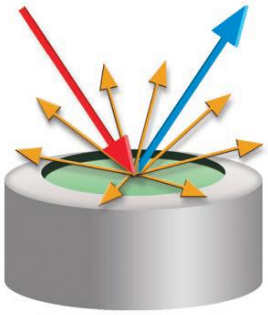

.. Incident Radiation

.. Diffuse Reflection

..Specular Reflection

Figure 2.5 (a). Incident and reflected beam through the sample under investigation.

The specular reflectance component can alter the band shapes, and their relative intensity. When the sample is diluted with a non-absorbing matrix, then these effects can be greatly reduced. In the present thesis the DRA machine used is shown in Fig. 2.5 (b).

Figure 2.5 (b). Perkin-Elmer Lambda 35 UV/Vis/NIR Spectrometer.

2.5.2. Fourier Transform infrared (FT-IR) spectroscopy: It is a prevailing in identifying bonding between atoms or functional group present in a molecule. The IR absorption bands identify the component and structure of an organic or inorganic composition. The basic principle on which FT-IR spectroscopy works is that the molecular bonds vibrate at frequencies attributed to particular element and the type of bonds. When IR radiation is incident on the molecule, the absorbed IR radiation excites the molecule from lower to higher vibrational level. The energy corresponding to such transitions falls in IR region of electromagnetic radiation. The FT-IR spectrometers employ a source of IR radiation, interferometer, detector and a display screen. The IR radiation from a broad source is modulated by using interferometer and

it interacts with the sample. The intensity of transmitted or reflected light is collected and recorded by detector as a function of its wavelength and known as interferogram. The interferogram is examined with a monitor using Fourier transform to obtain a single beam IR spectrum. The FT-IR spectrum is a plot of intensity (in percentage of light transmittance or absorbance) versus wavenumber (cm^{-1}). The FT-IR spectrometer used to record the spectrum for the work done in the present thesis is shown in Fig. 2.6.

Figure 2.6. Perkin Elmer's Frontier FT-IR spectrometer.

2.5.3. Photoluminescence (PL) excitation and emission: The excitation and emission spectra, lifetime and confocal images are important sampling tools to analyse the fluorescence behaviour of RE ions. When photons of electromagnetic radiation irradiate the sample, then RE ions get excited to higher states and spontaneously return to ground state giving off visible emission and the intensity is recorded as a function of wavelength, known as luminescence or fluorescence spectra. This is a contactless non-destructive tool to probe the materials under investigation. In the present thesis, RF-5301 PC spectrofluorometer was used to record the luminescence spectra, and fluorescence decay profiles were recorded using Edinburgh FLSP 900 spectrofluorophotometer as shown in Fig. 2.7 (a & b), respectively. The high-resolution

PL confocal image were obtained from confocal microscope (Olympus, BX51) equipped with XY-piezo stage and coupled with a 410 nm continuous wave (CW) diode laser. The RF-5301 PC spectrofluorometer is provided with excitation monochromator that allows particular wavelength from the light of Xenon flash lamp used as an excitation source having resolution of 0.1 nm to irradiate the sample. The emission monochromator selectively receives the light emitted by the sample and the light intensity is measured using a photomultiplier tube (PMT: detector). The spectral ranges of the monochromators are:

i. Excitation monochromator: 220 nm to 900 nm.
ii. Emission monochromator: 220 to 900 nm.

Figure 2.7 (a). RF-5301 PC spectrofluorometer.

Figure 2.7 (b). Edinburgh F900 Spectrometer.

For the high sensitivity of the instrument, RF-5301 PC utilizes a holographic grating, photomultiplier tube and digital circuit with high signal to noise ratio (S/N > 150). A PC manage the instrument for acquiring data and processing it. The sample slot measures 140x170x140 mm that allow the use of micro cells, high-sensitivity cells, LC flow cells, etc. to be utilize in diversified applications. Another spectrofluorometer used in recording PL and PL decay of few samples was manufactured by Edinburgh Instruments, UK (model F900). The spectrometer uses a Xenon lamp with monochromator to excite the samples for emission study. Microsecond Xenon flash lamp used as a source of excitation for the decay measurements of the samples with spectral resolution of 0.1 nm.

2.5.4. Thermoluminescence (TL): In TL a sample is irradiated by β, γ radiations and that create defects where the electron gets trapped in the material. When the temperature of the material in increased, the energy stored in the form of the trapped electrons is released and emanate luminescence. To measure the TL glow curve, PC controlled Nucleonix 1009I TL reader designed by Nucleonix Systems is used as shown in Fig. 2.8.

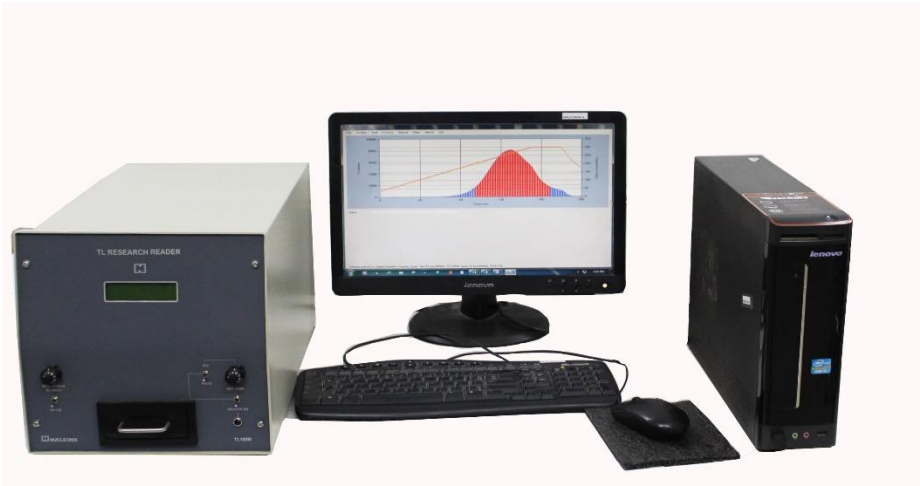

Figure 2.8. PC controlled Nucleonix 1009I Thermoluminescence system.

It is a controller-based unit include photomultiplier tube, temperature controller unit, heater transformer, heater strip (kanthal) which is used to heat the sample up to desired temperature and record TL glow curve. This unit employ 200 channels which can record the integral and digitized glow curve into EEPROM memory. This system is provided with an additional CCD spectrometer which allows user to record TL intensity versus wavelength. The sample placed on kanthal plate gets heated up at a desired heating rate (approximately 5 °C/sec) in the range between 50 and 400°C.

Chapter-3

Spectroscopic and photoluminescence characteristics of Sm^{3+} doped calcium aluminozincate phosphor for wLEDs application

Monophase CAZ phosphor activated with various concentrations of Sm^{3+} ions were synthesized at 1300°C by using SSR technique. The crystal structure and phase analysis of the CAZ phosphor was carried out by XRD studies. Morphology and functional groups present in the phosphor were examined thoroughly by employing SEM and FT-IR spectral measurements, respectively. Under 401 nm excitation, the as-prepared phosphors give intense visible orange emission at 601 nm. It was observed that 1.0 mol% of Sm^{3+} ions in the CAZ phosphor is most advantageous to give intense visible orange emission. The PL analysis discloses that the nature of interaction between Sm^{3+} ions was dipole-dipole due to which concentration quenching observed beyond 1.0 mol% of Sm^{3+} ions. The PL decay study reveals a bi-exponential behaviour of decay curves with an average lifetime of the order of microseconds. The CIE coordinates (x=0.574, y=0.424) measured for the optimized phosphor are very close to the intense orange emission coordinates specified by Nichia Corporation developed Amber LED NSPAR 70BS (0.570, 0.420). The spectroscopic, PL and PL decay studies suggest the potential use of Sm^{3+} doped CAZ phosphors for display and wLEDs.

3.1. Introduction:

In recent years, conventional light sources such as incandescent and fluorescent lamps have been replaced by SSL technology. SSL technology involves wLEDs, which are globally used for wide spread applications in consumer electronics and general illumination [87,88]. It offers many scientific and technological patronages such as environmental friendliness, lower operating temperature and effective energy utilization by saving 80% of energy consumption over conventional lighting devices. In the light of the aforementioned advantages, wLEDs are contemplated as the next generation lighting sources [89–92]. InGaN or GaN chip based wLEDs are gaining paramount attention because of their longevity, high luminous efficiency, high energy efficiency, smaller size, faster switching, excellent reliability with reduced operating expenses and capable of replacing conventional light sources [83,88,91–95]. The recent approach of generating white light is comprises of yellow phosphor encase over UV/blue LED. Though it has several drawbacks as it possess low CRI, high CCT, thermal quenching, narrow visible range and hence cannot meet the demand of warm white light needed for indoor and artificial lighting [96,97]. To circumvent the problem, red phosphors can be introduced to improve CRI and CCT. However, commercial red phosphor Y_2O_2S: Eu^{3+} has some shortcomings such as inimical decomposition products, chemical instability which degrades its luminescence efficiency over a period. This necessitate the development of a new orange-red emitting phosphor under n-UV or blue excitation [98,99]. Sm^{3+} doped phosphors are studied for the development of an orange-red phosphor due to their potential applications for color display, plasma display panels and solid state lighting [95,100–102]. For efficient white light emission with improved CRI and CCT, a new combination of cyan plus orange can be realized, where orange emission can be accomplished from Sm^{3+} ions doped phosphors [103]. Therefore, Sm^{3+} serves as one of the best activator/dopant for orange-red emission to augment the efficiency of wLEDs [104].

This chapter describes the synthesis of Sm^{3+} ions doped CAZ phosphors using traditional SSR technique. The as-synthesized phosphors have been used to study structural, morphological, luminescent, colorimetric properties and energy transfer processes in detailed for their utility in wLEDs.

3.2. Sample preparation:

Samarium ions doped CAZ phosphors at different concentrations of Sm^{3+} ions (i.e., 0.5, 1.0, 1.5, 2.0 and 2.5 mol%) are synthesized by using conventional SSR technique as described in section 2.3.1 and the detailed procedure is represented in Fig. 2.1 (a) of chapter 2. The analar grade chemicals CaO, ZnO, Al_2O_3 and Sm_2O_3 have been taken as raw materials in stoichiometric ratio.

3.3. Results and Discussion:

3.2.1. Phase analysis and crystal structure:

The XRD patterns of CAZ phosphor doped with different Sm^{3+} ions concentration (0.0, 0.5, 1.0, and 2.0 mol%) have been examined and compared with the International Crystallographic Diffraction Database (ICDD card no. 04-009-7304) of $Ca_3Al_4ZnO_{10}$ to verify the crystal structure, effect of doping concentration and to identify the phase as shown in Fig. 3.1 (a.) All the observed diffraction peaks are in complete agreement with the standard data and (h k l) planes have been well indexed as shown in Fig. 3.1 (a). The sharp XRD patterns without any additional peak confirm the formation of pure orthorhombic crystalline phase of CAZ phosphor. The results suggest the incorporation of Sm^{3+} ions in CAZ phosphor does not lead to noteworthy changes in the crystal structure of host. As the ionic radius of samarium is close to calcium (r_{sm3+} = 0.958 Å, r_{ca2+} = 1.0 Å with coordination number = 6) rather than aluminium (r_{Al3+} = 0.535 Å) and zinc (r_{zn2+} = 0.74 Å), it can incorporate into Ca^{2+} sites.

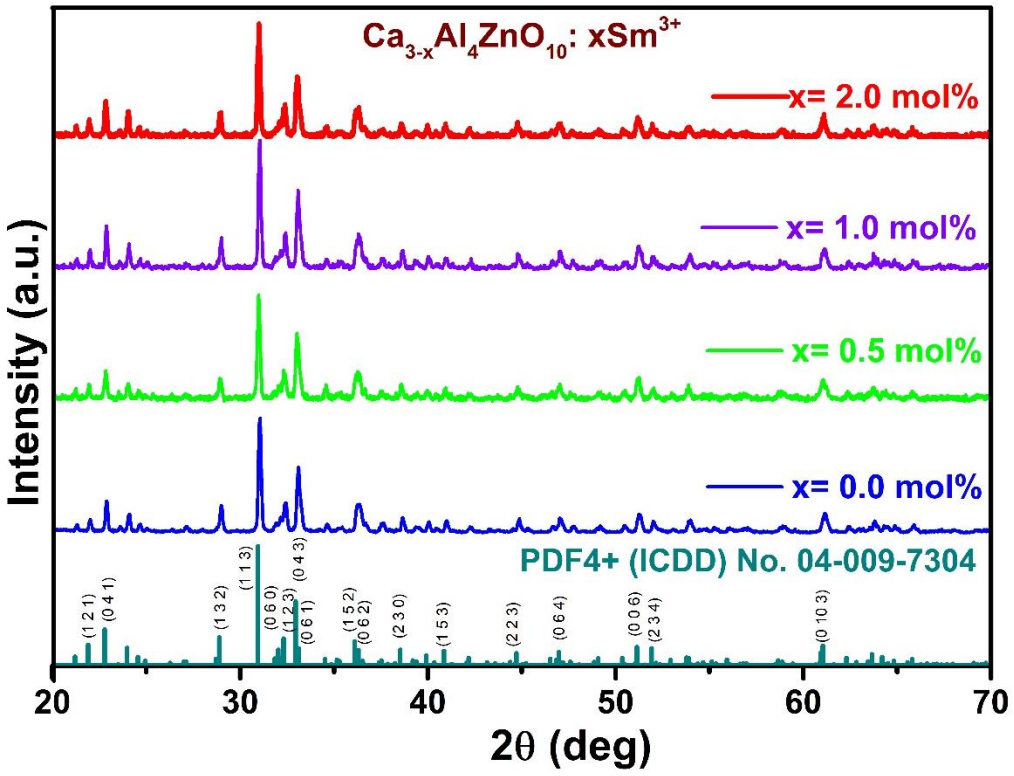

Figure 3.1 (a). XRD patterns of $Ca_{3-x}Al_4ZnO_{10}$: xSm^{3+} (x = 0.0, 0.5, 1.0 and 2.0 mol %) compared with reference diffraction pattern of $Ca_3Al_4ZnO_{10}$.

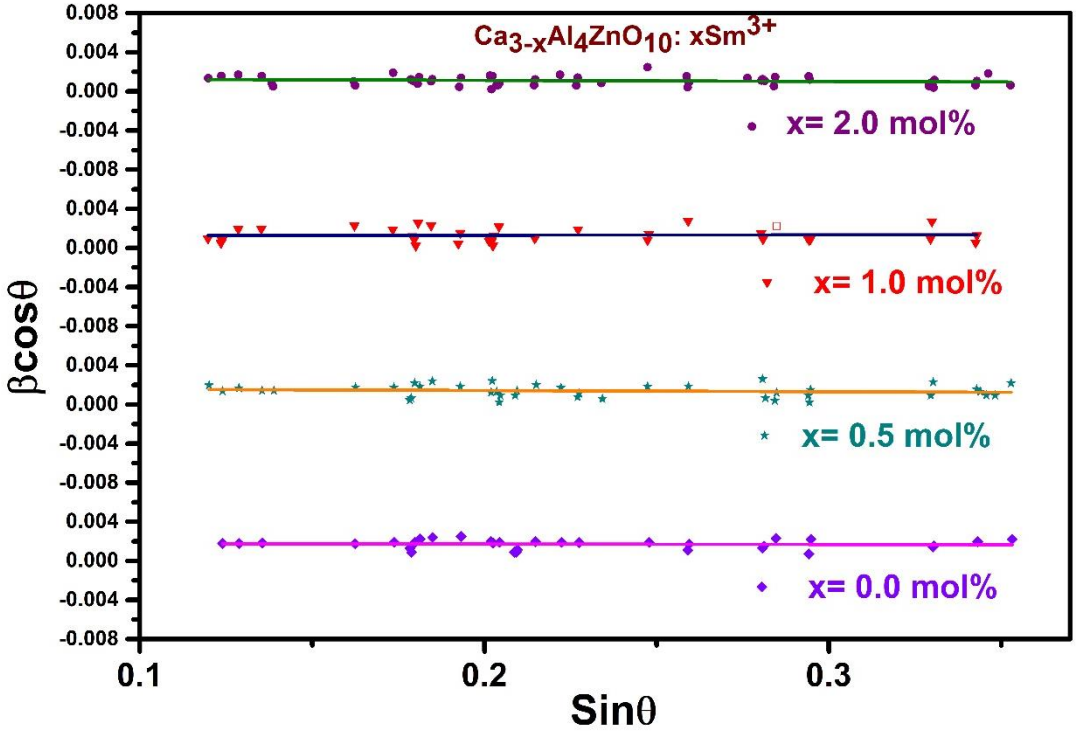

Figure 3.1 (b). W-H plot of $Ca_{3-x}Al_4ZnO_{10}$: xSm^{3+} (x = 0.0, 0.5, 1.0 and 2.0 mol%).

To measure average crystallite size, the Debye-Scherrer relation and W-H method has been used as discussed in section 2.4.2.3 of chapter 2. The evaluated average crystallite size using Debye-Scherrer relation reckoned in the range 61-110 nm for all the characterized CAZ phosphors. The W-H graph has been plotted between βcosθ versus sinθ as shown in Fig. 3.1 (b). From the intercept and slope of the plot, the average crystallite size (D) and the value of lattice strain (ε) can be estimated, respectively. The average crystallite size is in 52-75 nm range and strain (%) is 0.006–0.03 using W-H method for all the characterized CAZ phosphors.

3.3.2. Particle morphology:

To investigate morphology and particle size, SEM analysis has been carried out for the optimized $Ca_{2.99}Al_4ZnO_{10}$: $0.01Sm^{3+}$ phosphor as shown in Fig. 3.2. The phosphor exhibits solid microcrystalline structure of particles with agglomeration among crystalline grains and the average size of particles for $Ca_{3-x}Al_4ZnO_{10}$: xSm^{3+} (x=1.0 mol%) sample is found to be in the range of 2-15 μm. Most of the commercial phosphors currently available in the market contain particle size of the order of few micrometres [87].

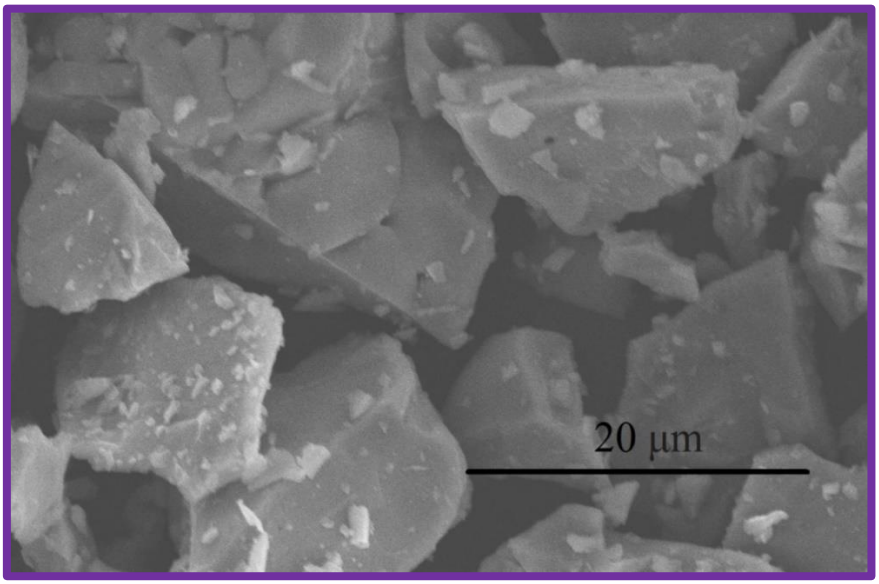

Figure 3.2. SEM micrograph of $Ca_{3-x}Al_4ZnO_{10}$: xSm^{3+} (x = 1.0 mol%).

3.3.3. FT-IR analysis:

Fig. 3.3 represents FT-IR spectrum of $Ca_{2.99}Al_4ZnO_{10}$: $0.01Sm^{3+}$ sample characterized into several peaks in the range 400-3800 cm^{-1} out of which some are broad, and others are moderate in bandwidth. The broad bands are formed due to degenerate vibrational energy states, mechanical scattering and broadened lattice dispersion, thermally [105,106]. The low intensity peaks in the region 400-650 cm^{-1} are accredited to metal-oxygen bond vibrations of Ca-O, Al-O [107].

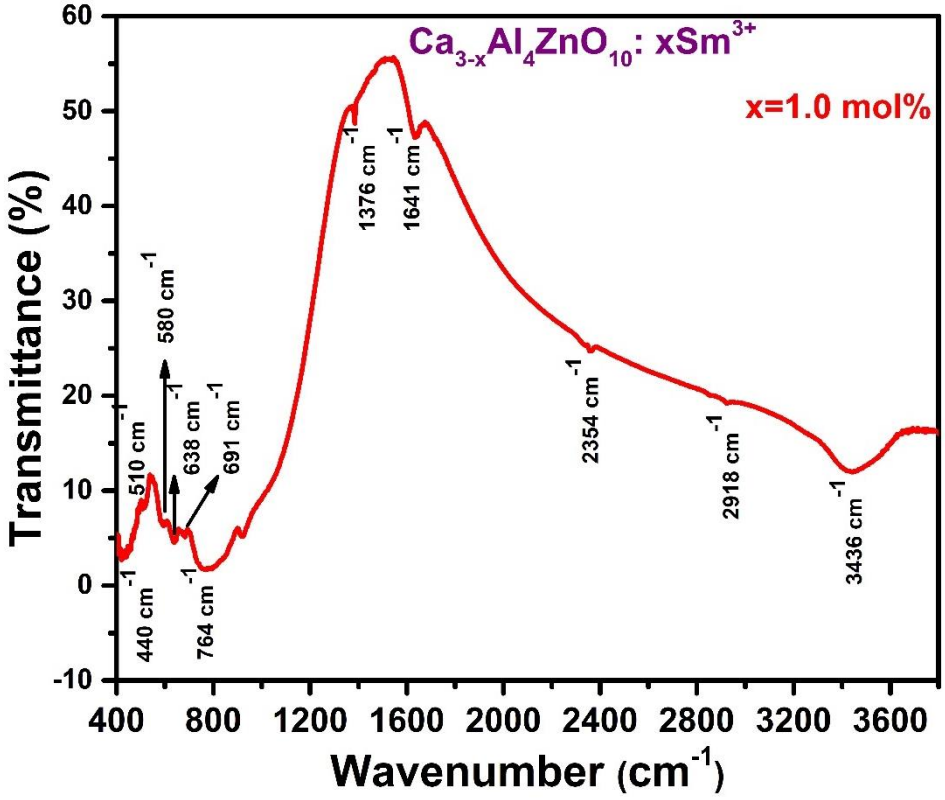

Figure 3.3. FT-IR analysis of $Ca_{3-x}Al_4ZnO_{10}$: xSm^{3+} (x = 1.0 mol%).

The spectrum reveals characteristic of absorption centered at 440 cm^{-1} as Zn-O stretching vibration. The peaks centered at 510 and 580 cm^{-1} correspond to Zn-O symmetric stretching vibration of ZnO_4 units. The peak at around 638 and 691 cm^{-1} assigned to Al-O bond vibration of AlO_4 units [108,109]. The broad peaks centered at around 764 cm^{-1} due to AlO_4 tetrahedral units [110]. The peaks at 1376 cm^{-1} is due to –OH vibrations [111]. The peak positioned at about 1641 cm^{-1} accredited to crystal water with H-O-H bending mode [112]. The peak at 2354

cm^{-1} ascribed to antisymmetric stretching of adsorbed water molecules [105]. The peaks centered at 2918 cm^{-1} confirms hydrogen bonding [106]. The band at about 3436 cm^{-1} accredited to fundamental stretching vibrations of hydroxyl group [113].

3.3.4. Luminescent properties:

Fig. 3.4 (a & b) shows the PLE and PL spectra of $Ca_{3-x}Al_4ZnO_{10}$: xSm^{3+} phosphor monitoring characteristic emission of Sm^{3+} at 601 nm and excitation at 401 nm, respectively. The concentration of trivalent samarium ion in $Ca_{3-x}Al_4ZnO_{10}$: xSm^{3+} is varied from x = 0.5 to x = 2.5 mol%. The excitation spectra manifests various sharp peaks at 343, 359, 373, 401, 412, 422, 439, 448, 461, 470, 480, 500 and 525 nm accredited to f-f transitions originated from ground state $^6H_{5/2}$ to $(^4K, ^4L)_{17/2}$, $(^4D, ^6P)_{5/2}$, $^4L_{17/2}$, $^4F_{7/2}$, $^4L_{13/2}$, $^4M_{19/2}$, $^4G_{9/2}$, $^4M_{17/2}$, $^4I_{13/2}$, $^4I_{11/2}$, $^4M_{15/2}$, $^4G_{7/2}$, and $^4F_{3/2}$ upper states, respectively [114–116]. Out of these transitions, the band corresponding to the $^6H_{5/2} \rightarrow {}^4F_{7/2}$ transition is the most intense, which suggests that the $^4F_{7/2}$ level is highly populated by 401 nm excitation, indicating the effective excitation of these phosphors using n-UV LEDs. Therefore, the emission spectra of $Ca_{3-x}Al_4ZnO_{10}$: xSm^{3+} was recorded under 401 nm excitation.

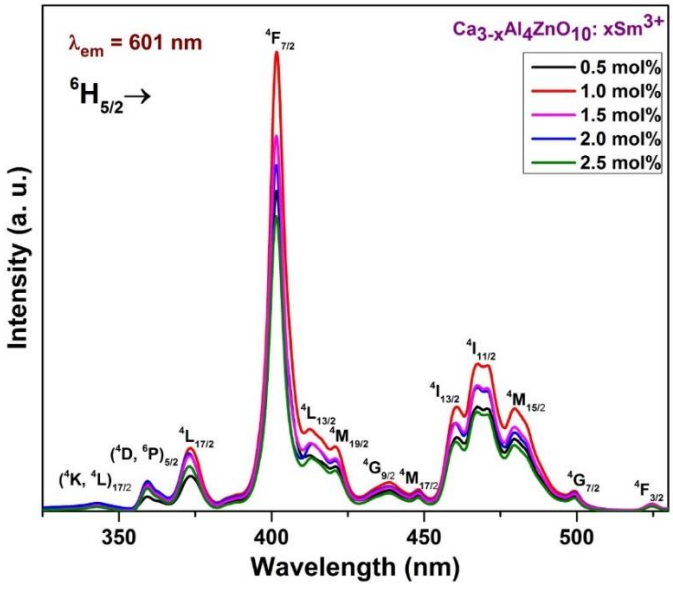

Figure 3.4 (a). Excitation spectra of $Ca_{3-x}Al_4ZnO_{10}$: xSm^{3+} ($0.5 \leq x \leq 2.5$ mol%) λ_{em} = 601 nm.

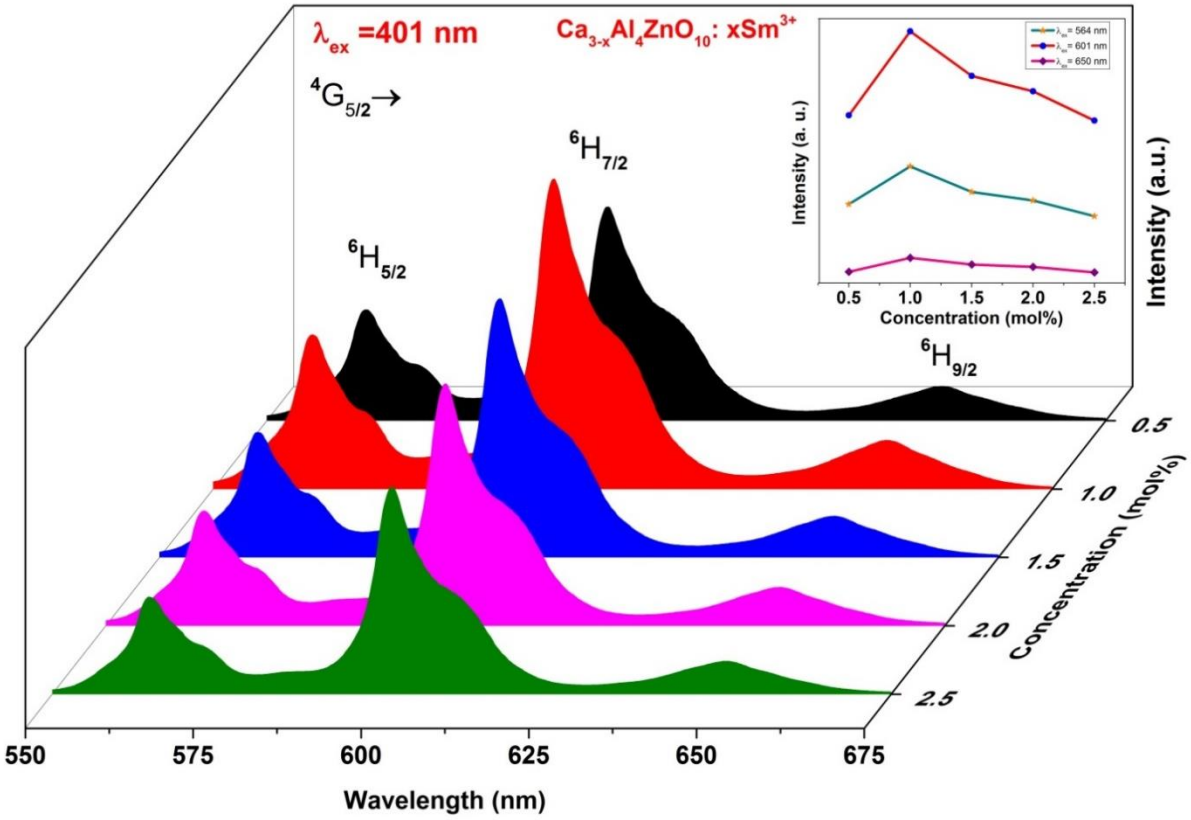

Figure 3.4 (b). Emission spectra of $Ca_{3-x}Al_4ZnO_{10}$: xSm^{3+} ($0.5 \leq x \leq 2.5$ mol%) λ_{ex} =401 nm (Inset: Plot of Intensity vs Concentration).

As shown in Fig. 3.4 (b), the PL spectra exhibit three emission bands centered at 564, 601, and 651 nm owing to $^4G_{5/2} \rightarrow {}^6H_{5/2}$, $^6H_{7/2}$, and $^6H_{9/2}$ transitions, respectively [87]. Fig. 3.5 represents the partial energy level diagram of Sm^{3+} ions in $Ca_3Al_4ZnO_{10}$ phosphor showing the radiative and non-radiative emissions. All the excitation levels above $^4G_{5/2}$ quickly undergo cascade non-radiative relaxation to $^4G_{5/2}$ state because the energy difference in their energy levels is small as shown in Fig. 3.5. The $^4G_{5/2}$ level undergo radiative transition to the lower levels $^6H_{5/2}$, $^6H_{7/2}$, and $^6H_{9/2}$ because of the presence of ample energy gap between them [117]. The non-radiative relaxation might have occurred through various possible cross relaxation channels. The possible cross relaxation channels are ($^4G_{5/2} \rightarrow {}^6F_{5/2}$; 10793 cm^{-1})⇋($^6H_{5/2} \rightarrow {}^6F_{11/2}$; 10471 cm^{-1}) , ($^4G_{5/2} \rightarrow {}^6F_{7/2}$; 9947 cm^{-1})⇋($^6H_{5/2} \rightarrow {}^6F_{9/2}$; 9090 cm^{-1}), ($^4G_{5/2} \rightarrow {}^6F_{9/2}$; 7784 cm^{-1}) ⇋($^6H_{5/2} \rightarrow {}^6F_{7/2}$; 7931 cm^{-1}) and ($^4G_{5/2} \rightarrow {}^6F_{11/2}$; 7407 cm^{-1})⇋($^6H_{5/2} \rightarrow {}^6F_{5/2}$; 7085 cm^{-1}) referred as CRC1, CRC2, CRC3, and CRC4 respectively as shown in Fig. 3.5 [118,119].

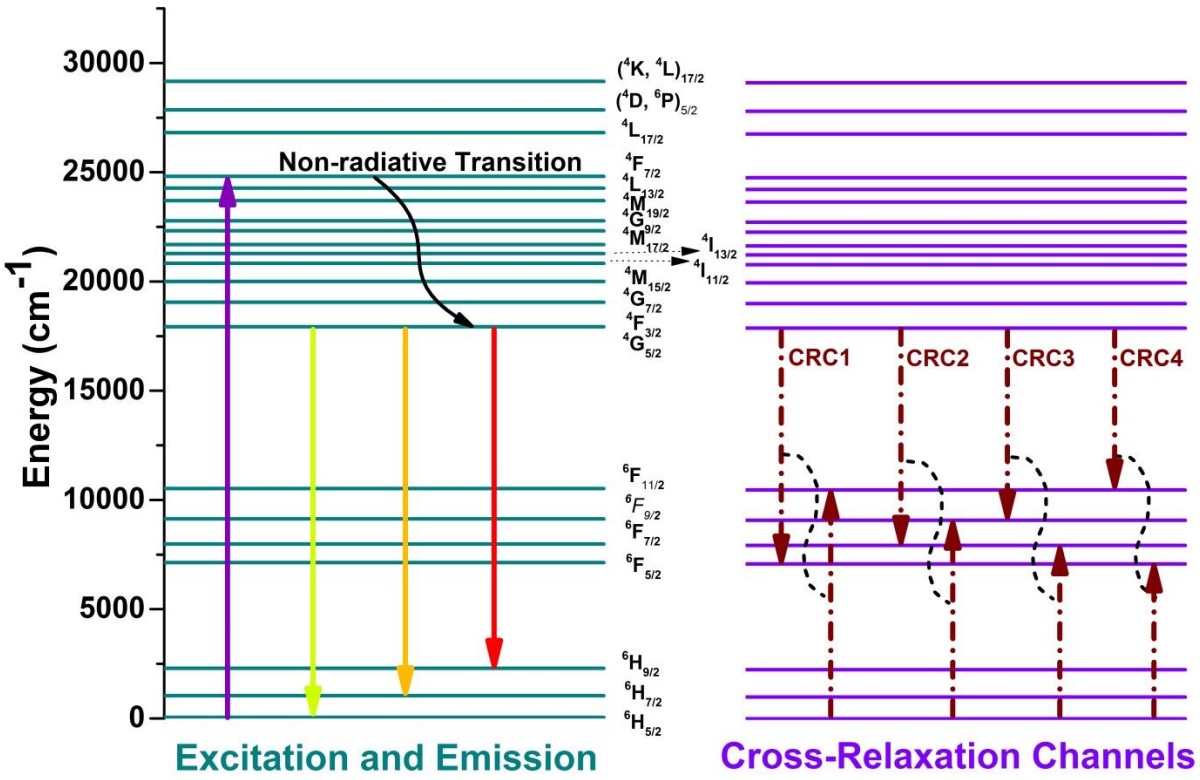

Figure 3.5. Partial energy level diagram and possible cross-relaxation channels of Sm^{3+} ions doped CAZ phosphor.

Among all the emission transitions shown in Fig. 3.4 (b), $^4G_{5/2} \rightarrow {}^6H_{7/2}$ transition in orange region (601 nm) is highly intense among others. The first transition at 564 nm assigned to $^4G_{5/2} \rightarrow {}^6H_{5/2}$ is purely magnetic dipole (MD) transition and is independent of crystal field obeying the selection rules ($\Delta J = 0, \pm 1$; J is angular momentum); the second one $^4G_{5/2} \rightarrow {}^6H_{7/2}$ at 601 nm obeys the selection rule ($\Delta J = \pm 1$) is a MD transition but here forced electric dipole (ED) transition dominates. Therefore, it is partially MD and partially forced ED transition. The third one $^4G_{5/2} \rightarrow {}^6H_{9/2}$ at 651 nm is purely forced ED crystal field sensitive transition according to the selection rules ($\Delta J \leq 6$; J or J' = 0, when J = 2, 4, 6) [119,120]. The asymmetricity is described by the intensity ratio of ED to MD transition that relates with the asymmetric nature of the local environment around luminescent center in the host system. Lower this intensity ratio, lesser is the distortion from the inversion symmetry. The calculated value of intensity ratio is found to be in the range 0.29 to 0.33. The lower values of intensity ratio suggests the

higher environmental symmetry of luminescent ion in the host lattice; which implies that Sm^{3+} ions have been substituted into symmetric nature [121].

3.3.5. Effect of Sm^{3+} concentration on emission:

It is observed from the PL spectra shown in Fig. 3.4 (b), all the prepared phosphors have insignificant change in spectral profile except the intensity variation with the increasing concentration of Sm^{3+} in $Ca_{3-x}Al_4ZnO_{10}$: xSm^{3+} ($0.5 \leq x \leq 2.5$ mol%) phosphors. Intensity increases up to 1.0 mol% of Sm^{3+} ions and beyond that quenching of luminescence is perceived. Thus, the optimized concentration of Sm^{3+} in the as-prepared phosphor is 1.0 mol%. The variation in emission intensity with Sm^{3+} ion concentration is manifested in the inset of Fig. 3.4 (b). Fundamentally, the concentration quenching is a phenomenon observed at higher doping concentration due to energy transfer among the activator ions i.e., Sm^{3+} to Sm^{3+}. At higher concentration, the distance among Sm^{3+} ions show decrement with rise in concentration. The energy states of these ions are close enough that energy migration from these states to quenching centers occurs with increasing concentration. The occurrence of non-radiative energy transfer from one luminescent center to another presented at diverse sites in the host lattice leads to decrease in luminous intensity. The exchange interaction, radiative re-absorption, multipole-multipole interaction are the three possible methods for non-radiative energy transfer [100]. The exchange interaction in short range order can occur up to a critical transfer distance, R_c of 5 Å which cannot be attributed for concentration quenching at very low concentration, since the distance between the two luminescent centers at low concentration will be sufficiently large. The mechanism of radiative re-absorption occurs when there is a broad overlap of excitation and emission spectra, which is not observed for the as-prepared phosphors. Therefore, the multipole-multipole interaction account for the quenching phenomenon. The multipole-multipole interaction mechanism is subvene by the critical transfer distance (R_c). The critical transfer distance can be defined as the distance where the

energy transfer probability equals the probability of radiative emission and can be proxime to two times the radius of the sphere with given volume [122]. The critical transfer distance [123] can be expressed as:

$$R_c \approx 2\left[\frac{3V}{4\pi X_c N}\right]^{\frac{1}{3}} \quad (1)$$

where, number of cations per unit cell is expressed as N (N = 4), V is the unit cell volume (V = 923.438 $Å^3$) and X_c represents critical concentration (X_c =0.01 mol). The value of R_c is computed to be 35.33 Å much greater than 5 Å. Hence the energy transfer due to multipole-multipole interaction causes the concentration quenching [100,124].

As stated in the Dexter theory [125], the emission intensity per dopant is described by the following relation:

$$\frac{I}{x} = K\{1 + \beta(x)^{\frac{Q}{3}}\}^{-1} \quad (2)$$

where x denotes the dopant concentration, K and β are some constants for a particular matrix. The value of Q defines the type of interaction among the nearest neighbour ions, Q = 3, 6, 8 and 10 for exchange interaction, dipole-dipole, dipole-quadrupole and quadrupole-quadrupole interaction, respectively.

Considering $\beta x^{Q/3} >> 1$, the above equation can be re-written as [123]:

$$log\frac{I}{x} = K' - \frac{Qlog(x)}{3}; \quad where\ (K' = logk - log\beta) \quad (3)$$

Therefore, to get the correct value of Q for Sm^{3+} sites in the host lattice, the graph of log(I/x) versus log (x) has been plotted as shown in Fig. 3.6 that yields a straight-line plot having slope -Q/3. In the present study, the slope comes out to be -1.714, which gives Q=5.142 close to 6, implying dipole-dipole interaction is the underlying mechanism for quenching of Sm^{3+} site emission centers in the host lattice [124].

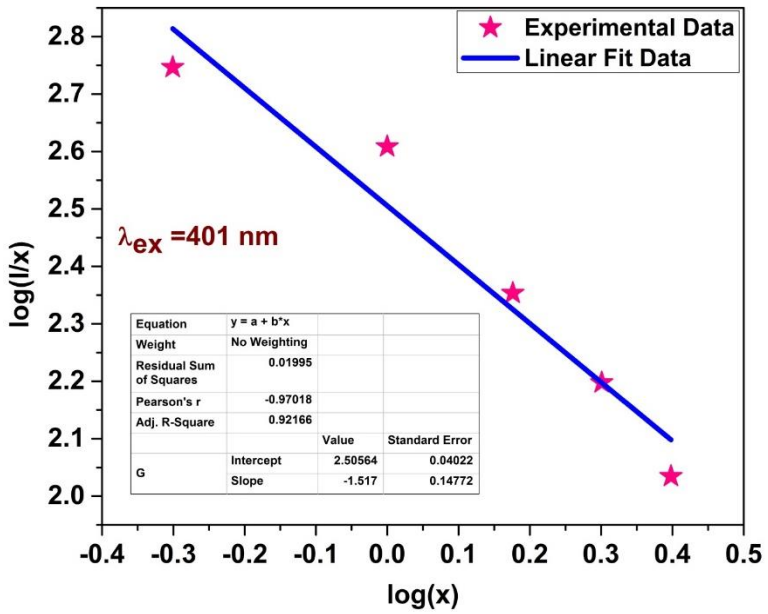

Figure 3.6. Plot of log (I/x) vs log (x).

3.3.6. Color chromaticity coordinates and CCT:

From the recorded emission spectra of CAZ phosphors, CIE chromaticity coordinates were calculated and found to be (0.571, 0.426), (0.574, 0.424), (0.576, 0.422), (0.575, 0.423) and (0.577, 0.421) for 0.5, 1.0, 1.5, 2.0 and 2.5 mol% of Sm^{3+} concentration, respectively. Fig. 3.7 shows the CIE coordinates for the optimized sample $Ca_{2.99}Al_4ZnO_{10}$: $0.01Sm^{3+}$. From the CIE diagram, it is discernible that $Ca_3Al_4ZnO_{10}$: Sm^{3+} phosphor exhibit pure orange color. The calculated CIE coordinates for all the samples are in close proximity to the coordinates of Amber LED NSPAR 70BS (0.570, 0.420) developed by Nichia Corporation [116]. The correlated color temperature (CCT) has been calculated empirically from the equation described in section 1.10 of chapter 1. The CCT values are found to be 1829, 1811, 1798, 1804 and 1792 K for $Ca_{3-x}Al_4ZnO_{10}$: xSm^{3+} where, x= 0.5, 1.0, 1.5, 2.0, and 2.5 mol% respectively. Therefore, it is expected that the samarium doped CAZ phosphors show favourable properties for n-UV driven orange component for warm white light display devices with low CCT.

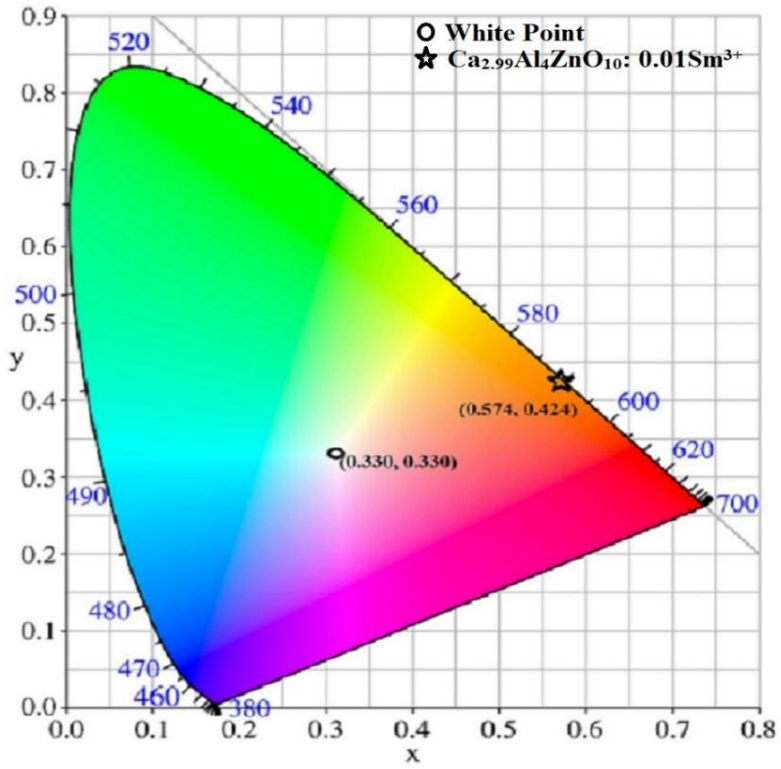

Figure 3.7. CIE Chromaticity diagram of CAZ phosphor doped with 1.0 mol% of Sm^{3+} ions (λ_{ex} = 401 nm).

3.3.7. Photoluminescence decay analysis:

The room temperature decay curves recorded for $^4G_{5/2}$ level of Sm^{3+} ions doped CAZ phosphors under 401 nm excitation is shown in Fig. 3.8. The decay profiles shown in Fig. 3.8 are nicely fit with a double exponential function:

$$I_t = I_0 + A_1 \exp\left(-\frac{t}{\tau_1}\right) + A_2 \exp\left(-\frac{t}{\tau_2}\right) \quad (4)$$

where I_t and I_0 denote the emission intensities at time t and 0, respectively; arbitrary constants are designated as A_1, and A_2; τ_1 and τ_2 are the representatives for fast and slow lifetimes for exponential components, respectively.

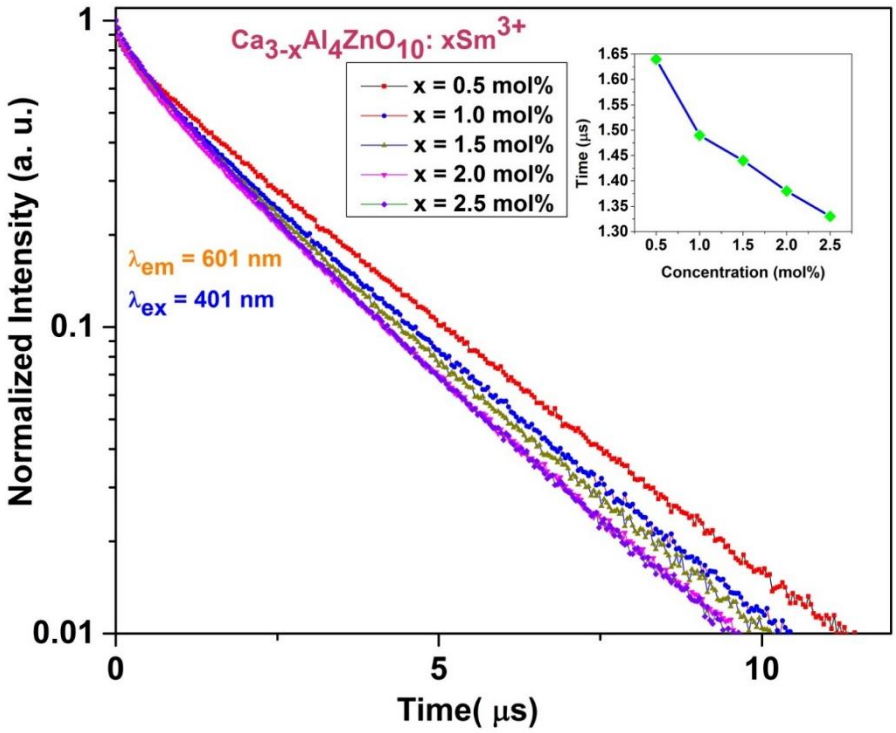

Figure 3.8. Decay curves of $Ca_{3-x}Al_4ZnO_{10}$: xSm^{3+} ($0.5 \leq x \leq 2.5$ mol%) λ_{ex} = 401 nm and λ_{em} = 601 nm. (Inset: Plot of lifetime of Sm^{3+} doped CAZ phosphor vs concentration of Sm^{3+}ions).

The average lifetime (τ) has been calculated for the series of CAZ phosphors by using the formula [119]:

$$\tau = \frac{A_1\tau_1^2 + A_2\tau_2^2}{A_1\tau_1 + A_2\tau_2} \qquad (5)$$

The lifetime values are found to be 1.64, 1.49, 1.44, 1.38 and 1.33 μs for 0.5, 1.0, 1.5, 2.0 and 2.5 mol% of Sm^{3+} in CAZ phosphor, respectively. It is computed that the average lifetime decreases by raising Sm^{3+} concentration due to the energy transfer among Sm^{3+} ions at shorter distances. The lifetime variation with Sm^{3+} ions concentration is plotted and shown in the inset of Fig. 3.8.

Chapter-4

Enhancement of red emission using flux in Eu^{3+} doped calcium aluminozincate phosphor for applications in w-LEDs

A series of novel CAZ phosphor doped with Eu^{3+} ions without and with different fluxes (NaF, NaCl, and $Na_2B_4O_7$) was synthesized by conventional SSR method. The XRD patterns depict the pure phase of $Ca_3Al_4ZnO_{10}$ phosphors with orthorhombic structure. The Judd-Ofelt (J-O) analysis has been carried out to get insights of optical properties. The as-synthesized phosphor has uneven agglomerated micron sized particles. The PL studies exhibit significant enhancement in the red emission for Eu^{3+} doped CAZ phosphor with the addition of $Na_2B_4O_7$. The emission intensity has been found to increase approximately 1.5 times using NaCl and 2.5 times using $Na_2B_4O_7$ in Eu^{3+} doped CAZ phosphor as compared to the phosphor without any flux. The emission spectrum of optimized Eu^{3+} doped CAZ phosphor added with $Na_2B_4O_7$ flux has been compared the commercial Y_2O_3: Eu^{3+} phosphor. The CIE chromaticity coordinates and color purity calculated for $Na_2B_4O_7$ in Eu^{3+} doped CAZ phosphor is close to commercial red phosphor. The decay curves show bi-exponential behaviour with experimental lifetimes in the range of microseconds for the as-prepared phosphors. All these results indicate that the $Na_2B_4O_7$ flux assisted Eu^{3+} doped CAZ phosphor can serve as an efficient red phosphor under blue light for applications in white light emitting devices.

4.1. Introduction:

In the pc-wLEDs approach, phosphors are coated on n-UV/blue LEDs in which part of n-UV/blue light is converted into white light either by the combination of blue LED and yellow phosphor or UV LED coupled with mixture of RGB phosphors. The commercially available blue-emitting LED (InGaN) with the combination of yellow phosphor (YAG: Ce^{3+}) gives white light having fast luminescence decay time. Despite the various advantages, its luminescence suffers some limitations due to lack of red component which restricts its application in SSL devices [126–130]. Moreover, tricolor pc-wLEDs consist of n-UV chip coated with appropriate mixture of RGB (red, green, and blue) phosphors. However, the disadvantage of using tricolor phosphors is the inconsistency in decay process of different components which leads to change in colour with time. At present, commercial red sulfide phosphor (Y_2O_2S: Eu^{3+}) suffers with low chemical stability and less efficient in comparison with the green (ZnS: Cu^{+}, Al^{3+}) and blue phosphors ($BaMgAl_{10}O_{17}$: Eu^{2+}) to get excited in n-UV and deep blue spectral region [131–134]. Nitride phosphor shows deep broad red emission and difficult to synthesize, which limit its applications [103,135,136]. Therefore, to develop a new red phosphor from the perspective of chemical stability and high luminescent efficiency for the preparation of pc-wLEDs, CAZ doped with Eu^{3+} ions has been explored for its luminescent properties. Moreover, the luminescent properties of phosphors are subjective to various other factors such as method of synthesis, concentration of activator, adding sensitizer or flux. Among these factors, flux added to the main composition can improve the quality of phosphor by reducing sintering temperature, improving size distribution uniformity and ennoble the intensity of emission [137,138]. In general, alkali halide fluxes have been reported in literature to enhance the emission intensity, for example Na_2CO_3-SiO_2-NaF in YAG: Ce, BaF_2 and CaF_2 in $BaMgAl_{10}O_{17}$: Eu^{2+}/Mn^{2+}, H_3BO_3, NH_4Cl, NH_4F, NH_4Br, $BaCl_2$, $BaBr_2$, CaF_2 and BaF_2 in Zn_2SiO_4:Mn^{2+} [138–140]. Apart from halide fluxes, boric acid (H_3BO_3) and borax ($Na_2B_4O_7$)

have also been reported in (Ca,Zn)TiO_3:Pr^{3+}, ($K_{0.5}Na_{0.5}$) NbO_3, and $SrAl_2O_4$:Eu^{2+} phosphors [141–143]. The flux had no harmful impact on the optical properties of the crystal [137]. The proper amount of flux in the synthesis process has a positive effect on the emissive characteristics of the phosphor.

In this chapter, Eu^{3+} doped CAZ phosphor without any flux and incorporating different fluxes, such as sodium fluoride (NaF), sodium chloride (NaCl), and borax ($Na_2B_4O_7$) have been synthesize for different concentration of Eu^{3+} ions to study the enhancement of red emission in it. Systematic studies on structural, morphological and PL have been carried out to analyse the suitability of the as-prepared phosphors along with the optimization for better luminescence efficiency and the feasibility of using them in pc-wLEDs. J-O analysis and PL decay analysis were carried out for the as-prepared phosphors with and without optimised flux. Confocal images and other colorimetric studies have also been performed and analysed to identify the potential candidature of the Eu^{3+} doped CAZ phosphor for visible emission.

4.2. Experimental:

Eu^{3+} doped CAZ phosphors for different concentrations of Eu^{3+} ions (0.0, 1.0, 2.0, 3.0 and 4.0 mol%) (CAZ: xEu^{3+}) were synthesized taking analytical grade CaO, Al_2O_3, ZnO and Eu_2O_3 as chemical precursors using the conventional SSR method described in section 2.3.1 of chapter 2. For flux assisted CAZ phosphor, the precursors were taken in stoichiometric ratio and mixed thoroughly in a dispersing medium (acetone) and grinded in an agate mortar for an hour, to which a predetermined quantity of NaF, NaCl and $Na_2B_4O_7$ were added separately as a flux. After sufficient grinding, samples were sintered at 1200°C with a consistent heating rate for five hours and then naturally cooled down to the room temperature in a programmable muffle furnace. The obtained powder samples were washed, dried and grinded for different characterizations. The synthesized 1.0 mol% Eu^{3+} doped CAZ phosphor with 5 wt% NaF, NaCl and $Na_2B_4O_7$ were named as NF1, NC1 and NB1, respectively. The as-synthesized Eu^{3+} doped

CAZ phosphor without flux are indicated as CAZ0, CAZ1, CAZ2, CAZ3 and CAZ4 for 0.0, 1.0, 2.0, 3.0 and 4.0 mol% of Eu^{3+} ions concentration, respectively.

4.3. Results and Discussion:

4.3.1. Phase identification:

Fig. 4.1(a) represent the XRD patterns for CAZ: xEu^{3+} (x = 0.0, 1.0, 2.0 and 3.0 mol%). No impurity peak was observed in diffraction patterns confirms the successful doping of Eu^{3+} ions in the host lattice. All the diffraction peaks of the CAZ phosphor sintered at 1300°C matches well with the standard PDF4 + International Crystallographic Diffraction Database (ICDD) card no. 04-009-7304 and confirms the single-phase formation of an orthorhombic structure with Pbc2 space group. The absence of any second phase implies that the Eu^{3+} ions are not influencing the structure of the host matrix due to similar ionic radii of six coordinated Ca^{2+} = 1.0 Å; Eu^{3+}=0.947 Å. The lattice parameters were found to be *a=5.142 Å, b=16.751 Å, c = 10.721 Å*, with cell volume $V = 923.438\ Å^3$ having number of atoms per unit cell, *N = 4*. The characteristic structural units for CAZ are five-membered tetrahedral rings with Ca^{2+} ion inside them. The oxygen atom forms deformed octahedral in the form of antiprisms. The aluminium and zinc form three-membered tetrahedral rings parallel to yx-plane which is connected with the similar rings along x-axis on their common vertex and with other two rings connected by double helical axis forming continuous layers. These layers are interconnected by metaaluminate chains of Al tetrahedral forming a continuous 3D structure [144]. XRD patterns measured for the CAZ1, NF1, NC1 and NB1 phosphors are shown in Fig. 4.1 (b). The XRD patterns of CAZ1, NC1 and NB1 phosphors are showing sharp peaks and are in complete agreement with the standard reference data. The XRD patterns observed for NC1 and NB1 are showing single phase orthorhombic structure of $Ca_3Al_4ZnO_{10}$ (CAZ) with Pbc2 space group. However, the XRD pattern of NF1 sample does not show pure phase of $Ca_3Al_4ZnO_{10}$ as shown

in Fig. 4.1(b). Furthermore, the XRD pattern of NB1 shows absence of any impurity peak and also it exhibits more crystallinity when compared to other samples. This might be due to larger solubility, faster diffusion and reaction rate of reactants in NB1 phosphor. This prompted us to increase the amount of flux ($Na_2B_4O_7$) to 10, 15 and 20 wt% in the CAZ host system to optimize the amount of flux. For convenience, these samples have been designated as NB2, NB3 and NB4 for 10, 15 and 20 wt% of flux in CAZ, respectively.

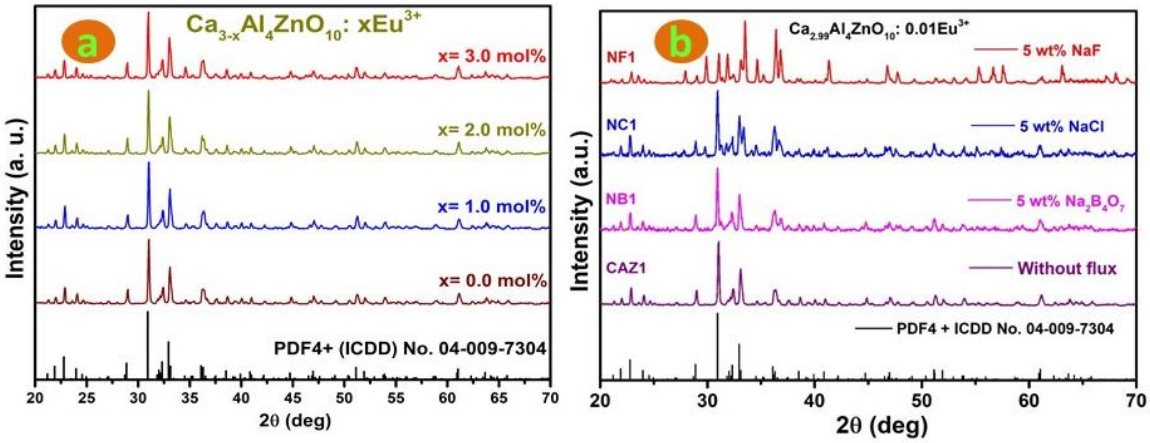

Figure 4.1. XRD patterns of (a) Eu^{3+} doped CAZ phosphor and (b) Eu^{3+} doped CAZ phosphor incorporated with 5 wt% of different fluxes.

The average crystallite sizes estimated by using Debye-Scherrer equation were found to be 51.6, 63.3, 70.5, 84.3, 52.2 and 50.0 nm for CAZ0, CAZ1, CAZ2, CAZ3, NC1 and NB1 respectively [52]. Moreover, the reduced crystallite size for NB1 signifies the better crystallinity of that phosphor with the addition of flux [145].

4.3.2. Morphology:

Fig. 4.2 (a) and (b) represents the surface morphology of CAZ1 and NB1, respectively. The observed SEM images exhibit agglomerated cluster of irregularly shaped particles and uneven particle distribution. The SEM images of CAZ1 and NB1 show that the particle size has been reduced by adding $Na_2B_4O_7$ flux to the host lattice. Different parameters such as solubility of raw materials, ionic radii of anion/cation, purity of flux, have a noteworthy

consequence on size and morphology of the as-prepared phosphors [141]. The average size of the particle in the as-prepared phosphors are found to be in the range of 2-15 μm which is comparable with the particle sizes of the commercially available phosphors [146].

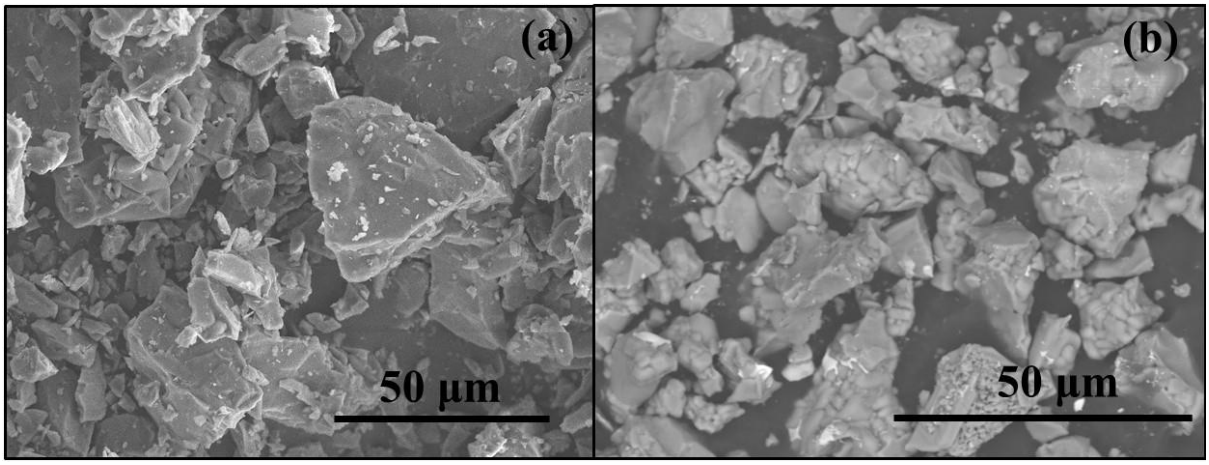

Figure 4.2. SEM images of (a) CAZ1 and (b) NB1.

4.3.3. Diffuse reflectance spectra:

Fig.4.3 shows the diffuse reflectance absorbance spectra of CAZ: xEu^{3+} (x = 0.0 and 2.0 mol%). Generally, the optical properties change when impurity ions are doped in the host matrix [147]. CAZ phosphor doped with 2.0 mol% Eu^{3+} ions shows the absorption band in the range 390-525 nm due to the presence of Eu^{3+} ions, which were found to be consistent with those observed in excitation spectra. In the process of finding the optical band gap, we have converted the diffuse reflectance into Kulbeka-Munk function as follows:

$$F(R) = (1 - R)^2/2R \quad (1)$$

where, *F(R) =K/S* represents the Kulbelka-Munk function symbolizes absolute reflectance of the host lattice, *K* stands for the molar absorption coefficient, *S* represent scattering coefficient [148]. The absorption coefficient *(α)* and energy band gap (E_g) can be related by Tauc equation as given below:

$$\alpha h\nu = C(h\nu - E_g)^n \quad (2)$$

where, *hv* gives the energy of photon, *C* is energy independent constant, and *n* is a constant whose values are related to the different types of transitions (*n* = 1/2, 2, 1/3, 3 for direct allowed, indirect allowed, direct forbidden, and indirect forbidden transitions, respectively). Since α is proportional to F(R), the above equation can be rewritten as:

$$F(R)h\nu = C(h\nu - E_g)^n \quad (3)$$

The band gap for CAZ0 and CAZ2 samples were measured by calculating *F(R)* and then a graph is plotted between $(F(R)h\nu)^2$ and *hv* (Tauc plot), for direct allowed transition as show in the inset of Fig. 4.3. The intercept of the tangent to the curve on the X-axis approximate the band gap energy.

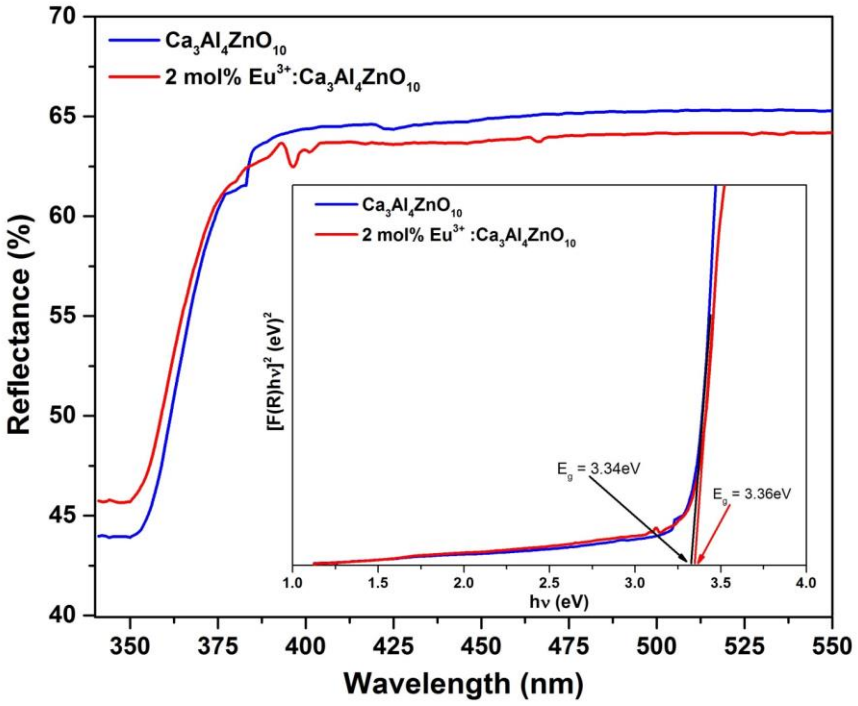

Figure 4.3. Diffuse Reflectance Absorbance of CAZ0 and CAZ2. (Inset: Tauc plot for band gap measurements).

The calculated band gap values for CAZ: xEu^{3+} (x = 0.0, and 2.0 mol% of Eu^{3+} ions) were observed to be approximately 3.34 and 3.36 eV, respectively, by extrapolating the Kulbelka-Munk absorption coefficient related spectrum. The calculated values of band gap represent insignificant change with the doping of activator ions [149]. By adding dopant into the host

lattice, a slight expansion in the unit cell tends to narrower the conduction and valence band which cause the broadening in the band gap [150].

4.3.4. Luminescent properties:

Fig.4.4 (a) shows the excitation spectra of CAZ: xEu^{3+} (x = 1.0, 2.0, 3.0, and 4.0 mol%) phosphor in the wavelength range 225-550 nm by monitoring emission wavelength at 615 nm. Two broad excitation bands were observed in the range 250-300 nm and 320-360 nm, indicates the presence of charge transfer band (CTB) and host band respectively in the host matrix. The CTB is attributed to the electronic transition from the 2p orbital of O^{2-} to the 4f orbital of Eu^{3+}, and it is allied to the covalency between O^{2-} and Eu^{3+} and associated with coordination environment of Eu^{3+} [59]. The narrow excitation peaks at a wavelength of 360, 379, 391, 412, 462 and 529 nm were observed as associated with intra-4f transitions of Eu^{3+} ions designated to $^7F_0 \rightarrow {}^5D_4$, $^7F_0 \rightarrow {}^5L_7$, $^7F_0 \rightarrow {}^5L_6$, $^7F_0 \rightarrow {}^5D_3$, $^7F_0 \rightarrow {}^5D_2$ and $^7F_0 \rightarrow {}^5D_1$ transitions, respectively [151–153]. Among all the peaks, the one at 462 nm wavelength has the highest intensity and the peak at 391 nm has the intensity closer to the intensity observed at 462 nm. These two intense peaks observed at 462 and 391 nm conspicuously speak that the phosphor under investigation can be excited by n-UV and blue LED chips. Fig. 4.4 (b) represents the PL emission spectra of CAZ phosphor doped with 2.0 mol % Eu^{3+} ions under different excitation wavelengths. From Fig. 4.4 (b), it can be seen that, the phosphor under investigation gives maximum emission intensity under 462 nm excitation. The emission intensity observed under 391 nm excitation wavelength is also very closer to that observed at 462 nm excitation. The two excitation peaks observed at 391 and 462 nm facilitates that the as-prepared phosphor can be effectively excited by both n-UV and blue LED chips. Fig. 4.4 (c) and Fig. 4.4 (d) represent the emission spectra of CAZ: xEu^{3+} (x = 1.0, 2.0, 3.0 and 4.0 mol%) recorded by exciting the samples at 391 and 462 nm wavelengths, respectively, which are similar from the perspective of peak position and intensity. Sharp emission peaks observed at 553, 578, 588, 615, 653 and

701 nm in both the emission spectra were assigned to $^5D_1 \rightarrow {}^7F_2$, $^5D_0 \rightarrow {}^7F_0$, $^5D_0 \rightarrow {}^7F_1$, $^5D_0 \rightarrow {}^7F_2$, $^5D_0 \rightarrow {}^7F_3$, and $^5D_0 \rightarrow {}^7F_4$ transitions, respectively [153,154]. Splitting of $^5D_0 \rightarrow {}^7F_1$, and $^5D_0 \rightarrow {}^7F_2$ levels into two peaks because of stark effect manifests tha the Eu^{3+} ions are present at two or more site symmetries in the phosphor under investigation [155].

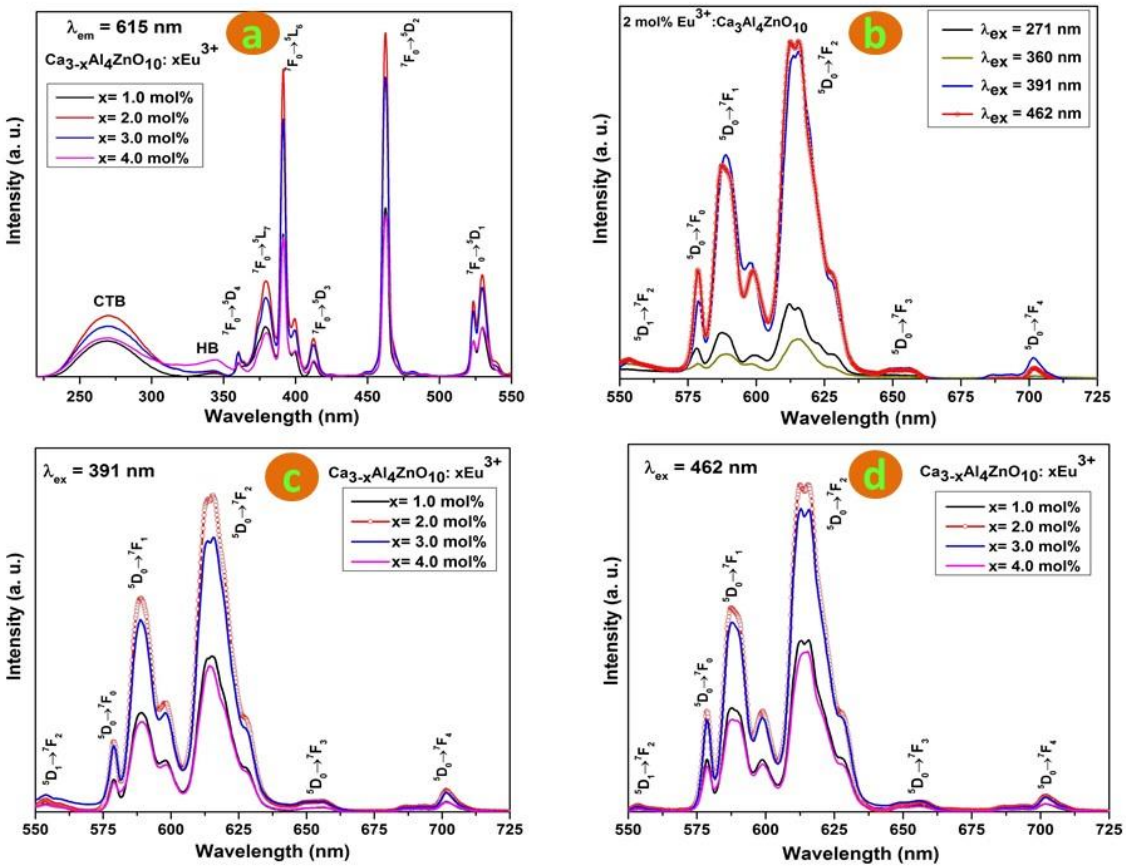

Figure 4.4. Excitation spectra of (a) CAZ1, CAZ2, CAZ3 and CAZ4 at 615 nm emission wavelength, emission spectra of (b) CAZ2 under different excitation wavelengths, (c & d) CAZ1, CAZ2, CAZ3 and CAZ4 under 391 and 462 nm excitation wavelength, respectively.

It is well known that because of stark effect, the emission transitions can split into a maximum of the *2J+1* stark levels, where *J* indicates total angular momentum [44]. The emission transitions $^5D_0 \rightarrow {}^7F_1$ and $^5D_0 \rightarrow {}^7F_2$ observed in the emission spectra are attributed to the magnetic dipole (MD) and forced electric dipole (ED) transitions, respectively. The hypersensitive forced ED transition is highly intense as compared with allowed MD transition indicating Eu^{3+} ions are located at the sites with no inversion symmetry [154,156]. The intensity

ratio of $^5D_0 \rightarrow {}^7F_2$ to $^5D_0 \rightarrow {}^7F_1$ transition gives the asymmetric ratio, which tells us the level of distortion on the inversion symmetry of Eu^{3+} ions in the host. Such ratio was found to be in the range from 1.4 to 1.6 for variable Eu^{3+} ions concentration in the phosphor under investigation indicates that the Eu^{3+} ions are dwelled at high symmetry site. The slight variation observed in asymmetric ratio indicates consistency in symmetry of Eu^{3+} ions with varying concentration [157,158]. It is discernible from the emission spectra that emission intensity initially increases up to 2.0 mol% of Eu^{3+} ions, and then gradually decreases with further increase in Eu^{3+} ion concentration. As the concentration of Eu^{3+} ion raises, the Eu^{3+} ions come closer due to reduced distance between them that favours the non-radiative pathway by energy transfer among Eu^{3+} ions which directs luminescence quenching. In general, there are three mechanisms responsible for non-radiative energy transfer through exchange interaction, radiation re-absorption and electric multipolar interaction among activator ions [159]. The energy transfer among Eu^{3+} ions depends on the shortest average distance (critical distance R_c) between Eu^{3+}-Eu^{3+} ions at a critical concentration X_c of Eu^{3+} ions. The critical distance R_c can be determined from the equation described in section3.3.5 of chapter 3. For Eu^{3+} doped CAZ system V = 923.438 Å^3, N = 4 and X_c = 0.02 (2.0 mol%). By using the above experimental data, the estimated value of critical distance was 29.16 Å. This is far more than R_c needed (5 Å) for exchange interaction to takes place. The huge difference in critical distance conspicuously speaks that the exchange interaction is not the plausible reason for energy transfer, and multipolar interaction may be the most appropriate mechanism in this case [160]. Dexter theory describes the probability of energy transfer via electric multiolar interaction between the activator ions is inversely proportional to the Q^{th} power of R (Q = 6, 8, and 10 corresponding to electric d-d, d-q and q-q interactions, respectively), where R indicates distance between activator ions. The emission intensities and the corresponding doping concentration of activator ions are related as [63]:

$$\frac{I}{x} = K\{1 + \beta(x)^{\frac{Q}{3}}\}^{-1} \quad (4)$$

where symbols have their usual menaing as described in chapter 3. From the Huang's description for luminous intensity and mole fraction [161], the luminous intensity and the mole fraction of activator ions can be reduced to:

$$log\frac{I}{x} = A - \frac{Qlog(x)}{3} \quad (5)$$

where, A remains invariant for varying doping concentration. To estimate the value of Q, the graph between *log(I/x)* versus *log(x)* is plotted as shown in Fig. 4.5. The calculated value of Q is 5.94, which is in proximity to 6 implying energy transfer mechanism is electric dipole-dipole interaction [123].

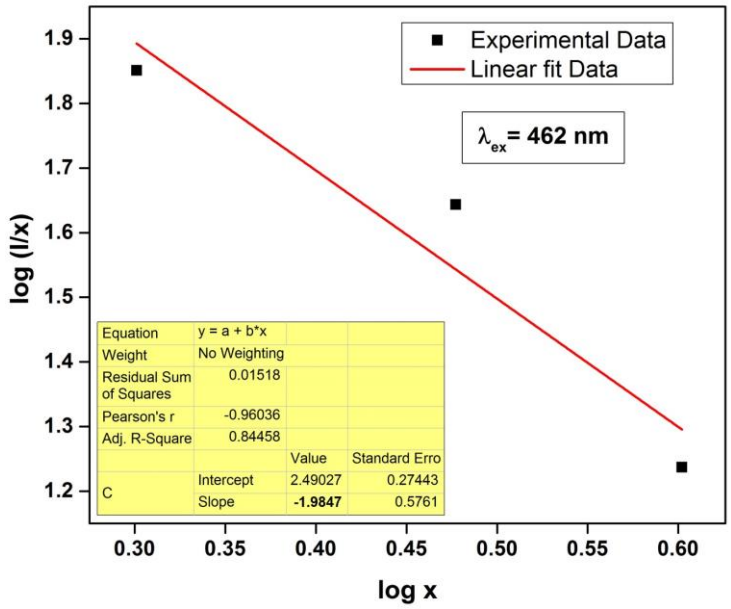

Figure 4.5. Plot of log(I/x) vs log(x).

4.3.4.1. Effect of added flux on the emission spectra:

Fig. 4.6 (a) shows the emission spectra of 1.0 mol% Eu^{3+} doped CAZ phosphor for CAZ1, NF1, NC1 and NB1 recorded under 462 nm excitation. The intensity variation with the addition of different fluxes can be clearly seen. From Fig. 4.6 (a), it is conspicuous that, $Na_2B_4O_7$ added as a flux significantly shows intensity enhancement in Eu^{3+} doped CAZ phosphor among all fluxes. Addition of NaCl flux can only increases the emission intensity

approximately 1.5 times to the CAZ1 phosphor; whereas the emission intensity for NB1 increased approximately 2.5 times to the CAZ1 phosphor. The emission spectrum for NF1 does not show any enhancement in the emission intensity, instead there is some loss of emission intensity which might be due to impure phase formation of CAZ phosphor. Therefore, the emission intensities shown by different fluxes added to CAZ phosphor allows us to conclude that, $Na_2B_4O_7$ serve as an optimized flux to show better luminescence efficiency. Addition of $Na_2B_4O_7$ flux reduces the temperature at which phosphor is sintered and increase the diffusion rate of Eu^{3+} in the host lattice, thereby enhancing the luminescent emission intensity [162]. Since the flux has lower melting point, it allows more particle to take part in reaction and accelerates the formation of phosphor by enhancing the diffusion rate, allowing reaction components to dissolve more and allowing larger content of reacting species to take part in reaction and improves the crystal structure and growth. When the flux melts during calcination, it removes solid-grain boundaries and make the surface of particles smooth. Among the three fluxes, $Na_2B_4O_7$ (743°C) has lowest melting point as compared to NaCl (801°C), and NaF (993°C). Therefore, the possibility of $Na_2B_4O_7$ to be emerged as a good flux is more, as it can allow more reacting component to take part in reaction comparatively at lower temperature as compared to other fluxes including NaF and NaCl. Since the luminescence intensity is highest for $Na_2B_4O_7$ added in Eu^{3+} doped CAZ phosphor, it can be said that flux $Na_2B_4O_7$ emerges as an excellent flux in Eu^{3+} doped CAZ phosphor [136,145]. Further, the integrated intensity ratios I_{ED}/I_{MD} for NC1 and NB1 are found to be 1.58 and 1.65, respectively. Therefore, it can be inferred from the calculated I_{ED}/I_{MD} ratio that the crystal environment of Eu^{3+} ions in NB1 is more distorted from the crystal field symmetry, and the nature of bonding between Eu^{3+} ions and anionic ligands is observed to be more covalent [163,164]. The emission spectra also show some splitting in the emission band which might be recognized as the stark effect. The emission

characteristics of RE ions in a crystal field relates with the symmetry of the coordination structure which results in splitting of the energy levels [162,165].

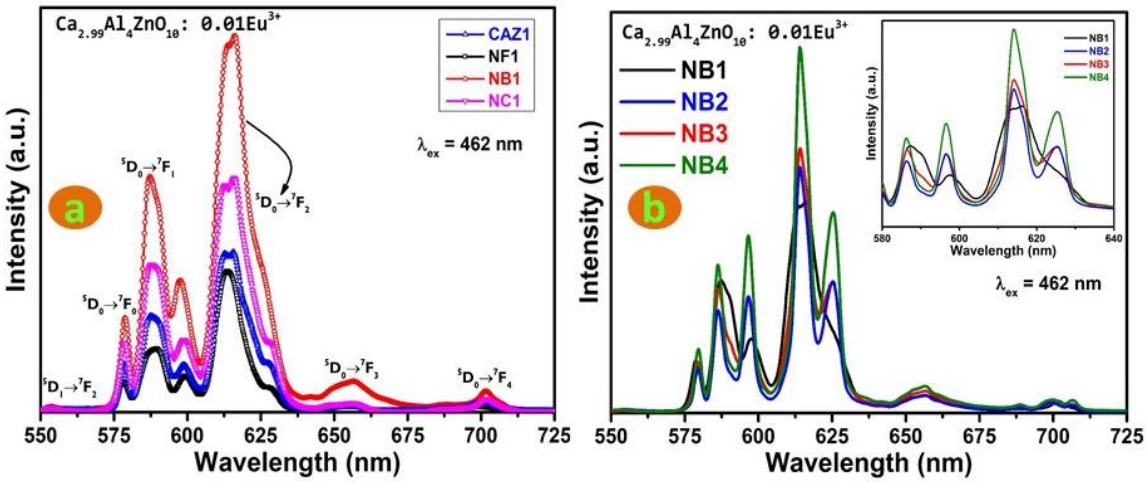

Figure 4.6. Emission spectra of (a) CAZ1, NF1, NC1 and NB1, and (b) NB1, NB2, NB3 and NB4 under 462 nm excitation (Inset shows magnified image of emission spectra (b) in the range 580-640 nm.).

Fig. 4.6 (b), shows the effect of flux dosage on the luminescent intensity of Eu^{3+} doped CAZ phosphor excited via blue (462 nm) light. The emission intensity gradually increases with increase in $Na_2B_4O_7$ amount from 5 wt% to 20 wt% (samples are named as NB1, NB2, NB3 and NB4 for 5, 10, 15 and 20 wt%, respectively) implying the enhancement in solubility of Eu^{3+} ions in the host matrix. Apart from this, as shown in the inset of Fig. 4.6 (b), the emission spectral profiles of NB2, NB3 and NB4 are little deviated from the spectral profiles of NB1. To understand the plausible reason for this deviation, the structural analysis has been done again for the higher concentration of $Na_2B_4O_7$, using XRD. Fig. 4.7 shows the XRD patterns of variable wt% $Na_2B_4O_7$ assisted Eu^{3+} doped CAZ. It is apparent from Fig. 4.7, that the pure phase of CAZ has not been obtained in the 10, 15 and 20 wt % $Na_2B_4O_7$ assisted CAZ phosphor.

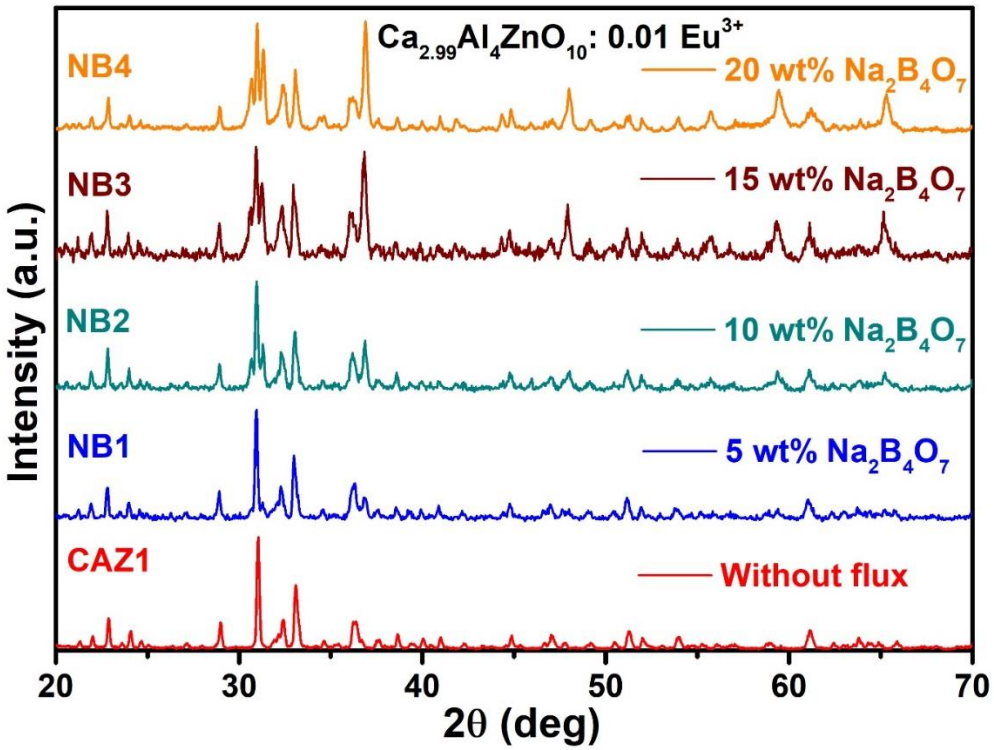

Figure 4.7. XRD patterns of NB1, NB2, NB3 and NB4, respectively.

The presence of few impurity peaks in the XRD patterns result in impure phase formation of $Ca_3Al_4ZnO_{10}$. This might be the plausible reason for the deviation of emission spectral profiles for these phosphors. The optimal amount of flux is therefore considered to be 5 wt% of $Na_2B_4O_7$. Furthermore, the emission intensity variation is also analysed for 2.0 mol% Eu^{3+} doped CAZ phosphor with and without $Na_2B_4O_7$ (named as NB5 and CAZ2, respectively) as shown in Fig. 4.8 (a). The obtained spectral profile is similar to that of NB1 and CAZ1. It is evident from Fig. 4.6 (a) and 4.8 (a) that, the emission intensity of $Na_2B_4O_7$ assisted Eu^{3+} doped CAZ phosphor increases more than twice to that of Eu^{3+} doped CAZ phosphor without flux. The emission spectrum of commercial phosphor (Y_2O_3:Eu^{3+}) has been compared with 2.0 mol% Eu^{3+} doped CAZ phosphor added $Na_2B_4O_7$ (NB5) as flux as shown in Fig. 4.8 (b). The intensity ratio of the intense peak of NB5 to Y_2O_3:Eu^{3+} corresponding to $^5D_0 \rightarrow {}^7F_2$ transition is 0.81, whereas for $^5D_0 \rightarrow {}^7F_0$, $^5D_0 \rightarrow {}^7F_1$, $^5D_0 \rightarrow {}^7F_3$ and $^5D_0 \rightarrow {}^7F_4$ transition the intensity ratio is 3.9, 4.3, 2.9 and 9.5, respectively. This symbolizes the emission of Eu^{3+} doped

CAZ phosphor added $Na_2B_4O_7$ is comparable with the commercial phosphor. Hence, $Na_2B_4O_7$ assisted Eu^{3+} doped CAZ phosphor is a potential candidate for red emitting phosphor for application in solid state lighting devices.

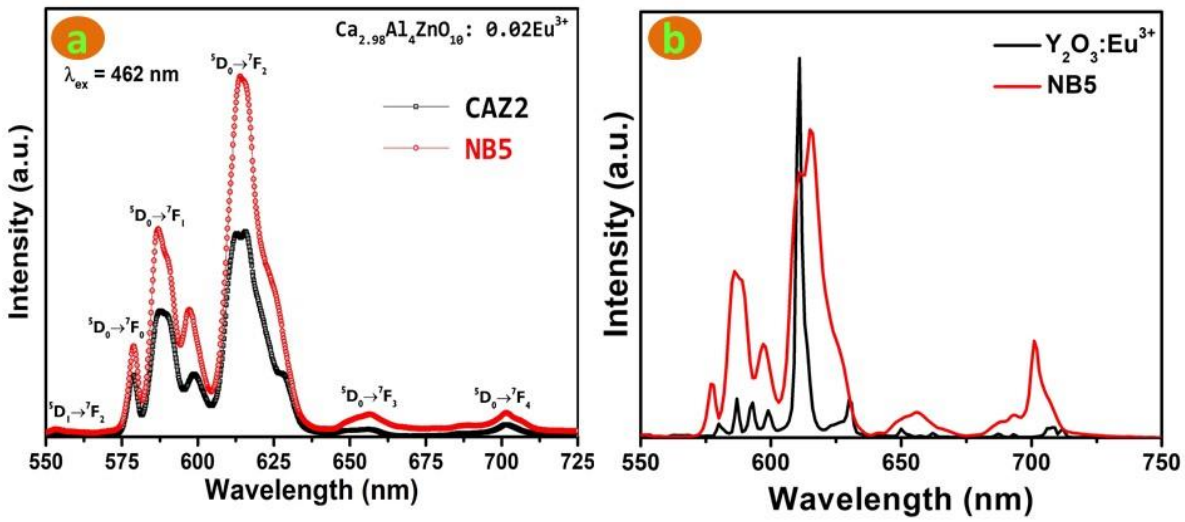

Figure 4.8. Emission spectra of (a) CAZ2 and NB5, and (b) NB5 and Y_2O_3: Eu^{3+} under 462 nm excitation.

On the basis of the observed photoluminescence spectrum of the as-prepared Eu^{3+} doped CAZ powder, schematic energy transfer mechanism is represented in Fig. 4.9 where the Eu^{3+} ions excited to higher energy levels and then returns to the lower energy levels either by the radiative or non-radiative transitions. The upward and downward arrows indicate the excitation and radiative emission, respectively which are shown by solid lines and non-radiative emission transitions are shown by dotted lines. The possible non-radiative transition channels might be either due to Resonant Energy Transfer (RET) or cross-relaxation (CR). The possible cross-relaxation channels for depopulating $^5D_1$,$^5D_2$ and $^5D_3$ higher levels are $^5D_1 + {}^7F_0 \rightarrow {}^5D_0 + {}^7F_3$ (CRC1), $^5D_2 + {}^7F_0 \rightarrow {}^5D_0 + {}^7F_5$ (CRC2), $^5D_2 + {}^7F_0 \rightarrow {}^5D_1 + {}^7F_4$ (CRC3), $^5D_3 + {}^7F_0 \rightarrow {}^5D_1 + {}^7F_6$ (CRC4) and $^5D_3 + {}^7F_0 \rightarrow {}^5D_2 + {}^7F_4$ (CRC5), respectively as shown in Fig. 4.9 [32].

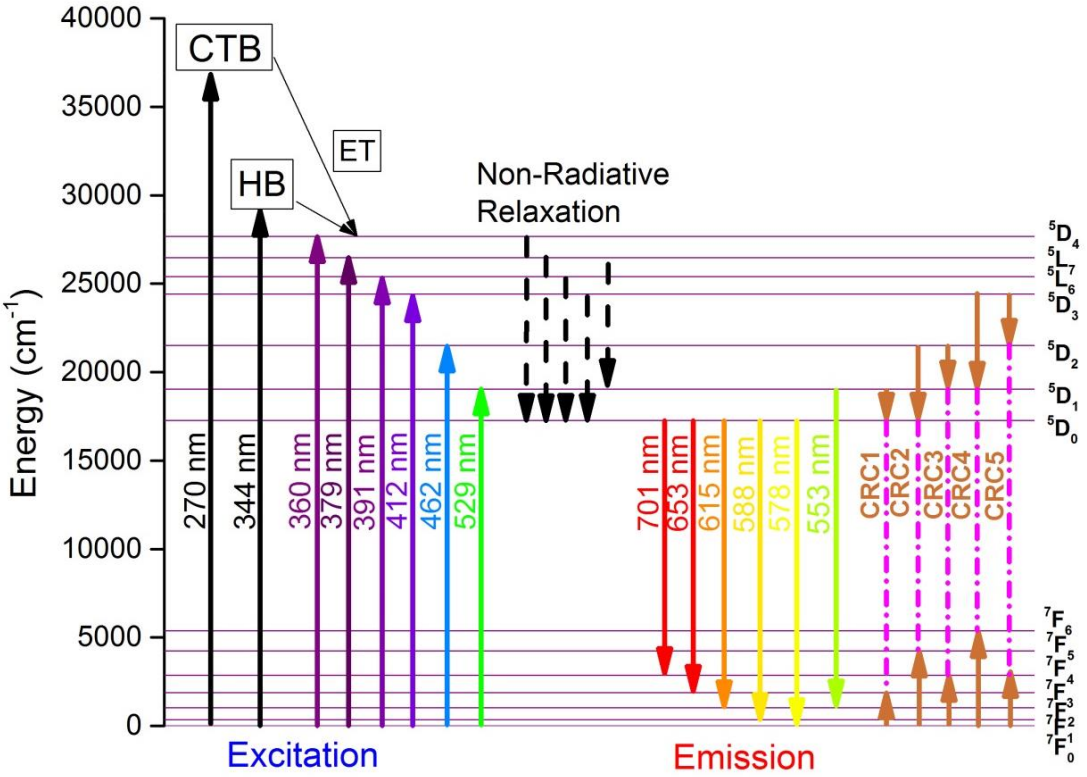

Figure 4.9. Partial energy level diagram of Eu^{3+} ions doped in CAZ phosphor.

4.3.5. Emission spectral analysis using Judd-Ofelt (J-O) theory:

The J-O intensity parameters (Ω_λ) have been evaluated using the emission spectra of RE ions in crystal lattice using the equations given in section 1.13 of chapter 1. The J-O intensity parameters (Ω_λ) provide the information pertaining to the local structure and bonding in the vicinity of RE ions [59]. The J-O analysis is also useful in calculating the radiative transition rates between various levels of the RE ions [60,61,166]. The radiative transition rates for MD and induced ED transitions have been calculated using equations described in section 1.13 of chapter 1. The radiative transition rates ($A_{0\text{-}J}$) corresponding to the MD and ED transitions are presented in Table 4.1. The branching ratios (β_R) evaluated using the expression given in section 1.13 of chapter 1 are listed in Table 4.1 [67]. The branching ratio characterizes that the emission transition possess lasing power if its value is more than 0.50 in comparison with other transitions originating from an excited level [67,68]. From Table 4.1, it is conspicuous that $^5D_0 \rightarrow {}^7F_2$ transition has branching ratio much greater than 0.50, indicating the

potentiality of the present system to serve as a good luminescent phosphor for laser applications under 462 nm excitation.

Table 4.1. Energy (in cm^{-1}), radiative transition rates ($A_{0\text{-}J}$) and branching ratio (β_J) of NB1 and CAZ1 phosphors.

	$^5D_0$-^7F_J	Energy (cm^{-1})	$A_{0\text{-}J}$ (s^{-1})	β_J
NB1	$^5D_0$-$^7F_1$	16893	50	0.03
	$^5D_0$-$^7F_2$	16287	1192	0.92
	$^5D_0$-$^7F_4$	14265	15	0.01
CAZ1	$^5D_0$-$^7F_1$	16893	50	0.04
	$^5D_0$-$^7F_2$	16287	1057	0.91
	$^5D_0$-$^7F_4$	14265	22	0.01

The J-O parameters and transition probabilities values evaluated are presented in Table 4.2. The Ω_6 value cannot be evaluated in the present case, since the transition $^5D_0 \rightarrow {}^7F_6$ is missing in the emission spectra. Higher the value of Ω_2, more structural changes around Eu^{3+} ions and higher covalence between metal-ligand bonds [167]. Higher covalence is due to the lowering of electronic levels of free ions which in turn enhances Ω_2 value. The structural distortion is more and covalent nature is strong in $Na_2B_4O_7$ assisted Eu^{3+} doped CAZ phosphor which has been confirmed from integrated emission intensity ratio I_{ED}/I_{MD} [168,169].

Table 4.2. J-O parameters (Ω_2, Ω_4), and total radiative transition rates (A_R) of NB1 and CAZ1 phosphors.

	Ω_2 (x 10^{-20}) cm^2	Ω_4 (x 10^{-20}) cm^2	A_R (s^{-1})
NB1	4.80	0.20	1291
CAZ1	4.77	0.29	1157

4.3.6. Color chromaticity coordinates and color purity:

To realize the potential of red emission in the as-prepared CAZ phosphors, the CIE chromaticity coordinates determined from luminescence spectra are represented in Table 4.3. Fig. 4.10 represents the CIE color chromaticity coordinates of NB5 lies in pure red region of chromaticity diagram. The obtained CIE coordinates for all the samples are close to NTSC standard value (0.670, 0.330) for red phosphor and also to the commercial red emitting phosphor Y_2O_2S: Eu^{3+} (0.622, 0.351) [170]. The CIE coordinates on the perimeter describes the monochromaticity of the color emission. To have a better understanding about the red emission, the color purity has been calculated using the expression given in section 1.9 of chapter 1. The color purity of the monochromatic emitters should be 100%. The calculated value of color purity for NB5 is found to be 99.09%, indicating extremely pure red emission. The Correlated Colour Temperature (CCT) has been estimated using McCamy's polynomial formula given in section 1.10 of chapter 1. The calculated CCT were found to be in the range of 1930-1994 K and 1788-1801K for the samples under 391 and 462 nm excitation wavelength. The above results suggest that the as-prepared CAZ: xEu^{3+} phosphor can be used as potential red phosphor in white LEDs.

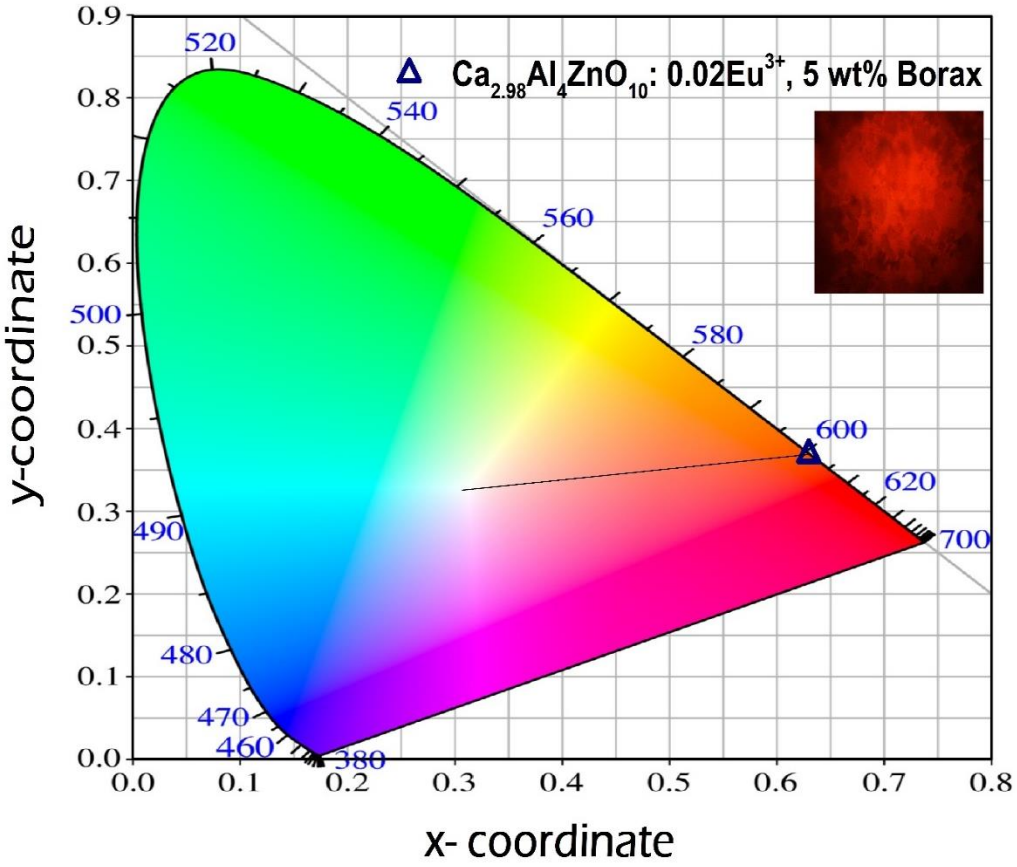

Figure 4.10. CIE chromaticity diagram for NB5 (Inset shows confocal image for the same).

Table 4.3. CIE coordinates and decay time of all the phosphors.

Excitation Wavelength (nm)	**Sample**	**CIE co-ordinates (x, y)**
391	CAZ1	(0.627, 0.372)
	CAZ2	(0.629, 0.370)
	CAZ3	(0.626, 0.374)
	CAZ4	(0.627, 0.372)
462	CAZ1	(0.614, 0.384)
	CAZ2	(0.614, 0.385)
	CAZ3	(0.615, 0.384)

	CAZ4	(0.615, 0.383)
	NF1	(0.631, 0.368)
	NC1	(0.630, 0.368)
	NB1	(0.632, 0.367)
	NB2	(0.635, 0.364)
	NB3	(0.633, 0.365)
	NB4	(0.636, 0.362)
	NB5	(0.630, 0.369)

4.3.7. PL decay analysis:

Fig. 4.11 represents the PL decay spectral features recorded at 615 nm for all the phosphors under 462 nm excitation, namely CAZ1, CAZ2, NF1, NC1, NB1, NB2, NB3, NB4 and NB5, respectively.

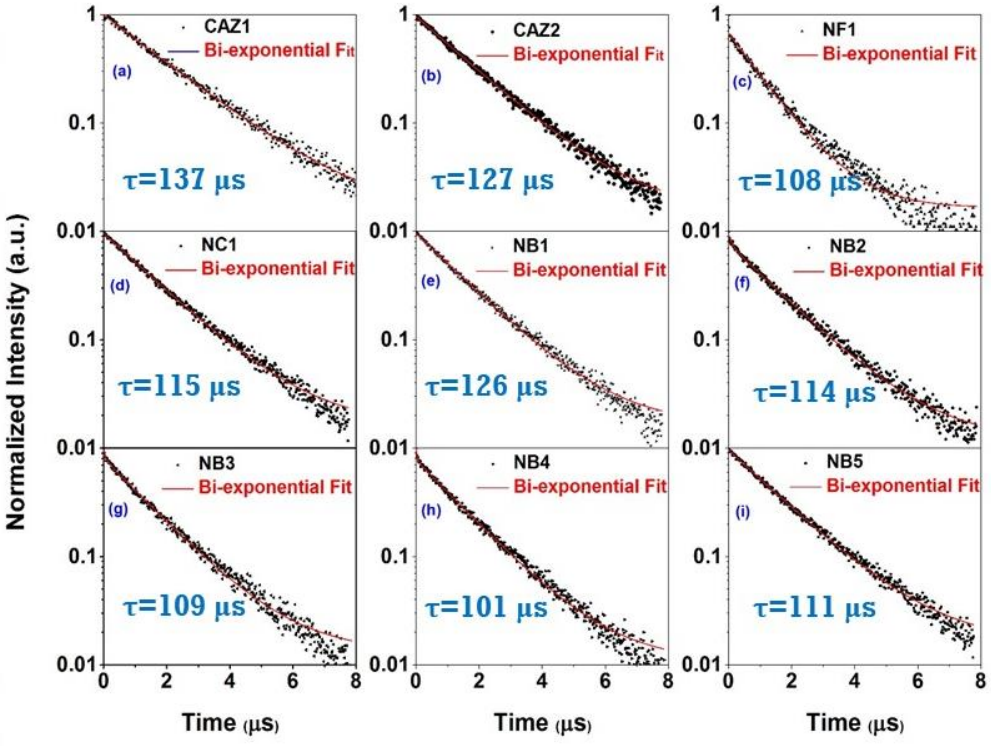

Figure 4.11. PL decay curves for $^5D_0$ level under 462 nm excitation.

The decay curves aptly fitted to bi-exponential equation as discussed in previous chapter (chapter 3). The bi-exponential fit of the decay curves indicates the presence of metal ion in two different environments due to which it has two components of lifetime [171]. The bi-exponential fitting suggests the energy transfer between the activator ions takes place via cross-relaxation process. The average value of lifetime for all the phosphors has been found to be in the range of microseconds. The lifetime values for 1.0 and 2.0 mol% Eu^{3+} doped CAZ phosphor with and without $Na_2B_4O_7$ decreases with increase in Eu^{3+} ions concentration shows energy transfer between Eu^{3+} ions.

Chapter-5

Optimization of synthesis method for Eu^{3+} doped calcium aluminozincate phosphor

CAZ doped with Eu^{3+} has been synthesized using SSR, combustion (CS) and Pechini sol-gel (SG) methods for relatively improved luminescence performance and to optimize synthesis method. The XRD peaks confirm the complete matching of diffraction peaks of the as-synthesized sample with the standard data for $Ca_3Al_4ZnO_{10}$. The morphology of the sample synthesized via SG method shows agglomerated particles with average particle size smaller than the samples synthesized via CS and SSR method. The detail investigation of PL spectra shows significant red emission enhancement in Eu^{3+} doped CAZ phosphor synthesized via SG method. The thermoluminescence (TL) spectral study has been done to estimate the trap depth of the defect centres. The aforesaid results recommend that the Eu^{3+} doped CAZ phosphor synthesized via SG method could be a great choice as red emitter for applications in SSL technology.

5.1. Introduction:

In recent years, pc-wLEDs are enjoying the supremacy over conventional lighting sources (incandescent lamps and CFLs) due to their proficient and promising characteristics such as long-time reliability, power saving ability, energy efficiency, and environment friendliness [172–174]. The remarkable properties of pc-wLEDs have empowered wider variety of lighting, display and scintillation applications. Generally, there are three distinct methods to fabricate wLEDs. The currently used tri-color phosphor materials include Y_2O_2S: Eu^{3+} as red, ZnS:(Cu^{+}, Al^{3+}) as green, and $BaMgAl_{10}O_{17}$: Eu^{2+} (BAM) as blue. Unfortunately, there is some loss of energy in this method and also since blue light gets re-absorbed by green and red emitting phosphors that deteriorate the quality of white light generation [175]. Moreover, the chemical stability of the sulphide phosphors is very low and they are not environment friendly as they are prone to emit sulphur gas into the environment [176–178]. Therefore, it is highly desirable to make superior red phosphors that absorb in the n-UV & blue region and emits in the red to enhance the color rendition, CCT, and energy efficiency of pc-wLEDs. Among various RE ions, Eu^{3+} acts as an efficient red luminescent centre in numerous phosphors, and it is extensively used in lighting applications such as color television and lamp phosphors [179]. Therefore, Eu^{3+} doped inorganic oxide phosphors have attracted much interest for their application in pc-wLEDs due to physical, chemical stability and good luminescence efficiency [77]. In general, high temperature SSR method is used to synthesize various phosphors due to ease of synthesis, low preparation cost and time. The SSR method has some limitations such as inhomogeneous mixing, high sintering temperature with subsequent grinding, which damages the phosphor surface and hence loss in emission intensity [180]. Alternatively, different chemical synthesis methods such as combustion, Pechini sol-gel, molten salt and hydrothermal gained much attention because these methods excel in purity, homogeneity, regular morphology with smaller particles size and low reaction temperature [174,181]. The

chemical synthesis route allows the uniform mixing of chemical and it helps in uniform distribution of particles which upgrade the luminescence characteristics of the phosphor material. For instance, the use of oxidizer and type of fuel, ignition temperature and the amount of water can influence the combustion and hence the particles distribution [182,183]. The unique properties obtained with chemical synthesis method results in enhancement of luminescence of the as synthesized phosphor [177].

In this chapter, synthesis and optimization of luminescence properties for Eu^{3+} doped CAZ phosphor, the synthesis process and the amount of activator ion has been varied. The properties of diversely synthesized Eu^{3+} doped CAZ phosphors, i.e., via solid-state reaction, combustion, and Pechini sol-gel method were investigated. The TL glow curve has been recorded and evaluated trap depth or activation energy and other related parameters.

5.2. Phosphor preparation:

The CAZ phosphors doped with Eu^{3+} ions were synthesized by SSR, combustion, Pechini sol-gel method as described in section 2.3.(1, 2 and 3) of chapter 2. The protocol details of SSR, combustion and sol-gel synthesis methods are represented in Fig. 2.1 (a & b) of chapter 2. The samples prepared by using different methods are coded as mentioned in Table 5.1.

Table 5.1. Sample code for different synthesis method and Eu^{3+} ion concentration.

Synthesis Method	**Eu^{3+} ion concentration (mol%)**	**Sample Code**
Solid state Reaction (SSR)	1.0	CSS1
Combustion (CS)	1.0	CCS1
Pechini Sol-Gel (SG)	1.0	CSG1
	2.0	CSG2
	3.0	CSG3
	4.0	CSG4

5.3. Results and Discussion:

5.3.1. Thermogravimetric analysis (TGA):

The thermal behaviour of dried powder precursor $Ca_3Al_4ZnO_{10}$ phosphor obtained by Pechini sol-gel method has been shown in Fig. 5.1. TGA curve shows three distinct weight loss stages in the temperature range of 70-838˚C. The first weight loss (~7.38 %) occur from 80-183˚C. The second and major weight loss (~59.81 %) occur from 183- 516˚C and the third weight loss (~2.84 %) observed from 516-838˚C.

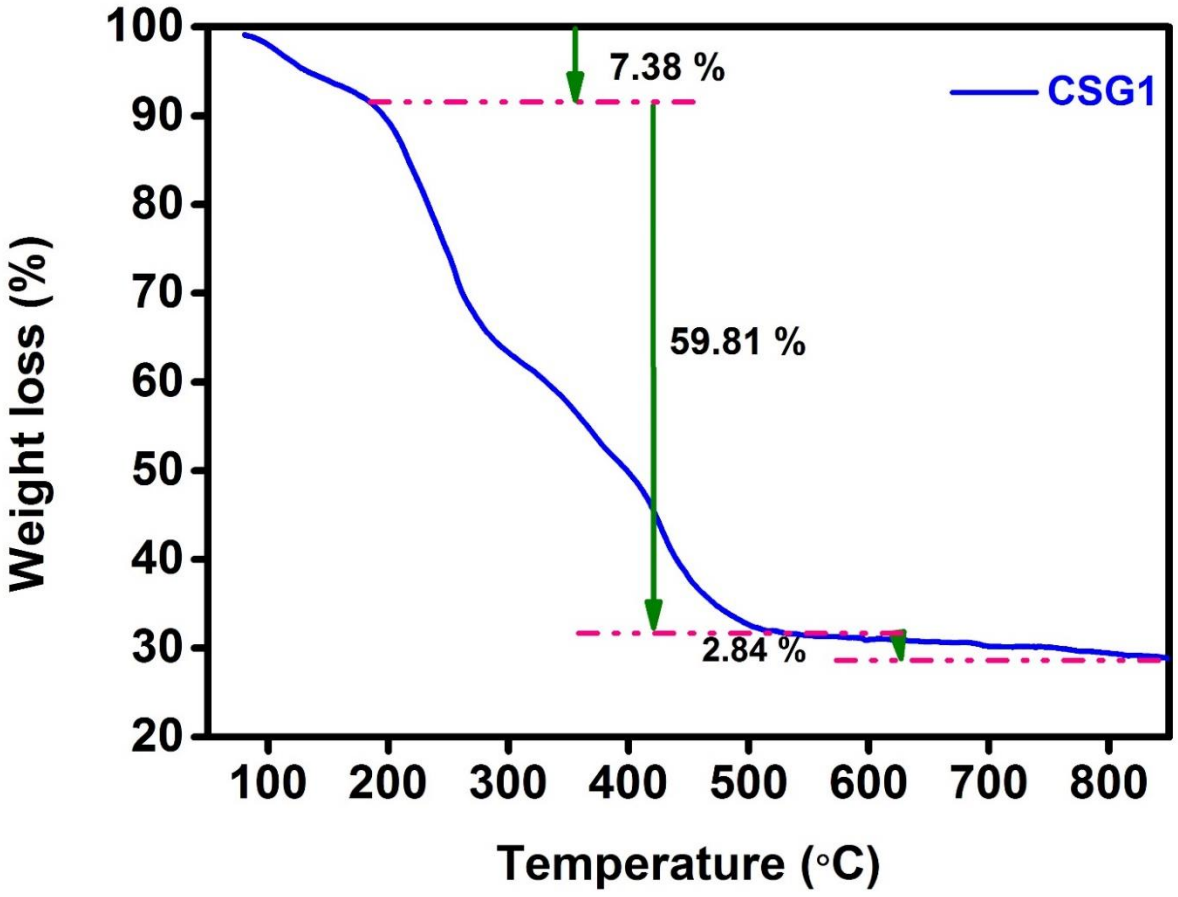

Figure 5.1. Thermogravimetric analysis (TGA) curve for Pechini sol-gel synthesized sample.

The initial two stages of weight loss observed might be due to loss of moisture, exhaustion of organic species, CA and PEG. The next minimal weight loss could be due to the beginning of crystallization of $Ca_3Al_4ZnO_{10}$. The total weight loss in the formation of $Ca_3Al_4ZnO_{10}$ is

about 70%, which is due to the evaporation of different gases and exhaustion of organic species. Therefore, the samples have been sintered at 1000˚C after analysing TGA curve.

5.3.2. Phase analysis: The XRD patterns of three diversely synthesized Eu^{3+} doped CAZ phosphor denoted as CSS1, CCS1, CSG1 & CSG2, CSG3, CSG4 have been recorded and shown in Fig. 5.2 (a) & 5.2(b), respectively. The XRD peak profile of all the samples are indistinguishable and the peaks can be indexed to diffraction peaks of $Ca_3Al_4ZnO_{10}$ having orthorhombic phase with Pca21 space group with reference to the standard data shown in Fig. 5.2 (a & b). This symbolizes that the host lattice synthesized via three different methods has been crystalizes to pure and single-phase CAZ phosphor. Further, this manifest that doping does not cause any remarkable change in the crystal structure of CAZ host. The Eu^{3+} ions have been successfully incorporated into the Ca^{2+} sites owing to the similar ionic radii (r_{Eu3+} = 0.947 Å pm, r_{ca2+} = 1.00 Å) in six coordinated atoms. The close observation of the XRD pattern reveals the CSG1 peaks are relatively sharp and more intense. The sharpness of the diffraction peaks epitomizes high crystallinity of the lattice [75]. The higher crystallinity can be attributed to the addition of PEG in sol-gel synthesis which promotes the formation of crystalline CAZ phosphor and stimulates the growth process [184]. Moreover, in Fig. 5.2 (b), it is conspicuous that the doping concentration has negligible influence on the crystal structure of $Ca_3Al_4ZnO_{10}$ since there is no impurity peak observable in diffraction peaks. Further, Rietveld refinement has been performed on CAZ phosphor synthesized by three different routes, using Fullprof suite software to study the phase purity. The refinement of XRD profile has been described by pseudo-Voigt function (combination of Lorentz and Gaussian function). The unit cell parameters, space group and atom co-ordinate values have been utilized from elsewhere [144]. The Rietveld refinement results affirm that the CAZ lattice synthesized via three different routes crystallizes in orthorhombic structure with Pca21 space group. Fig. 5.2 (c-e) shows Rietveld refinement of CSS1, CCS1 and CSG1, respectively. The structural parameters, unit

cell parameters have been converged and refined. Table 5.2 represents the crystallographic data and detailed refined parameters for CSS1, CCS1 and CSG1 samples, in which the residual factors R_{wp}, R_p and χ^2 are satisfactory.

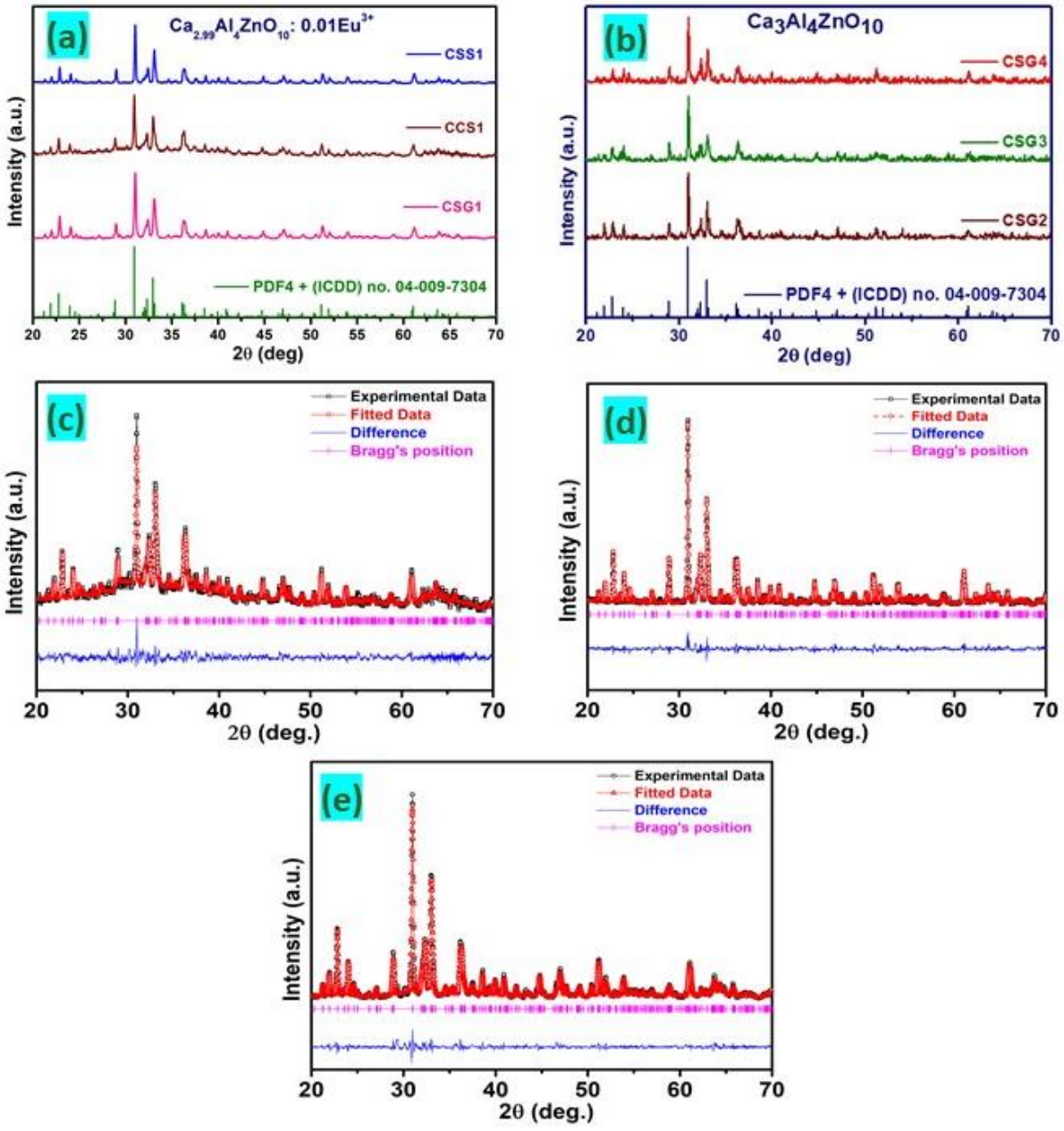

Figure 5.2 (a). XRD patterns of (a) CSS1, CCS1, CSG1; (b) CSG2, CSG3, CSG4; Rietveld refinement of (c) CSS1, (d) CCS1 and (e) CSG1.

The refinement results further indicating pure phase formation of CAZ sample. The goodness of fit (χ^2) value are 1.958 and 1.938 for CSS1 and CSG1, respectively, whereas its

value is slightly higher for CCS1 (4.443). These results indicate that the CAZ phosphor has been successfully synthesized by three different methods without inducing any impurity phase. The crystallite size has been calculated using conventional Debye-Scherrer formula [185]. The calculated average crystallite sizes are found to be 52.8, 38.0, 33.9, 32.5, 31.9 and 30.4 nm for CSS1, CCS1, CSG1, CSG2, CSG3 and CSG4 phosphors, respectively. The decrease in average crystallite size might be due to decrease in sintering temperature. Further, the decrease in crystallite size with increasing dopant concentration might be attributed to lattice distortion due to difference in ionic radii of Eu^{3+} ions and Ca^{2+} ions and increase in crystal field strength [186,187].

Table 5.2. Calculated crystallographic data of CSS1, CCS1, and CSG1 by Rietveld refinement method.

Sample	**CSS1**	**CCS1**	**CSG1**
Symmetry	orthorhombic	orthorhombic	orthorhombic
Space group	Pca21 (29)	Pca21 (29)	Pca21 (29)
a (Å)	16.7424	16.7301	16.7363
b (Å)	5.1375	5.1387	5.1377
c (Å)	10.7132	10.7070	10.7129
V ($Å^3$)	921.497	920.491	921.161
Density (g/cm^3)	3.338	2.747	3.089
R_p (%)	23.0	14.7	31.6
R_{wp} (%)	26.2	17.6	27.1
X^2 (%)	1.935	4.443	1.958

5.3.3. Morphology:

The SEM images for CSS1, CCS1, and CSG1 (two figures with different resolution) are shown in Fig. 5.3 (a-d), respectively. Fig. 5.3 (a) shows the agglomerated particles exhibiting irregular morphology with an average particle size of 1-8 μm. Fig. 5.3 (b) also shows the agglomerated particles with inhomogeneous particles of size 2-10 μm. Fig. 5.3 (c & d) show CSG1 sample at different resolutions that exhibit agglomerated particles with some homogeneity in particle structure. The SEM image of CSG1 sample exhibit dense distribution of particles with an average particle size of 1-3 μm.

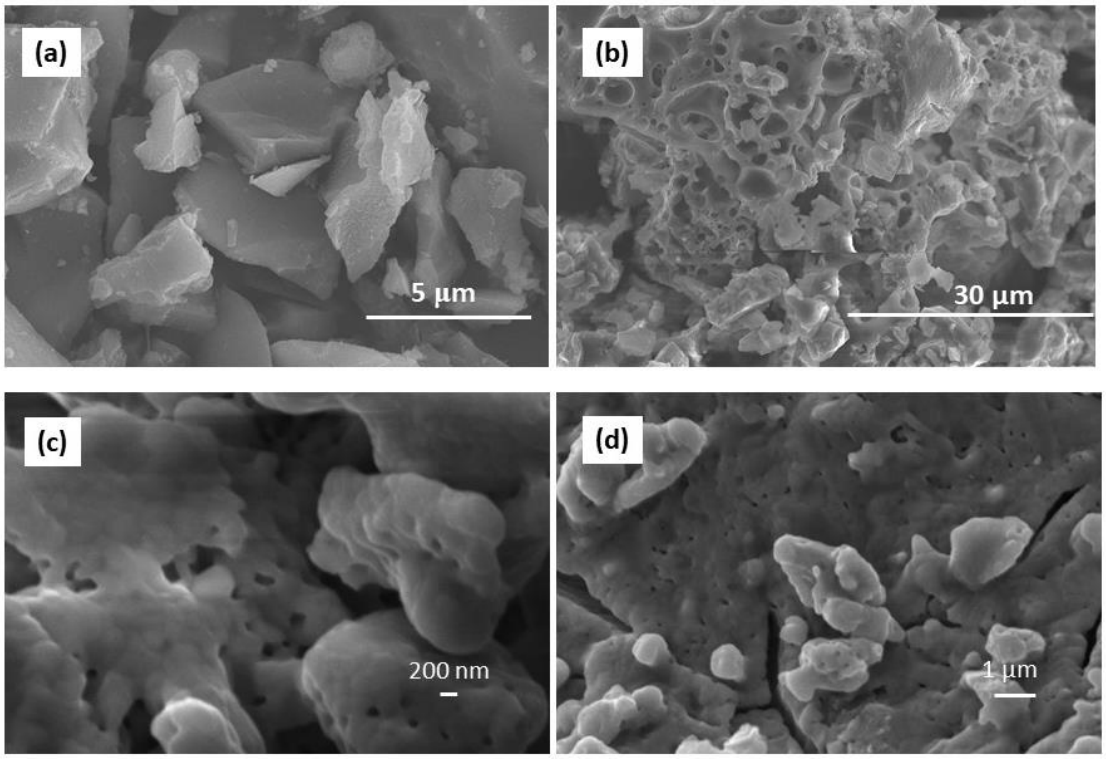

Figure 5.3. SEM micrographs of (a) Solid-state (CSS1), (b) Combustion (CCS1) and (c & d) Pechini sol-gel (CSG1) synthesized phosphors.

The improved morphology of the phosphor can significantly enhance the luminescent properties of phosphor [19]. The improved morphology in sol-gel synthesized phosphors may be due to mixing of chemicals uniformly and slow evaporation of gases during stirring. The

marked difference in morphology of the as-synthesized phosphors via different synthesis methods might be due to different reaction essence [75].

5.3.4. Photoluminescence study: Fig. 5.4 (a) depicts the PL excitation spectra of differently synthesized 1.0 mol% Eu^{3+} doped CAZ phosphor recorded under 618 nm emission wavelength. The spectrum shows peaks at wavelengths 360, 379, 391, 413 and 462 nm, which are attributed to $^7F_0 \rightarrow {}^5D_4$, $^7F_0 \rightarrow {}^5L_7$, $^7F_0 \rightarrow {}^5L_6$, $^7F_0 \rightarrow {}^5D_3$ and $^7F_0 \rightarrow {}^5D_2$ transitions of Eu^{3+} ions, respectively [188,189]. The emission spectra recorded for CSG1 under aforementioned different excitation wavelengths are shown in Fig. 5.4 (b).

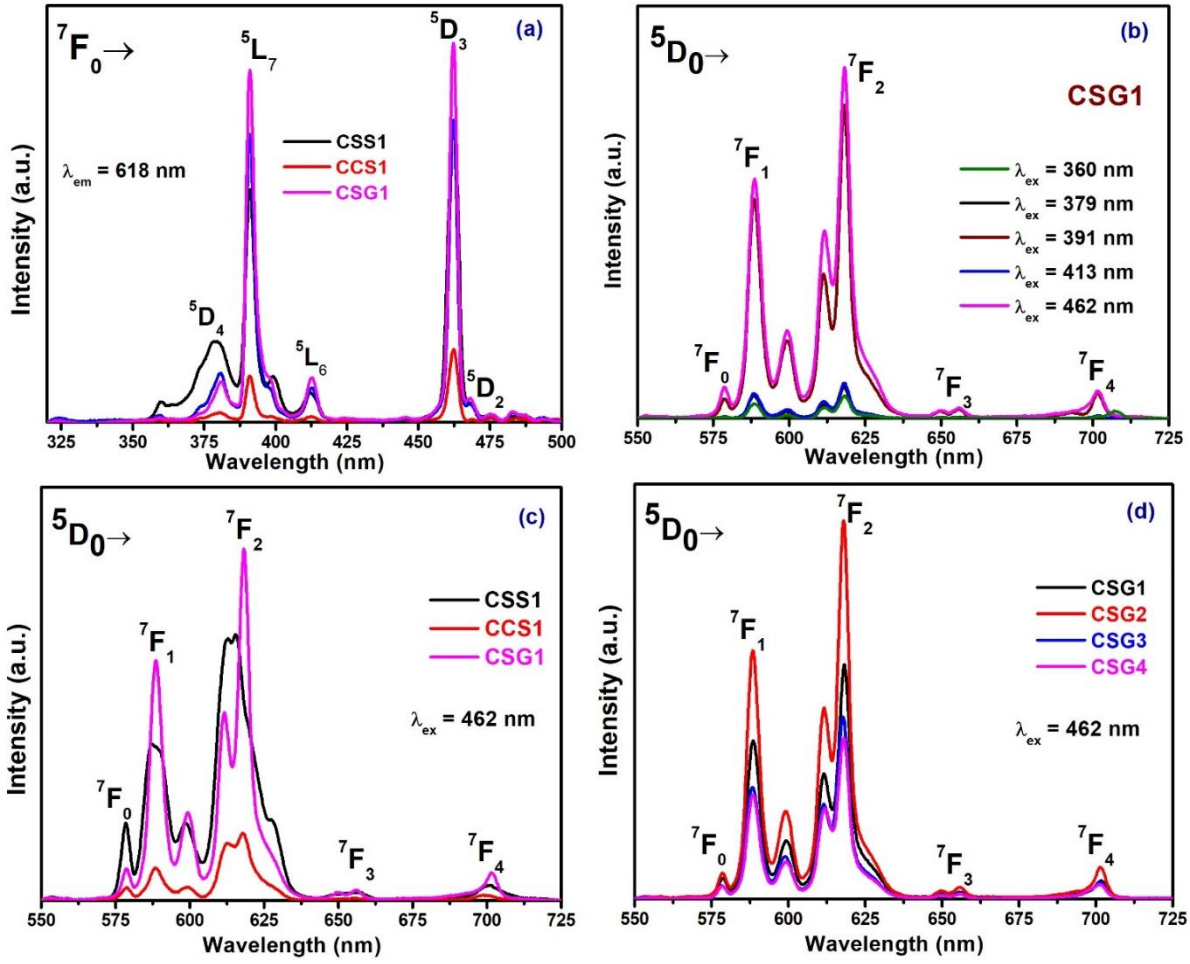

Figure 5.4 (a). Photoluminescence Excitation (PLE) spectra of CSS1, CCS1 and CSG1 (λ_{em} = 618 nm), Emission spectra of (b) CSG1 under different excitation wavelengths, (c) CSS1, CCS1 and CSG1 under 462 nm excitation wavelength and (d) CSG1, CSG2, CSG3 and CSG4 under 462 nm excitation wavelength.

The emission spectra recorded under different excitation exhibit maximum intensity of emission under 462 nm excitation wavelength. The observed emission intensity under 391 nm is also close to the one observed under 462 nm excitation. This conspicuously speaks that the phosphor under investigation can be successfully excited by n-UV and blue light. This prompted us to record the emission spectra for all samples under 462 nm excitation.

5.3.4.1. Comparison of PL spectra:

Fig. 5.4 (c) shows PL spectra of 1.0 mol% Eu^{3+} doped CAZ phosphor synthesized via solid-state (CSS1), combustion (CCS1) and Pechini sol-gel (CSG1) synthesis methods under 462 nm excitation. The emission spectra of all the aforementioned samples show five transitions $^5D_0 \rightarrow {}^7F_0$, $^5D_0 \rightarrow {}^7F_1$, $^5D_0 \rightarrow {}^7F_2$, $^5D_0 \rightarrow {}^7F_3$ and $^5D_0 \rightarrow {}^7F_4$ at 578, 588, 618, 653 and 701 nm respectively with significant change in their intensities [190,191]. The PL intensity is found to be the highest and lowest in case of phosphor synthesized via sol-gel and combustion method, respectively. The sample synthesized via SSR method has moderate emission intensity. Noteworthy, the emission spectra reveal that the sample CSG1 shows significant enhancement in emission intensity as compared to CCS1 and CSS1. From the integrated intensity calculations, we came to know that the emission intensity of CSG1 sample is relatively 5 times more than CCS1 and 1.5 times more than CSS1 phosphor. This suggests the morphology of the phosphor which influences the luminescent properties of phosphors can be changed by changing the synthesis method. The smaller sized particles owe to less scattering losses and can improve the optical properties [192]. As discussed in the previous section, CSS1 sample has agglomerated structure, CCS1 has porous agglomerated particles, and CSG1 has agglomerated particles with uniform morphology and homogeneous structure. This might be due to citric acid which helps in grain growth and homogeneous morphology that improves crystallinity in CSG1 phosphor. Furthermore, very low emission intensity of CCS1 phosphor in comparison with CSS1 and CSG1 can be attributed to the large defect formation on the

surface with rapid evolution of gases which acts as luminescence quenching centres [73,193]. It can be ascertained from the above discussion that, Pechini sol-gel synthesis method is more effective to synthesize CAZ phosphor for its applications in lighting and other display devices. Also, it can be inferred from emission spectra that, Eu^{3+} ions have occupied sites with no inversion centre, since ED ($^5D_0 \rightarrow {}^7F_2$) transition correspond to red emission is dominant over MD ($^5D_0 \rightarrow {}^7F_1$) transition corresponds to orange emission. The ED to MD intensity ratio has been estimated as 1.68, 1.95 and 1.46 for CSS1, CCS1 and CSG1, respectively. The ED to MD intensity ratio also reflects the bonding characteristics of Eu^{3+} with other constituents of the host system. Higher the ED to MD intensity ratio, higher is the covalency [194]. In the emission spectra, CCS1 shows highest covalency among other synthesized phosphors, which indicate most distorted structure of CCS1 as compared to CSS1 and CSG1.

Further, the optimized synthesis method (Pechini sol-gel method) has been taken to optimize the Eu^{3+} concentration in the host system. Fig. 5.4 (d) represents the PL spectra of sol-gel synthesized Eu^{3+} doped CAZ phosphor with varying concentration of activator (1.0, 2.0, 3.0 and 4.0 mol% of Eu^{3+} ions) named as CSG1, CSG2, CSG3 and CSG4, respectively. It can be witnessed from the emission spectra that the integrated emission intensity increases gradually up to 2.0 mol% of Eu^{3+} concentration and decreases beyond. This contemplate that, 2.0 mol% of Eu^{3+} ion concentration in CAZ phosphor is optimum to fabricate single phase red emitting phosphor useful in designing wLEDs. Lowering of emission intensity beyond optimum concentration is due to concentration quenching of luminescence ensuing from non-radiative energy transfer between the activator ions. In such cases, the average critical distance, R_c responsible for energy transfer via exchange interaction can be evaluated using the following expression as already discussed in chapter 3. The value of critical distance is calculated to be 28.04 Å which is much greater than 5 Å. The energy transfer of forbidden transition via exchange interaction occurs mainly due to large overlap between donor and

acceptor ions at shorter critical distance (5 Å) [195]. From the calculated value of critical distance, it can be inferred that the exchange interactions are not responsible for non-radiative transitions and despite multipolar interactions are responsible for energy transfer between Eu^{3+} ions.

Further, the comparison of emission spectra of all the prepared samples along with the standard red phosphor Y_2O_3: Eu^{3+} recorded under 462 nm is shown in Fig. 5.5. It can be observed from the figure that the emission intensity of the optimized phosphor (CSG2) is comparable with the standard phosphor. Also, the integrated emission intensity ratio of CSS1, CCS1, CSG1, CSG2, CSG3 and CSG4 to Y_2O_3: Eu^{3+} for $^5D_0 \rightarrow {}^7F_2$ transition is found to be 0.26, 0.12, 0.40, 1.25, 0.54 and 0.29, respectively under 462 nm excitation. It can be concluded that the Pechini sol-gel synthesized sample is apt for its utility in lighting devices.

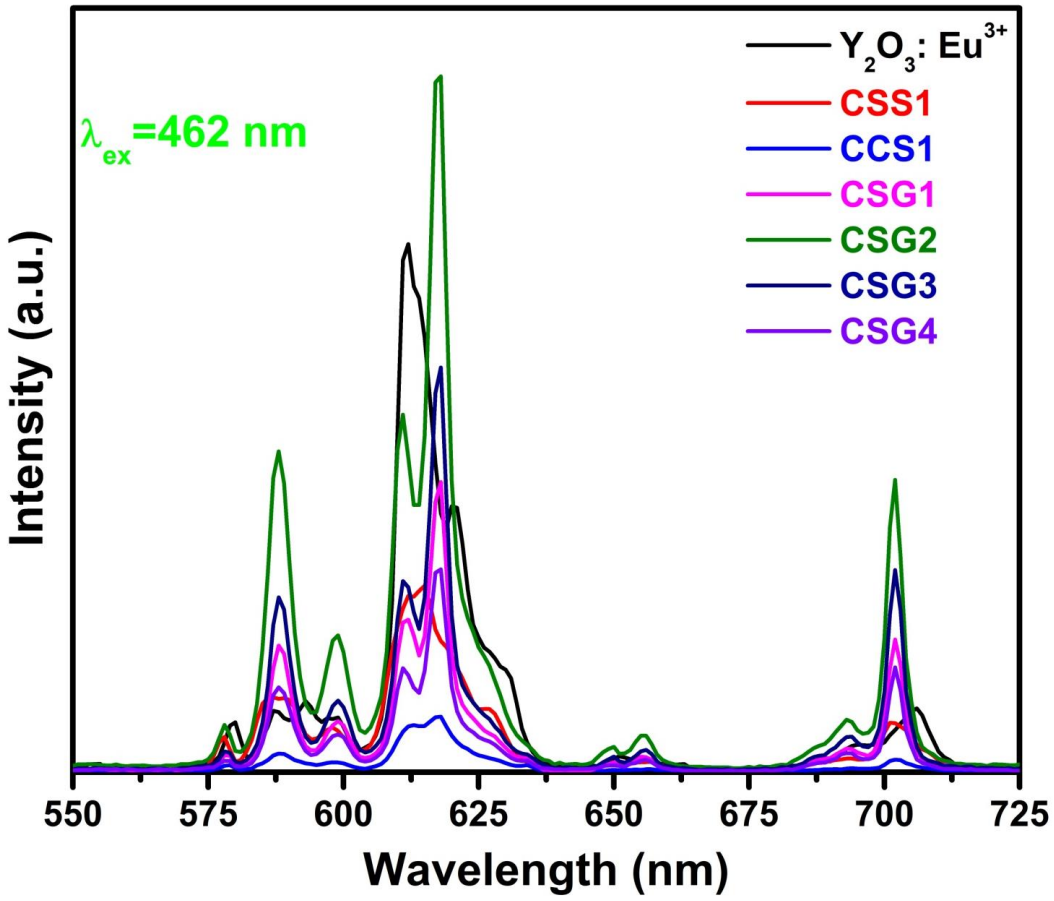

Figure 5.5. Emission spectra of all the prepared samples compared with Y_2O_3: Eu^{3+} under 462 nm excitation.

5.3.4. Color chromaticity coordinates and CCT:

The CIE color chromaticity coordinates for all the as-synthesized phosphors have been calculated and are shown in Table 5.3. The CIE coordinates for all the as-prepared phosphors lie in red region of CIE chromaticity diagram and are in proximity with the coordinates for commercial red phosphor Y_2O_2S: Eu^{3+} (0.622, 0.351). The CIE coordinates for the all the samples are shown in Fig. 5.6. The correlated color temperature (CCT) for the as-prepared phosphors is calculated from the equation given in section 1.10 of chapter 1 and the values are given in Table 5.3.

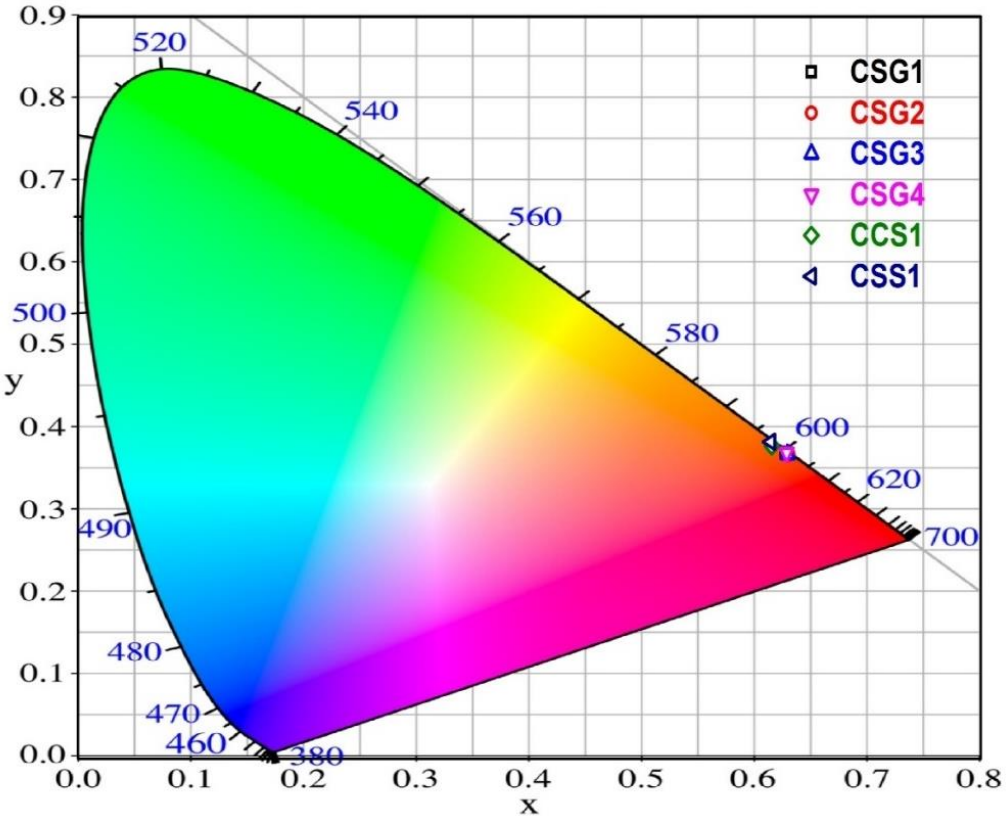

Figure 5.6. Color chromaticity diagram represents CIE coordinates of all the phosphors.

Table 5.3. CIE coordinates, CCT, and decay time, energy transfer parameter (Q), N_0, and R_0 of all the samples.

Samples	CIE Co-ordinates (x, y)	CCT (K)	Decay Time (μs)	Q	N_0 (10^{19} ions/cm^3)	R_0 (Å)
CSS1	(0.614, 0.384)	1792	1.33	-	-	-
CCS1	(0.615, 0.379)	1825	0.88	-	-	-
CSG1	(0.627, 0.371)	1959	1.30	0.38	1.08	3.61
CSG2	(0.630, 0.369)	2006	1.25	0.60	2.17	3.34
CSG3	(0.629, 0.369)	2002	1.18	0.62	3.25	2.95
CSG4	(0.628, 0.371)	1971	0.98	0.68	4.34	2.76

5.3.5. PL decay analysis:

The room temperature PL decay at 618 nm ($^5D_0 \rightarrow {}^7F_2$) recorded for Eu^{3+} in CAZ phosphors synthesized by three different routes and for various concentrations of Eu^{3+} ions under 462 nm (blue) excitation has been shown in Fig. 5.7. The decay curves possess bi-exponential fitting. The average luminescence lifetime (τ) values evaluated are shown in Table. 5.3. The average lifetime decreases from CSG1 to CSG4 with increase in Eu^{3+} ion concentration signifying the energy transfer between Eu^{3+} ions.

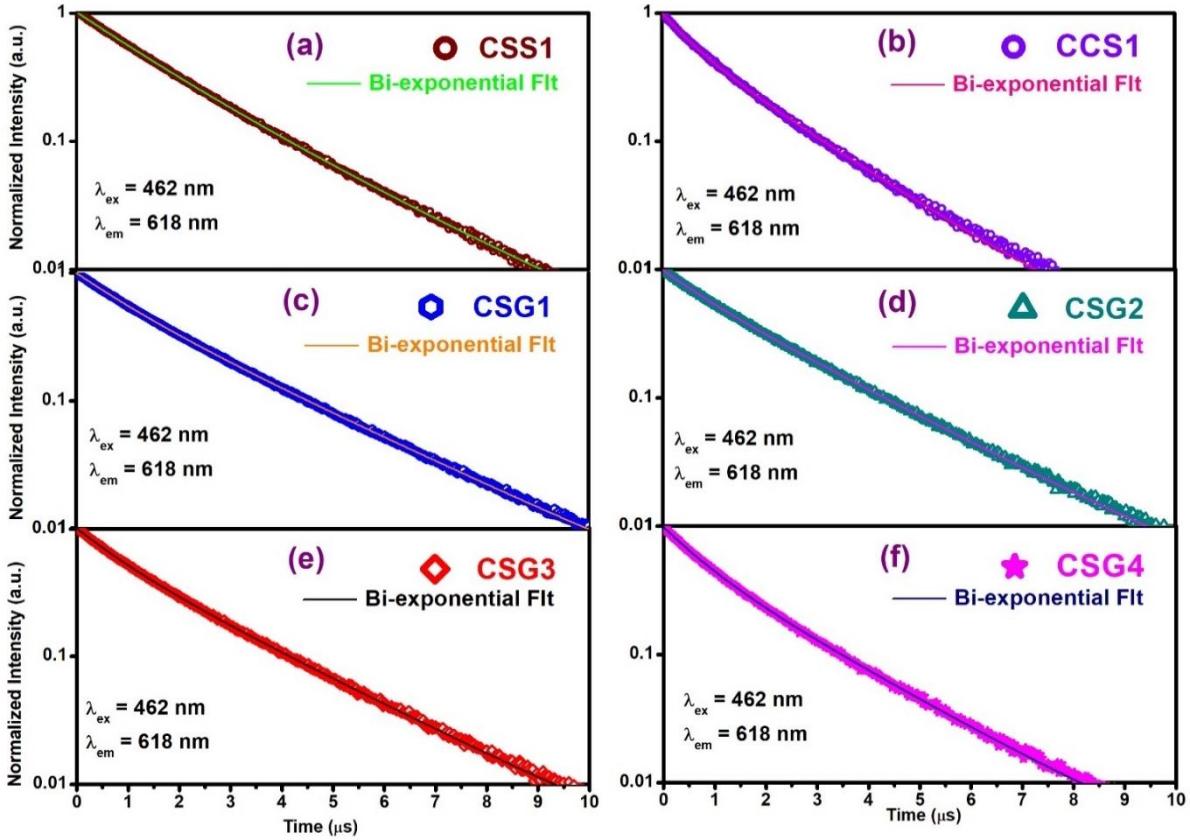

Figure 5.7. Decay curves for $^5D_0$ level of Eu^{3+} for all the synthesized phosphors.

According to Inokuti-Hirayama (I-H) model, the energy transfer via multipolar interaction between Eu^{3+} ions is responsible for the non-exponential behaviour of PL decay. The I-H model has been applied on decay curves to further explore the energy transfer mechanism involved between Eu^{3+} ions. In the I-H model, the luminescence decay intensity relates with time as described in section 1.12 of chapter 1. Fig. 5.8 shows the I-H fitting of the decay curves for s=6 indicating dipole-dipole interaction between Eu^{3+} ions.

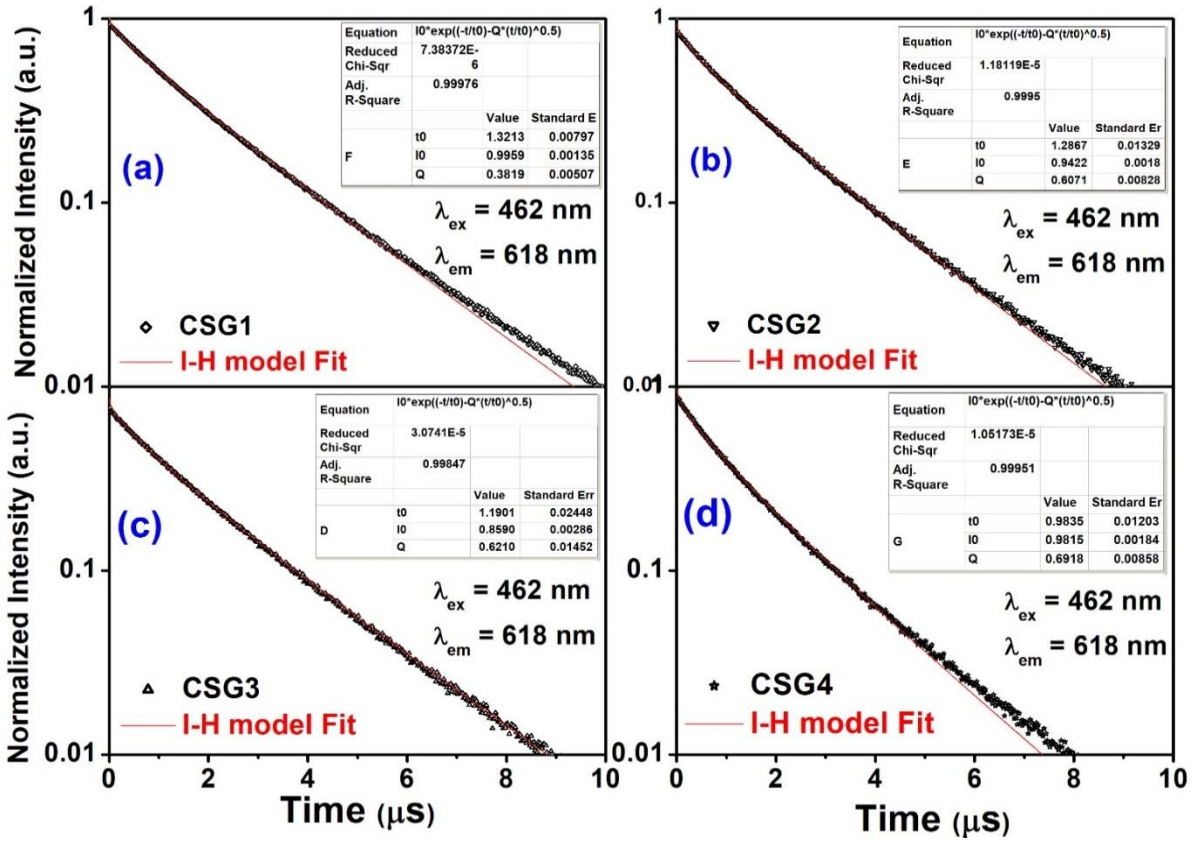

Figure 5.8. I-H fitting of decay curves for CSG1, CSG2, CSG3, and CSG4.

The energy transfer parameter (Q) is defined as:

$$Q = \frac{4\pi}{3}\Gamma\left(1-\frac{3}{s}\right)N_0R_0^3 \qquad (2)$$

where the Euler function is represented as Γ(s) whose value is taken to be 1.77, 1.43 and 1.30 for s=6, 8 and 10, respectively. N_0 is the acceptor concentration per cubic centimetre and R_0 is the critical distance defined as distance between donor and acceptor for which energy transfer rate to the acceptor is equal to the rate of intrinsic decay of the donor [196,197]. The energy transfer parameter, Q has been evaluated from the fitting of decay curves, and R_0 values have been evaluated by using Q values in equation 6. Fig. 5.9 shows the variation of decay time and fitting parameter with Eu^{3+} concentration. The value of Q and N_0 increases, whereas R_0 decreases with increase in concentration of Eu^{3+} ions as given in Table 5.3. This may be due

to enhancement in the energy transfer from the excited Eu^{3+} ions to the unexcited Eu^{3+} ions and finally due to other quenching centres [198].

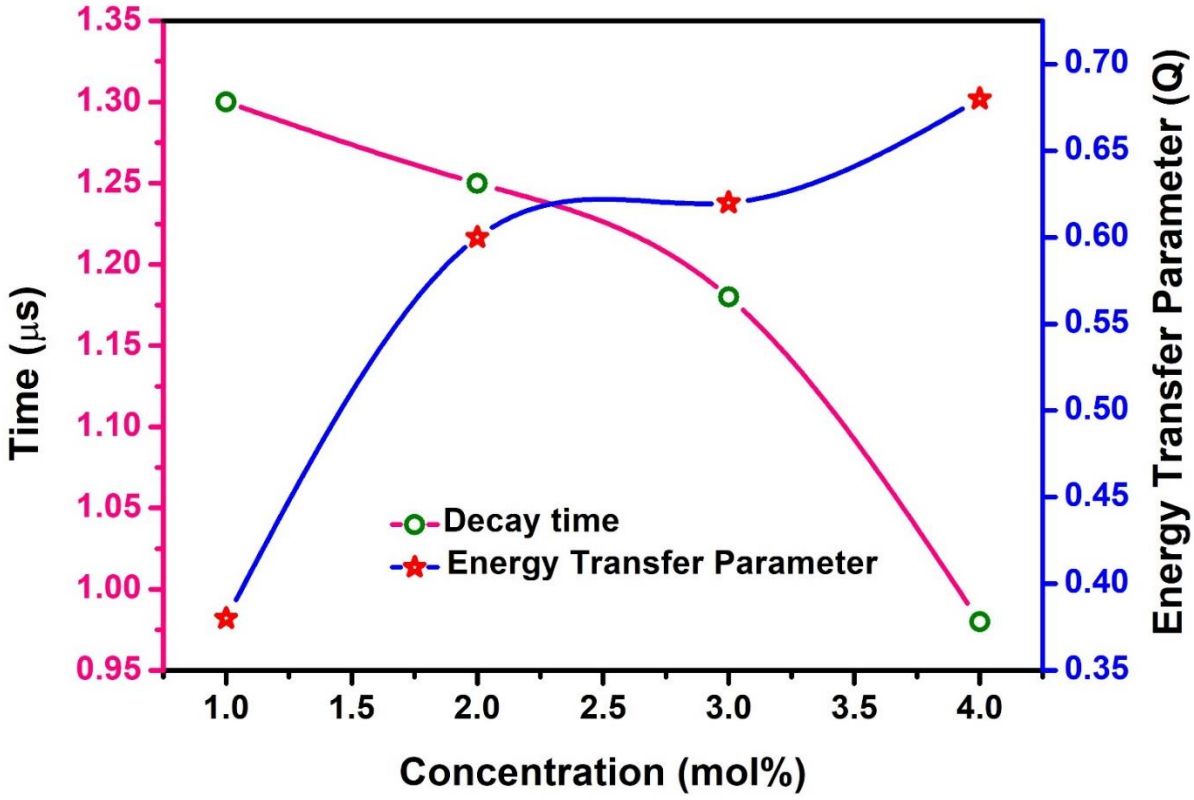

Figure 5.9. Variation of decay time and energy transfer parameter with Eu^{3+} ions concentration.

5.3.6. Thermoluminescence (TL) properties:

The TL glow curve of Pechini sol-gel synthesized 1.0 mol% Eu^{3+} doped CAZ phosphor (CSG1) irradiated by β-radiations for a dose of 1.0 kGy at different temperature is shown in Fig. 5.10. The TL glow curve exhibit maximum intensity at 225°C. TL is a phenomenon in which luminescence occurs via thermal stimulation. In thermally stimulated luminescence (TSL or TL), free charge carriers get trapped at defect centres on exposure to radiations. Such trapped charges re-combine (electron and hole) to produce luminescence [199]. In Fig. 5.10, the TL curve shows maximum intensity at higher temperature region indicating the presence of deep trap centres [200]. The TL phenomenon is having its applications in dating

archaeology, dosimetry and determination of defect centres and impurities in rocks [201]. Peak shape method has been used to explore the properties of trapping centres.

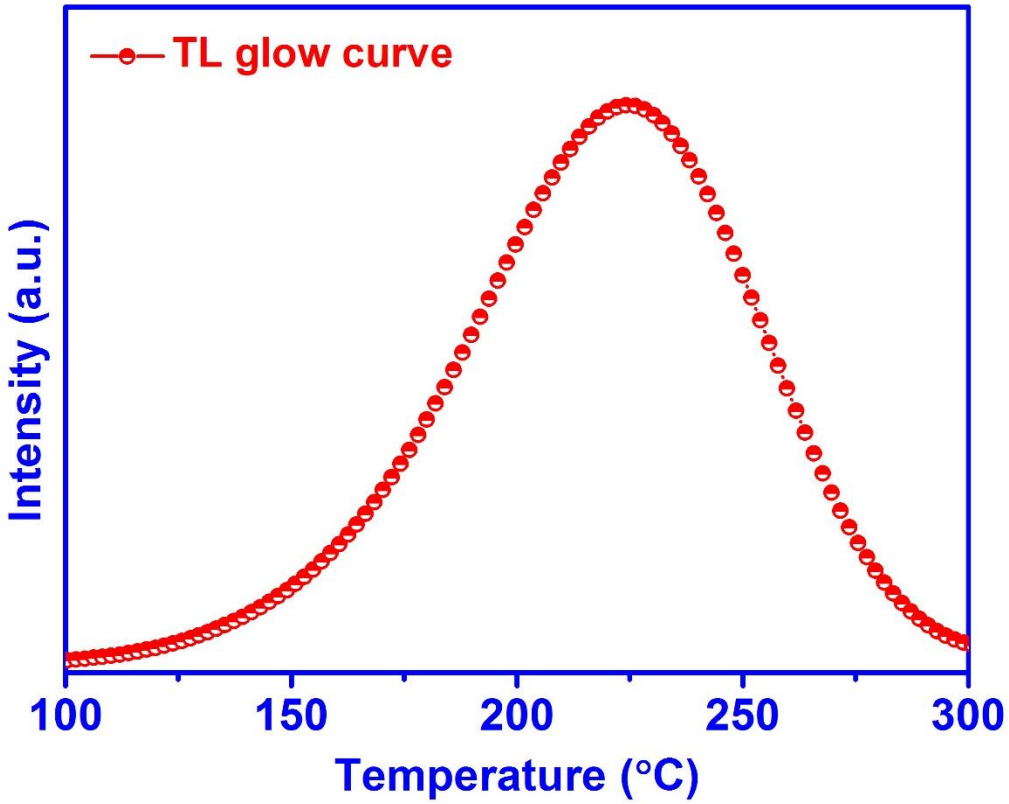

Figure 5.10. TL glow curve of β-irradiated 1.0 mol% Eu^{3+} doped CAZ phosphor (CSG1).

From the recorded TL curve, employing peak shape method, the peak trapping parameters such as trap depth/activation energy (E), order of kinetics (b), rate of electron ejection also known as escape frequency (s) have been evaluated. The empirical formula used to derive the parameters is given by:

$$E_\alpha = C_\alpha \left(\frac{kT_m^2}{\alpha}\right) - b_\alpha kT_m \qquad (7)$$

here, k indicates Boltzmann constant, T_m represents the peak temperature, C_α and b_α are the parameters relative to α (α = τ, δ, and ω), where, τ (τ = T_m-T_1) is low temperature half width, δ (δ = T_2-T_m) is high temperature half width and ω (ω = T_2-T_1) is full width at half maximum. The parameters C_α and b_α can be evaluated using the following set of equations [202,203]:

$$C_\tau = 1.51 + 3(\mu_g - 0.42);\ b_\tau = 1.58 + 4.2(\mu_g - 0.42) \quad (8a\&b)$$

$$C_\delta = 0.98 + 7.3(\mu_g - 0.42);\ b_\delta = 0 \quad (9a\&b)$$

$$C_\omega = 2.52 + 10.2(\mu_g - 0.42);\ b_\omega = 1 \quad (10a\&b)$$

here, $\mu_g = \frac{\delta}{\omega}$ is the geometrical form factor. It relates with the order of kinetics (b). The values of C_α are 1.63, 1.27 and 2.92, and b_α are 1.74, 0 and 1 for α=τ, δ and ω, respectively. Theoretically geometrical form factor value close to 0.42 implies the first order kinetics and closer to 0.52 indicates second order kinetics [185,204]. The activation energy (E) is an average value of E_α. In the present case, T_m=225°C, T_1=184°C, T_2=260°C. The calculated E_α values are 0.698, 0.775 and 0.736 eV for α=τ, δ and ω; b_α values are 1.748, 0, and 1 for α=τ, δ and ω respectively. Thus, the mean activation energy is found to be 0.736 eV for 225°C and the order of kinetics is general order kinetics (b=1.8). After evaluating the activation energy and order of kinetics, escape frequency can be estimated using the following expression:

$$s = \frac{\beta E}{kT_m^2} \exp\left(\frac{E}{KT_m}\right)(1 + (b-1)\Delta_m)^{-1};\ \Delta_m = \frac{2KT_m}{E} \quad (11)$$

β is heating rate [203]. The evaluated escape frequency (s) is found to be 6.8 x10^7, 3.7 x10^8 and 1.5 x10^8 Hz for τ, δ and ω, respectively. The mean value of escape frequency is 2.0 x10^8 Hz. All these results suggest the candidature of as-prepared phosphors in dosimetry applications.

Chapter-6

Color tunability and energy transfer studies of Dy^{3+}/Eu^{3+} co-doped calcium aluminozincate phosphor for solid state lighting applications

Dy^{3+} doped and Dy^{3+}/Eu^{3+} co-doped CAZ phosphors have been synthesized by using Pechini sol-gel method. Structural and morphological analysis was carried out by using XRD and FE-SEM. The PL spectra were recorded and energy transfer mechanism between Dy^{3+} and Eu^{3+} ions were studied using Dexter and Reisfeld's approximation. The colorimetric properties were studied by evaluating CIE coordinates and correlated color temperature. The energy transfer mechanism was analysed by applying Inokuti-Hirayama model on decay curves as well. The thermoluminescence glow curve analysis reveals two trap centres in the present host. The obtained results indicate that the CCT can be tuned from warm to cool region and color tunability can also be achieved in Dy^{3+}/Eu^{3+} co-activated CAZ phosphor by varying the excitation wavelength or activator concentration in the host lattice and hence can be effectively utilized in wLEDs.

6.1. Introduction:

Nowadays, wLEDs have pursued great attention due to their properties of low toxicity, low power consumption, high efficiency, and higher durability as compared with conventional lighting sources [205–207]. There are diverse ways to mimic sunlight artificially using white light emitters: (i) by making an assembly of red, green and blue LED. Since it requires independent output power control on each LED, it is difficult to achieve white light using tri-color LEDs and also it is expensive [208]. (ii) By coupling yellow phosphor (YAG: Ce) and blue LED (InGaN) chip. The spectral emission in this method results in poor color rendering index (CRI) and insufficient color temperature due to halo effect making it less efficient [209,210]. (iii) By coating a mixture of red, green, and blue phosphor on n-UV/UV LED, which is well-known as multiphase phosphor converted white LED (pc-wLED). However, trichromatic phosphors based pc-wLED offers low luminescence efficiency due to re-absorption of blue light by red and green emitting phosphors [209,211]. To achieve sunlight like emission with high CRI ($R_a > 80$) and low correlated color temperature (CCT < 4500K), it is expected that coactivated single phase phosphor will give full color emission for application in display devices. The development of co-doped single-phase phosphor provides color tunability and relaxed perception to human eyes [45,212].

Quite recently, RE doped inorganic phosphors have attracted interest to tune the emission properties by co-doping RE ions. Among various RE ions, Dy^{3+} doped in inorganic phosphor is used in single phase phosphor for achieving white light emitting phosphor. The Dy^{3+} doped phosphor gives strong emission in yellow and blue spectral region, which also lacks in red component. In order to tune the nature of white light from cool to warm white light, and to improve the CRI by introducing red component in the emission spectral profile, Eu^{3+} can serve as co-activator in Dy^{3+} doped inorganic phosphor [213,214]. In Dy^{3+}/Eu^{3+} co-doped phosphor,

the energy transfer from Dy^{3+} to Eu^{3+} ions arise, since the emission band of Dy^{3+} overlap with excitation band of Eu^{3+} indicating Dy^{3+} not only act as an activator but also as sensitizer.

In this chapter, Dy^{3+} activated and Dy^{3+}/Eu^{3+} co-activated CAZ have been synthesized via Pechini sol-gel method. The structural, morphological, and PL properties have been examined to explore its potentiality. The PL decay spectra have been recorded to study the energy transfer process in detail. The colorimetric properties have also been investigated for its vital significant application in display devices. The TL study has been conducted to observe the defects/trap centres in the host.

6.2. Sample preparation:

To prepare CAZ phosphors doped with Dy^{3+} ions and co-doped with Dy^{3+}/ Eu^{3+} ions, the stoichiometric ratio of nitrate precursors ($Ca(NO_3)_2.4H_2O$, $Zn(NO_3)_2.6H_2O$, $Al(NO_3).6H_2O$) were taken and then individually dissolved in de-ionized (DI) water. RE oxides (Eu_2O_3 and Dy_2O_3) were individually dissolved in nitic acid. All the nitrate precursors dissolved in DI water were mixed and then RE oxides dissolved in nitric acid were added into the solution. The detail synthesis procedure is described in section 2.3 and Fig. 2.1 (b) of chapter 2. The samples are named as D1, D2, D3, D4 and D5 for 1.0, 2.0, 3.0, 4.0 and 5.0 mol% of Dy^{3+} respectively in CAZ. The sample D1E1 represents 1.0-1.0 mol% of Dy^{3+}-Eu^{3+} co-doped CAZ phosphor. Samples named as DE1, DE2, DE3, and DE4 represents 3.0 mol% Dy^{3+} with 1.0, 2.0, 3.0 and 4.0 mol% of Eu^{3+} respectively in CAZ phosphor.

6.3. Results and Discussion:

6.3.1. Structure and phase analysis:

The XRD patterns of Dy^{3+} and Dy^{3+}/Eu^{3+} co-activated CAZ phosphors for variable sensitizer and activator concentration (namely D0, D1, D5, DE1 and DE4) annealed at 1000°C were recorded and shown in Fig. 6.1 (a). The diffraction peaks of represented samples

under investigation possess complete matching with the standard data of $Ca_3Al_4ZnO_{10}$. No impurity peak was observed in XRD patterns of the samples. The absence of any impurity peak in XRD patterns of the samples indicate single phase formation of CAZ phosphor having orthorhombic structure in Pbc2 space group. No structural changes were observed for Dy^{3+} activated and Dy^{3+}/Eu^{3+} co-activated CAZ phosphor by varying sensitizer concentration and/or by increasing activator concentration. Since the ionic radii of six coordinated Dy^{3+} (0.912 Å) and Eu^{3+} (0.947 Å) ions is similar to the Ca^{2+} ion (1.0 Å) in six coordination, it is expected that Dy^{3+} and Eu^{3+} ions successfully substitute the Ca^{2+} sites. The observed diffraction peaks are strong and sharp indicate high crystallinity in the as-prepared phosphors which is desirable for good luminescence.

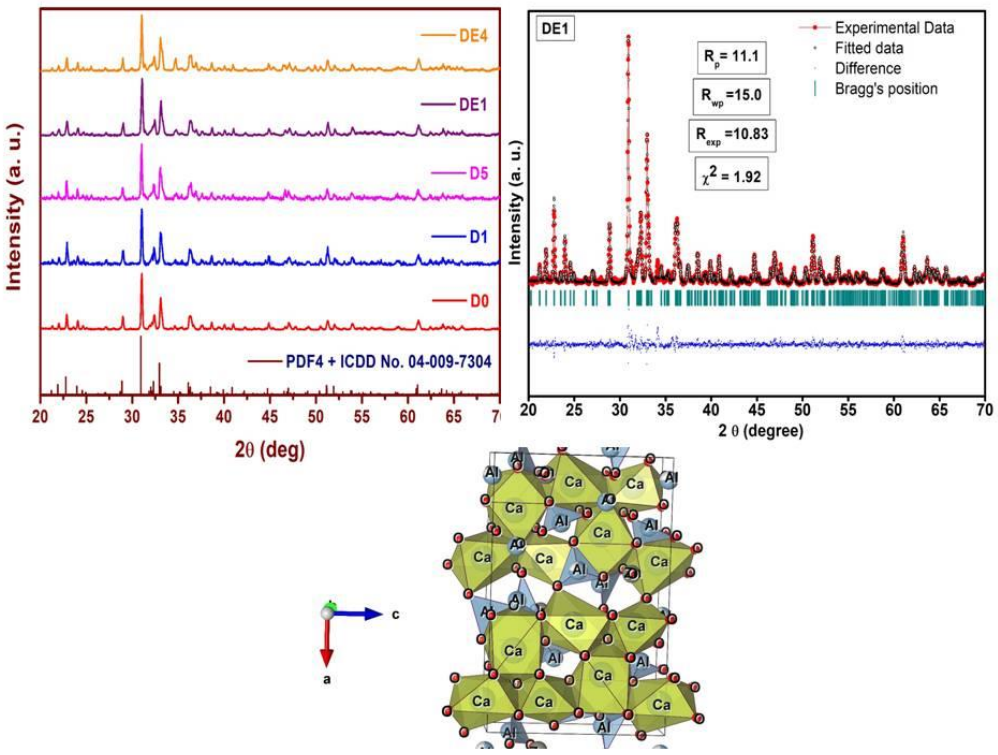

Figure 6.1 (a). XRD patterns of D0, D1, D5, DE1 and DE4. (b) Rietveld refinement of DE1 and (c) crystal structure of $Ca_3Al_4ZnO_{10}$.

To ascertain the crystal structure of the as synthesized phosphor, the Rietveld refinement of DE1 has been conducted using Fullprof suite software. The refinement pattern of DE1 is shown in Fig. 6.1 (b) and various parameters obtained are presented in Table 6.1. The profile

shape refinement has been described by pseudo-Voigt function. The initial parameters, space group and atom co-ordinates have been taken from elsewhere [144]. The refinement results indicate the phosphor crystallizes in pure phase orthorhombic structure of $Ca_3Al_4ZnO_{10}$ with Pca21 space group. The goodness of fit ($\chi 2$) value for DE1 is 1.92, which indicates pure phase for $Ca_3Al_4ZnO_{10}$ phosphor under investigation.

Table 6.1. Rietveld refinement parameters.

Sample	**DE1**
Symmetry	orthorhombic
Space group	Pca21 (29)
a (Å)	16.7541
b (Å)	5.1423
c (Å)	10.7204
V ($Å^3$)	923.643
Density (g/cm^3)	3.603
R_p (%)	11.1
R_{wp} (%)	10.83
χ^2 (%)	1.92

The average crystallite sizes using Debye-Scherrer equation have been estimated for D0, D1, D5, DE1 and DE4 are 37.4, 43.8, 33.0, 37.6 and 42.2 nm, respectively. Fig. 6.1 (c) shows the crystal structure of $Ca_3Al_4ZnO_{10}$ modelled using Vesta software based on the obtained atomic coordinates from XRD refinement. The basic structural units of $Ca_3Al_4ZnO_{10}$ is a continuous 3D structure of (Al, Zn) and Zn tetrahedra in which the characteristic structural unit is five membered rings with calcium ions inside them and three membered rings from aluminium-zinc tetrahedra parallel to yx plane. Oxygen atoms form distorted octahedra in the

form of antiprisms. These rings are connected translationally with each other along the x-axis on their common vertex, and with the other two rings, connected by double helical axis forming continuous layers. These layers are interconnected by meta-aluminate chains of Al-tetrahedra (forming a continuous 3D network) [144].

6.3.2. Morphology:

FE-SEM image of DE1 represents surface morphology as shown in Fig. 6.2. The FE-SEM image depicts uniform and denser distribution of grains. The particles are well separated with textural boundaries. The average particle size of DE1 is approximately between 10-50 nm.

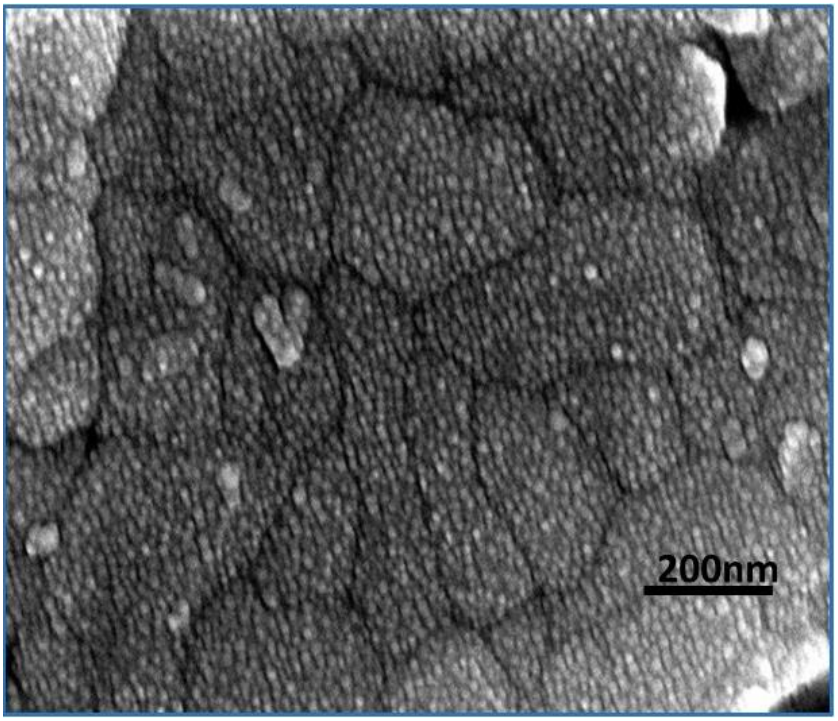

Figure 6.2. FE-SEM image of DE1.

6.3.3. Photoluminescence analysis:

The luminescence behaviour of Dy^{3+} doped and Dy^{3+}/Eu^{3+} co-doped CAZ phosphor was examined from PL spectral measurements. Fig. 6.3 (a & b) show the PL excitation and PL emission spectra of $Ca_{3-x}Al_4ZnO_{10}$: xDy^{3+} ($1.0 \leq x \leq 5.0$ mol%) recorded under 577 nm emission and 384 nm excitation wavelength, respectively. The PLE spectra revealed four bands located

at 345, 363, 384, and 424 nm due to intra f-f transitions attributed to the $^6H_{15/2}\rightarrow{}^6P_{7/2}$, $^6H_{15/2}\rightarrow{}^6P_{5/2}$, $^6H_{15/2}\rightarrow{}^4I_{13/2}$ and $^6H_{15/2}\rightarrow{}^4G_{11/2}$ electronic transitions, respectively as shown in Fig. 6.3 (a) [215]. Highly intense excitation peak at 384 nm has been ascribed to $^6H_{15/2}\rightarrow{}^4I_{13/2}$ transition. This might be due to highest absorption at this particular wavelength.

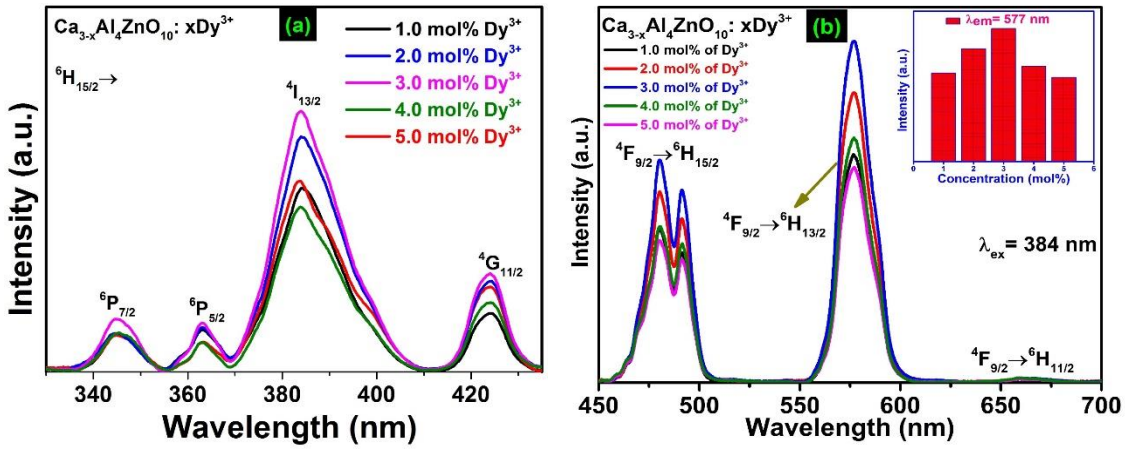

Figure 6.3. Photoluminescence (a) excitation and (b) emission spectra of D1, D2, D3, D4 and D5. (Inset: Histogram showing intensity variation of emission at 577 nm with Dy^{3+} concentration).

Therefore, the PLE spectra of Dy^{3+} doped CAZ phosphors authenticate the usage of n-UV LED as an effective excitation source to pump these ions to obtain intense emission. It is conspicuous that, with increase in Dy^{3+} ion concentration, the intensity of the excitation bands enhances up to 3 mol% and then show decrement with increase in Dy^{3+} ion concentration. Fig. 6.3 (b) represent the PL spectra recorded for D1, D2, D3, D4 and D5 phosphors, which reveals two intense bands at 480, 577 nm and a very weak peak at 663 nm attributed to $^4F_{9/2}\rightarrow{}^6H_{15/2}$, $^4F_{9/2}\rightarrow{}^6H_{13/2}$ and $^4F_{9/2}\rightarrow{}^6H_{11/2}$ electronic transitions respectively. Among these transitions, $^4F_{9/2}\rightarrow{}^6H_{13/2}$ transition observed in yellow region at 577 nm and $^4F_{9/2}\rightarrow{}^6H_{15/2}$ transition observed in blue region at 480 nm are ascribed to forced ED and MD transitions, respectively [40,214,215]. In the PL spectra, ED transition is more pronounced indicating that Dy^{3+} ions are located at a site without an inversion centre. Since the ionic radii of Dy^{3+} (0.912 Å) is smaller than the ionic radii of Ca^{2+} (1.0 Å) coordinated with six atoms, Dy^{3+} ions can easily enter into Ca^{2+} sites having low symmetry. Moreover, it can be readily observable that $^4F_{9/2}\rightarrow{}^6H_{15/2}$

transition splits into a maximum of J+1/2 (J is total angular momentum) stark manifolds in the blue emission region due to crystal field effect caused by surrounding ions [40,216,217].

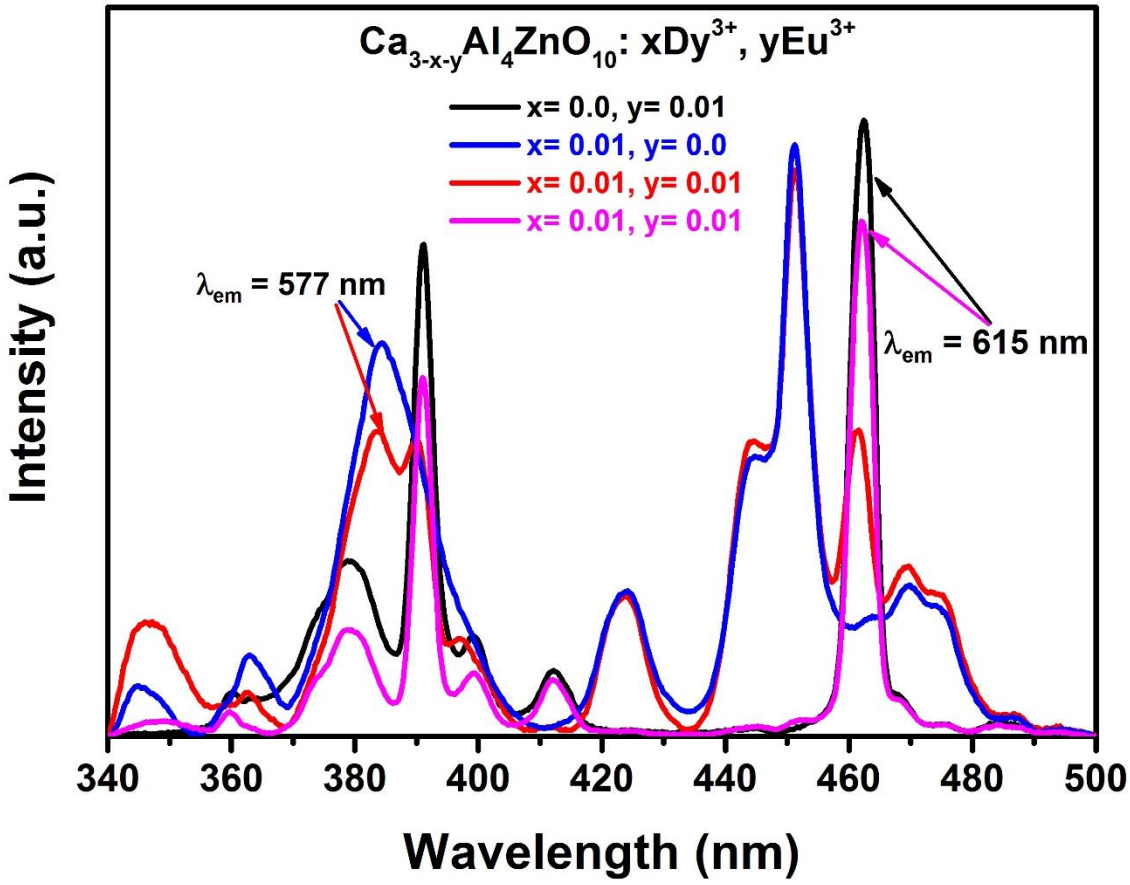

Figure 6.4. Excitation spectra of 1.0 mol% Dy^{3+}, 1.0 mol% Eu^{3+}, and 1.0 mol% of Dy^{3+}/1.0 mol% of Eu^{3+} co-doped in CAZ phosphor monitored at 577 and 615 nm emission wavelength.

Furthermore, the yellow to blue (Y/B) ratio, also known as asymmetry ratio, is the ratio of intensities of peak at 577 nm to 480 nm, which is calculated to evaluate the performance of Dy^{3+} doped phosphors. In general, the Y/B ratio of different host lattices doped with Dy^{3+} varies, since the $^4F_{9/2} \rightarrow {}^6H_{13/2}$ transition is hypersensitive to the host environment which may lead to variable intensity in different host composition, whereas the $^4F_{9/2} \rightarrow {}^6H_{15/2}$ transition is insensitive to the crystal environment [57,218]. The value of asymmetry ratio close to 1 implies that the near white emission can be obtained for the as-prepared phosphor doped with Dy^{3+}. In the present case, the Y/B ratio is found to be 1.5 which suggest that Dy^{3+} ions were distributed at non-inversion symmetry sites in the host matrix [57,217,219]. Further, the intensity of

emission increases gradually with Dy^{3+} concentration from 1.0 to 3.0 mol% in the host lattice and decreases beyond 3.0 mol%. The well-known phenomenon of concentration quenching is responsible for decrease in emission intensity after certain concentration of activator in the host. Since the energy is being transferred non-radiatively to the quenching sites which results in decrement of intensity [45,220].

In the present case, 3.0 mol% is the optimized concentration of Dy^{3+} in the host lattice for white emission. Fig. 6.4 shows excitation spectra of 1.0 mol% Dy^{3+}, 1.0 mol% Eu^{3+}, D1E1 phosphor by monitoring emission wavelength at 577 and 615 nm. It can be observed from Fig. 4, that 1.0 mol% Dy^{3+} shows excitation peaks as discussed above. 1.0 mol% Eu^{3+} doped CAZ phosphor exhibits characteristic transitions ($^7F_0 \rightarrow {}^5D_4$) at 361 nm, ($^7F_0 \rightarrow {}^5L_7$) at 380 nm, ($^7F_0 \rightarrow {}^5L_6$) at 391 nm, ($^7F_0 \rightarrow {}^5D_3$) at 412 nm, and ($^7F_0 \rightarrow {}^5D_2$) at 462 nm of Eu^{3+} ions in the host. The excitation spectra D1E1 phosphor monitored at 577 nm emission wavelength exhibit excitation peaks occurred due to f-f transitions of Dy^{3+} and Eu^{3+} ions. The various excitation peaks are attributed to ($^6H_{15/2} \rightarrow {}^6P_{7/2}$) at 347 nm, ($^6H_{15/2} \rightarrow {}^6P_{5/2}$) at 363 nm, ($^6H_{15/2} \rightarrow {}^4I_{13/2}$) at 384 nm, ($^6H_{15/2} \rightarrow {}^4G_{11/2}$) at 424 nm transitions of Dy^{3+} ions and Eu^{3+} ($^7F_0 \rightarrow {}^5L_6$) at 389 nm and ($^7F_0 \rightarrow {}^5D_2$) at 462 nm transitions of Eu^{3+} ions [221,222]. The excitation spectra of D1E1 under 615 nm emission wavelength shows a similar kind of excitation spectra under 577 nm wavelength with more intensity of peaks attributed to f-f transitions of Eu^{3+} ions. The overlap of excitation bands of Dy^{3+} and Eu^{3+} in n-UV region of electromagnetic spectrum shows that co-doped phosphor can be successfully pumped by n-UV excitation source.

Furthermore, Fig. 6.5 (a-d) shows the emission spectra of Dy^{3+}/Eu^{3+} co-doped CAZ phosphor for different excitation wavelength 363, 380, 384, and 391 nm respectively, where Dy^{3+} concentration is fixed at 3.0 mol% and Eu^{3+} concentration has been varied from 1.0-4.0 mol%. The PL spectra manifest emission peaks originating from certain transition levels of Eu^{3+} and Dy^{3+}, which gives emission in yellow, orange, red and blue regions of the

visible spectrum. The emission band at 468 nm assigned to $^5D_2 \rightarrow {}^7F_0$ transition with splitting at 474 nm, and the peak assigned to $^4F_{9/2} \rightarrow {}^6H_{15/2}$ transition which splits into peak at 480, and 493 nm. The emission at 577 nm and 586 nm are assigned to $^4F_{9/2} \rightarrow {}^6H_{13/2}$ of Dy^{3+} and $^5D_0 \rightarrow {}^7F_1$ level of Eu^{3+}.

A small peak at 663 nm assigned to $^4F_{9/2} \rightarrow {}^6H_{11/2}$ of Dy^{3+} and at 702 nm assigned to $^5D_0 \rightarrow {}^7F_4$ transition of Eu^{3+} ions [214,223]. By varying the excitation wavelength, the emission spectral profile shows the variation in the intensity of characteristic bands of Dy^{3+} and Eu^{3+} ions. Fig. 6.5 (a & c) shows the emission spectra recorded under 363 and 384 nm excitation (characteristic excitation of Dy^{3+} ions). The emission band corresponding to the characteristic emission of Dy^{3+} ions dominate over the emission bands of Eu^{3+} ions. In Fig. 6.5 (a), the emission bands in blue region shows four peaks as assigned above, since 363 nm excitation band exists in both Dy^{3+} and Eu^{3+} excitation spectrum. In Fig. 6.5 (c), the splitting of emission band in blue and yellow region is not so pronounced as in Fig. 6.5 (a). In Fig. 6.5 (b), the emission spectra have been recorded under 380 nm excitation wavelength which is central overlap of excitation band of Eu^{3+} and excitation band of Dy^{3+} ions centred at 384 nm and therefore the emission spectra arises from both the transitions of Dy^{3+} ions and Eu^{3+} ions. In Fig. 6.5 (d), the emission bands of Eu^{3+} ion dominates over Dy^{3+} with splitting in blue and yellow emission bands owing to the emission bands of Dy^{3+} and Eu^{3+} ions. Further, the peak at 586 nm become more pronounced under the excitation wavelength which is predominately attributed to Eu^{3+} transitions due to overlapping of the tail of $^4F_{9/2} \rightarrow {}^6H_{13/2}$ emission of Dy^{3+} with the $^5D_0 \rightarrow {}^7F_1$ emission of Eu^{3+} as shown in Fig. 6.5 (d).

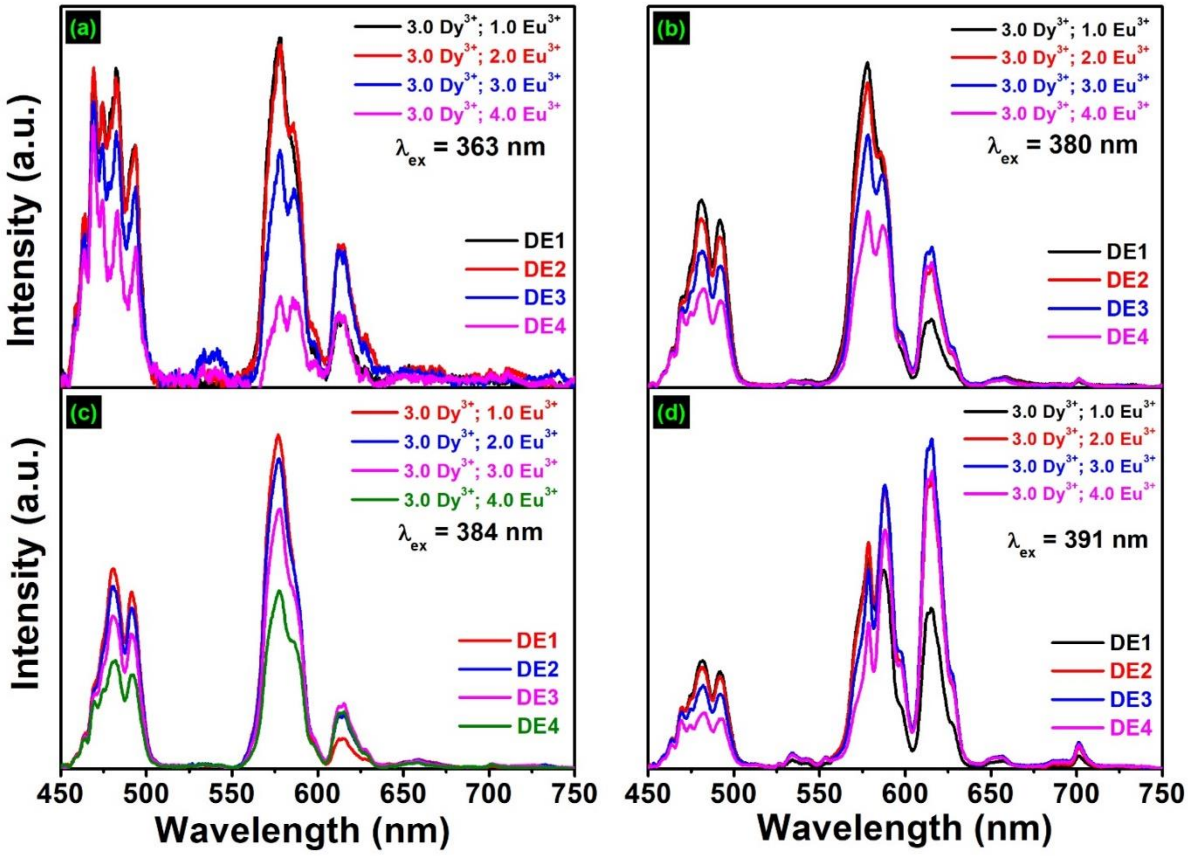

Figure 6.5. PL spectra of DE1, DE2, DE3 and DE4 under (a) 363, (b) 380, (c) 384 and (d) 391 nm excitation wavelength.

Also, by increasing Eu^{3+} ion concentration at constant Dy^{3+} ion concentration, the emission intensity of peaks originating from Dy^{3+} levels decrease, whereas emission intensity of peaks originating from Eu^{3+} levels increases. This behaviour is observable in all emission spectral profile of Dy^{3+}/Eu^{3+} co-doped CAZ phosphor monitored at different excitation wavelength. This indicates that Dy^{3+} sensitizes Eu^{3+} and thereby gives visible emission and the energy transfer from Dy^{3+} to Eu^{3+} ions occur, since the energy levels of Dy^{3+} are slightly higher than those of Eu^{3+} ions [214]. Nevertheless, the emission intensities originating from different transitions of Eu^{3+} and Dy^{3+} vary with excitation wavelength and the concentration of Eu^{3+} ions in the host matrix. Therefore, by varying the excitation wavelength or Eu^{3+} concentration, color tunability in CAZ phosphor can be realized.

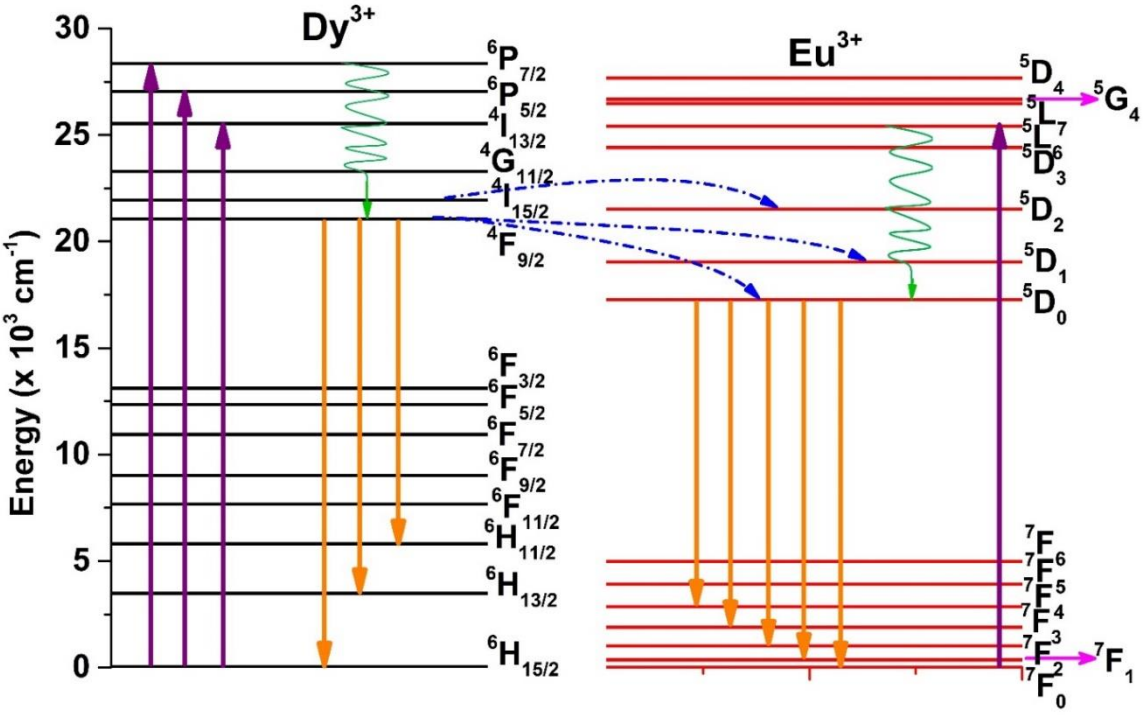

Figure 6.6. Partial energy level diagram representing energy level of Dy^{3+} and Eu^{3+} ions and transitions.

Fig. 6.6 shows partial energy level diagram showing excitation from ground state to various excited states. As it can be seen from Fig. 6.6, that the $^4I_{15/2}$ energy level of Dy^{3+} ion is near to $^5D_2$ energy level of Eu^{3+}, and that of $^4F_{9/2}$ is closer to $^5D_1$, and $^5D_0$ energy level of Eu^{3+} ions; so energy transfer from the excited state of Dy^{3+} to Eu^{3+} ions takes place due to phonon-aided non-radiative relaxation [215]. When the as-prepared phosphors are pumped by n-UV excitation, Dy^{3+} ions absorb the energy and gets excited to higher energy level. Subsequently after some non-radiative relaxation to intermediate levels, the Dy^{3+} ions give blue and yellow emissions and simultaneously transfers some energy to Eu^{3+} ions. This instigates Eu^{3+} ions to give red emission as depicted in Fig. 6.6.

The energy transfer between sensitizer (Dy^{3+}) and activator (Eu^{3+}) might occur non-radiatively, via exchange interaction, or multipolar interaction. The exchange interaction between sensitizer and activator occurs, if the critical distance is below 5 Å. The critical transfer distance can be calculated using the relation given in chapter 3.The critical concentration X_c,

is the total concentration of Dy^{3+} and Eu^{3+}, at which the intensity of Dy^{3+} is half of that in absence of Eu^{3+} (X_c = 4.0 mol%) [209,211]. The critical distance has reckoned to be 22.25 Å. Thus, it can be concluded that, the energy transfer occurs via multipolar interaction. Further, to identify the type of multipolar interaction, Dexter theory and Reisfeld's approximation has been employed. By employing Dexter's theory of multipolar interaction and Reisfeld's approximation as discussed in section 1.12 of chapter 1, a plot between I_{s0}/I_s versus $C^{n/3}$ for n = 6, 8, and 10 has been plotted as shown in Fig. 6.7.

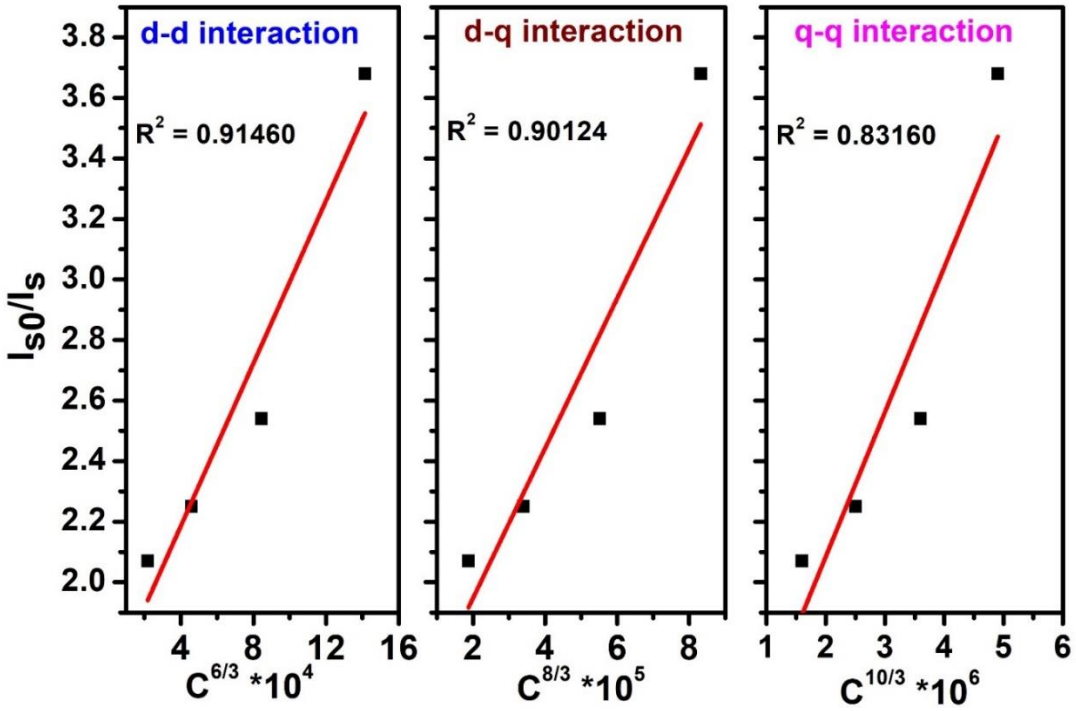

Figure 6.7. Plot of I_{s0}/I_s versus $C^{n/3}$.

The best linear fitting has been obtained for n=6, indicating the energy transfer mechanism between sensitizer and activator is d-d in nature. The energy transfer efficiency from sensitizer to activator has been calculated by using the following relation [224,225]:

$$\eta = 1 - \frac{I_s}{I_{s0}} \qquad (5)$$

The energy transfer efficiencies calculated for DE1, DE2, DE3 and DE4, are found to be 51.70, 55.62, 60.76 and 72.89, respectively. Thus, Eu^{3+} co-doped with Dy^{3+} in CAZ phosphor

can effectively be used for white light generation with the flexibility of tuning the emission by varying excitation wavelength.

6.3.4. Colorimetric properties:

To evaluate the potential of white emission in the as-prepared CAZ phosphors, the CIE chromaticity coordinates can be calculated from the emission spectra presented in Table 6.2. The color chromaticity CIE coordinates for Dy^{3+}/Eu^{3+} co-doped CAZ phosphor have been evaluated from emission spectra recorded under different excitation wavelengths (363, 380, 384 and 391 nm) and are shown in Fig. 6.8.

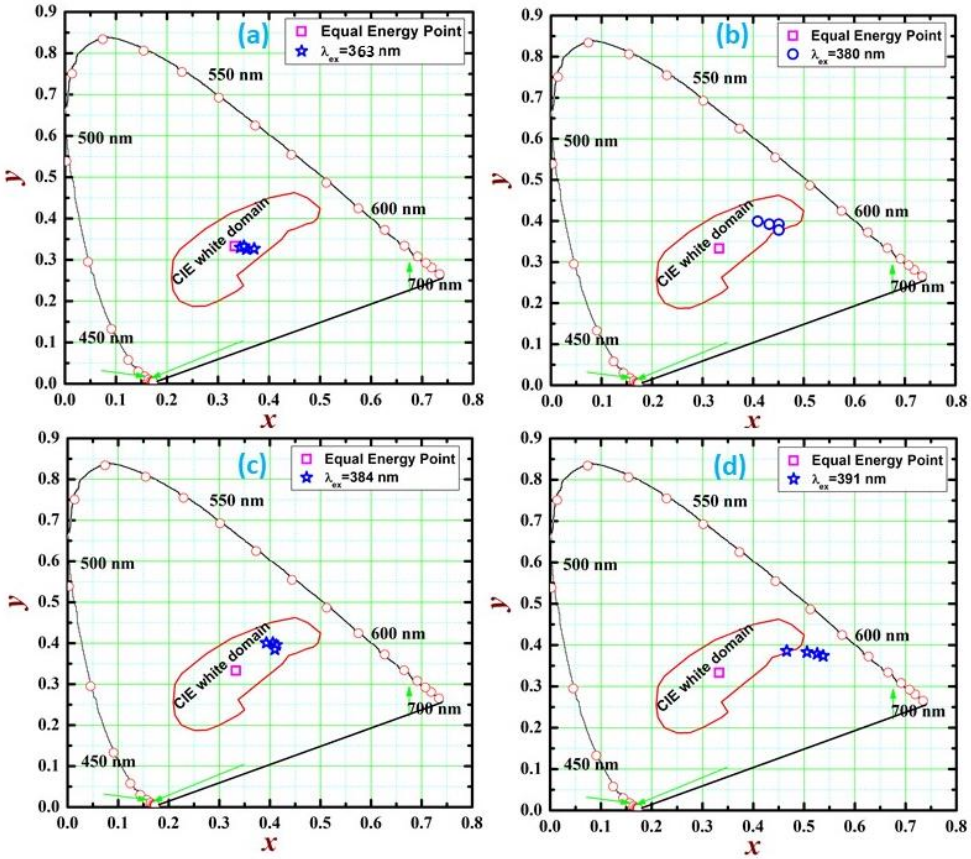

Figure 6.8. CIE chromaticity diagram of DE1, DE2, DE3 and DE4 under (a) 363, (b) 380, (c) 384 and (d) 391 nm excitation wavelength.

Correlated color temperature (CCT) for the as-prepared phosphors has been evaluated using the equation given by McCamy [53]. The calculated CIE coordinates and corresponding value of CCT have been reported in Table 6.2. The variation in CIE coordinates and CCT with

excitation wavelength suggest the possibility of tuning white light emission from warm to neutral to cool white light and also from white to yellow to reddish orange region of visible spectrum with variation in concentration of activator keeping sensitizer concentration constant. By selecting the excitation wavelength, one can tune the emission of Dy^{3+}/Eu^{3+} co-doped CAZ phosphor for the desired application. Therefore, it can be established from the aforementioned data that Dy^{3+}/Eu^{3+} co-doped CAZ phosphor is quite appropriate for its applications in wLEDs.

Table 6.2. CIE and CCT values for DE1, DE2, DE3, and DE4 under different excitations.

Excitation Wavelength (nm)	Sample	CIE co-ordinates (x, y)	CCT (K)
363	**DE1**	(0.344, 0.330)	4978
	DE2	(0.371, 0.327)	3882
	DE3	(0.356, 0.326)	4447
	DE4	(0.351, 0.333)	4565
380	**DE1**	(0.409, 0.399)	3479
	DE2	(0.432, 0.392)	2996
	DE3	(0.451, 0.390)	2654
	DE4	(0.450, 0.378	2549
384	**DE1**	(0.393, 0.401)	3855
	DE2	(0.406, 0.401)	3569
	DE3	(0.413, 0.395)	3379
	DE4	(0.410, 0.385)	3359
391	**DE1**	(0.466, 0.386)	2407
	DE2	(0.506, 0.383)	1970
	DE3	(0.526, 0.379)	1826
	DE4	(0.538, 0.374)	1756

6.3.5. Photoluminescence decay analysis:

The PL decay measurements have been recorded by monitoring 577 nm emission wavelength excited by n-UV (384 nm) excitation source, to analyse the lifetime of Dy^{3+} doped and Dy^{3+}/Eu^{3+} co-doped CAZ phosphors. Fig. 6.9 (a-e) show decay curves well-fitted to a bi-exponential function [52,226]. The evaluated lifetime values are 1.034, 1.013, 0.988, 0.949 and 0.910 ms for the Dy^{3+} doped and Dy^{3+}/Eu^{3+} co-doped CAZ phosphors. The lifetime values for Dy^{3+}/Eu^{3+} co-doped CAZ phosphor show decrease with increase in Eu^{3+} concentration. This clearly indicates efficient energy transfer from sensitizer (Dy^{3+}) to activator (Eu^{3+}).

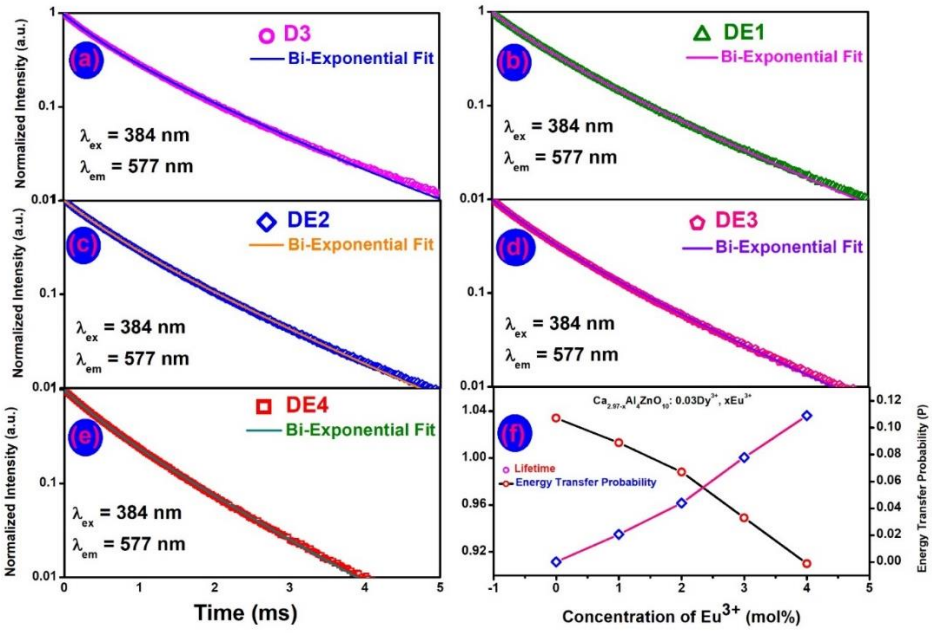

Figure 6.9. Decay curves of (a) D3, (b) DE1, (c) DE2, (d) DE3, (e) DE4 and (f) Plot of lifetime and energy transfer probability versus concentration (λ_{ex} = 384 nm, λ_{em} = 577 nm).

The energy transfer probability (P), for d-d energy transfer from Dy^{3+} to Eu^{3+} ions can be expressed by the equation below [227]:

$$P_{Dy^{3+}-Eu^{3+}} = \frac{1}{\tau} - \frac{1}{\tau_0} \qquad (6)$$

where, τ and τ_0 are the lifetime values of Dy^{3+} with and without Eu^{3+} ions, respectively. The energy transfer probabilities are estimated to be 0.0205, 0.0450, 0.0866 and 0.1317 for

DE1, DE2, DE3 and DE4, respectively. The energy transfer probability values are increasing with increase in Eu^{3+} ion concentration in the as-prepared phosphors. The energy transfer probability and lifetime values of D3, DE1, DE2, DE3 and DE4 samples have been plotted in Fig. 6.9 (f). To understand the nature of energy transfer process between Dy^{3+} and Eu^{3+} ions, I-H model has been employed. The non-exponential decay curve for DE4 has been fitted by applying I-H model for s = 6, 8, and 10 using the equation given in section 1.12 of chapter 1 is shown in Fig. 6.10.

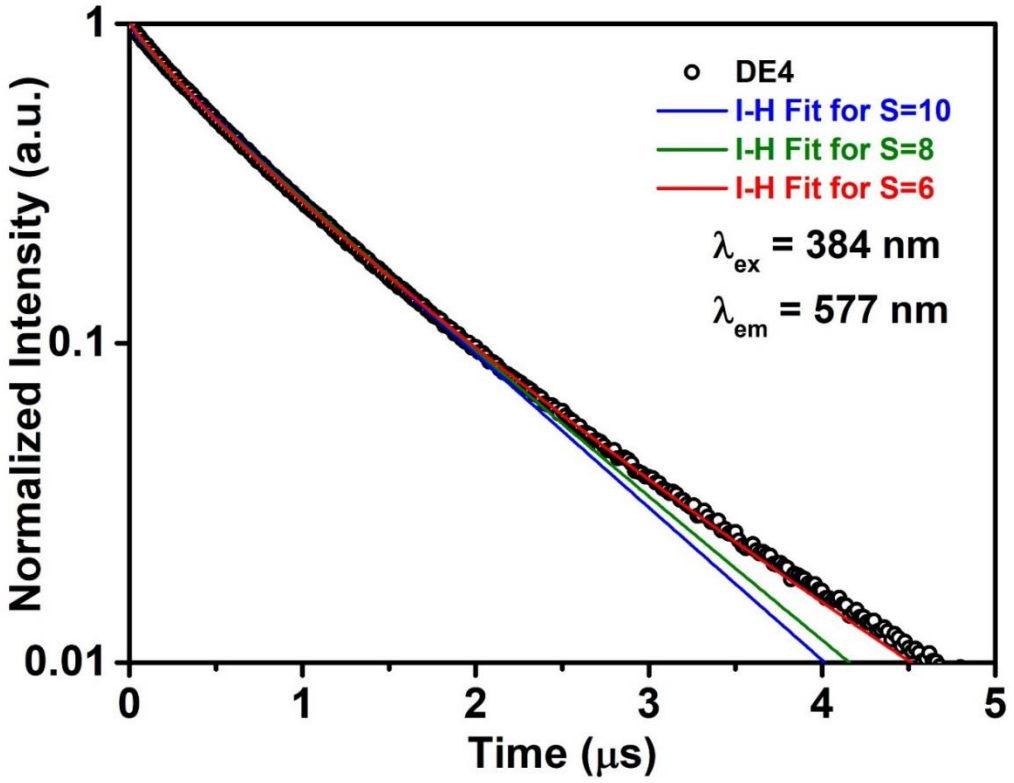

Figure 6.10. I-H fit of DE1 for S= 6, 8, and 10 (λ_{ex} = 384 nm, λ_{em} = 577 nm).

As the curve in Fig. 6.10 shows best fitting for s= 6, for all the co-doped phosphors, the I-H fitting was done for s=6 as shown in Fig. 6.11. From Figs. 6.10 & 6.11 it is conspicuous that the energy transfer mechanism involved in reducing lifetimes is dipole-dipole in nature. Thus, the results obtained from Dexter theory, Reisfeld's approximation and I-H model confirms the occurrence of dipole-dipole interaction between Dy^{3+} and Eu^{3+} ions in CAZ phosphor.

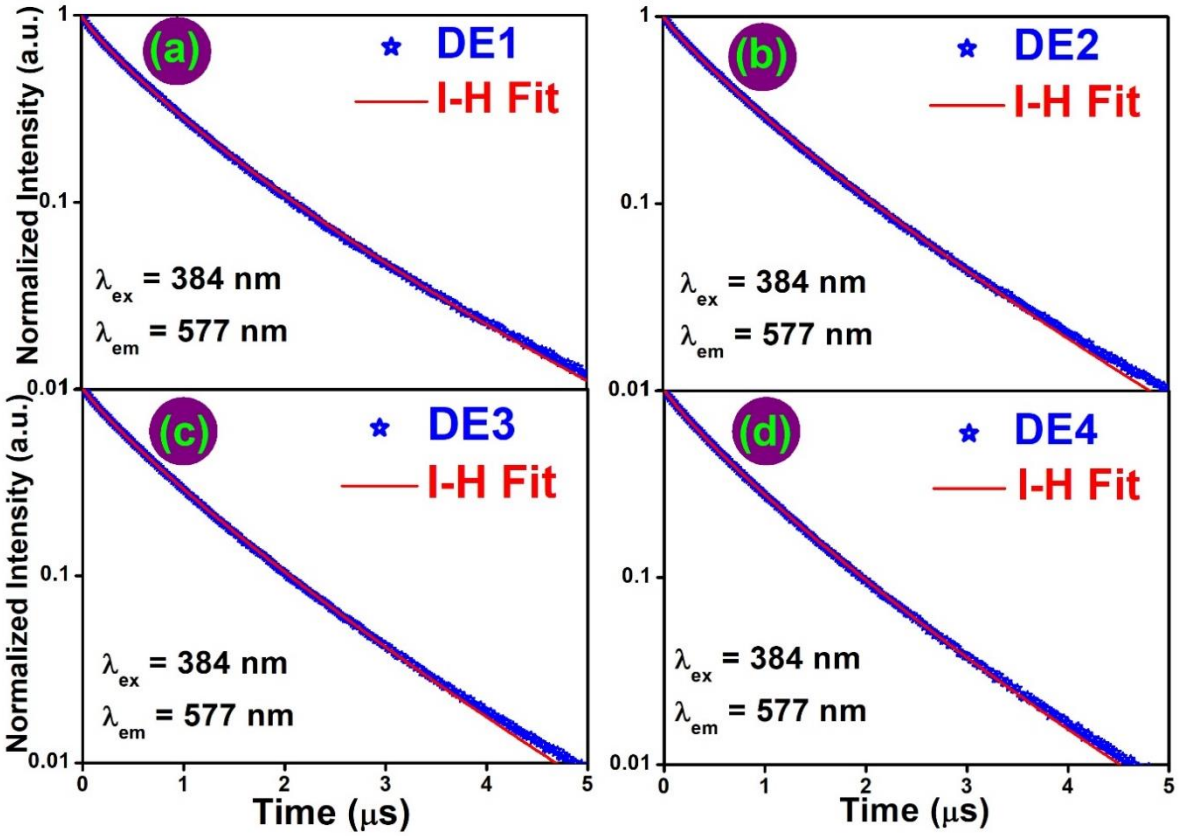

Figure 6.11. I-H fit of (a) DE1, (b) DE2, (c) DE3 and (d) DE4 (λ_{ex} = 384 nm, λ_{em} = 577 nm).

3.7. TL glow curve analysis:

The phenomenon of TL is the emission of photons via thermal stimulation. In the TL process, electrons get trapped during excitation with ionizing radiations into defects created by some impurities. The consumption of ionizing radiation dislocates electrons from valence band to reach to the conduction band. The trapped charge carrier release due to heating of the sample and recombination of electrons and holes at the luminescent centre leads to thermoluminescence [228]. The TL glow curve has been observed for DE1 phosphor irradiated by β-radiations with a dose of 1kGy. The TL glow curve deconvolute and gets resolved into two peaks with a maximum at 132 and 230°C as shown in Fig. 6.12. The TL glow peaks represents the different trapping levels of electrons in forbidden energy gap of materials under investigation. The glow peak at lower temperature indicate shallow trap centres and at higher temperature indicate deeper trap centers [200,229].

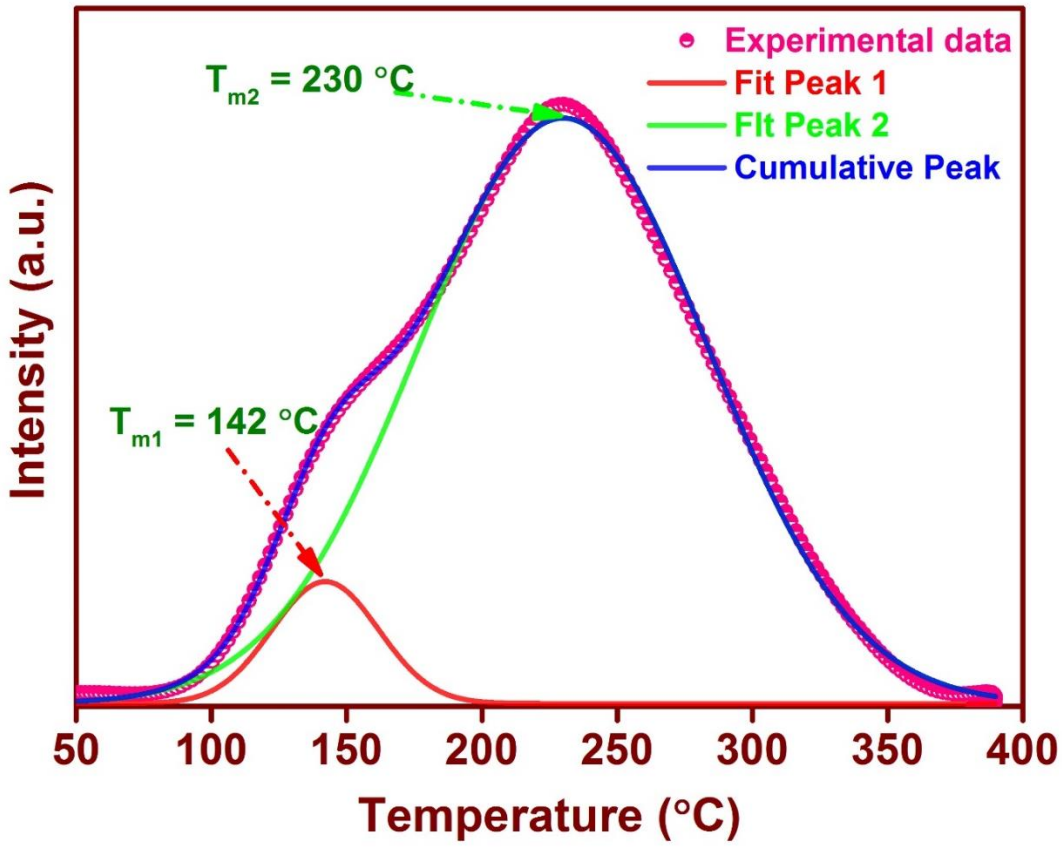

Figure 6.12. TL glow curve of β-irradiated DE1 sample.

The TL characterization peaks have been analysed to ascertain various trapping parameters such as trap depth/activation energy (E_α), order of kinetics (b), escape frequency/frequency factor or probability per second for de-trapping (s). To estimate the aforementioned parameters, Chen's peak shape method has been applied to the obtained TL glow curve.

Table 6.3: Glow peak parameters for DE1 sample.

	Temp. (°C)	**α**	**C_α**	**b_α**	**E_α (eV)**	**s_α (Hz)**
Peak 1	T_1=117	τ=25	1.69	1.83	0.870	$1.26*10^{11}$
	T_2=166	δ=24	1.41	0	0.875	$1.43*10^{11}$
	T_{m1}=142	ω=49	3.13	1	0.875	$1.44*10^{11}$
		μ_g=0.48		**b**=1.5	**E_m** = 0.873	Mean **s** = $1.38*10^{11}$
Peak 2	T_1=165	τ=25	1.72	1.87	0.413	$1.32*10^{5}$
	T_2=294	δ=24	1.49	0	0.506	$9.56*10^{5}$
	T_{m1}=230	ω=49	3.23	1	0.459	$3.43*10^{5}$
		μ_g=0.49		**b**=1.5	**E_m** = 0.459	Mean **s** = $4.78*10^{5}$

The activation energy (E_α), C_α, b_α for a given "α" and escape frequency (s) has been estimated from the empirical formula described in the previous chapter (chapter 5). The value of geometric form factor μ_g ($\mu_g=\delta/\omega$) is 0.48 and 0.49 for T_{m1} and T_{m2}, respectively. Theoretically, the geometric form factor value 0.42 indicates first order kinetics and 0.52 for second order kinetics. In the present analysis $0.42<\mu_g<0.52$, it indicates general order kinetics with b=1.5 [185,204]. The evaluated escape frequency (s) and other kinetic parameters are shown in Table.6.3. These results indicate the applicability of the as synthesized phosphor in radiation dosimetry.

Chapter-7

Summary and Future Scope

7.1. Summary:

The main emphasis of this thesis work is to synthesize and characterize RE ions activated CAZ phosphor for the solid-state lighting applications. Intense orange, red and white light emitting monophasic CAZ phosphors were successfully synthesized by using solid state reaction, combustion and Pechini sol-gel methods by incorporating single or double RE ions (Sm^{3+}, Eu^{3+}, and Dy^{3+} ions) as dopants. Emphasis was also given to the enhancement in emission with the addition of flux or by varying synthesis methods.

As discussed in the previous chapters, pc-wLEDs are overpowering SSL technology due to their idiosyncratic features such as power saving, longevity, environment friendly and outstanding luminescence efficiency for application in sensors, artificial lighting, display devices and other medical applications [230]. The study on structural, morphological and photoluminescent properties of Sm^{3+} doped CAZ phosphors were successfully prepared by traditional SSR method to achieve orange emission that can act as orange/red component to generate white light in pc-wLEDs. Moreover, the as-prepared Sm^{3+} doped CAZ phosphors prone to emit orange color can be coupled with cyan to generate white light.

The commercial pc-wLEDs based on YAG: Ce and blue LED lack in red component due to which its CRI is low, which can be surpassed if an efficient red phosphor is blended with YAG: Ce phosphor and then coated on blue LED chip. The commercially available red phosphors exhibit weak emission due to poor chemical stability, and poor absorption [70,231]. Therefore, CAZ phosphors doped with Eu^{3+} were successfully synthesized by SSR method. The structural and luminescent properties were thoroughly discussed for its utilization as red

phosphor that can be pumped with n-UV and blue LED. Furthermore, the red enhancement in Eu^{3+} doped CAZ phosphor is achieved by incorporating different fluxes and optimizing synthesis method as Pechini sol-gel method. Moreover, the optimization of synthesis methods is conducted by synthesizing CAZ phosphors via three different routes, namely, SSR, combustion and Pechini sol-gel. By analysing the structural and luminescent properties for CAZ phosphors synthesized by three different routes, the Pechini sol-gel method was considered to be the best among others. The luminescence enhancement was observed in Pechini sol-gel synthesized CAZ phosphor in comparison with other methods. For single phase phosphor to generate white light, Dy^{3+} doped and Dy^{3+}/Eu^{3+} doped CAZ phosphors were synthesized via Pechini sol-gel method. The structure, morphology, photoluminescent, and thermoluminescence (TL) properties were systematically studied.

7.2. Important findings of research work:

The thermal analysis of sol-gel synthesized CAZ phosphor was accomplished to analyse the crystallization of the $Ca_3Al_4ZnO_{10}$. The crystallization of CAZ phosphor began beyond 800°C. Therefore, these samples were sintered at 1000°C to achieve pure phase of $Ca_3Al_4ZnO_{10}$. The structural properties of differently synthesized CAZ phosphor doped with various RE ions were investigated to analyse crystallinity, phase purity, and crystallite size by using XRD and also Rietveld refinement for phase confirmation. The XRD patterns for all the prepared samples were in complete agreement with the standard PDF4+ICDD card no. 04-009-7304 signifies the pure phase formation of with orthorhombic structure and Pbc2 space group.

The morphological analysis of RE doped $Ca_3Al_4ZnO_{10}$ was accomplished by recording SEM/FE-SEM images. Among the three synthesis methods discussed in the previous chapters, SSR, and combustion methods show irregular agglomerated particles and sol-gel synthesized phosphors shows homogeneous regular morphology of particles.

The PL study reveals that the Sm^{3+} doped CAZ phosphors have three emission bands with the intense emission at 601 nm for $^4G_{5/2} \rightarrow {}^6H_{7/2}$ transition when pumped from $^6H_{5/2} \rightarrow {}^4F_{7/2}$ at 401 nm wavelength. The concentration quenching has been obtained beyond 1.0 mol% of Sm^{3+}. The calculated result reveals that the dipole-dipole interaction plays a major role in the quenching phenomenon. The calculated CIE chromaticity coordinates for all the samples lie in the orange region and the chromaticity values for the optimized sample are (0.574, 0.424) showing insignificant deviation from the coordinates specified by Nichia Corporation developed Amber LED NSPAR 70BS (0.570, 0.420). The PL decay study reveals the bi-exponential behaviour of the decay curves with decay time in 1.64-1.33 μs range. All these results indicate that the prepared $Ca_{3-x}Al_4ZnO_{10}$: xSm^{3+} powder phosphor serve as an efficient orange emitting phosphor for display and solid-state lighting devices.

The PL study shows that the Eu^{3+} doped CAZ phosphors exhibit two strong emission bands at 588 and 615 nm corresponding to $^5D_0 \rightarrow {}^7F_1$, and $^5D_0 \rightarrow {}^7F_2$ transitions respectively, of which, the band at 615 nm is more intense under n-UV and blue excitations than the other one. By optimizing the flux, enhancement of red emission observed to be more than twice in 5 wt% $Na_2B_4O_7$ assisted Eu^{3+} doped CAZ phosphor under blue excitation. The integrated emission intensity of 5 wt% $Na_2B_4O_7$ assisted Eu^{3+} doped CAZ phosphor found to be 81% of the commercial phosphor (Y_2O_3: Eu^{3+}) for 615 nm emission peak. The J-O theory has been applied to analyses optical properties. The CIE chromaticity coordinates for all the studied samples are found to lie in red region and are close to the coordinates of commercial red phosphor Y_2O_2S: Eu^{3+} (x=0.622, y=0.351) as well as NTSC system (x=0.670, y=0.330). The calculated color purity found to be 99.09 % for 5 wt% $Na_2B_4O_7$ in 2.0 mol % Eu^{3+} doped CAZ phosphor which confirms the highly pure red emission. The $^5D_0$ level decay curves of Eu^{3+} doped CAZ phosphor shows bi-exponential behaviour with an average lifetime of microseconds. All the aforementioned results allow us to conclude that 5wt% $Na_2B_4O_7$ in 2.0 mol% Eu^{3+} doped CAZ

phosphor is a promising phosphor for intense red emission and is aptly suitable for the development of wLEDs.

The emission spectra show significant enhancement in the red emission of Eu^{3+} doped CAZ phosphor via Pechini sol-gel method under blue excitation when compared with samples prepared by combustion and SSR methods. The optimization of Eu^{3+} concentration in CAZ phosphor found to be 2.0 mol%. The integrated emission intensity of the optimized CAZ phosphor is compared with commercial Y_2O_3: Eu^{3+} and found to be 1.25 of the Y_2O_3: Eu^{3+} phosphor. The decay profile indicates decrease in lifetime values and critical distance (R_0) with increase in the dopant concentration indicating energy transfer through dipole-dipole interaction. Further, the TL analysis of sol-gel synthesized Eu^{3+} doped CAZ phosphor confirms the presence of deep trap centres with a mean trap depth (E) of 0.736 eV. All the aforementioned studies finally allow me to contemplate that, the sol-gel method synthesized Eu^{3+} doped CAZ phosphors are more competent in giving red component useful for fabricating wLEDs.

The luminescent analysis of Dy^{3+}/Eu^{3+} co-doped CAZ phosphor recorded under different excitation wavelengths reveal white emission with varying CCT from cool to neutral to warm light. Also, by varying activator ion concentration, color tunability can be achieved in Dy^{3+}/Eu^{3+} co-doped CAZ phosphor. The Dexter theory & Reisfeld's approximation on emission spectra and I-H model applied on decay profile confirms the energy mechanism responsible for decrease in lifetime values is dipole-dipole in nature. The TL glow peaks at 142 and 230°C have been well resolved indicating the presence of shallow and deep trap centres and the activation energy is found to be 0.873 and 0.459 eV, respectively under β-irradiations. All these results suggest that the Dy^{3+} activated and Dy^{3+}/Eu^{3+} co-activated CAZ phosphor show potentiality for fabricating wLEDs and other display devices.

The aforementioned results confirm that RE doped $Ca_3Al_4ZnO_{10}$ phosphors developed in this thesis could be useful for solid state lighting applications and especially for wLEDs.

7.3. Future Scope:

1. To enhance the luminescence properties for Eu^{3+} doped $Ca_3Al_4ZnO_{10}$ phosphor by using suitable co-dopant. (for ex: Bi^{3+} may act as sensitizer; as the excitation peak of Eu^{3+} is exactly matches with Bi^{3+} emission)
2. To explore other synthesis method to improve the particle morphology, reduce the particle size to nano which in turn further improves the luminescence properties.
3. To compute CRI and improve it for white light generation by mixing red emitting $Ca_3Al_4ZnO_{10}$ phosphor to the commercial Ce^{3+}: YAG phosphor.
4. To fabricate prototype pc-wLED by using $Ca_3Al_4ZnO_{10}$ phosphor and UV/n-UV/blue LED chip.
5. To extend the utility of this phosphor for applications in plasma display panels and solar cells.

References

[1] B. Valeur, N. Berberan-santos, J. Chem. Educ. 88 (2011) 731–738.

[2] M. Shang, C. Li, J. Lin, Chem. Soc. Rev. 43 (2014) 1372–1386.

[3] D. Macisaac, G. Kanner, G. Anderson, Phys. Teach. 37 (1999) 520–525.

[4] G. Annadurai, S.M. Moses, V. Sivakumar, Superlattices Microstruct. 93 (2016) 57–66.

[5] C.N. Banwell, Fundamentals of Molecular Spectroscopy, Third Edit, McGRAW-HILL International (UK) Limited, 1972.

[6] C.. Parker, W.T. Rees, RSC Adv. 87 (1962) 83–111.

[7] N. Hafsi, H. Bouridah, Optik (Stuttg). 168 (2018) 244–252.

[8] H. Xu, Q. Sun, Z. An, Y. Wei, X. Liu, Coord. Chem. Rev. 293–294 (2015) 228–249.

[9] N. Siraj, B. El-zahab, S. Hamdan, T.E. Karam, L.H. Haber, M. Li, S.O. Fakayode, S. Das, B. Valle, R.M. Strongin, G. Patonay, H.O. Sintim, G.A. Baker, A. Powe, M. Lowry, J.O. Karolin, C.D. Geddes, I.M. Warner, Anal. Chem. 88 (2016) 170–202.

[10] L.V.S. França, L.C. Oliveira, O. Baffa, Meas. J. Int. Meas. Confed. 134 (2019) 492–499.

[11] M. Koshimizu, T. Yanagida, K. Shinsho, S. Yanagisawa, Y. Fujimoto, H. Yagi, T. Yanagitani, K. Asai, Nucl. Instruments Methods Phys. Res. Sect. B Beam Interact. with Mater. Atoms 435 (2018) 285–289.

[12] Z. Xia, Q. Liu, Prog. Mater. Sci. 84 (2016) 59–117.

[13] V.F. Guimaraes, L.J.Q. Maia, I. Gautier-Luneau, C. Bouchard, A.C. Hernandes, F. Thomas, A. Ferrier, B. Viana, A. Ibanez, J. Mater. Chem. C 3 (2015) 5795–5802.

[14] J. Huo, W. Lü, B. Shao, Y. Song, Y. Feng, S. Zhao, J. Lumin. 180 (2016) 46–50.

[15] P. Du, X. Huang, J.S. Yu, Chem. Eng. J. 337 (2018) 91–100.

[16] K. Li, J. Fan, X. Mi, Y. Zhang, H. Lian, M. Shang, J. Lin, Inorg. Chem. 53 (2014) 12141–12150.

[17] G. Blasse, B.. Grabmaier, Luminescent Materials, 1994th ed., Springer-Verlag Telos, 1994.

[18] S. Ye, F. Xiao, Y.X. Pan, Y.Y. Ma, Q.Y. Zhang, Mater. Sci. Eng. B 71 (2010) 1–34.

[19] X. Zhang, L. Zhou, Q. Pang, J. Shi, M. Gong, J. Phys. Chem. C 118 (2014) 7591–7598.

[20] C.J. Summers, B. Wagner, H. Menkara, Proc. Third Int. Conf. Solid State Light. 5187 (2004) 123–132.

[21] K. Li, M. Shang, H. Lian, J. Lin, J. Mater. Chem. C 4 (2016) 5507–5530.

[22] M. Strobl, T. Mayr, I. Klimant, S.M. Borisov, Sensors Actuators B. Chem. 245 (2017)

972–979.

[23] A. Ruivo, V.S.F. Muralha, H. Águas, A.P. de Matos, C.A.T. Laia, J. Quant. Spectrosc. Radiat. Transf. 134 (2014) 29–38.

[24] D.R. Dreyer, S. Park, C.W. Bielawski, R.S. Ruoff, Chem. Soc. Rev. 39 (2010) 189–227.

[25] S. Saha, S. Das, U.K. Ghorai, N. Mazumder, D. Ganguly, K.K. Chattopadhyay, J. Phys. Chem. C 119 (2015) 16824–16835.

[26] M. V Dacosta, S. Doughan, Y. Han, U.J. Krull, Anal. Chim. Acta 832 (2014) 1–33.

[27] A. Kalaji, M. Mikami, A.K. Cheetham, Chem. Mater. 26 (2014) 3966–3975.

[28] M. De Jong, D. Biner, K.W. Kra, L. Seijo, J. Phys. Chem. Lett. 7 (2016) 2730–2734.

[29] M.P. Hehlen, M.G. Brik, K.W. Krämer, J. Lumin. 136 (2013) 221–239.

[30] Y. Zhang, W. Gong, G. Ning, New J. Chem. 40 (2016) 10136–10143.

[31] L. Yang, Y. Wan, Y. Huang, C. Chen, H. Jin, J. Alloys Compd. 684 (2016) 40–46.

[32] B. Tian, B. Chen, Y. Tian, X. Li, J. Zhang, J. Sun, H. Zhong, L. Cheng, S. Fu, H. Zhong, Y. Wang, X. Zhang, H. Xia, R. Hua, J. Mater. Chem. C 1 (2013) 2338–2344.

[33] J. Mckittrick, M.E. Hannah, A. Piquette, J.K. Han, J.I. Choi, M. Anc, M. Galvez, H. Lugauer, J.B. Talbot, K.C. Mishra, ECS J. Solid State Sci. Technol. 2 (2013) 3119–3131.

[34] J.C.G. Bünzli, C. Piguet, Chem. Soc. Rev. 34 (2005) 1048–1077.

[35] M. Hatanaka, S. Yabushita, Theor. Chem. Acc. 133 (2014) 1517–1531.

[36] J. Sucher, Reports Prog. Phys. 41 (1978) 1781–1837.

[37] J.G. Bu, S. V Eliseeva, Basics of Lanthanide Photophysics, Springer, Berlin, Heidelberg, 2010.

[38] S. V Eliseeva, J.-C.G. Bünzli, Chem. Soc. Rev. 39 (2010) 189–227.

[39] N.C. George, K.A. Denault, R. Seshadri, Annu. Rev. Mater. Res. 43 (2013) 481–501.

[40] Y. Il Jeon, L. Krishna Bharat, J.S. Yu, J. Alloys Compd. 620 (2015) 263–268.

[41] W.P. Lustig, F. Wang, S.J. Teat, Z. Hu, Q. Gong, J. Li, Inorg. Chem. 55 (2016) 7250–7256.

[42] T. Suehiro, ACS Appl. Mater. Interfaces 3 (2011) 811–816.

[43] Y. Wei, L. Cao, L. Lv, G. Li, J. Hao, J. Gao, C. Su, Chem. Mater. Mater. 30 (2018) 2389–2399.

[44] C. Grieco, K.F. Hirsekorn, A.T. Heitsch, A.C. Thomas, M.H. Mcadon, B.A. Vanchura, M.M. Romanelli, L.L. Brehm, A. Leugers, A.N. Sokolov, J.B. Asbury, ACS Appl. Mater. Interfaces 9 (2017) 12547–12555.

[45] J. Du, D. Xu, X. Gao, S. Ji, H. Li, J. Sun, Optik (Stuttg). 147 (2017) 290–299.

[46] H. Yu, D. Deng, D. Zhou, W. Yuan, Q. Zhao, Y. Hua, J. Mater. Chem. C 3 (2013) 5577–5582.

[47] Y. Chang, C. Liang, S. Yan, Y. Chang, J. Phys. Chem. C 3 (2010) 3645–3652.

[48] C. Chiu, C. Liu, S. Huang, T.-M. Chen, J. Electrochem. Soc. 154 (2007) J181–J184.

[49] P. Rekha Rani, M. Venkateswarlu, S. Mahamuda, K. Swapna, N. Deopa, A.S. Rao, J. Alloys Compd. 787 (2019) 503–518.

[50] N. Guo, Y. Huang, H. You, M. Yang, Y. Song, K. Liu, Y. Zheng, Inorg. Chem. 49 (2010) 10907–10913.

[51] J.I. Choi, M. Anc, A. Piquette, M.E. Hannah, K.C. Mishra, J. Mckittrick, J.B. Talbot, ECS J. Solid State Sci. Technol. 2 (2013) 153–159.

[52] A.K. Vishwakarma, K. Jha, M. Jayasimhadri, B. Sivaiah, B. Gahtori, D. Haranath, Dalt. Trans. 44 (2015) 17166–17174.

[53] C.S. McCamy, Color Res. Appl. 17 (1992) 142–144.

[54] L.G. Van Uitert, J. Electrochem. Soc. 114 (1967) 1048–1053.

[55] V.B. Pawade, H.C. Swart, S.J. Dhoble, Renew. Sustain. Energy Rev. 52 (2015) 596–612.

[56] Y. Zhang, D. Geng, X. Li, J. Fan, K. Li, H. Lian, M. Shang, J. Lin, J. Phys. Chem. C 118 (2014) 17983–17991.

[57] U. Caldiño, A. Lira, A.N. Meza-Rocha, I. Camarillo, R. Lozada-Morales, J. Lumin. 194 (2018) 231–239.

[58] V. Uma, K. Maheshvaran, K. Marimuthu, G. Muralidharan, J. Lumin. 176 (2016) 15–24.

[59] Y. Tian, X. Qi, X. Wu, R. Hua, B. Chen, J. Phys. Chem. C 113 (2009) 10767–10772.

[60] B.R. Judd, Phys. Rev. 127 (1962) 750–761.

[61] G.S. Ofelt, J. Chem. Phys. 37 (1962) 511–520.

[62] K. Jha, M. Jayasimhadri, J. Am. Ceram. Soc. 100 (2017) 1402–1411.

[63] Y. Tian, B. Chen, R. Hua, J. Sun, L. Cheng, H. Zhong, X. Li, J. Zhang, Y. Zheng, T. Yu, L. Huang, H. Yu, J. Appl. Phys. 109 (2015) 053511–053517.

[64] E.E.S. Teotonio, G.P. Espı, H.F. Brito, O.L. Malta, S.F. Oliveira, D.L.A. de Faria, C.M.S. Izumi, Polyhedron 21 (2002) 1837–1844.

[65] J. Xue, Y. Guo, B. Kee, S. Heum, J. Hyun, J. Hwan, L. Wang, Opt. Mater. (Amst). 66 (2017) 220–229.

[66] A. Kodaira, H.F. Brito, M. Cla, F.C. Felinto, J. Solid State Chem. 171 (2003) 401–407.

[67] C.B. Annapurna, S. Mahamuda, M. Venkateswarlu, K. Swapna, A.S. Rao, G.V. Prakash,

Opt. Mater. (Amst). 62 (2016) 569–577.

[68] M. Venkateswarlu, M.V.V.K.S. Prasad, K. Swapna, S. Mahamuda, Ceram. Int. 40 (2014) 6261–6269.

[69] L. Dacanin, S.R. Lukic, D.M. Petrovic, M. Nikolic, M.D. Dramicanin, Phys. B Phys. Condens. Matter 406 (2011) 2319–2322.

[70] P. Halappa, B. Devakumar, C. Shivakumara, New J. Chem. 43 (2019) 63–71.

[71] C. Zhang, J. Lin, Chem. Soc. Rev. 41 (2012) 7938–7961.

[72] H. Terraschke, C. Wickleder, Chem. Rev. 115 (2015) 11352–11378.

[73] R.K. Tamrakar, D.P. Bisen, N. Brahme, J. Radiat. Res. Appl. Sci. 7 (2014) 550–559.

[74] C.C. Lin, R. Liu, J. Phys. Chem. Lett. 2 (2011) 1268–1277.

[75] Z.M. Chen, S.X. Jiang, R.H. Guo, B.J. Xin, D.G. Miao, Mater. Technol. Adv. Perform. Mater. 29 (2014) 198–203.

[76] T. Qian, B. Fan, H. Wang, S. Zhu, Chem. Phys. Lett. 715 (2019) 34–39.

[77] S. Som, S. Das, S. Dutta, H.G. Visser, M.K. Pandey, P. Kumar, R.K. Dubey, S.K. Sharma, RSC Adv. 5 (2015) 70887–70898.

[78] J.K. Han, J.I. Choi, A. Piquette, M. Hannah, M. Anc, M. Galvez, J.B. Talbot, J. Mckittrick, ECS J. Solid State Sci. Technol. 2 (2013) 3138–3147.

[79] A.E. Danks, S.R. Hall, Z. Schnepp, Mater. Horizons 3 (2016) 91–112.

[80] G. Paul, Principles and Applications of Thermal Analysis, Ist editio, Blackwell, 2008.

[81] B.D. Cullity, M. Cohen, Elements of X-RAY DIFFRACTION, 2nd ed., ADDISON-WESLEY PUBLISHING COMPANY INC>, 1978.

[82] A.L. Patterson, Phys. Rev. 56 (1939) 978–982.

[83] V. Bedekar, D.P. Dutta, M. Mohapatra, S. V Godbole, R. Ghildiyal, a K. Tyagi, Nanotechnology 20 (2009) 125707–125715.

[84] P. Biswas, V. Kumar, G. Agarwal, O.M. Ntwaeaborwa, H.C. Swart, Ceram. Int. 42 (2016) 2317–2323.

[85] K. Sabri, A. Rais, K. Taibi, M. Moreau, B. Ouddane, A. Addou, Phys. B Condens. Matter 501 (2016) 38–44.

[86] R.W. Frei, H. Zeitlin, C R C Crit. Rev. Anal. Chem. 2 (1971) 179–246.

[87] R. Yu, Y. Guo, L. Wang, H.M. Noh, B.K. Moon, B.C. Choi, J.H. Jeong, J. Lumin. 155 (2014) 317–321.

[88] X. Chen, J. Zhao, L. Yu, C. Rong, C. Li, S. Lian, J. Lumin. 131 (2011) 2697–2702.

[89] G.M. Rao, S.K. Hussain, G. Seeta Rama Raju, P.S.V. Subba Rao, J.S. Yu, J. Alloys Compd. 660 (2016) 437–445.

[90] B. Bondzior, D. Stefańska, A. Kubiak, P.J. Dereń, J. Lumin. 173 (2016) 38–43.

[91] F. Yang, Z. Yang, Q. Yu, Y. Liu, X. Li, F. Lu, Spectrochim. Acta - Part A Mol. Biomol. Spectrosc. 105 (2013) 626–631.

[92] G. He, L. Mei, L. Wang, G. Liu, J. Li, Cryst. Growth Des. 11 (2011) 5355–5361.

[93] Z. Yang, H. Dong, P. Liu, C. Hou, X. Liang, C. Wang, F. Lu, J. Rare Earths 32 (2014) 404–408.

[94] Z. Wang, P. Li, Z. Yang, Q. Guo, J. Lumin. 132 (2012) 1944–1948.

[95] L. Wang, H.M. Noh, B.K. Moon, B.C. Choi, J.H. Jeong, J. Shi, J. Alloys Compd. 663 (2016) 808–817.

[96] N.S. Choi, K.W. Park, B.W. Park, X.M. Zhang, J.S. Kim, P. Kung, S. Margaret Kim, J. Lumin. 130 (2010) 560–566.

[97] G. Zhu, Y. Wang, Z. Ci, B. Liu, Y. Shi, S. Xin, J. Lumin. 132 (2012) 531–536.

[98] R. Yu, H. Mi Noh, B. Kee Moon, B. Chun Choi, J. Hyun Jeong, H. Sueb Lee, K. Jang, S. Soo Yi, J. Lumin. 152 (2014) 133–137.

[99] R. Yu, H. Mi Noh, B. Kee Moon, B. Chun Choi, J. Hyun Jeong, H. Sueb Lee, K. Jang, S. Soo Yi, J. Lumin. 145 (2014) 717–722.

[100] Maheshwary, B.P. Singh, R.A. Singh, New J. Chem. 39 (2015) 4494–4507.

[101] J. Xu, Z. Ju, X. Gao, Y. An, X. Tang, W. Liu, Inorg. Chem. 52 (2013) 13875–13881.

[102] N. Kiran, A.P. Baker, G. Wang, J. Mol. Struct. 1129 (2017) 211–215.

[103] A.K. Vishwakarma, M. Jayasimhadri, J. Lumin. 176 (2016) 112–117.

[104] Q. Li, Y. Yuan, T. Wei, Y. Li, Z. Chen, X. Jin, Y. Qin, W. Sun, Sol. Energy Mater. Sol. Cells 130 (2014) 426–434.

[105] K. Swapna, S. Mahamuda, A.S. Rao, S. Shakya, T. Sasikala, D. Haranath, G.V. Prakash, Spectrochim. ACTA PART A Mol. Biomol. Spectrosc. 125 (2014) 53–60.

[106] S. Mahamuda, K. Swapna, M. Venkateswarlu, A.S. Rao, S. Shakya, G.V. Prakash, J. Lumin. 154 (2014) 410–424.

[107] J.S. Kumar, K. Pavani, A.M. Babu, N. Kumar, S.B. Rai, L.R. Moorthy, J. Lumin. 130 (2010) 1916–1923.

[108] G.P. Singh, S. Kaur, P. Kaur, D.P. Singh, Phys. B Phys. Condens. Matter 407 (2012) 1250–1255.

[109] A. Tarafder, A. Rahaman, S. Mukhopadhyay, B. Karmakar, Opt. Mater. Mater. 36 (2014) 1463–1470.

[110] G.J. Mohini, N. Krishnamacharyulu, G.S. Baskaran, P.V. Rao, N. Veeraiah, Appl. Surf. Sci. 287 (2013) 46–53.

[111] C.S. Pappas, P.A. Tarantilis, P.C. Harizanis, M.G. Polissiou, 57 (2003) 23–27.

[112] L. Balachander, G. Ramadevudu, R. Sayanna, Y.C. Venudhar, Sci. Asia 39 (2013) 278–283.

[113] P.F. Wang, Z.H. Li, J. Li, Y.M. Zhu, Solid State Sci. 11 (2009) 1427–1432.

[114] Q. Xu, D. Xu, J. Sun, Opt. Mater. (Amst). 42 (2015) 210–214.

[115] C.K. Jayasankar, P. Babu, J. Alloys Compd. 307 (2000) 82–95.

[116] G.U. Xiguang, F.U. Renli, J. Weina, Z. Pengfei, T. Ye, J. Rare Earths 33 (2015) 954–960.

[117] B.C. Jamalaiah, J.S. Kumar, A.M. Babu, T. Suhasini, L.R.M. Ã, J. Lumin. 129 (2009) 363–369.

[118] P. Karthikeyan, S. Arunkumar, C. Basavapoornima, K. Marimuthu, J. Lumin. 178 (2016) 43–53.

[119] L. Wang, H.M. Noh, B.K. Moon, S.H. Park, K.H. Kim, J. Shi, J.H. Jeong, J. Phys. Chem. C 119 (2015) 15517–15525.

[120] W. Zhang, Y. Zhang, S. Ouyang, Z. Zhang, H. Xia, Mater. Lett. 160 (2015) 459–462.

[121] M. Mariyappan, S. Arunkumar, K. Marimuthu, J. Mol. Struct. 1105 (2016) 214–224.

[122] S. Som, V. Kumar, V. Kumar, M. Gohain, A. Pandey, M.M. Duvenhage, J.J. Terblans, B.C.B. Bezuindenhoud, H.C. Swart, Ultrason. Sonochem. 28 (2016) 79–89.

[123] G.P. Darshan, H.B. Premkumar, H. Nagabhushana, S.C. Sharma, S.C. Prashanth, B.D. Prasad, J. Colloid Interface Sci. 464 (2016) 206–218.

[124] B.S.O. Ce, Z. Xia, Y. Liang, D. Yu, M. Zhang, W. Huang, Opt. Laser Technol. 56 (2014) 387–392.

[125] D.L. Dexter, J. Chem. Phys. 21 (1953) 836–850.

[126] Y. Li, Y. Shi, Y. Wang, ECS J. Solid State Sci. Technol. 2 (2013) R208–R212.

[127] A. Fernández-Carrión, M. Ocañ, J. García-Sevillan, E. Cantelar, A.I. Becerro, J. Phys. Chem. CJournal Phys. Chem. C 118 (2014) 18035–18043.

[128] W. Bin Im, S. Brinkley, J. Hu, A. Mikhailovsky, S.P. Denbaars, R. Seshadri, Chem. Mater. 22 (2010) 2842–2849.

[129] X. Yang, J. Liu, H. Yang, X. Yu, Y. Guo, Y. Zhou, J. Mater. Chem. 19 (2009) 3771–3774.

[130] X. Li, J.D. Budai, F. Liu, J.Y. Howe, J. Zhang, X.-J. Wang, Z. Gu, C. Sun, R.S. Meltzer, Z. Pan, Light Sci. Appl. 2 (2013) e50.

[131] S. Som, P. Mitra, V. Kumar, V. Kumar, J.J. Terblans, H.C. Swart, S.K. Sharma, Dalton Trans. 43 (2014) 9860–9871.

[132] B. Hallstedt, J. Am. Ceram. Soc. 78 (1995) 193–198.
[133] S. Neeraj, N. Kijima, A.K. Cheetham, Chem. Phys. Lett. 387 (2004) 2–6.
[134] E. Pavitra, G.S.R. Raju, J.Y. Park, L. Wang, B.K. Moon, Sci. Rep. 5 (2015) 10296–10309.
[135] S. Long, J. Hou, G. Zhang, F. Huang, Y. Zeng, Ceram. Int. 39 (2013) 6013–6017.
[136] H. Zhang, H. Zhang, J. Zhuang, H. Dong, Y. Zhu, X. Ye, Ceram. Int. 42 (2016) 13011–13017.
[137] H. Wu, Y. Hu, W. Zhang, H. Duan, L. Chen, X. Wang, J. Non. Cryst. Solids 358 (2012) 2734–2740.
[138] Y.E. Linqin, P. Xingping, Z. Shuihe, W. Yuhua, J. Rare Earths 32 (2014) 1109–1113.
[139] B. Sundarakannan, M. Kottaisamy, Mater. Res. Bull. 74 (2016) 485–490.
[140] V. Sivakumar, A. Lakshmanan, J. Lumin. 145 (2014) 420–424.
[141] G. Swati, S. Bishnoi, P. Singh, B. Rajesh, G. Kumar, P. Seth, D. Haranath, J. Alloys Compd. 698 (2017) 930–937.
[142] K. Chen, J. Zhou, F. Zhang, X. Zhang, C. Li, L. An, J. Am. Ceram. Soc. Ceram. Soc. 1701 (2015) 1698–1701.
[143] R. Sharma, U. Sharma, J. Alloys Compd. 649 (2015) 440–446.
[144] V.D. Barbanyagre, T.I. Timoshenko, A.M. Ilyinets, V.M. Shamshurov, Powder Diffr. 12 (1997) 22–26.
[145] A.K. Vishwakarma, M. Jayasimhadri, J. Alloys Compd. 683 (2016) 379–386.
[146] S. Kaur, A.S. Rao, M. Jayasimhadri, Ceram. Int. 43 (2017) 7401–7407.
[147] Y. Li, Z. Zhao, Z. Song, R. Wan, J. Qiu, Z. Yang, Z. Yin, X. Liu, Q. Liu, Y. Zhou, J. Am. Ceram. Soc. 98 (2015) 2170–2176.
[148] Y. Wu, D. Wang, T. Chen, C. Lee, K. Chen, H. Kuo, ACS Appl. Mater. Interfaces 3 (2011) 3195–3199.
[149] R. Köferstein, L. Jäger, S.G. Ebbinghaus, Solid State Ionics 249–250 (2013) 1–5.
[150] B.Y. Huang, B.L. Feng, L. Luo, C.L. Han, Y.T. He, Z.R. Qiu, Mater. Sci. Eng. B Solid-State Mater. Adv. Technol. 212 (2016) 71–77.
[151] Y. Wu, Z. Sun, K. Ruan, Y. Xu, H. Zhang, J. Lumin. 155 (2014) 269–274.
[152] Q. Xiao, Y. Liu, L. Liu, R. Li, W. Luo, X. Chen, J. Phys. Chem. C 114 (2010) 9314–9321.
[153] Q. Ju, Y. Liu, R. Li, L. Liu, W. Luo, X. Chen, 113 (2009) 2309–2315.
[154] V. Marcos, S. Rezende, C. William, A. Paschoal, Opt. Mater. (Amst). 46 (2015) 530–535.

[155] V.R.L. Constantino, M. a. Bizeto, H.F. Brito, J. Alloys Compd. 278 (1998) 142–148.

[156] T.C. Ozawa, K. Fukuda, K. Akatsuka, Y. Ebina, T. Sasaki, Chem. Mater. 19 (2007) 6575–6580.

[157] J. Hou, P. Chen, G. Zhang, Y. Fang, W. Jiang, F. Huang, Z. Ma, J. Lumin. 146 (2014) 97–101.

[158] Z. Zhang, L. Wang, L. Han, F. Han, X. Ma, X. Li, D. Wang, Mater. Lett. 160 (2015) 302–304.

[159] Q. Xu, J. Sun, D. Cui, Q. Di, J. Zeng, J. Lumin. 158 (2015) 301–305.

[160] J. Zhong, W. Zhuang, X. Xing, R. Liu, Y. Li, Y. Liu, Y. Hu, J. Phys. Chem. C 119 (2015) 5562–5569.

[161] Y. Tian, B. Chen, B. Tian, R. Hua, J. Sun, L. Cheng, H. Zhong, X. Li, J. Zhang, Y. Zheng, T. Yu, L. Huang, Q. Meng, J. Alloys Compd. 509 (2011) 6096–6101.

[162] G. Ramakrishna, H. Nagabhushana, S.C. Prashantha, S.C. Sharma, B.M. Nagabhushana, Spectrochim. Acta Part A Mol. Biomol. Spectrosc. 136 (2015) 356–365.

[163] M. Nogami, N. Umehara, T. Hayakawa, Phys. Rev. B 58 (1998) 6166–6171.

[164] D.A. Hakeem, K. Park, New J. Chem. 39 (2015) 7768–7772.

[165] S. Kaur, M. Jayasimhadri, A.S. Rao, J. Alloys Compd. 697 (2017) 367–373.

[166] R. Reisfeld, J. Less-Common Met. 112 (1985) 9–18.

[167] S. Mahamuda, K. Swapna, A.S. Rao, T. Sasikala, L.R. Moorthy, Phys. B Phys. Condens. Matter 428 (2013) 36–42.

[168] K. Binnemans, C. Görller-Walrand, J. Phys. Condens. Matter 10 (1999) L167–L170.

[169] R. Reisfeld, E. Greenberg, R.N. Brown, M.C. Drexhage, C.K. Jorgensen, Chem. Phys. Lett. 95 (1983) 91–94.

[170] A.K. Vishwakarma, K. Jha, M. Jayasimhadri, A.S. Rao, K. Jang, B. Sivaiah, D. Haranath, J. Alloys Compd. 622 (2015) 97–101.

[171] M. Mohapatra, V. Natarajan, S. V. Godbole, J. Non. Cryst. Solids 386 (2014) 115–120.

[172] W.-L. Feng, X. Qin, P. Su, Optik (Stuttg). 131 (2017) 1007–1015.

[173] Y. Du, Y. Zhang, K. Huang, S. Wang, L. Yuan, S. Feng, Dalt. Trans. 42 (2013) 8041–8048.

[174] H. Sameie, R. Salimi, A.A. Sarabi, A.A.S. Alvani, S. Nargesian, H.E. Mohammadloo, Y. Ebrahimi, Mater. Tehnol. 47 (2013) 685–687.

[175] T. Fukui, K. Kamon, J. Takeshita, H. Hayashi, T. Miyachi, Y. Uchida, S. Kurai, T. Taguchi, Jpn. J. Appl. Phys. 48 (2009) 112101–112106.

[176] U. Rambabu, N.R. Munirathnam, B.S. Reddy, S. Chatterjee, Luminescence 31 (2016)

141–151.

[177] Y.S. Chang, Z.R. Shi, Y.Y. Tsai, S. Wu, H.L. Chen, Opt. Mater. (Amst). 33 (2011) 375–380.

[178] S.E. Brinkley, N. Pfaff, K.A. Denault, Z. Zhang, H.T. Hintzen, R. Seshadri, S. Nakamura, S.P. Denbaars, Appl. Phys. Lett. 99 (2011) 2009–2012.

[179] D. Tu, Y. Liang, R. Liu, Z. Cheng, F. Yang, W. Yang, J. Alloys Compd. 509 (2011) 5596–5599.

[180] C. Guo, H.K. Yang, Z. Fu, L. Li, B.C. Choi, J.H. Jeong, J. Am. Ceram. Soc. 92 (2009) 1713–1718.

[181] J. Ohyama, C. Zhu, G. Saito, M. Haga, T. Nomura, N. Sakaguchi, T. Akiyama, J. Rare Earths (2017) 1–9.

[182] A. Verma, S.K. Pathak, A. Verma, G. V. Bramhe, I.P. Sahu, J. Alloys Compd. 764 (2018) 1021–1032.

[183] A. Verma, A. Verma, G. V. Bramhe, J. Alloys Compd. 774 (2019) 1168–1180.

[184] T. Thirugnanam, J. Nanomater. 2013 (2013) 1–7.

[185] V. Dubey, R. Tiwari, M. Pradhan, G. Rathore, C. Sharma, R. Tamrakar, J. Lumin. Appl. 1 (2014) 30–39.

[186] M. Pal, U. Pal, J.M.G.Y. Jiménez, F. Pérez-Rodríguez, Nanoscale Res. Lett. 7 (2012) 1–12.

[187] S. Mavengere, J.S. Kim, Appl. Surf. Sci. 444 (2018) 491–496.

[188] M.M. Haque, M. Kudrat-E-Zahan, N.A. Jahan, H.I. Lee, Optik (Stuttg). 133 (2017) 1–8.

[189] C.R. Garcia, J. Oliva, M.A. Garcia-Lobato, A.I. Martínez, R. Ochoa-Valiente, G.A. Hirata, Ceram. Int. 43 (2017) 12876–12881.

[190] M. Janulevicius, P. Marmokas, M. Misevicius, J. Grigorjevaite, L. Mikoliunaite, S. Sakirzanovas, A. Katelnikovas, Sci. Rep. 6 (2016) 1–12.

[191] M. Chandrasekhar, H. Nagabhushana, Y.S. Vidya, K.S. Anantharaju, S.C. Sharma, H.P. Nagaswarupa, J. Mol. Catal. A 409 (2015) 26–41.

[192] A. Verma, A. Verma, G. V. Bramhe, I.P. Sahu, J. Alloys Compd. 769 (2018) 831–842.

[193] K. V. Dabre, S.J. Dhoble, RSC Adv. 5 (2015) 60409–60418.

[194] R. Reisfeld, E. Zigansky, M. Gaft, Mol. Phys. 102 (2004) 1319–1330.

[195] L.R. Hatwar, S.P. Wankhede, S. V. Moharil, P.L. Muthal, S.M. Dhopte, Luminescence 30 (2015) 904–909.

[196] V. Uma, M. Vijayakumar, K. Marimuthu, G. Muralidharan, J. Mol. Struct. 1151 (2018)

266–276.
[197] M. Vijayakumar, K. Marimuthu, J. Lumin. 178 (2016) 414–424.
[198] L. Guerbous, M. Derbal, J.P. Chaminade, J. Lumin. 130 (2010) 2469–2475.
[199] K.R. Nagabhushana, D. Prakash, F. Singh, S.H. Tatumi, R.R. Rocca, S. Watanabe, J. Alloys Compd. 735 (2018) 1949–1954.
[200] P. Dewangan, D.P. Bisen, N. Brahme, R.K. Tamrakar, K. Upadhyay, S. Sharma, I.P. Sahu, J. Alloys Compd. 735 (2018) 1383–1388.
[201] R.K. Tamrakar, D.P. Bisen, Res. Chem. Intermed. 39 (2013) 3043–3048.
[202] S. Delice, M. Isik, E. Bulur, N.M. Gasanly, J. Appl. Phys. 113 (2013) 193510–193514.
[203] R. Chen, J. Electrostat. 3 (1977) 15–24.
[204] R. Chen, J. Electrochem. Soc. 116 (1969) 1254–1257.
[205] Y. Zhou, C. Zhu, M. Zhang, J. Liu, J. Alloys Compd. 688 (2016) 715–720.
[206] R. Krishnan, J. Thirumalai, V. Mahalingam, S. Mantha, M. Lavanya, Mater. Chem. Phys. 162 (2015) 41–49.
[207] D. Wang, J. Fan, M. Shang, K. Li, Y. Zhang, H. Lian, J. Lin, Opt. Mater. (Amst). 51 (2016) 162–170.
[208] J. Kaur, Y. Parganiha, V. Dubey, D. Singh, D. Chandrakar, Superlattices Microstruct. 73 (2014) 38–53.
[209] G. Li, D. Geng, M. Shang, C. Peng, Z. Cheng, J. Lin, J. Mater. Chem. 21 (2011) 13334–13344.
[210] L. Zhao, D. Wang, C. Chen, Y. Wang, Mater. Res. Bull. 70 (2015) 817–821.
[211] K.H. Kwon, W. Bin Im, H.S. Jang, H.S. Yoo, D.Y. Jeon, Inorg. Chem. 48 (2009) 11525–11532.
[212] X.-F. Wang, Q. Yang, Wang, Gui-gen, X.-Z. Wang, J.-C. Han, RSC Adv. 5 (2015) 92988–92994.
[213] F. Li, X. Liu, T. He, Chem. Phys. Lett. 686 (2017) 78–82.
[214] M. Vijayakumar, K. Marimuthu, J. Lumin. 178 (2016) 414–424.
[215] H. Guan, Y. Song, P. Ma, M. Chang, J. Chen, Y. Wang, B. Yuan, H. Zou, RSC Adv. 6 (2016) 53444–53453.
[216] J.L. Fry, H.H. Caspers, H.E. Rast, S.A. Miller, J. Chem. Phys. 48 (1968) 2342–2348.
[217] P. Karthikeyan, S. Arunkumar, K. Annapoorani, K. Marimuthu, Spectrochim. Acta - Part A Mol. Biomol. Spectrosc. 193 (2018) 422–431.
[218] Y. Wang, X. Liu, L. Jing, P. Niu, Ceram. Int. 42 (2016) 13004–13010.
[219] B.C. Jamalaiah, G. Pakardin, G. V. Lokeswara Reddy, M. V. Vijaya Kumar, Opt. Mater.

(Amst). 73 (2017) 545–549.
[220] P. Du, J.S. Yu, J. Alloys Compd. 653 (2015) 468–473.
[221] W.T. Carnall, P.R. Fields, K. Rajnak, J. Chem. Phys. 49 (1968) 4450–4455.
[222] W.T. Carnall, P.R. Fields, K. Rajnak, J. Chem. Phys. 49 (1968) 4424–4442.
[223] J. Wang, Y. Bu, X. Wang, H.J. Seo, Sci. Rep. 7 (2017) 1–11.
[224] Y. Liu, G. Liu, J. Wang, X. Dong, W. Yu, Inorg. Chem. 53 (2014) 11457–11466.
[225] K. Li, M. Shang, D. Geng, H. Lian, Y. Zhang, J. Fan, J. Lin, Inorg. Chem. 53 (2014) 6743–6751.
[226] Y. Zhang, W. Gong, J. Yu, Z. Cheng, G. Ning, RSC Adv. 6 (2016) 30866–30894.
[227] B. Zhang, H. Zou, H. Guan, Y. Dai, Y. Song, X. Zhou, Y. Sheng, CrystEngComm 18 (2016) 7620–7628.
[228] A.J.J. Bos, Materials (Basel). 10 (2017) 1357–1379.
[229] S. Basun, G.F. Imbusch, D.D. Jia, W.M. Yen, J. Lumin. 104 (2003) 283–294.
[230] C.H. Huang, T.M. Chen, Inorg. Chem. 50 (2011) 5725–5730.
[231] Q. Cheng, F. Ren, Q. Lin, H. Tong, X. Miao, J. Alloys Compd. 772 (2018) 905–911.

CURRICULUM VITAE

PERSONAL INFORMATION:	
Name:	**SUMANDEEP KAUR**
Father's Name:	**JATINDER SINGH**
Date of Birth:	**28th January, 1990**
Nationality:	**Indian**
Sex:	**Female**
Marital Status:	**Single**
Address for Communication:	**Sumandeep Kaur** **H. No. B-65, Uday Vihar, Chander Vihar** **New Delhi-110 041, INDIA.** **Mob. No.: +91-8860853010**
E-mail Address:	**suman28gill@gmail.com**

CURRENT EDUCATIONAL STATUS:
Highest Academic Degree: **Doctor of Philosophy (Ph.D.)**
Subject: **Physics**
Present State of Degree: **Ph.D. Synopsis has been successfully submitted on 28th March, 2019.**
Institute/University: **Delhi Technological University (formerly known as the Delhi College of Engineering), Delhi- 110 042, India.**
Title of the Ph.D. Thesis: **Structural and Luminescent Properties of Rare Earth Activated Calcium Aluminozincate Phosphor for Solid State Lighting Applications**

ACADEMIC PERFORMANCE:

- **2011: Received Master of Science (M.Sc.) degree in Physics with 66% (First division) from Delhi University, Delhi ş 110021 India.**
- **2009: Received Bachelor of Science in Honours (B.Sc Hon's) degree with 63% (First division) from Delhi University, Delhi ş 110021 India.**
- **2006: 10+2 with 75% (absolute ş First division) from CBSE Board, New Delhi, India.**
- **2004: Matriculation (10^{th} std.) with 65% (First division) from CBSE Board, New Delhi, India.**

SCI JOURNAL PUBLICATIONS:

1. **Synthesis optimization, photoluminescence and thermoluminescence studies of Eu^{3+} doped calcium aluminozincate phosphor**

   ***Sumandeep Kaur, M. Jayasimhadri, A.S.Rao, B. Sivaiah, D. Haranath*, J. Alloys Compd., 802 (2019) 129-138.**

2. **Color tunability and energy transfer studies of Dy^{3+}/ Eu^{3+} co-doped calcium aluminozincate phosphor for lighting applications**

   ***Sumandeep Kaur, A.S.Rao, M. Jayasimhadri,* Mater. Res. Bull., 116 (2019) 79-88.**

3. **Enhanced red down-conversion luminescence and high color purity from flux assisted Eu^{3+} doped calcium aluminozincate phosphor**

   ***Sumandeep Kaur, M. Jayasimhadri, A.S.Rao,* J. Lumin., 202 (2018) 461-468.**

4. **Spectroscopic and photoluminescence characteristics of Sm^{3+} doped calcium aluminozincate phosphor for applications in w-LED**

   ***Sumandeep Kaur, M. Jayasimhadri, A.S.Rao,* Ceram Int., 43 (2017) 7401-7407.**

5. **A novel red emitting Eu^{3+} doped calcium aluminozincate phosphor for Applications in w-LEDs**

   ***Sumandeep Kaur, M. Jayasimhadri, A.S.Rao*, J. Alloys Compd., 697 (2017) 367-373.**

6. **Spectroscopic studies of Dy^{3+} doped borate glasses for cool white light generation**

   ***Sumandeep Kaur, Amit kumar Vishwakarma, Nisha Deopa, Aman Prasad, M. Jayasimhadri, A.S. Rao,* Mater Res. Bull., 104 (2018) 77-82.**

7. **Intense green emission from Tb^{3+} ions doped zinc lead alumino borate glasses for laser and w-LEDs applications**

   ***Sumandeep Kaur, Nisha Deopa, Aman Prasad, Rajat Bajaj, A.S. Rao,* Opt. Mater. 84 (2018) 318-323.**

8. **Spectral studies of Eu^{3+} doped lithium lead alumino borate glasses for visible photonic applications**

   ***Nisha Deopa, Sumandeep Kaur, Aman Prasad, Bipin Joshi, A.S. Rao*, Opt Laser Technol., 108 (2018) 434-440.**

9. **Spectroscopic investigations on Dy^{3+} ions doped zinc lead alumino borate glasses for photonic device applications**

   ***Nisha Deopa, Shubham Saini, Sumandeep Kaur, Aman Prasad, A.S. Rao,* J. Rare Earth 37 (2019) 52-59.**

10. **UV radiation emitting Gd^{3+} activated Sr_2SiO_4 host system prepared by sol¸gel procedure: structural, electron paramagnetic resonance, and luminescence studies**

    ***V. Singh, N. Singh, M. S. Pathak, Sumandeep Kaur, M Jayasimhadri, S Watanabe*, J. Mater. Sci.: Mater. Electron. 29 (2018) 20759¸20767.**

11. **UV emitting Pb^{2+} doped $SrZrO_3$ phosphors prepared by sol-gel procedure¿**

    ***V. Singh, N. Singh, Sumandeep Kaur, M. Jayasimhadri, M. S. Pathak, S. Watanabe, T.K. Gundu,* Ceram. Inter., 44 (2018) 17074-17078.**

12. **An Electron Paramagnetic Resonance and Photoluminescence Investigation of UVB Radiation Emitting Gadolinium-Activated $CaY_2Al_4SiO_{12}$ Garnet Compound**

    ***V. Singh, Sumandeep Kaur, A.S. Rao, N. Singh, M. S. Pathak, J. L. Rao*, J. Electron. Mater., 48 (2019) 4092-4098.**

13. **Spectroscopic properties of deep Red Emitting Tm^{3+} doped ZnPbWTe Glasses for Optoelectronic and Laser Applications**

    ***Ritu Sharma, Aman Prasad, Sumandeep Kaur, Nisha Deopa, Rekha Rani, M. Venkateswarlu, A. S. Rao*, J. Non-cryst. Solids, 516 (2019) 82-88.**

PUBLICATIONS COMMUNICATED TO SCI JOURNAL:

1. **Spectral studies of Er^{3+} ions doped Lithium Lead Alumino Borate glasses for Visible and 1.5 µm Photonic Application**

   ***Nisha Deopa, Mukesh K. Sahu, Sumandeep Kaur, Aman Prasad, K. Swapna, A.S. Rao*, Optics and Laser Technology (2019).**

2. **Judd-Ofelt parametrization and Radiative analysis of Dy^{3+} ions doped Sodium Bismuth Strontium Phosphate glasses**

   ***Haruka George, Nisha Deopa, Sumandeep Kaur, Aman Prasad, M. Sreenivasulu, M. Jayasimhadri, A. S. Rao*, Journal of Luminescence (2019)**

NATIONAL & INTERNATIONAL CONFERENCES:

1. **Presented oral talk on topic entitled Ș*Highly pure red emitting flux assisted Eu^{3+} doped calcium aluminozincate phosphor for display lighting applications*¿ in International Conference on Advanced Functional Materials and Devices (ICAFMD-2019) during 26th -28th February 2019 organized by National Institute of Technology, Warangal, Telangana, India.**
2. **Presented oral talk on topic entitled Ș*Color tunable and energy transfer properties of Dy^{3+}/Eu^{3+} co-doped calcium aluminozincate phosphor*¿ in International Conference on Luminescence and its Applications (ICLA-2019) during 7th-10th January 2019 organized by Luminescence Society of India at Pt. R. S. University, Raipur.**
3. **Presented poster entitled Ș*Red emission enhancement in flux assisted Eu^{3+} doped calcium aluminozincate phosphor*¿ in National Conference on Luminescence and its Applications (NCLA-2018), held during 14th-16th February 2018 in CSIR-National Institute for Interdisciplinary Science and Technology, Trivandrum, India.**
4. **Presented paper entitled Ș*Intense white light emission from Dy^{3+} doped $Ca_3Bi(PO_4)_3$ phosphor for w-LEDs application*¿ in 2nd International Conference on Advanced Production and Industrial Engineering (ICAPIE-2017) during 6th-7th October, 2018, at Delhi Technological University, Delhi, India.**
5. **Presented Poster entitled Ș*Tunable luminescence and energy transfer properties of Sm^{3+}/Tb^{3+} co-doped ZPBT glasses for n-UV based solid state lighting applications*¿ in 10th Biennial National Conference of ISCAS in Solid State Chemistry and Allied areas held during 1st-3rd July 2017 at Delhi Technological University, Delhi, India.**
6. **Presented paper entitled Ș*Warm white light emitting Calcium Aluminozincate phosphor for Display Applications*¿ in National Conference on Luminescence and its Application (NCLA-2017) from 9th-11th January 2017 at CSIR-IICT Hyderabad.**
7. **Presented paper entitled Ș*Trivalent europium doped $BaZnP_2O_7$ phosphors for white LED applications*¿ in International Conference on Advanced Production and Industrial Engineering (ICAPIE-2016) from 9th-10th December 2016 at Delhi Technological University, Delhi.**
8. **Presented paper entitled Ș*Studies of Eu^{3+} ions doped alkaline earth zinc aluminate phosphor for solid-state lighting applications*¿ in National Conference on Luminescence and its Application (NCLA-2016) during 18th-20th February 2016 organized by Luminescence Society of India at RTM University, Nagpur.**
9. **Presented paper entitled Ș*Dysprosium doped B_2O_3-Al_2O_3-ZnO-Na_2O glass phosphor for w-LEDs applications*¿ in International Conference on Luminescence and its Applications (ICLA-2015) during 9th-12th February 2016 organized by Luminescence Society of India at PES University, Bangalore, India.**

TRANING & WORKSHOPS:

- **One week TEQIP-III sponsored Faculty Development Programme (FDP) on ȘRecent Trends in Material Science and Engineering¿ 17th-21st September, 2018 at Delhi Technological University, Delhi-42.**
- **One-week FDP programme on ȘAdvances in Microelectronics and Plasma Diagnostics¿ 29th August 2016 - 2nd September 2016 at Delhi Technological University, Delhi-42.**
- **National Seminar on Frontiers in Applied Science and Technology (FAST-2016) 22nd March 2016 at Delhi Technological University, Delhi-42.**
- **Attended ȘNational Seminar on Recent Advances in Physics¿ at Delhi Technological University, Delhi-42.**
- **Attended National workshop on ȘPower Eelctronics¿ (NWPE-2015) 6th & 7th November 2015 at Delhi Technological University, Delhi-42**

HONORS/AWARDS:

- **Qualified CSIR-UGC JRF in Physical Sciences with AIR-99 in June 2014.**
- **Qualified GATE in Physics in March 2013 with AIR-722.**
- **Awarded Junior Research Fellowship (JRF) by UGC-Govt. of India since January 2015 to Till Date.**
- **Awarded Best Poster (First) Prize in 10th Biennial National Conference of ISCAS in Solid State Chemistry and Allied areas during 1-3rd July 2017 organized by DTU, Delhi, India.**
- **Awarded Best Poster (Third) Prize in National Conference on Luminescence and Applications (NCLA-2018) during 14th-16th February 2018 organized by CSIR-NIIST, Trivandrum, Kerala.**
- **Received Commendable Research Award for excellence for two consecutive years (2018 & 2019) from Research and Council Board of DTU, Delhi.**

TEACHING EXPERIENCE (2012- 2014):

Post Designation: **Lecturer in Physics**

Institute/University: **Guru Teg Bahadur Institute of Technology, GGSIP University, Delhi, India.**

Teaching Tenure: **Date of Joining: 20th January 2012**

Date of Relieving: 31st July 2014

RESEARCH FIELDS OF INTEREST:
➢ **Luminescent Materials and their applications.** ➢ **Glasses and Glass Ceramics** ➢ **Naonophotonics** ➢ **Optical Physics**

Journal of Alloys and Compounds 802 (2019) 129–138

Contents lists available at ScienceDirect

Journal of Alloys and Compounds

journal homepage: http://www.elsevier.com/locate/jalcom

Synthesis optimization, photoluminescence and thermoluminescence studies of Eu^{3+} doped calcium aluminozincate phosphor

Sumandeep Kaur [a], A.S. Rao [a, *], M. Jayasimhadri [a, **], B. Sivaiah [b], D. Haranath [c]

[a] Department of Applied Physics, Delhi Technological University, Bawana Road, New Delhi, 110 042, India
[b] CSIR-National Physical Laboratory, Dr. K.S. Krishnan Road, New Delhi, 110 012, India
[c] Department of Physics, National Institute of Technology, Warangal, 506 004, Telangana, India

ARTICLE INFO

Article history:
Received 4 April 2019
Received in revised form
10 June 2019
Accepted 13 June 2019
Available online 14 June 2019

Keywords:
Sol-gel
Combustion
Photoluminescence
CIE chromaticity coordinates
Activation energy

ABSTRACT

Calcium aluminozincate phosphor, $Ca_3Al_4ZnO_{10}$ (CAZ) doped with Eu^{3+} has been synthesized using solid-state reaction (SSR), combustion (CS) and sol-gel (SG) methods for relatively improved luminescence performance and to optimize synthesis method. The X-ray diffraction (XRD), scanning electron microscope (SEM), photoluminescence (PL) and PL decay measurements have been recorded for the detailed investigation of the luminescence properties of the as-synthesized phosphor. The thermoluminescence (TL) spectral study has been done to estimate the trap depth of the defect centres. The XRD peaks confirm the complete matching of the diffraction peaks of the as-synthesized sample with the standard data for $Ca_3Al_4ZnO_{10}$. The morphology of the sample synthesized via SG method shows agglomerated particles with average particle size smaller than the samples synthesized via CS and SSR method. The detailed investigation shows significant red emission enhancement in Eu^{3+} doped CAZ phosphor synthesized via SG method. The obtained results suggest that the Eu^{3+} doped CAZ phosphor synthesized via SG method could be a great choice as red emitter for applications in solid state lighting.

1. Introduction

In recent years, phosphor converted white light emitting diodes (pc-wLEDs) are enjoying the supremacy over conventional lighting sources (incandescent lamps and CFLs) due to their proficient and promising characteristics such as long-time reliability, power saving ability, energy efficiency, and environment friendliness [1–3]. The remarkable properties of pc-wLEDs have empowered wider variety of lighting, display and scintillation applications. Generally, there are three distinct methods to fabricate wLEDs. One of those methods is to enclose blue LED with yellow emitting phosphor, $Y_3Al_5O_{12}$: Ce^{3+} (YAG: Ce) [4]. However, this combination for generating white light suffers few limitations such as high correlated color temperature (CCT) and poor color rendering index (CRI), $R_a < 80$ caused by scarcity of red color component in luminescence spectra of the phosphor [5,6]. The another alternative way to achieve full color gamut is by using tri-color (red, green, and blue) phosphors combining with n-UV LED chip [7–9]. The currently used tri-color phosphor materials are Y_2O_2S: Eu^{3+} for red, ZnS:(Cu^{+}, Al^{3+}) for green, and $BaMgAl_{10}O_{17}$: Eu^{2+} (BAM) for blue. Unfortunately, there is some loss of energy in this method due to re-absorption of blue light by green and red emitting phosphors that deteriorate the quality of white light generation [10]. Also, the efficiency of the Y_2O_2S: Eu^{3+} red phosphor is very much less than that of the green and blue phosphors [7,11]. Moreover, the chemical stability of the sulphide phosphors is very low and they are not environment friendly as they are prone to emit sulphur gas into the environment [12–14]. Therefore, it is highly desirable to make superior red phosphors that absorb in the near-UV (n-UV) and blue, emit in the red to enhance the color rendition, CCT, and energy efficiency of pc-wLEDs.

For an efficient red-emitting phosphor, it has two basic requirements: (1) the phosphor host or the activator that shows strong absorption in the n-UV spectral region; (2) the phosphor could convert the n-UV light into red light efficiently. Among various rare earth (RE) ions, Eu^{3+} acts as an efficient red luminescent centre in numerous phosphors, and it is extensively used in lighting applications such as color television and lamp phosphors [15]. Therefore, Eu^{3+} doped inorganic oxide phosphors have

* Corresponding author.
** Corresponding author.
E-mail addresses: drsrallam@gmail.com (A.S. Rao), jayaphysics@yahoo.com (M. Jayasimhadri).

https://doi.org/10.1016/j.jallcom.2019.06.169
0925-8388/

Materials Research Bulletin 116 (2019) 79–88

Contents lists available at ScienceDirect

Materials Research Bulletin

journal homepage: www.elsevier.com/locate/matresbu

Color tunability and energy transfer studies of Dy^{3+} / Eu^{3+} co-doped calcium aluminozincate phosphor for lighting applications

Sumandeep Kaur, A.S. Rao*, M. Jayasimhadri*

Department of Applied Physics, Delhi Technological University, Bawana Road, New Delhi, 110 042, India

ARTICLE INFO

Keywords:
Calcium aluminozincate phosphors
XRD
FE-SEM
Photoluminescence
Activation energy

ABSTRACT

Dy^{3+} doped and Dy^{3+}/Eu^{3+} co-doped calcium aluminozincate (CAZ) phosphor synthesized by Pechini sol-gel method. Structural and morphological analysis were carried out by using X-ray diffractometer (XRD) and field emission scanning electron microscope (FE-SEM). The photoluminescent (PL) spectra were recorded and energy transfer mechanism between Dy^{3+} and Eu^{3+} ions were studied using Dexter and Reisfeld's approximation. The colorimetric properties were studied by evaluating CIE coordinates and correlated color temperature (CCT). The energy transfer mechanism was analysed by applying Inokuti-Hirayama (I-H) model on decay curves as well. The thermoluminescence (TL) glow curve analysis reveals two trap centres in the present host. The obtained results indicate that the CCT can be tuned from warm to cool region and color tunability can also be achieved in Dy^{3+}/Eu^{3+} co-activated CAZ phosphor by varying the excitation wavelength or activator concentration in the host lattice and hence can be effectively utilized in white light emitting diodes (wLEDs).

1. Introduction

Nowadays, white light emitting devices (wLEDs) have pursued great attention due to their properties of low toxicity, low power consumption, high efficiency, and higher durability as compared with conventional lighting sources [1–3]. There are diverse ways to mimic sunlight artificially using white light emitters:

(i) By making an assembly of red, green and blue LEDs. Since it requires independent output power control on each LED, it is difficult to achieve white light using tri-color LEDs and also it is expensive [4];
(ii) By coupling yellow phosphor (YAG: Ce) and blue LED (InGaN) chip. The spectral emission in this method results in poor color rendering index (CRI) and insufficient color temperature due to halo effect making it less efficient [5,6];
(iii) By coating a mixture of red, green, and blue phosphor on n-UV/UV LED, which is well-known as multiphase phosphor converted white LED (pc-wLED) [7]. However, trichromatic phosphors based pc-wLED offers low luminescence efficiency due to re-absorption of blue light by red and green emitting phosphors [5,8–10].

To achieve sunlight like emission with high CRI (Ra > 80) and low correlated color temperature (CCT < 4500 K), it is expected that coactivated single phase phosphor will give full color emission for application in display devices. The development of co-doped single-phase phosphor provides color tunability and relaxed perception to human eyes [11,12].

Over the past few decades, the development of inorganic oxides has been a subject of keen interest owing to their special merits such as high chemical and thermal stability, and photo stability. Apart from their excellent stable behaviour, they are environment friendly which captivates researchers to explore further [13–15]. Earlier reports suggest many inorganic materials, for instance, molybdates, borates, phosphates, aluminates, zincates, tungstates etc. have been studied extensively for their luminescent properties [3,6,16–19]. Among these inorganic hosts, zincates have emerged as an excellent host due to their prevalent optical and luminescent properties. Therefore, in this report calcium aluminozincate doped with rare earth (RE) ions have been established for the desired luminescent properties. The RE ions play an irreplaceable role in lighting and display devices. Their unique luminescence properties attributed to transitions from incompletely filled 4f energy levels whose position depends on the local environment of the RE ion due to the intermixing between atomic orbitals of oxygen atoms in the host and RE ions [20]. Owed to outstanding luminescent efficiency, researchers are engrossed in RE doped inorganic phosphors for their indispensable applications in lighting fields such as full color displays, LEDs, fluorescence imaging, lasers, and scintillators

* Corresponding authors.
E-mail addresses: drsrallam@gmail.com (A.S. Rao), jayaphysics@yahoo.com (M. Jayasimhadri).

https://doi.org/10.1016/j.materresbull.2019.04.022
Received 19 February 2019; Received in revised form 13 April 2019; Accepted 13 April 2019
Available online 15 April 2019

Journal of Luminescence 202 (2018) 461–468

Contents lists available at ScienceDirect

Journal of Luminescence

journal homepage: www.elsevier.com/locate/jlumin

Enhanced red down-conversion luminescence and high color purity from flux assisted Eu^{3+} doped calcium aluminozincate phosphor

Sumandeep Kaur, A.S. Rao*, M. Jayasimhadri*

Department of Applied Physics, Delhi Technological University, Bawana Road, New Delhi 110042, India

A B S T R A C T

Trivalent europium ions (Eu^{3+}) doped calcium aluminozincate (CAZ) phosphors blended with various fluxes (NaF, NaCl and $Na_2B_4O_7$) have been synthesized by conventional solid-state reaction method. The structural, morphological and luminescent properties along with lifetimes have been investigated in detailed. The Judd-Ofelt (J-O) analysis has been carried out to get insight of optical properties. The X-ray diffraction (XRD) pattern confirms the single phase orthorhombic structure for Eu^{3+} doped CAZ phosphor with NaCl and $Na_2B_4O_7$ fluxes; whereas the phase purity has not been achieved in NaF assisted Eu^{3+} doped CAZ phosphor. The as-synthesized phosphor has uneven agglomerated micron sized particles. The photoluminescence (PL) studies exhibit significant enhancement in the red emission for Eu^{3+} doped CAZ phosphor with the addition of $Na_2B_4O_7$. The emission intensity has been found to increase approximately 1.5 times using NaCl and 2.5 times for $Na_2B_4O_7$ in Eu^{3+} doped CAZ phosphor as compared to the phosphor without any flux. The emission spectrum of optimized Eu^{3+} doped CAZ phosphor added with $Na_2B_4O_7$ flux has been compared with the commercial Y_2O_3: Eu^{3+} phosphor. The CIE chromaticity coordinates and color purity calculated for $Na_2B_4O_7$ in Eu^{3+} doped CAZ phosphor is close to commercial red phosphor. The decay curves show bi-exponential behaviour with experimental lifetimes in the range of microseconds for the as-prepared phosphors. All these results indicate that the $Na_2B_4O_7$ flux assisted Eu^{3+} doped CAZ phosphor can serve as an efficient red phosphor under blue light for applications in white light emitting devices.

1. Introduction

In recent years, research and development of phosphor converted white light emitting diodes (pc-WLEDs) have gained considerable interest owing to their high efficiency, long lifetime, mercury free and low power consumption [1–4]. White light emitting diodes (WLEDs) have been employed in various applications, such as illumination systems, optical communication, optical storage and sensors [5–7]. The commercial pc-WLED is an integrated assembly of high efficiency blue (InGaN) LED chip and yellow (YAG: Ce) phosphor [8,9]. The combination of blue and yellow light emits white light. Since commercial pc-WLEDs are in deficit of red component in the emission spectrum of the YAG: Ce phosphor, they have a lower color rendering index (CRI) ($Ra < 80$) and high correlated color temperature ($CCT \sim 7750$ K) [8,10–12]. Aiming to solve this inexorable problem, a red light emitting phosphor is needed to enrich the red region in the pc-WLED to improve the CRI and CCT of the device [13–15]. At present, commercial red sulphide phosphor (Y_2O_2S: Eu^{3+}) suffers with low chemical stability and less efficient to get excited in n-UV and deep blue spectral region [16]. Nitride phosphor shows deep broad red emission and difficult to synthesize, which limit its applications [3,8,17]. Therefore, it has become important to develop a new red phosphor for pc-WLEDs. The rare earth (RE) ions enriched in f-f energy levels give abundant emission color in visible region depending upon the transition it undergoes in the host lattice [7]. Among various RE ions, Eu^{3+} serves as an excellent dopant for red light emitting phosphors to improve CRI and stability in WLEDs for optoelectronic applications [18–20].

The luminescent properties of phosphors also get influenced by some other factors such as synthesis technique, concentration of activator, use of sensitizer, and addition of flux. Among these factors, addition of flux improves the quality of phosphor by lowering calcining temperature, improving size distribution uniformity and enhancing the luminescence intensity [21,22]. In general, alkali halide fluxes have been reported in literature to enhance the emission intensity, for example Na_2CO_3-SiO_2-NaF in YAG: Ce, BaF_2 and CaF_2 in $BaMgAl_{10}O_{17}$: Eu^{2+}/Mn^{2+}, H_3BO_3, NH_4Cl, NH_4F, NH_4Br, $BaCl_2$, $BaBr_2$, CaF_2 and BaF_2 in Zn_2SiO_4:Mn^{2+} [22–24]. Apart from halide fluxes, boric acid (H_3BO_3) and borax ($Na_2B_4O_7$) have also been reported in (Ca,Zn)TiO_3: Pr^{3+},

* Corresponding authors.
E-mail addresses: drsrallam@gmail.com (A.S. Rao), jayaphysics@yahoo.com (M. Jayasimhadri).

https://doi.org/10.1016/j.jlumin.2018.06.015
Received 24 January 2018; Received in revised form 8 May 2018; Accepted 6 June 2018
Available online 07 June 2018

Ceramics International 43 (2017) 7401–7407

Contents lists available at ScienceDirect

Ceramics International

journal homepage: www.elsevier.com/locate/ceramint

Spectroscopic and photoluminescence characteristics of Sm^{3+} doped calcium aluminozincate phosphor for applications in w-LED

Sumandeep Kaur, A.S. Rao*, M. Jayasimhadri*

Department of Applied Physics, Delhi Technological University, Bawana Road, New Delhi 110042, India

ARTICLE INFO

Keywords:
XRD
Calcium aluminozincate phosphor
PL
TR-PL
FT-IR
Solid state reaction

ABSTRACT

Monophase Calcium Aluminozincate ($Ca_3Al_4ZnO_{10}$) phosphor doped with Sm^{3+} ions by varying concentrations have been prepared at 1300 °C using conventional solid state reaction technique. The crystal structure and phase analysis of the as-prepared phosphor has been carried out by X-ray Diffraction (XRD) studies. Morphology and functional groups present in the phosphor have been investigated thoroughly by using Scanning Electron Microscope (SEM) and Fourier Transform Infrared (FT-IR) spectral measurements, respectively. Under 401 nm excitation, the as-prepared phosphor exhibit intense visible orange emission at 601 nm. It has been observed that 1.0 mol% of Sm^{3+} ions concentration is optimum to give intense visible orange emission. The PL analysis reveals that the dipole-dipole interaction is primarily responsible for the concentration quenching observed beyond 1.0 mol% of Sm^{3+} ions. The TR-PL study reveals a bi-exponential behavior of decay curves with an average lifetime of the order of microseconds. The CIE coordinates (x=0.574 and y=0.424) measured for the optimized phosphor are very close to the intense orange emission coordinates specified by Nichia Corporation developed Amber LED NSPAR 70BS (0.570, 0.420). The spectroscopic, PL and TR-PL studies suggest the potential use of Sm^{3+} doped calcium aluminozincate phosphors for display and white light emitting devices.

1. Introduction

In recent years, conventional light sources such as incandescent and fluorescent lamps have been replaced by solid state lighting (SSL) technology. SSL technology involves white Light Emitting Diodes (w-LEDs), which are globally used for wide spread applications in consumer electronics and general illumination [1,2]. It offers many scientific and technological patronages such as environmental friendliness, lower operating temperature and effective energy utilization by saving 80% of energy consumption over conventional lighting devices. In the light of the aforementioned advantages, w-LEDs are considered to be the next generation lighting sources [3–6]. Indium Gallium Nitride (InGaN) or Gallium Nitride (GaN) chip based w-LEDs are gaining paramount attention because of their longevity, high luminous efficiency, high energy efficiency, smaller size, faster switching, excellent reliability with reduced operating expenses and capable of replacing conventional light sources [2,5–10]. The current strategy of achieving white light is based on yellow phosphor encapsulated over UV/blue LED chip, which utilizes UV/blue light for excitation. However, this strategy suffers from several drawbacks such as lower color rendering index (CRI), high correlated color temperature (CCT), thermal quenching, narrow visible range and hence cannot meet the demand of warm white light needed for indoor and artificial lighting [11,12]. To circumvent the problem, red phosphors can be introduced to improve CRI and CCT. However, commercial red phosphor $Y_2O_2S:Eu^{3+}$ has some shortcomings such as inimical decomposition products, chemical instability which degrades its luminescence efficiency over a period. This necessitate the development of a new orange-red emitting phosphor that can be excited by n-UV or blue LED [13,14].

Rare earth (RE) ions play a vital role in display devices and lighting fields due to f-f and f-d transitions, which give narrow and broad emission, respectively. At present, Sm^{3+} doped phosphors are studied for the development of an orange-red phosphor due to their potential applications for color display, plasma display panels and solid state lighting [10,15–17]. For efficient white light emission with improved CRI and CCT, a new combination of cyan plus orange can be realized, where orange emission can be accomplished from Sm^{3+} ions doped phosphors [18]. Therefore, Sm^{3+} serves as one of the best activator/dopant for orange-red emission to augment the efficiency of w-LEDs [19].

Inorganic oxide based compounds, including zincates, aluminates [20–26] doped with RE ions are better luminescent materials over

* Corresponding authors.
E-mail addresses: drsrallam@gmail.com (A.S. Rao), jayaphysics@yahoo.com (M. Jayasimhadri).

http://dx.doi.org/10.1016/j.ceramint.2017.02.129
Received 3 January 2017; Received in revised form 22 February 2017; Accepted 24 February 2017
Available online 28 February 2017

Journal of Alloys and Compounds 697 (2017) 367–373

Contents lists available at ScienceDirect

Journal of Alloys and Compounds

journal homepage: http://www.elsevier.com/locate/jalcom

A novel red emitting Eu^{3+} doped calcium aluminozincate phosphor for applications in w-LEDs

Sumandeep Kaur, M. Jayasimhadri*, A.S. Rao*

Department of Applied Physics, Delhi Technological University, Bawana Road, New Delhi 110 042, India

ARTICLE INFO

Article history:
Received 9 August 2016
Received in revised form
28 October 2016
Accepted 12 December 2016
Available online 13 December 2016

Keywords:
Phosphors
White LEDs
Solid state reaction
Photoluminescence
XRD
Band gap

ABSTRACT

A novel calcium aluminozincate phosphor doped with Eu^{3+} ions has been synthesized by conventional solid state reaction method and characterized by using X-ray diffraction (XRD), Scanning Electron Microscope (SEM), Diffuse Reflectance Absorbance (DRA) and Spectrofluorophotometer to study the structural, morphological and photoluminescence (PL) properties. All the XRD peaks are matching well with the standard ICDD card confirm that the prepared phosphors consist of single phase orthorhombic structure ($Ca_3Al_4ZnO_{10}$) having Pbc2 space group. The PL spectra recorded under near-UV/blue excitations demonstrates a very distinct and intense red emission from all the phosphors. In the present investigation, we found that 2 mol% of Eu^{3+} ions concentration is optimum in this host to give intense red emission. This result is also in consistent with the CIE chromaticity coordinates measured from the PL spectra of the samples under investigation. The results obtained for the optimized phosphor in the present investigation such as PL and CIE coordinates (x = 0.629 and y = 0.370) are close to the commercial red phosphor Y_2O_2S: Eu^{3+} (x = 0.622 and y = 0.351) and also very near to the coordinates specified by National Television Standard Committee (NTSC).

1. Introduction

Energy became an essential commodity in our lives and the demand for energy in various sectors of the present society is increasing day by day. Lighting plays a vital role in our lives as well as in commerce and industry worldwide as it consumes large amount of the total energy produced. Energy efficiency is one of the most effective and challenging means to meet the ever growing demand of energy worldwide. Realizing the need of high efficiency lighting devices, various scientists across the world are working to meet this challenge. The rapid scientific quest for achieving the energy efficient light sources, white light emitting diodes (w-LEDs) open up opportunities in the general lighting market. Lighting applications using LEDs, organic LEDs, or light emitting polymers are commonly refers to Solid State Lighting (SSL). Now a days, SSL technology is emerging as a promising one to replace the conventional lighting sources such as incandescent bulbs, fluorescent lamps and high intensity discharge lamps due to their unique features such as high efficiency, compact and rigid structure, longer lifetime and their efficiency in power saving [1,2]. SSL technology also contributes immensely to the reduction of greenhouse gases and thereby helps in protecting the environment [3,4]. The history of solid state lighting dates back to 1907 when H.J. Round discovered a green glow in the silicon carbide diode junction [5]. However this major invention remained unnoticed for a longer period. A significant development in this direction took place when Shuji Nakamura fabricated double-hetrostructured InGaN/GAN blue LED chips in 1993 [6]. The first white light emitting diode was brought in to the commercial market by Nichia Corporation in 1996 [7]. From that time onwards, the search for the most efficient w-LEDs became a thrust area and the scientists are striving hard to bring out financially viable and environmental friendly w-LEDs needed for lighting industries.

There are various approaches to get efficient solid state sources for white light generation [8,9]. However two different prominent methods are employed most commonly. The first one is using phosphor free RGB-LEDs. In this method light from three monochromatic LED sources, red, green and blue (RGB) are mixed directly so as to produce a white light. Second one is phosphor based, i.e., phosphor-converted white LEDs (pc-white LEDs) method. Nowaday pc-white LEDs approach has been paid much attention when compared with phosphor free RGB-LED approach

* Corresponding authors.
E-mail addresses: jayaphysics@yahoo.com (M. Jayasimhadri), drsrallam@gmail.com (A.S. Rao).

http://dx.doi.org/10.1016/j.jallcom.2016.12.150
0925-8388/

Materials Research Bulletin 104 (2018) 77–82

Contents lists available at ScienceDirect

Materials Research Bulletin

journal homepage: www.elsevier.com/locate/matresbu

Spectroscopic studies of Dy^{3+} doped borate glasses for cool white light generation

Sumandeep Kaur, Amit K. Vishwakarma, Nisha Deopa, Aman Prasad, M. Jayasimhadri, A.S. Rao*

Department of Applied Physics, Delhi Technological University, Bawana Road, New Delhi, 110 042, India

ARTICLE INFO

Keywords:
Glasses
FT-IR
Luminescence
Dexter theory
Concentration quenching

ABSTRACT

The Dy^{3+} ions doped Na_2O-ZnO-Al_2O_3-B_2O_3 (BAZN) glasses with variable doping concentrations were synthesized by melt-quenching technique. The XRD pattern reveals amorphous nature of the as-synthesized glass. The FT-IR spectrum reveals various stretching and bending vibration of aluminates, borate and some other groups. The emission spectra exhibit two intense bands at around 482 nm (blue) and 575 nm (yellow) corresponding to the $^4F_{9/2} \rightarrow {}^6H_{15/2}$ and $F_{9/2} \rightarrow {}^6H_{13/2}$ transitions respectively. The CIE chromaticity coordinates of the as-synthesized glasses are lying in white region and in proximity to the coordinates for white light specified by National Television Standard Committee and commercial phosphor converted white light emitting devices. The decay profile of BAZN glasses showed bi-exponential behavior due to the energy transfer mechanism from excited donor ion to unexcited acceptor ion. The above-mentioned studies show potential of the as-synthesized Dy^{3+} doped BAZN glasses in solid state lighting applications.

1. Introduction

In quite recent years, awareness about climate change, environmental problems and harmful impact of using fossil fuels as a source of energy on environmental issues has increased to an extent where people are now seeking some alternatives for fossil fuels, which are less hazardous to environment. Lighting consumes major fraction of energy; therefore, research is highly targeting on reducing consumption of energy for lighting purposes. Quite recently, white Light Emitting Diodes (w-LEDs) have replaced the conventional incandescent and fluorescent lamps to reduce the usage of fossil fuels and also to meet global power requirements by producing more efficient light. The phosphor based w-LEDs have attracted great attention due to its extraordinary luminescent efficiency, low power consumption, small volume, long persistence and environment friendliness [1–4]. These phosphor based w-LEDs exhibit high color rendering index, but these w-LEDs have disadvantage that phosphor material used to produce it requires a coating of organic resin having poor heat resistance which reduces the luminous efficacy [4–7]. Therefore, it is needed to develop a phosphor free w-LED that can emit white light with improved luminous efficacy and color rendering index with stable color temperature and cost effective in comparison to the conventional w-LEDs. Now-a-days, glasses are found to be a suitable alternative for resin based phosphors. The rare earth (RE) doped glasses have several advantages over RE doped phosphors such as high brightness, low power consumption, possibility of wavelength tuning, high doping proficiency, shape and size control, no aging effects and free of organic resin [8–10]. Moreover, glasses doped with RE ions are receiving great attention for its wide range of applications such as solid-state lighting, photovoltaic cells, FED applications, X-ray sensors, optical temperature sensors, optical amplifiers, UV–vis converters, plasma display devices, bio imaging and bio sensing, w-LEDs [11–20].

The optical and fluorescence properties of RE ions depend upon the local environment and phonon energies of the host glass system [21]. Borate glasses are well studied due to its ease of preparation, good strength, high transparency, and excellent isotropic nature. Borate glasses are generally known for their high thermal stability, low melting point, different coordination numbers and good solubility of RE ions, but their phonon energy is quite high (1300 cm^{-1}) which makes them unsuitable for lighting purposes [22–24]. In general, heavy metal oxides having low phonon energy are mixed with borates to reduce the redundant phonon energy of borate glasses and make it more suitable to be used in the development of optoelectronic devices, solar energy converters, gas sensors and UV lasers [25–27]. Based on the concentration of heavy metal oxides in the glass, it can act as a glass former as well as glass modifier. ZnO have attracted many researchers because of its optical, electrical and magnetic properties along with its non-toxic and non-hygroscopic nature and having wide direct band gap, large exciting binding energy and intrinsic emitting property [28]. It also improves chemical durability, stability and RE ion solubility in the glass. By adding Al_2O_3 in oxide glasses, devitrification of glass is

* Corresponding author.
E-mail address: drsrallam@dce.ac.in (A.S. Rao).

https://doi.org/10.1016/j.materresbull.2018.04.002
Received 27 January 2018; Received in revised form 18 March 2018; Accepted 1 April 2018
Available online 03 April 2018

Optical Materials 84 (2018) 318–323

Contents lists available at ScienceDirect

Optical Materials

journal homepage: www.elsevier.com/locate/optmat

Intense green emission from Tb^{3+} ions doped zinc lead alumino borate glasses for laser and w-LEDs applications

Sumandeep Kaur, Nisha Deopa, Aman Prasad, Rajat Bajaj, A.S. Rao*

Department of Applied Physics, Delhi Technological University, Bawana Road, New Delhi, 110 042, India

ARTICLE INFO

Keywords:
Glasses
Photoluminescence
FT-IR
Photoluminescence decay
CIE coordinates

ABSTRACT

Zinc Lead Alumino Borate (ZPAB) glasses doped with varying concentrations of Terbium (Tb^{3+}) ions have been prepared via melt quenching technique. Structural studies like XRD and FT-IR were performed to ascertain the amorphous nature and functional groups present in the as prepared glasses respectively. Photoluminescence (PL) properties of the as prepared glasses were investigated by performing excitation and emission spectral studies under 545 nm and 369 nm wavelengths respectively. Under n-UV excitation, these glasses exhibit four emission peaks due to transitions from the excited $^5D_4$ level of Tb^{3+} to ^7F_J (J = 3 to 6) ground level. Among all, the intense emission band was observed at 545 nm corresponding to the $^5D_4 \rightarrow {}^7F_5$ transition and the emission intensity increases up to 1 mol%, beyond concentration quenching took place. The Dexter theory confirms the possibility of energy transfer via electric dipole-dipole interaction between Tb^{3+}-Tb^{3+} ions. The CIE chromaticity coordinates and color purity were evaluated which falls in intense green region and close to European Broadcasting Union illuminant green. The PL decay studies were carried out to know the experimental lifetimes of the fluorescent levels of Tb^{3+} ions. The lifetime measured for $^5D_4 \rightarrow {}^7F_5$ transition of the as prepared glasses decreasing with increase in Tb^{3+} ions concentration, may be due to efficient energy transfer between Tb^{3+}-Tb^{3+} ions. The aforementioned results confirm potentiality of these glasses in solid state green laser and as a green component in tricolor w-LEDs.

1. Introduction

Over the past few decades, rare earth (RE) ions doped materials have drawn significant attention of researchers for practical application in solid state lasers, light converters, sensors, field emission displays, scintillators, optoelectronic applications, and thermo-luminescent dosimeters [1–5]. Phosphor based w-LEDs have seen numerous advances in the field of solid state lighting (SSL) and different approaches are used to design them. The first method involves a blue emitting InGaN LED chip in conjunction with a yellow emitting phosphor (YAG: Ce^{3+}). But, halo effect due to blue/yellow color separation and poor color rendering index (CRI) because of lack of red component makes this approach unsuitable for SSL. The temperature and drive current are also detrimental to the blue LED chip. In second approach, the combination of near ultraviolet (NUV) LEDs with RGB phosphors is used to overcome the aforementioned shortcomings. This significantly improves CRI and reduces halo effect [6,7]. However, in both the approaches phosphor is suspended in the form of powder in an epoxy resin which is made up of an organic material. Due to high temperatures and high energy/power excitation light sources, the epoxy resin gets damaged. This affects the luminous efficiency and CRI in a detrimental manner [8]. The need to develop a monolithic material with high durability having superior emission property prompted us to propose an inorganic glass as a potential candidate for SSL applications. The decrement of re-absorption of light only adds to the advantages of using glass as a luminescent material [9]. Owing to the ease of alteration in composition, glasses have been involved in various applications. Glasses have been considered as excellent luminescent materials due to excellent thermal, chemical and mechanical stability, high solubility of RE ions, ease of preparation, easy shaping of elements and low cost [3].

Among various glass formers, borate groups have been considered as one of the best glass formers due to low melting point, robust, high optical transparency, chemical durability and inexpensive [10,11]. However, borate glasses have some shortcomings as it shows hygroscopic nature and can easily absorb water in moist environment and stretching vibrations of borate groups in forming network exhibit high phonon energy which results in non-radiative energy losses [12]. To inculcate these shortcomings of borate glasses, network modifiers can be added to the borate glasses and the optical and chemical properties of borate glasses can be enhanced significantly [12]. Heavy metal

* Corresponding author.
E-mail address: drsrallam@gmail.com (A.S. Rao).

https://doi.org/10.1016/j.optmat.2018.07.020
Received 16 May 2018; Received in revised form 7 July 2018; Accepted 8 July 2018
Available online 14 July 2018
0925-3467/

Optics and Laser Technology 108 (2018) 434–440

Contents lists available at ScienceDirect

Optics and Laser Technology

journal homepage: www.elsevier.com/locate/optlastec

Full length article

Spectral studies of Eu^{3+} doped lithium lead alumino borate glasses for visible photonic applications

Nisha Deopa [a], Sumandeep Kaur [a], Aman Prasad [a], Bipin Joshi [b], A.S. Rao [a,*]

[a] Department of Applied Physics, Delhi Technological University, Bawana Road, New Delhi 110042, India
[b] Department of Science and Technology, Technology Bhavan, New Mehrauli Road, Delhi 110016, India

ARTICLE INFO

Article history:
Received 9 May 2018
Received in revised form 9 June 2018
Accepted 12 July 2018
Available online 24 July 2018

ABSTRACT

Quaternary lithium lead alumino borate (LiPbAlB) glasses doped with different concentration of Eu^{3+} ions have been synthesized by melt quench technique and characterized by using XRD, Photoluminescence (PL), PL decay and CIE-chromaticity co-ordinates to understand their luminescence behavior. A broad hump observed in the XRD spectrum confirms glassy nature of the as-prepared un-doped glasses. By applying Judd-Ofelt (J-O) theory to the emission spectra, various radiative parameters for the prominent fluorescent levels of Eu^{3+} have been evaluated. An intense excitation peak observed at 393 nm matches well with the excitation wavelength of n-UV LED chip. The PL intensity increases up to 7 mol% of Eu^{3+} in LiPbAlB glasses and beyond quenching observed. The decay profiles observed for the prominent emission line $^5D_0 \rightarrow {}^7F_2$ were well fitted to bi-exponential function and lifetime are decreasing with increase in Eu^{3+} ion concentration which may be due to efficient energy transfer between Eu^{3+}-Eu^{3+} through cross relaxation channels. CIE chromaticity co-ordinates evaluated from the emission spectra, are found to be in red region of the visible spectrum. The enhanced color purity and quantum efficiency values were also evaluated from the emission spectral data. From the emission cross-sections, branching ratios, quantum efficiency, CIE coordinates and color purity, it was concluded that 7 mol% of Eu^{3+} ion concentration (glass C) is optimum in LiPbAlB glasses for visible red photonic device application.

1. Introduction

Rare Earth (RE) ions doped glassy matrix have found immense usage today in the field of lighting technologies, lasers, photovoltaic devices and development of new modes of telecommunication [1–5]. What catches immense attention is the present day development of such compounds for solid state lighting (SSL) applications in the form of w-LEDs. Now, w-LEDs are conventionally fabricated via two synthesis techniques. First is when YAG: Ce^{3+} yellow phosphor is excited by blue LED InGaN chip [2,6]. Second one is when mixed RGB phosphors are excited with the help of UV LEDs [2,6]. But low color rendering index (CRI) and high color correlated temperature (CCT = 7750 K) in the case of former and low luminescence efficiency in the case of later are some of the well-known drawbacks of such synthesis techniques [7,8]. Also, a polymer based epoxy material is used in the construction of LEDs that encapsulate the phosphor [9]. The emission of such w-LED depends on the thickness of the epoxy material and on the phosphor. But this epoxy material can deteriorate under high energy excitation and high temperature [10]. Therefore, RE ions doped glasses are a good alternative to such phosphors as there is no epoxy resin involved. Also they are highly durable and exhibit enhance luminescence. Glasses can be produced in high volume and have optical uniformity so they are mostly favored over crystalline host. Glasses doped with RE ions have attracted significant attention because they can be fabricated easily in several forms [11,12]. Apart from having low non-linear refractive indices, these glasses behave like a good elastic matrix and therefore can accept high amount of RE ions [13].

Boron Trioxide (B_2O_3) is one of the best glass former because of its high transparency, low melting point, high thermal stability, high mechanical and chemical strength with high solubility of RE ions [14,15]. However, B_2O_3 possess high phonon energy (1300 cm^{-1}) due to stretching vibrations of network forming oxides. This, in turn, enhances the non-radiative emission. However such redundant phonon energies can be reduced drastically by adding heavy metal oxides (HMO) such as PbO to the borate glasses [16]. Greater quantum efficiencies are therefore expected due to smaller multi-phonon decay rates and larger radiative transition probabilities. Lithium Oxide (Li_2O) is used in the glass matrix to improve the chemical stability and also to modify its chemical

* Corresponding author.
E-mail address: drsrallam@gmail.com (A.S. Rao).

https://doi.org/10.1016/j.optlastec.2018.07.010
0030-3992/

Journal of Rare Earths 37 (2019) 52–59

Contents lists available at ScienceDirect

Journal of Rare Earths

journal homepage: http://www.journals.elsevier.com/journal-of-rare-earths

Spectroscopic investigations on Dy^{3+} ions doped zinc lead alumino borate glasses for photonic device applications

Nisha Deopa, Shubham Saini, Sumandeep Kaur, Aman Prasad, A.S. Rao*

Department of Applied Physics, Delhi Technological University, Bawana Road, New Delhi 110042, India

ARTICLE INFO

Article history:
Received 22 February 2018
Received in revised form
30 March 2018
Accepted 3 April 2018
Available online 10 August 2018

Keywords:
Glasses
J-O parameters
Luminescence
Inokuti-Hirayama model
Energy transfer
Rare earths

ABSTRACT

This paper presents the structural, optical absorption, photoluminescence (PL) and decay spectral properties of Dy^{3+} ions doped zinc lead alumino borate (ZPAB) glasses to elucidate their possible usage in photonic devices such as w-LEDs and lasers. A broad hump shown by the XRD spectrum recorded for an un-doped ZPAB glass confirms its non-crystalline nature. The Judd-Ofelt (J-O) intensity parameter evaluated from the measured oscillator strengths of the absorption spectral features were used to estimate various radiative parameters and also to understand the nature of bonding between Dy^{3+} ions and oxygen ligands. Under 350 nm excitation, the as-prepared glasses are exhibiting two emission bands $^4F_{9/2} \rightarrow {}^6H_{15/2}$ (blue), and $^4F_{9/2} \rightarrow {}^6H_{13/2}$ (yellow) at 483 and 575 nm, respectively. From the PL spectra, the Y/B ratio values, CIE chromaticity color coordinates and color correlated temperature (CCT) were evaluated. The experimental lifetimes measured from the decay profiles are decreasing with increase in Dy^{3+} ions concentration in these glasses which may be attributed to the cross-relaxation and non-radiative multiphonon relaxation process. Decay profiles observed for higher concentration were well fitted to Inokuti-Hirayama (I-H) model to understand the energy transfer process and subsequent decrease in experimental lifetimes. The higher values of radiative parameters, emission cross-sections, quantum efficiency, optical gain and gain band width suggest the suitability of 0.5 mol% of Dy^{3+} ions in these ZPAB glasses for the photonic device application.

1. Introduction

Solid state lighting (SSL) has received considerable attention recently in the field of luminescent technology due to its eco-friendly nature and ability to consume less energy. Apart from this, SSL based devices are playing significant role in the development of white LEDs and seeking immense research due to their long life span, high efficiency and less power consumption as compared to conventional incandescent bulbs and CFLs.[1–5] The aforementioned applications have encouraged researchers to develop luminescent technology that is highly color tunable as well as efficient. Nowadays, LEDs have been fabricated by taking a combination of blue/n-UV excitation chips and phosphor wavelength converter models.[6–8] Phosphors are usually encapsulated in an epoxy resin which is made up of a polymer material. The epoxy resin can get damaged at high temperature or high energy excitation sources. Hence rare earth (RE) doped glasses are best alternatives to phosphors as they are highly durable and exhibit enhanced luminescence. Since glasses can be produced in high volume having optical uniformity, they are mostly favored over crystalline host. Glasses doped with RE ions have attracted significant attention because they can be fabricated easily in several forms, have higher transparency, require a simple manufacture procedure and exhibit homogeneous light emission. Also, they are less susceptible to damage due to heat and have low production cost.[9]

Among all the glass formers available, B_2O_3 is one of the best glass formers because of its low melting point, high thermal stability, high mechanical and chemical strength with high solubility of RE ions.[10,11] However, B_2O_3 possesses high phonon energy (1300 cm^{-1}) due to stretching vibrations of network forming oxides.[12] Such high phonon energies in turn enhance the non-radiative emissions and hampers the luminescence efficiency. Therefore, to reduce such redundant phonon energies, preferably a heavy metal oxide (HMO) such as PbO is added to the borate glasses.[13] Consequently, larger quantum efficiencies are expected due to smaller multi-phonon decay rates and larger radiative transition probabilities. ZnO in any host glass is having special

* Corresponding author. Fax: +91 01127871023.
E-mail address: drsrallam@gmail.com (A.S. Rao).

https://doi.org/10.1016/j.jre.2018.04.013
1002-0721/

Journal of Materials Science: Materials in Electronics (2018) 29:20759–20767
https://doi.org/10.1007/s10854-018-0217-4

UV radiation emitting Gd^{3+} activated Sr_2SiO_4 host system prepared by sol–gel procedure: structural, electron paramagnetic resonance, and luminescence studies

Vijay Singh[1] · N. Singh[1] · M. S. Pathak[1] · Sumandeep Kaur[2] · M. Jayasimhadri[2] · S. Watanabe[3] · T. K. Gundu Rao[3]

Received: 6 September 2018 / Accepted: 11 October 2018 / Published online: 16 October 2018

Abstract
Trivalent gadolinium (Gd^{3+}) activated strontium silicate (Sr_2SiO_4:xGd^{3+}; $0.01 \le x \le 0.11$) systems have been synthesized via sol–gel technique. The structural, morphological, luminescent, and magnetic properties have been investigated using X-ray diffraction patterns, scanning electron microscopy (SEM), photoluminescence (PL), and electron paramagnetic resonance (EPR) technique, respectively. The synthesized strontium silicate samples exhibit a mixed phase of α′ and β-Sr_2SiO_4. The SEM images show irregular morphologies with a random distribution of particles. The PL spectra confirm the ultraviolet emission from the synthesized samples and the optimum concentration of Gd^{3+} ions is observed at 0.05 mol. With low dopant concentrations, Sr_2SiO_4:Gd^{3+} sample displays EPR lines, mainly in the low field region with effective g-values 5.8, 4.5, 3.1, and 2.7. As dopant concentration increases, a broad line appears with $g_{eff} \sim 2.1$ along with the low field lines. A relatively strong crystal field is experienced by Gd^{3+} ion due to distortions in the immediate environment of the ion, which lead to low field EPR lines. These studies allow the use of gadolinium-activated strontium silicate in phototherapy lamps.

1 Introduction

Lanthanide activated inorganic materials have been extensively investigated due to their unique electronic, optical, and magnetic properties [1–3]. Among various inorganic hosts, silicates are known as excellent host materials for many technological applications due to their admirable chemical, physical, thermal, and high irradiation power stability [4–8]. Alkaline earth metal orthosilicates (M_2SiO_4; M = Ca, Sr, Ba) have attracted much attention in the recent years [9–14]. Alkaline earth silicates are resistant to many chemicals and air moisture [15]. Strontium orthosilicate (Sr_2SiO_4), in particular, has attracted attention due to its special structural features, excellent physical, and chemical stability [16]. The Eu^{2+} activated Sr_2SiO_4 has been used commercially in white LEDs in place of YAG:Ce [17, 18]. The luminescence properties of Sr_2SiO_4 activated with different rare earth (RE) ions such as Eu^{3+}, Sm^{3+}, Eu^{2+}, Ce^{3+}, Tb^{3+}, Pr^{3+}, and Dy^{3+} have been extensively investigated due to their applications in white LEDs [12, 15, 19–22]. However, a lack of information exists regarding the exploration of the luminescence properties of the Gd^{3+} activated Sr_2SiO_4 system.

Among the lanthanide activated inorganic materials, trivalent gadolinium (Gd^{3+}) based systems have gained significant importance because of their simple electronic energy level scheme that can be used as a spectroscopic probe for host-dopant energy transfer dynamics, site swapping, point group symmetry, intricate structure-photoluminescence correlation, etc. [23–25]. In addition, Gd^{3+} ion contains seven unpaired electrons which make it an important ion as a water relaxation agent in MRI applications. Currently, Gd^{3+} ions are attracting more attention as neutron capture therapy agents in targeted radiotherapy for cancer treatment [26, 27]. In addition, a Gd ion can act as an auxiliary ion to serve as a trap center in several hosts for energy storage in long afterglow materials, and ionizing radiation detectors [28].

Ultraviolet (UV) radiations have been segregated into three different types: long wavelength UV rays (UV-A: 380–320 nm), medium wavelength UV rays

✉ Vijay Singh
vijayjiin2006@yahoo.com

[1] Department of Chemical Engineering, Konkuk University, Seoul 05029, Republic of Korea

[2] Department of Applied Physics, Delhi Technological University, Delhi 110 042, India

[3] Institute of Physics, University of Sao Paulo, Sao Paulo, SP 05508-090, Brazil

Ceramics International 44 (2018) 17074–17078

Contents lists available at ScienceDirect

Ceramics International

journal homepage: www.elsevier.com/locate/ceramint

UV emitting Pb^{2+} doped $SrZrO_3$ phosphors prepared by sol-gel procedure

N. Singh[a], Sumandeep Kaur[b], M. Jayasimhadri[b], M.S. Pathak[a], S. Watanabe[c], T.K. Gundu Rao[c], Jung-Kul Lee[a,*], Vijay Singh[a,*]

[a] Department of Chemical Engineering, Konkuk University, Seoul 05029, Republic of Korea
[b] Department of Applied Physics, Delhi Technological University, Delhi 110042, India
[c] Institute of Physics, University of Sao Paulo, SP 05508-090, Brazil

ARTICLE INFO

Keywords:
Sol-gel
XRD
EPR
Pb^{2+} ions
$SrZrO_3$
Photoluminescence

ABSTRACT

A series of Pb^{2+}-doped $SrZrO_3$ phosphors with a varying Pb^{2+} concentration has been successfully synthesized using the sol-gel method. The structural, morphological, and luminescence properties along with the electron paramagnetic resonance (EPR) properties have been investigated in details. The structural analysis was carried out by recording X-ray diffraction (XRD) patterns, which confirms the pure-phase formation of the synthesized phosphors. The morphological study was performed using a scanning electron microscope (SEM) that showed micron-sized particles with irregular morphologies. The photoluminescence excitation and emission spectra were also recorded. The emission intensity shows the maximum at 360 nm that was pumped at 278 nm for $SrZrO_3$:Pb^{2+}. The optimized Pb^{2+} concentration is 0.015 mol. Investigations of un-doped and Pb^{2+} doped $SrZrO_3$ phosphor have been carried out using electron paramagnetic resonance (EPR) technique. Pure $SrZrO_3$ exhibits an axially symmetric EPR line with $g_{||} = 1.93$ and $g_{\perp} = 1.99$. These lines are ascribed to Zr^{3+} ion. Additional lines are not observed in the Pb^{2+} doped phosphors.

1. Introduction

In recent years, the development of lighting technology has attracted researchers to the exploration of different hosts for diversified applications. The inorganic phosphors have various applications in field emission displays (FED), plasma display panels (PDP), fluorescent lamps, sensors, and optical-communication and imaging devices [1–5]. Due to the diversified applications, researchers have deeply investigated the properties of different hosts doped with different ions to ascertain their potential in terms of the previously mentioned applications.

The alkaline earth zirconates of the perovskite structure with the general formula ABO_3 (A = calcium [Ca], strontium [Sr], barium [Ba], lead [Pb]; B = titanium [Ti], silicon [Si], zirconium [Zr]) are of a high technological interest due to their high thermal and chemical stability, high refractive indices, and wide bandgaps with ferroelectric and piezoelectric properties [6]. Owing to the outstanding properties of the alkaline earth zirconates, various applications including sensors, ceramics, filters, memory and microelectronic devices have been identified [6,7]. The chemical and physical properties of these materials can be easily tuned through the addition of some dopants into the host. Among the heavy-metal ions, the Pb^{2+} can be used as an activator that emits diverse spectral lines in different hosts. Inorganics oxide phosphors doped with the Pb^{2+} have been applied in X-ray imaging devices, low-pressure lamps, high-energy physics, photocopying lamps, sensing, and phototherapy [7–10]. Among the various zirconates, the cubic-structure strontium zirconate ($SrZrO_3$) host lattice is also favored for its application in X-ray imaging, which is an important tool in the medical sciences, material engineering, and security screening [11,12].

The luminescence properties of a phosphor are dependent on the size, morphology, and synthesis temperature. The citrate sol-gel method provides an attractive alternative to the traditional synthesis methods. The sol-gel synthesis method not only reduces the synthesis temperature, but it also improves the morphology of the prepared phosphors and enhances the luminescence properties [13].

As far as we know, there are no previous reports on Pb^{2+}-doped $SrZrO_3$ phosphors. In the present article, the Pb^{2+}-doped $SrZrO_3$ phosphor has been synthesized using a citrate sol-gel method for which the dopant concentration was varied from 0 to 0.090 mol. The structural, morphological, and luminescence studies, along with an EPR analysis, have been realized in detail for the application of the phosphor in imaging devices.

2. Materials preparation and analysis

A series of the phosphors of $Sr_{1-x}ZrO_3$:Pb_x (x = 0.005, 0.015, 0.03,

* Corresponding authors.
E-mail addresses: jkrhee@konkuk.ac.kr (J.-K. Lee), vijayjiin2006@yahoo.com (V. Singh).

https://doi.org/10.1016/j.ceramint.2018.06.153
Received 26 May 2018; Received in revised form 16 June 2018; Accepted 18 June 2018
Available online 19 June 2018

Journal of ELECTRONIC MATERIALS, Vol. 48, No. 6, 2019
https://doi.org/10.1007/s11664-019-07175-w

An Electron Paramagnetic Resonance and Photoluminescence Investigation of UVB Radiation Emitting Gadolinium-Activated $CaY_2Al_4SiO_{12}$ Garnet Compound

VIJAY SINGH,[1,4] SUMANDEEP KAUR,[2] A.S. RAO,[2] N. SINGH,[1] M.S. PATHAK,[1] and J.L. RAO[3]

1.—Department of Chemical Engineering, Konkuk University, Seoul 05029, Korea. 2.—Department of Applied Physics, Delhi Technological University, Bawana Road, Delhi 110042, India. 3.—Department of Physics, S.V. University, Tirupati, Andhra Pradesh 517502, India. 4.—e-mail: vijayjiin2006@yahoo.com

Trivalent gadolinium (Gd^{3+}) activated $CaY_2Al_4SiO_{12}$ garnet compounds with a variable concentration of Gd^{3+} ions were synthesized by a sol–gel method. The synthesized garnet compounds were characterized for their structural, morphological, luminescent, and magnetic properties. The x-ray diffraction data of Gd^{3+} activated $CaY_2Al_4SiO_{12}$ garnet compound reveal the cubic structure with I*a3d* space group. The scanning electron microscope images represent the morphology of the particles. The photoluminescence properties were analyzed from the excitation and emission spectra. The emission spectra of the $CaY_2Al_4SiO_{12}$:Gd^{3+} garnet compound under 273 nm excitation exhibit two emission peaks at 308 nm and 314 nm and are attributed to $^6P_{5/2} \rightarrow {}^8S_{7/2}$ and $^6P_{7/2} \rightarrow {}^8S_{7/2}$ transitions, respectively. The emission peak observed at 314 nm is more intense than the peak observed at 308 nm. The high-intensity peak at 314 nm is used to cure various skin disorders, and hence is beneficial in phototherapy. The intensity of the emission peaks increases up to 0.09 mol of Gd^{3+} ion concentration in the $CaY_2Al_4SiO_{12}$ garnet compound, and beyond, then decreases, showing concentration quenching. The electron paramagnetic resonance of Gd^{3+} ions in the prepared garnet compound exhibits resonance signals with effective g values at $g \approx 6.5$, 5.0, 2.6, 2.2, 2.0, and 1.6 of the U-spectrum, due to cubic, octahedral, or tetrahedral distorted sites.

Key words: Sol–gel, EPR, Gd^{3+}, $CaY_2Al_4SiO_{12}$, garnet, luminescence

INTRODUCTION

Garnet host materials are one of the most important host materials for rare earth (RE) ions, because of their physical stability, high luminescent efficiency, good chemical stability, and high thermal properties.[1–5] Garnet-type structure offers promising candidates for electrolytes in solid-state electrochemical devices, and in rechargeable lithium batteries.[6,7] Garnet compounds have the general crystal formula $\{A_3\}[B_2](C_3)O_{12}$, where A, B, and C are in dodecahedral, octahedral, and tetrahedral coordinates, respectively.[8,9] In recent years, by combining the ions of different valence states, such as A = RE^{3+}, Ca^{2+}, Ba^{2+}, Sr^{2+}, or Mg^{2+}; B = Sc^{3+}, Ga^{3+}, or Al^{3+}; and C = Ga^{3+}, Al^{3+}, or Si^{4+} at various crystallographic sites, a significant number of different compositions were obtained, without changing the garnet structure.[10,11] Although the structure of garnet does not show any change, the local coordination structure of the sites can be changed, depending on the garnet composition. Exploiting the isomorphism in garnets is another approach to obtain new compounds with garnet structure that belong to the *Ia3d* space group.[12] In recent years, $MY_2Al_4SiO_{12}$ (where M = Ca, Ba, Sr,

(Received September 14, 2018; accepted March 28, 2019; published online April 8, 2019)

Journal of Non-Crystalline Solids 516 (2019) 82–88

Contents lists available at ScienceDirect

Journal of Non-Crystalline Solids

journal homepage: www.elsevier.com/locate/jnoncrysol

Spectroscopic properties of deep red emitting Tm^{3+} doped ZnPbWTe glasses for optoelectronic and laser applications

Ritu Sharma[a], Aman Prasad[a], Sumandeep Kaur[a], Nisha Deopa[b], Rekha Rani[c], M. Venkateswarlu[c], A.S. Rao[a,*]

[a] Department of Applied Physics, Delhi Technological University, Bawana Road, New Delhi 110 042, India
[b] Department of Physics, Chaudhary Ranbir Singh University, Rohtak bypass Road, Jind, Haryana 26102, India
[c] Department of Physics, Koneru Lakshmaiah Educational Foundation, Vaddeswaram-Guntur, AP, India

ARTICLE INFO

Keywords:
Tellurite glasses
Absorption
Photolumienscence
J-O parameters
Melt quench technique
CIE coordinates

ABSTRACT

Thulium (Tm^{3+}) doped Zinc Lead Tungsten Tellurite (ZnPbWTe) glasses having the composition 5ZnO-15PbO-20WO_3-(60-x)TeO_2-xTm_2O_3 were prepared by using melt quenching technique and analysed with optical absorption, photoluminescence (PL) and PL decay spectral measurements. The absorption data was used to calculate oscillator strengths and the Judd-Ofelt (J-O) parameters. The emission spectra were recorded under 472 nm excitation exhibit intense fluorescent peaks 650 nm and 806 nm. The emission spectral data correlated with J-O theory was used to determine radiative parameters like radiative transition probability (A_R), total radiative transition probability (A_T), branching ratio (β_R) and radiative lifetimes (τ_R) for the fluorescent levels of Tm^{3+} ions in ZnPbWTe glasses. The decay curves for the $^1G_4 \rightarrow {}^3F_4$ transition under 472 nm excitation were investigated to calculate experimental lifetimes (τ_{exp}) and quantum efficiency (η). The σ_{se} and η reveals that ZnPbWTe glasses doped with 1 mol% of Tm^{3+} ions are most suitable for fabricating deep red emitting optoelectronic devices and lasers.

1. Introduction

Emerging scientific trends and immense technological developments in the field of rare earth (RE) doped glassy and crystalline systems today are a researcher's treat due to the various applications that these systems find in the field of solid state laser systems, modern lighting technologies, display, photovoltaics etc. [1–5]. Homogenous light emitting property along with high thermal stability, low manufacturing procedure, free from organic polymer and cost make these RE doped glasses superior to other crystalline materials. Also, RE ion doped materials show diverse applications due to their emissive properties which arise due to intra 4f transitions. Among all the RE ions, Tm^{3+} doped materials exhibit emission in red and NIR region of electromagnetic spectrum. Therefore, such materials show potentiality in white light emitting diodes (w-LEDs), NIR lasers, sensors in atmosphere pollution monitoring, laser surgery and other applications [6–8]. Tm^{3+} ions emission in NIR and MID-IR regions have numerous applications that include Light Detection and Ranging (LIDAR), welding and coherent Doppler velocimetry. The energy level structure of Tm^{3+} is such that it increases the quantum efficiency of materials by aiding cross relaxation ($^3H_4 + {}^3H_6 \rightarrow {}^3F_4 + {}^3F_4$). Such critical scientific advantages make Tm^{3+} systems very important in the field of optoelectronic devices [9]. Moreover, in visible emission for white light generation, Tm^{3+} doped materials are studied along with co-doping of Dy^{3+} ions to improve the CRI and CCT of white light generated [10]. The transitions of Tm^{3+} ions are host dependent and crystal field effect can greatly influence the red and NIR region emissions. Among lanthanides, the energy level transitions of Tm^{3+}: $^3F_4 \rightarrow {}^3H_6$ is responsible for the emission in the 2 μm region. These transitions operate in the 3-level quantum scheme, and the luminescence spectrum emitted from this transition is relatively broad [11–14]. The transition $^1G_4 \rightarrow {}^3F_4$ of Tm^{3+} is responsible for red light emission [15]. Further, among all the RE ions, Tm^{3+} ions also show color tunability in various host matrices. The previous results present interesting properties of different materials singly and doubly doped with Tm^{3+} ions. G. Lakshmi Narayana et al. reported the optical absorption and gamma-radiation-shielding parameter studies of Tm^{3+}-doped multicomponent borosilicate glasses [16]. They observed that addition of Tm_2O_3 content leads to the improvement of the shielding efficiency of the prepared Li and Mg glasses. Spectroscopy and energy transfer in lead borate glasses doubly doped with Tm^{3+} and Dy^{3+} ions were thoroughly investigated by Agata Górny et al. [10]. They estimated the efficiencies of energy transfer

* Corresponding author.
E-mail address: drsrallam@gmail.com (A.S. Rao).

https://doi.org/10.1016/j.jnoncrysol.2019.04.032
Received 6 February 2019; Received in revised form 23 April 2019; Accepted 24 April 2019